Kinetochore-driven control of meiotic DNA break formation and recombination at centromere-proximal regions

Inaugural-Dissertation
zur
Erlangung des Doktorgrades
Dr. rer. nat.

der Fakultät für Biologie
an der
Universität Duisburg-Essen

vorgelegt von
Lisa-Marie Kuhl
aus Witten

durchgeführt am
Max Planck Institut für molekulare Physiologie
Abteilung für mechanistische Zellbiologie

Februar 2018

Die der vorliegenden Arbeit zugrunde liegenden Experimente wurden am Max Planck Institut für molekulare Physiologie in der Abteilung für mechanistische Zellbiologie durchgeführt.

1. Gutachter: Prof. Dr. Andrea Musacchio
2. Gutachter: Prof. Dr. Stefan Westermann

Vorsitzender des Prüfungsausschusses: Prof. Dr. Hemmo Meyer

Tag der mündlichen Prüfung: 13. April 2018

DOI: 10.17185/duepublico/46030
URN: urn:nbn:de:hbz:464-20190418-114218-2

In the context of this doctoral work, the following article was published:

- Vincenten, N., Kuhl, LM., Lam, I., Oke, A., Kerr, ARW., Hochwagen, A., Fung, J., Keeney, S., Vader, G., Marston, AL. (2015). The kinetochore prevents centromere-proximal crossover recombination during meiosis. *Elife* 4: e10850

Content

List of Figures

List of Tables

List of Abbreviations

BEs	boundary elements
CDE	centromere DNA element
CDKs	cyclin-dependent kinases
CEN	centromere
CENP	centromeric protein
CFP	cyan fluorescent protein
ChIP	chromatin immunoprecipitation
cM	centimorgan
CO	crossover
Co-IP	Co-immunoprecipitation
COMA	Ctf19, Okp1, Mcm21, Ame1
CRISPR	clustered regularly interspaced short palindromic repeats
Ctf19-C	Ctf19 complex
dCas9	deactivated CRISPR associated protein 9
DDK	Dbf4-dependent kinase
DMSO	Dimethyl sulfoxide
DSB	double-strand break
FKBP12	FK506-binding-protein
Frb domain	FKBP12-rapamycin-binding domain
G1 phase	gap1 phase
G2 phase	gap2 phase
GFP	green fluorescent protein
LEFs	loop extruding factors
M phase	mitosis phase
Mtw1-C	Mtw1 complex
NCO	non-crossover
Ndc80-C	Ndc80 complex
PAM	proto-spacer adjacent motif
PP2A	protein phosphatase 2A
qPCR	real time quantitative PCR
Rapa	rapamycin
RFP	red fluorescent protein

SAC	spindle assembly checkpoint
S phase	synthesis phase
Sgo1	Shugoshin1
sgRNA	single guide RNA
Spc105-C	Spc105 complex
YPD	Yeast extract peptone dextrose

1 Introduction

Sexual reproduction is a feature of eukaryotic life. To enable sexual reproduction, organisms produce specialized reproductive cells, known as gametes. In multicellular organisms, gametes are termed egg in females and sperm in males, whereas gametes in unicellular organisms such as yeasts are called spores. Gametes are the final outcome of a special type of cell division program, referred to as meiosis. The meiotic program involves the duplication of the genome of a progenitor cell followed by two consecutive rounds of chromosome segregation. The newly produced gametes contain half the number of chromosomes of the progenitor cell. Fusion of two gametes restores proper ploidy and gives rise to the development of a new organism (Hochwagen, 2008; Lee and Amon, 2001; Marston and Amon, 2004; Nasmyth, 2001). Errors in meiosis can cause chromosome segregation defects leading to the production of aneuploid gametes. This is often referred to as developmental aneuploidy. In humans, developmental aneuploidy is associated with infertility, miscarriages and birth defects, such as Trisomy 21 (Down's syndrome) (Hassold and Hunt, 2001).

1.1 An overview of meiosis: Similarities and differences from mitosis

Meiosis is a modification of a cell division program, termed mitosis (Petronczki et al., 2003). Mitosis produces two cells that contain exactly the same chromosome complement (*i.e.* they have the same ploidy) as a progenitor cell. The mitotic division program starts with DNA replication of the homologous chromosomes during synthesis (S) phase. Homologous chromosomes are pairs of chromosomes that are similar but not identical in their DNA sequence. These chromosomes are originally inherited from the maternal and paternal organisms. After DNA replication, homologous chromosomes are duplicated. The two identical copies of the chromosomes are referred to as sister chromatids. The newly synthesized sister chromatids are held together by cohesin, a ring-shaped multi-protein complex (Michaelis et al., 1997). After S phase and a gap (G2) phase, the sister chromatids are pulled apart and segregate equally into two daughter cells during the mitotic (M) phase. Consequently, the newly produced daughter cells are genetically identical (Figure 1-1 A). Meiosis relies on factors and mechanisms that are similar to mitosis, although there are some additional events required to ensure the proper execution of the meiotic program. Unlike mitosis, meiosis generates cells that are genetically

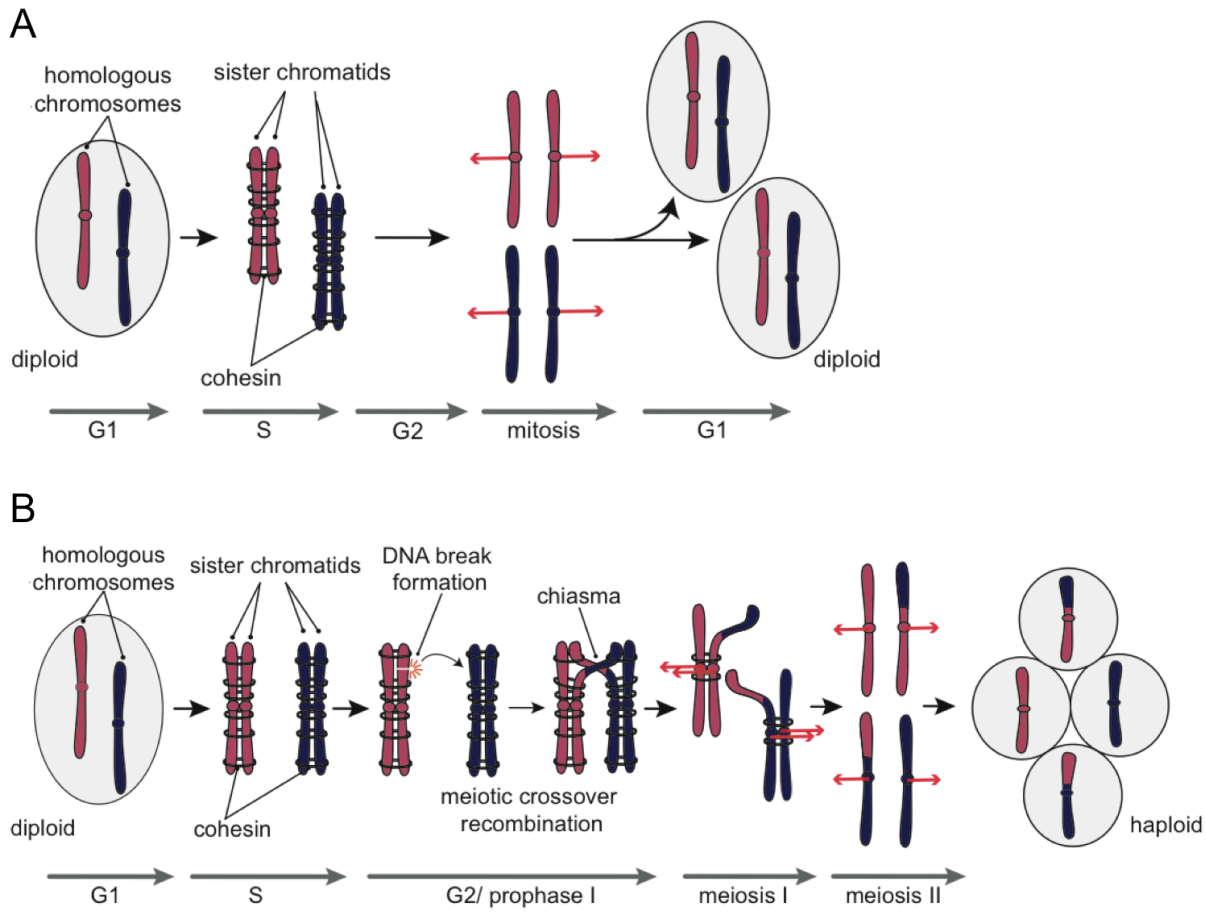

Figure 1-1 An overview of mitosis and meiosis

Scheme of a cell that commits the mitotic (A) or meiotic (B) division program. A+ B) A diploid cell contains pairs of chromosomes that are similar but not identical in their sequence composition, termed homologous chromosomes (red and blue). The decision whether the cell commits the mitotic or meiotic program is made in G1 phase. The cell first undergoes a single round of DNA replication in S phase, in which a copy of each homologous chromosome is synthesized. The two identical chromosomes that result from DNA replication are called sister chromatids. From the moment of their synthesis until their separation, sister chromatids are closely associated by ring-like protein complexes, termed cohesin. A) Following pre-mitotic S phase, a cell then undergoes G2 phase in which the cell growths and prepares for the upcoming division. In M phase, the newly synthesized sister chromatids are equally separated into two daughter cells upon removal of cohesin. Thus, the daughter cells contain a chromosome complement that is identical to that of the progenitor cell. B) Following pre-meiotic S phase, a cell undergoes controlled DNA fragmentation (*i.e.* DNA break formation) and repair (*i.e.* meiotic recombination) to establish physical connections between homologous chromosomes, referred to as chiasmata, in G2/ prophase I. The establishment of chiasmata is essential for accurate chromosome segregation during meiosis. In the first meiotic division (meiosis I), the homologous chromosomes are pulled apart (reductional segregation), whereas in the second meiotic division (meiosis II) the sister chromatids are separated (equational segregation). In meiosis I, cohesin is lost along chromosome arms, whereas remaining

Figure 1-1 continued.

cohesin at chromosomal regions close to centromeres is removed in meiosis II. The final outcome of the meiotic program are four haploid genetically non-identical cells.
G1= gap 1, S= synthesis, G2= gap 2, M= mitosis. Centromeres are indicated as red and blue circles on the chromosomes. Pulling forces are shown as red arrows.

distinct from each other and contain only half the ploidy of a progenitor cell. The meiotic program begins with DNA replication during S phase, which is similar to mitosis. The newly synthesized sister chromatids are closely associated by cohesin. After S phase, controlled DNA fragmentation (*i.e.* DNA break formation) and repair (*i.e.* meiotic recombination) occur to establish physical linkages, called chiasmata (singular: chiasma), between homologous chromosomes. A chiasma is the final outcome of a DNA repair pathway that uses the homologous chromosome as a repair template, known as inter-homolog crossover (CO) recombination. The establishment of at least one chiasma between the homologous chromosomes is required for the faithful segregation of the chromosomes during two following meiotic divisions. The meiotic divisions are referred to as meiosis I and meiosis II. In meiosis I, homologous chromosomes separate upon cohesin is removed along chromosome arms. Cohesin close to defined chromosomal loci, termed centromeres, is retained until sister chromatids disjoin in meiosis II. The end result of the meiotic program is four genetically non-identical haploid cells. The non-identical nature comes from the exchange of genetic material during inter-homolog recombination (Figure 1-1 B) (Brar and Amon, 2008; Lee and Amon, 2001; Marston and Amon, 2004; Nasmyth, 2001).
Meiosis has been studied in various organisms, which range from yeasts to mammals, including humans (Clift and Schuh, 2013; Gray and Cohen, 2016). Basic principles and proteins that govern progression through the meiotic program are conserved among species (Gray and Cohen, 2016). In this PhD study, the budding yeast *Saccharomyces cerevisiae* (*S. cerevisiae*) was used as a model organism. The following introduction is therefore focused on meiosis with respect to similarities and differences from mitosis in *S. cerevisiae*.

1.1.1 Cell cycle phases

A common feature of both mitotic and meiotic division programs is the classical segmentation into the discrete phases G1 (gap 1), S (synthesis) and G2 (gap 2) that a cell passes through before it divides. However, a significant difference between

both programs is the division process: A mitotic cell separates its chromosomes in one division, called M (Mitosis) phase, whereas a meiotic cell disjoins its chromosomes in the two segregation events meiosis I and meiosis II (Figure 1-1). The division phases of both programs (M phase and meiosis I and meiosis II) are divided into prophase, prometaphase, metaphase, anaphase and telophase. The final step in the production of two identical daughter cells in mitosis and four non-identical gametes in meiosis involves the division of the cytoplasm, termed cytokinesis (Alberts et al., 2008; Marston and Amon, 2004).

1.1.2 G1 phase

The fate of a cell, whether it enters the meiotic or mitotic division program, depends on external stimuli (van Werven and Amon, 2011). Budding yeast cells induce the meiotic program in response to starvation that involves nitrogen depletion and the presence of a non-fermentable carbon source (*e.g.* acetate) (Freese et al., 1982; Mitchell, 1988). These external factors temporarily induce the transcription of early meiotic genes required for the exit from the mitotic cycle in G1 phase and entry into pre-meiotic S phase (Chu et al., 1998; Smith et al., 1990; Vershon and Pierce, 2000). Induction of meiosis is restricted to diploid budding yeast cells that are heterozygous for the mating type locus (being *MATa*/ *MATα*) (Mitchell, 1994). In contrast to starvation, budding yeast cells that are exposed to a nutrient-rich environment (presence of glucose and nitrogen) commit the mitotic division program (also known as vegetative growth or proliferation). During vegetative growth, many genes that are essential for meiosis and thus spore formation (termed sporulation) are transcriptionally repressed (Kassir et al., 1988).

1.1.3 S phase

In the mitotic and meiotic programs, DNA replication during S phase occurs in a similar fashion. The machinery of DNA replication is identical in both pre-meiotic and pre-mitotic S phase (Simchen, 1974) and uses the same replicating origins (Collins and Newlon, 1994). As mentioned earlier, DNA replication results in the synthesis of an identical copy of each chromosome. The two identical chromosomes that are synthesized during S phase are referred to as sister chromatids. From the moment of their synthesis during S phase until their separation, sister chromatids are closely associated by the ring-shaped multi-protein cohesin complex (Michaelis et al., 1997).

In budding yeast, cohesin complexes loaded onto chromosomes in late G1 phase topologically embrace and entrap newly replicated sister chromatids during S phase, which is required for the establishment of cohesion (Haering et al., 2008; Uhlmann and Nasmyth, 1998). Sister chromatid cohesion is crucial for the faithful chromosome segregation during mitosis and meiosis (Buonomo et al., 2000; Nasmyth, 2001) and loss of cohesion leads to precocious separation of sister chromatids (Michaelis et al., 1997). Cohesin complexes loaded after DNA replication mostly do not mediate sister chromatid cohesion (Haering et al., 2004; Lengronne et al., 2006). The loading of cohesin along chromosomes depends on the Scc2-Scc4 complex (Ciosk et al., 2000; Kogut et al., 2009). Studies revealed that cohesin complexes are non-uniformly distributed along chromosomes. Cohesin complexes are associated with centromeres, the chromosomal regions surrounding centromeres, termed pericentromeres, and at specific sites along chromosome arms. Overall, levels of cohesin localization are highly enriched at centromeric and pericentromeric regions when compared to chromosome arms (Glynn et al., 2004; Lengronne et al., 2006; Tanaka et al., 1999; Weber et al., 2004).

1.1.4 G2/ prophase I

DNA replication during pre-meiotic S phase is followed by chromosome fragmentation and repair in G2/ prophase I (Figures 1-1, 1-2; Hochwagen and Amon, 2006). The fragmentation and repair of chromosomes is required for the establishment of at least one chiasma per homologous chromosome pair, which in turn is a prerequisite for faithful meiotic chromosome segregation. G2/ prophase I is sub-divided into five stages known as leptonema, zygonema, pachynema, diplonema and diakinesis. In leptonema, chromosome fragmentation occurs via the active formation of meiotic DNA double-strand breaks (DSBs). Meiotic DSB formation depends on, among other factors, structural changes of the chromosomes. The newly replicated chromosomes assemble in chromosomal loops that emanate from proteinaceous axes (Klein et al., 1999; Blat et al., 2002; Panizza et al., 2011). In budding yeast, chromosomal axes are made up of at least three major components. These components are two meiosis-specific proteins, called Hop1 and Red1, and cohesin complexes (Hollingsworth et al., 1990; Klein et al., 1999; Smith and Roeder, 1997). The “loop-axis” organization is completed in leptonema and plays an important role for meiotic DSB formation and repair processes (Blat et al., 2002; Carballo et al., 2008; Kim et al., 2010; Panizza et al., 2011; Storlazzi et al., 2003).

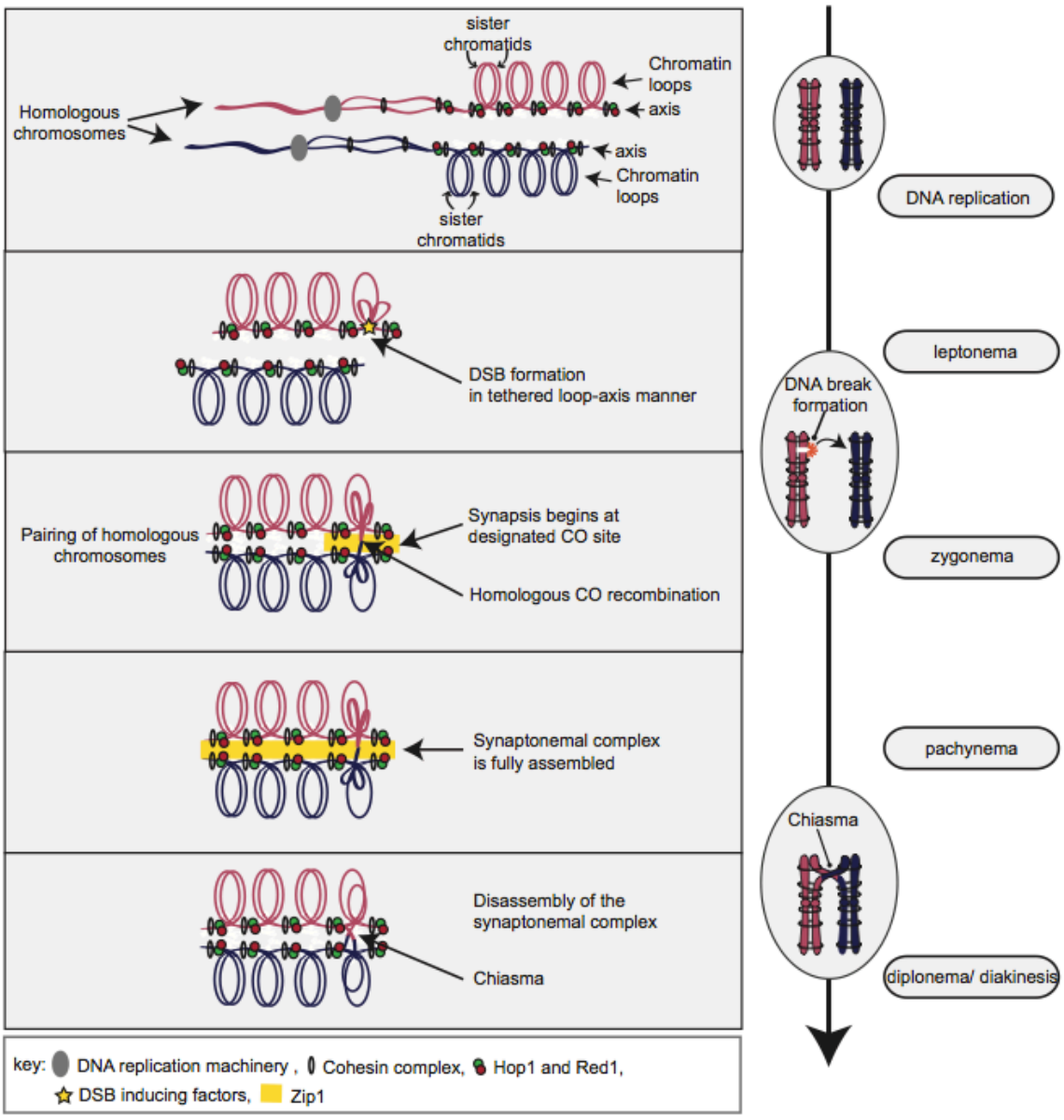

Figure 1-2 Meiotic DSB formation followed by inter-homolog CO recombination culminates in chiasmata establishment during G2/ prophase I

A prerequisite for faithful chromosome segregation during meiosis is the establishment of at least one chiasma per homologous chromosome pair. The establishment of chiasmata occurs in a cell division phase, termed G2/ prophase I, which follows DNA replication during S phase. G2/ prophase I is sub-divided into leptonema, zygonema, pchynema, diplonema and diakinesis. Upon meiotic entry chromosomes undergo structural changes through which chromosomal loops emanate from chromosomal axes. Among other proteins, chromosomal axes are made up of the meiosis-specific proteins Red1, Hop1 and DSB inducing factors as well as cohesin. In leptonema, programmed DSB formation, the initiating event of meiotic recombination and thus chiasma formation, mostly occurs within the chromosomal loops, which are tethered to the axes. In zygonema, DSB repair processes are initiated. For chiasmata formation, DSBs are repaired via inter-homolog CO recombination that uses the homologous chromosome as a repair template. Although, there are other DSB repair

Figure 1-2 continued.

pathways, only inter-homolog CO recombination ensures chiasma establishment. The CO recombination pathway involves homology search, pairing and synapsis of chromosomes. Synapsis is facilitated by the synaptonemal complex, which is composed of two lateral elements (Red1 and Hop1) and one central element (Zip1). Synapsis was proposed to begin at designated CO sites. In pachynema, the synaptonemal complex is fully assembled along chromosomes. In diplonema, the synaptonemal complex disassembles upon completion of meiotic DSB repair. In diakinesis, homologous chromosome pairs are physically linked (*i.e*. chiasma) as the final outcome of CO recombination. DSB, Double-strand break; CO, crossover.

DSBs are mostly formed in the loops in a “tethered loop-axis” manner, whereby DSB inducing factors are localized at chromosomal axes (Ito et al., 2014; Panizza et al., 2011). In the following stages, these meiotic DSBs engage a repair pathway in which the homologous chromosome is the preferred repair template rather than the sister chromatid (Schwacha and Kleckner, 1997). We refer to this repair pathway as inter-homolog repair. In zygonema, meiotic DSBs are processed as homologous chromosomes undergo homology search and align their axes, also known as pairing. Homolog pairing is then converted into a physical juxtaposition of the homologous chromosomes, an event called synapsis. Synapsis of homologous chromosome pairs is facilitated by a tripartite proteinaceous structure, referred to as the synaptonemal complex (Page and Hawley, 2004). In *S. cerevisiae*, the synaptonemal complex is composed of two outer lateral elements, which are the axis-associated proteins Hop1 and Red1, and a central element, which is an additional meiosis-specific protein, termed Zip1 (Sym et al., 1993). It is thought that meiotic DSBs designated for CO recombination are the sites where homologous chromosomes begin to synapse (Zickler and Kleckner, 2015). CO recombination is the reciprocal exchange of DNA fragments between homologous chromosomes that occurs in the context of the assembly of the synaptonemal complex. All chromosomes are fully synapsed in pachynema. The synaptonemal complex disassembles from chromosomes at diplonema when all DSBs are repaired. In diakinesis, homologous chromosome pairs are attached through chiasmata, which are the final outcome of CO recombination (Brar and Amon, 2008; Subramanian and Hochwagen, 2014).

The programmed formation of DSBs is one of the major differences between the meiotic and mitotic division programs. It is important to note that in the mitotic cell cycle, chromosomes can be damaged by environmental factors such as radiation or

chemicals rather than DNA break-inducing factors within cells (Jasin and Rothstein, 2013).

1.1.5 Meiosis I and meiosis II

Following meiotic recombination, a cell undergoes two sequential chromosome segregations events, termed meiosis I and meiosis II, that allow for the transmission of a haploid set of chromosomes into each of the four gametes. Homologous chromosome pairs that are linked through chiasmata disjoin in meiosis I, whereas sister chromatids separate in meiosis II (Figure 1-3, upper panels). During each segregation event, spindle microtubules attach to chromosomes via kinetochores, multi-subunit protein assemblies anchored to centromeres (Musacchio and Desai, 2017). In metaphase I, the kinetochores of homologous chromosome pairs become connected to microtubules from opposite spindle poles. Unlike homolog kinetochores, sister kinetochores (kinetochores of sister chromatids) are co-oriented, meaning that they are captured by microtubules from the same pole. Proper chromosome alignment on the metaphase plate does not only depend on the “pulling” forces generated by the microtubules, it also requires cohesive forces mediated by cohesin complexes that resist the microtubule-mediated pulling forces. Thus, tension is generated between the homologous chromosomes on the metaphase I plate. Once proper attachment of homologous chromosome pairs is achieved, a protease called separase cleaves cohesin complexes along chromosome arms, thereby triggering the separation of the homologous chromosomes at the onset of anaphase I. By contrast, cohesin complexes are preserved at centromeres and pericentromeres to hold sister chromatids together until meiosis II. To facilitate the separation of the sister chromatids, kinetochores are bi-oriented and attached to spindle microtubules from opposite poles at metaphase II. Sister chromatids come under tension due to the persisting cohesin complexes at centromeres and pericentromeres. Removal of the cohesin complexes by separase in anaphase II leads to the disjunction of sister chromatids (Watanabe, 2012).

The chromosome segregation pattern of meiosis II resembles that of a mitotically dividing cell. In M phase, sister chromatids are bi-oriented on the spindle plate while connected by microtubules that emanate from opposite sites (Watanabe, 2012). In budding yeast mitosis, the separation of sister chromatids is triggered by the simultaneous loss of cohesin complexes along the entire length of the chromosomes (Figure 3-1, lower panel; Uhlmann et al., 1999). This is in contrast to mammalian

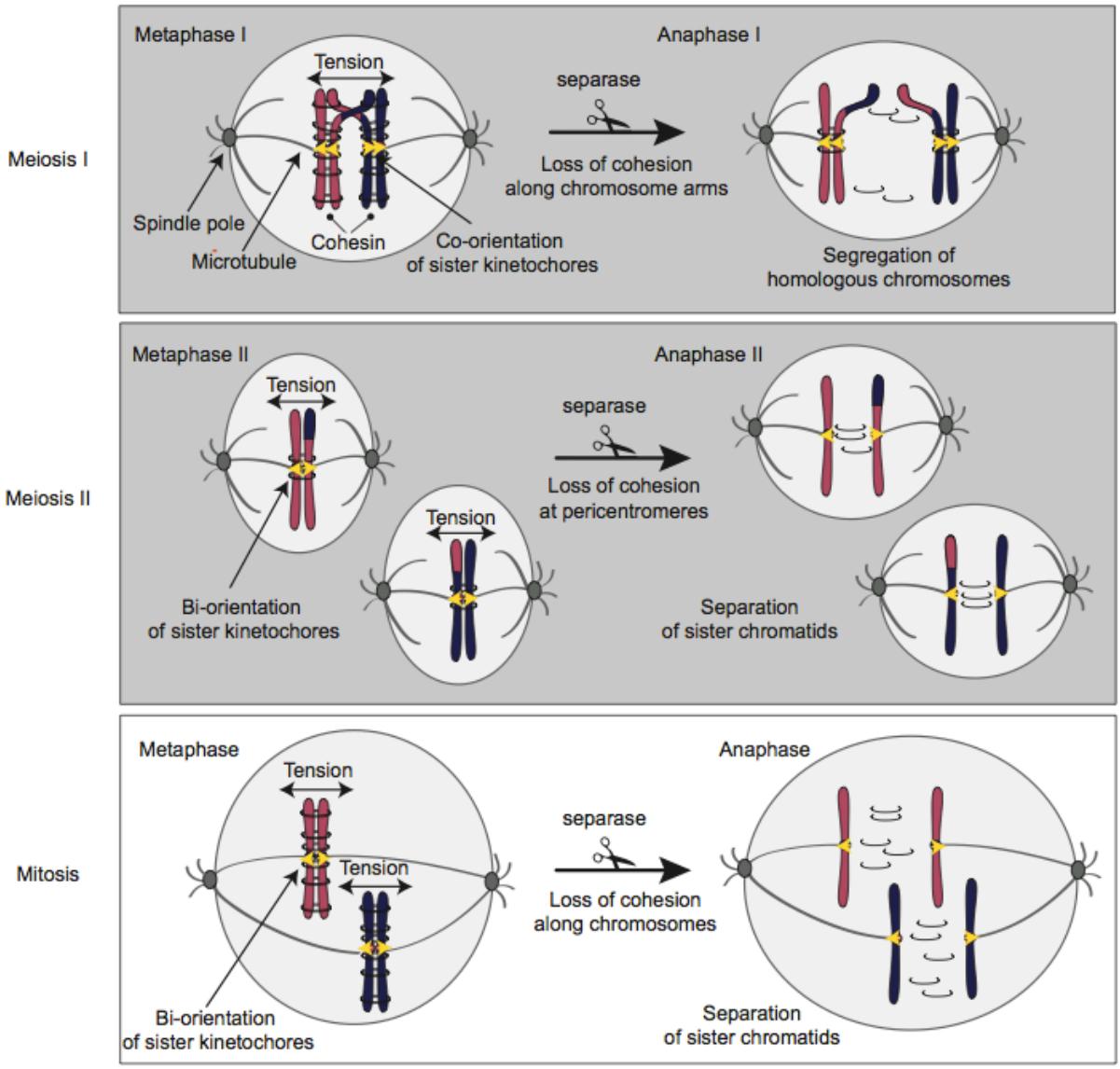

Figure 1-3 Chromosome segregation patterns in meiosis and mitosis

A cell in the meiotic program undergoes two sequential chromosome segregation events, termed meiosis I and meiosis II. In meiosis I, homologous chromosomes segregate, whereas sister chromatids separate in meiosis II. To enable homologous chromosome segregation, the kinetochores (multi-protein complexes that assemble onto centromeres and attach to microtubules, here indicated as yellow arrow heads) of physically linked homologous chromosomes must be bi-orientated on the spindle plate in metaphase I, which enables the attachment of microtubules from opposite spindle poles. On the contrary, the kinetochores of sister chromatids are co-oriented on the spindle plate in metaphase I, so that they are attached to microtubules from the same pole. Consequently, tension is generated between homologous chromosomes but not sister chromatids. Separase-mediated cleavage of cohesin along chromosome arms but not centromeres and pericentromeres at the onset of anaphase I allows for the separation of homologous chromosomes. In metaphase II, the kinetochores of sister chromatids are bi-oriented, thereby captured from microtubules of opposite spindle poles. Destruction of cohesin at centromeric and pericentromeric regions at the onset of

Figure 1-3 continued.

anaphase II enables the separation of sister chromatids. The chromosome segregation pattern in meiosis II resembles the pattern in mitosis. In metaphase of the mitotic cell cycle, sister chromatid kinetochores are bi-oriented, thereby attached to microtubules from opposite spindle poles. In budding yeast mitosis, separase-mediated cleavage of cohesin occurs simultaneously along whole chromosomes, which allows for the separation of the sisters.
Yellow arrow heads indicate kinetochore orientation on the spindle plate. (Meiotic and mitotic chromosome segregation patterns are reviewed in Watanabe, 2012.)

mitosis, in which cohesin complexes are lost through two distinct steps. The first step involves the cleavage of cohesin complexes from chromosome arms during prophase in a fashion that is independent of separase activity (termed prophase pathway; Losada et al., 2002; Sumara et al., 2002). The residual cohesin proteins around centromeres are required for the bi-orientation of the sister chromatids on the metaphase spindle. Once sister chromatids are correctly aligned, the second step comprises the separase dependent cleavage of centromeric and pericentromeric cohesin complexes, thereby triggering the separation of sister chromatids in anaphase (Hauf et al., 2001; Waizenegger et al., 2000).

1.1.6 Cyclin dependent kinases and Dbf4/ Cdc7 kinase

The progression of both mitotic and meiotic cell division programs highly depends on the acitivity of two types of serine/ threonine kinases, the cyclin dependent kinases (CDKs) and the Dbf4/ Cdc7 kinase (also referred to as the Dbf4-dependent kinase, DDK) (Gómez-Escoda and Wu, 2017). The activity of CDKs relies on the binding of a regulatory subunit, a cyclin (Cln). In budding yeast, the major CDK, termed Cdc28, associates with distinct Clns in a temporally coordinated manner to tightly control the transition from one phase to the next (Marston and Amon, 2004). In the mitotic cell cycle, Cdc28 binds to the G1 phase cyclins Cln1-3 to promote the transition from G1 to S phase. In budding yeast, there are six B type cyclins, called Clb1-6. In both mitosis and meiosis, Cdc28 forms a complex with the S phase cyclins Clb5 and Clb6 to drive genome duplication. The activity of Cdc7 depends on the binding to its subunit, Dbf4 (Jackson et al., 1993; Johnston et al., 1999; Sclafani, 2000). Like the kinase complexes Cdc28-Clb5 and Cdc28-Clb6, the activity of the Dbf4/ Cdc7 kinase is required for the initiation of DNA replication in both pre-mitotic and pre-meiotic S phase (Bousslet and Diffley, 1998; Donaldson et al., 1998; Dirick et al., 1998; Stuart and Wittenberg, 1998). As described earlier, the meiotic division program is an

adaptation of mitosis with additional meiosis-specific events. These meiosis-specific events comprise the extended G2/ prophase I, in which meiotic DSB formation and recombination occur, and two consecutive chromosome segregation events. Therefore, the control of meiotic progression via CDKs and the Dbf4/ Cdc7 kinase requires some modifications. In addition to the activity of the kinase complexes Cdc28-Clb5 and Cdc28-Clb6 as well as Dbf4/ Cdc7 during pre-mitotic and pre-meiotic S phase, these kinases are required for the initiation of meiotic recombination in G2/ prophase I (Henderson et al., 2006; Murakami and Keeney 2008; Wan et al. 2008). After G2/ prophase I, the activation of Cdc28 via the binding to Clb1, 3 and 4 is essential for the following meiotic divisions (Carlile and Amon, 2008). The B type cyclin Clb2 is mitosis-specific and not expressed in meiosis (Grandin and Reed, 1993).

1.1.7 Checkpoints

To maintain the integrity of the genome, the cell cycle contains surveillance mechanisms, termed checkpoints, which can delay or arrest cells in a certain stage when earlier events are not accurately completed (Hartwell and Weinert, 1989; Subramanian and Hochwagen, 2014). There are four major checkpoints in budding yeast mitosis. These checkpoints are known as the G1/ S checkpoint, intra S phase checkpoint, G2/ M checkpoint and spindle assembly checkpoint (SAC) (Murray, 1994; Weinert, 1998). The G1/ S checkpoint, intra S phase checkpoint, G2/ M checkpoint response to DNA damage (Gerald et al., 2002; Longhese, 1998). Activation of these checkpoints temporary inhibits cell cycle progression to prevent replication and/ or segregation of damaged DNA. The SAC, the fourth checkpoint, allows for chromosome disjunction only when all kinetochores are properly attached to spindle microtubules (Musacchio and Salmon, 2007).

The meiotic program is controlled by checkpoints that are similar to the ones found in mitosis, although some specific checkpoints are required while cells undergo homologous recombination in G2/ prophase I (Hochwagen and Amon, 2006; Subramanian and Hochwagen, 2014). First, DNA replication is linked to DSB formation, the initiating event of meiotic recombination, through the replication checkpoint. The replication checkpoint blocks the formation of meiotic DSBs when replication forks are stalled and DNA replication is incomplete (Blitzblau and Hochwagen, 2013; Ogino and Masai, 2006; Tonami et al., 2005). Second, the formation of meiotic DSBs triggers the activation of the recombination checkpoint. As

mentioned earlier, the repair of meiotic DSBs has a strong bias towards the homologous chromosome as a repair template (Schwacha and Kleckner, 1997). In *S. cerevisae*, inter-homolog bias is controlled by two kinases, called Tel1 and Mec1, which phosphorylate the meiosis-specific protein Hop1 (Carballo et al., 2008). Phosphorylation of Hop1 in turn leads to the recruitment of a kinase, termed Mek1, whose activity inhibits inter-sister recombination (Carballo et al., 2008; Niu et al., 2005, 2007, 2009). The meiotic recombination checkpoint, also referred to as pachytene checkpoint, is active before a cell commits to enter the meiotic divisions (Lydall et al., 1996; MacQueen and Hochwagen, 2011; Roeder and Bailis, 2000). This checkpoint prevents cells to exit meiotic prophase via controlling the expression and localization of a transcription factor, termed Ndt80, and inhibiting CDK activity when recombination events are incomplete (Chu and Herskowitz, 1998; Sourirajan and Lichten, 2008). A generally conserved member of the AAA^+ ATPase family, called Pch2, is also involved in meiotic recombination checkpoint responses in G2/ prophase I (Vader, 2015). In budding yeast, Pch2 plays a role in the same pathway as the Tel1 kinase leading to the phosphorylation of Hop1 (Ho and Burges, 2011; Wu and Burges, 2006). In addition, Pch2 responds to synapsis defects, leading to an arrest in the meiotic program (Bhalla and Dernburg, 2005; San Segundo and Roeder, 1999). After checkpoint responses in G2/ prophase I, the SAC is also active in the meiotic division program (Sun and Kim, 2011).

1.2 An overview of meiotic recombination in *S. cerevisiae*

Inter-homolog recombination is a prerequisite for accurate chromosome disjunction in meiosis. The following section 1.2.1 gives an overview of meiotic DSB formation and repair pathways. Section 1.2.2 describes factors that influence the distribution of meiotic recombination events along chromosomes.

1.2.1 Meiotic recombination: From DSB formation to inter-homolog repair

Meiotic recombination begins with the programmed formation of DSBs throughout the genome. The subsequent repair of the DSBs via homologous recombination can yield several types of recombination products. In meiosis, the preferred repair template is the homologous chromosome (Schwacha and Kleckner, 1997). The recombination pathway that uses the homologous chromosome as a repair template generates either a CO or a non-crossover (NCO) (Figure 1-4). Inter-homolog CO recombination is the reciprocal exchange of DNA fragments between homologous

chromosomes that culminates in the establishment of chiasmata. The inter-homolog NCO recombination pathway does not involve the reciprocal exchange between homologous chromosomes, so chiasmata are not formed. Therefore, only inter-homolog CO products ensure both genetic variation and chiasmata, which is required for faithful chromosome segregation during meiosis.

The initiating event of meiotic recombination, the DSB formation, is dependent on four interacting protein sub-complexes, termed Mre11-Rad50-Xrs2 (MRX), Mer2-Rec114-Mei4, Rec102-Rec104 and Spo11-Ski8 that act together as the “DSB machinery” (Keeney 2001; Keeney and Neale 2006; Lam and Keeney, 2014). The initiating step in DSB formation is the chromosomal localization of the protein Mer2 by the axis-associated proteins Red1 and Hop1 (Panizza et al., 2011). Mer2 is phosphorylated by the S phase kinase complexes Cdc28-Clb5 and Cdc28-Clb6 as well as the Dbf4/ Cdc7 kinase (Henderson et al., 2006; Murakami and Keeney 2008; Wan et al. 2008). Phosphorylated Mer2 leads to the recruitment of the DSB factors Rec114 and Mei4 to axis sites (Henderson et al. 2006; Panizza et al. 2011). It is thought that the proteins Rec102 and Rec104 act as an interface between the Mer2-Rec114-Mei4 and Spo11-Ski8 complexes, which supports chromatin association of Spo11 (Arora et al. 2004; Maleki et al. 2007; Prieler et al. 2005).

The conserved topoisomerase-like enzyme Spo11 is the catalytic core of the DSB machinery (Keeney and Kleckner, 1995; Keeney et al., 1997). A dimer of Spo11 cleaves the strands of a DNA molecule, thereby generating a DSB with covalent links between the 5’ DNA ends and the catalytic tyrosine residue of each Spo11 monomer (Keeney and Kleckner, 1995; Keeney 2001). After DSB formation, other components of the DSB machinery catalyze endonucleolytic removal of Spo11, which is covalently bound to oligonucleotides (Keeney and Kleckner, 1995; Usui et al. 1998). The ends of a DSB undergo nucleolytic degradation to expose single-stranded DNA tails, which allow exchange proteins Rad51 and Dmc1 to be loaded. The proteins Rad51 and Dmc1, orthologs of the bacterial RecA protein (Bishop et al. 1992; Shinohara et al. 1992), execute homologous DNA pairing and strand exchange activities (Sehorn and Sung, 2004). While Rad51 plays a critical role in recombination of both mitotic and meiotic division programs, Dmc1 is specifically expressed in meiosis to conduct recombination (Bishop et al. 1992; Shinohara et al. 1992). Absence of any of the two exchange proteins causes a delay or arrest

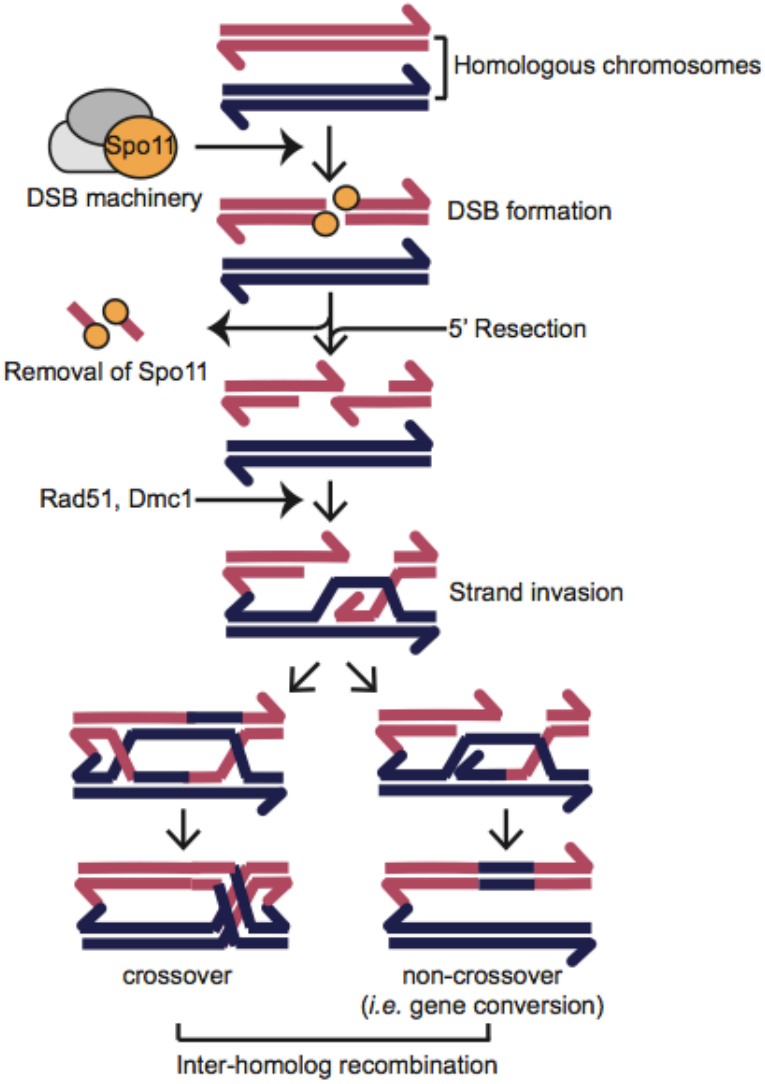

Figure 1-4 Inter-homolog CO and NCO recombination

The DSB machinery, including the proteins Mre11-Rad50-Xrs2, Mer2-Rec114-Mei4, Rec102-Rec104 and Spo11-Ski8, is recruited to chromosomes. After DSB formation, Spo11, the catalytic core of the DSB machinery, is covalently attached to DSB sites. Enzymatic cleavage of Spo11, which is bound to short DNA fragments, is followed 5' resection of the cleaved DNA strands. This leads to single-stranded DNA overhangs. These overhangs are then occupied by the proteins Rad51 and Dmc1, which are required for DSB repair. After scanning the genome for the homologous chromosome as a repair template, the resected strand invades into the homolog. Stabilization of the strand invasion gives rise to a double-Holliday junction, whose resolution generates CO recombination product. On the contrary, failure to stabilize the strand invasion yields a NCO recombination product (*i.e.* gene conversion). CO, crossover; NCO, non-crossover; DSB, double-strand break. Adapted from Vincenten et al. (2015).

with unprocessed recombination intermediates (Bishop et al.1992; Shinohara et al. 1992). The single-stranded DNA tails occupied by the exchange proteins then scan the genome for the homologous chromosome as a repair template. After homology search, the resected DSB is processed into a strand invasion intermediate, whose stabilization leads to the formation of a double-Holliday junction (Schwacha and Kleckner, 1995). Resolution of the double-Holliday junction yields a CO recombination product (Storlazzi et al. 1995). Failure to stabilize the strand invasion intermediate generates a NCO. Homologous NCO recombination is characterized by gene conversions, which is the copying of genetic material between homologous chromosomes at the site of DNA breakage (without the exchange of flanking chromosomal regions) (Carpenter, 1987; Fink and Petes, 1984). Although inter-homolog homologous recombination is the preferred repair pathway in meiosis, DSBs can be repaired via inter-sister recombination, whereby the sister chromatid serves as a repair template (Goldfarb and Lichten, 2010). In the budding yeast *S. cerevisiae*, for example, ~160 meiotic DSBs are induced per cell (Pan et al., 2011). While, ~95 of these are processed into a CO (Chen et al., 2008), the remainder of breaks are repaired as NCOs and via the inter-sister recombination pathways.

1.2.2 Non-random genome-wide distribution of meiotic recombination events

Meiotic DSB formation and recombination are non-randomly distributed across the genome, meaning that these events occur in some genomic regions more often than in others (de Massy, 2013; Kauppi et al., 2004; Lichten and Goldman, 1995; Petes, 2001). Chromosomal regions in which meiotic DSBs frequently occur are termed hot regions. Hot regions in turn contain short DNA sequences, called hot spots. On the contrary, chromosomal domains in which DSBs are less likely induced are known as cold regions (Blitzblau et al., 2007; Buhler et al., 2007; Gerton et al., 2000; Pan et al., 2011). Meiotic DSB formation and repair most likely underly local control within chromosomal cold regions (Chen et al., 2008; Vader et al., 2011). Often, cold regions fall within genomic regions that can threaten genome stability and/ or negatively influence chromosome segregation, when they undergo meiotic DSB formation and recombination. For example, in budding yeast, chromosomal cold regions are found at pericentromeres repetitive DNA arrays and telomeres (Blitzblau et al., 2007; Buhler et al., 2007; Gerton et al., 2000; Pan et al., 2011).

The overall distribution of meiotic DSBs is influenced by several factors that operate

on different levels of chromosome and chromatin organization (Figure 1-5; Cooper et al., 2016). On a large scale, DSB distribution is dictated by the structural organization of the chromosomes. As described in section 1.1.4, meiotic DSB formation and repair occur in the context of chromosomes that are organized in chromatin loops and proteinaceous axes (Baudat et al., 2013; Blat et al., 2002; Klein et al., 1999; Panizza et al., 2011). Within this structural arrangement, DSB hot spots are predominantly found in the loops (Klein et al., 1999). By contrast, axis associated sites are cold regions for meiotic DSB formation (Ito et al., 2014). The DSB machinery, including Spo11 as the catalytic core, is localized at axis sites and induces DNA breakage in a tethered loop-axis fashion (Ito et al., 2014; Panizza et al., 2011). On a small scale, DSB distribution is influenced by the underlying chromatin organization within the loops. In *S. cerevisiae*, meiotic DNA break hot spots are associated with nucleosome depleted sites, which are often found in promoter regions (Fan and Petes, 1996; Pan et al., 2011). In particular, promoter regions of divergent gene pairs are preferred regions for meiotic DSB formation (Blitzblau et al., 2007). Moreover, it was revealed that certain histone modifications such as trimethylation of lysine 4 of histone H3 (H3K4me3) create an environment favorable for Spo11 activity (Borde et al., 2009; Kniewel and Keeney, 2009; Tischfield and Keeney, 2012).

In other species, factors that designate DSB hot spots differ on a small scale. For example, in the fission yeast *Schizosaccharomyces pombe* (*S. pombe*), DNA breaks are mostly formed within intergenic regions, which do not necessarily are nucleosome depleted (Fowler et al., 2014). In mice and humans, DSB hotspots are associated with the binding of the methyltransferase PRDM9, which can methylate H3K4 (Baudat et al., 2010).

There is evidence that the choice of the repair pathways of meiotic DSBs (*i.e.* inter-homolog vs. inter-sister repair and CO vs. NCO) is tightly regulated across the genome (Chen et al., 2008; Medhi et al., 2016; Phadnis et al., 2011). As mentioned earlier, DSBs can be repaired using either the homologous chromosome or the sister chromatid as a repair template, although the preference is towards the use of the homolous chromosome in meiosis (Schwacha and Kleckner, 1994, 1997). The choice of using the homologous chromosome or the sister chromatid as the repair template depends on several factors. For example, the axis-associated proteins Red1 and Hop1 and the meiotic kinase Mek1 were suggested to promote inter-homolog recombination (Niu et al., 2005; Terentyev et al., 2010; Wan et al., 2004).

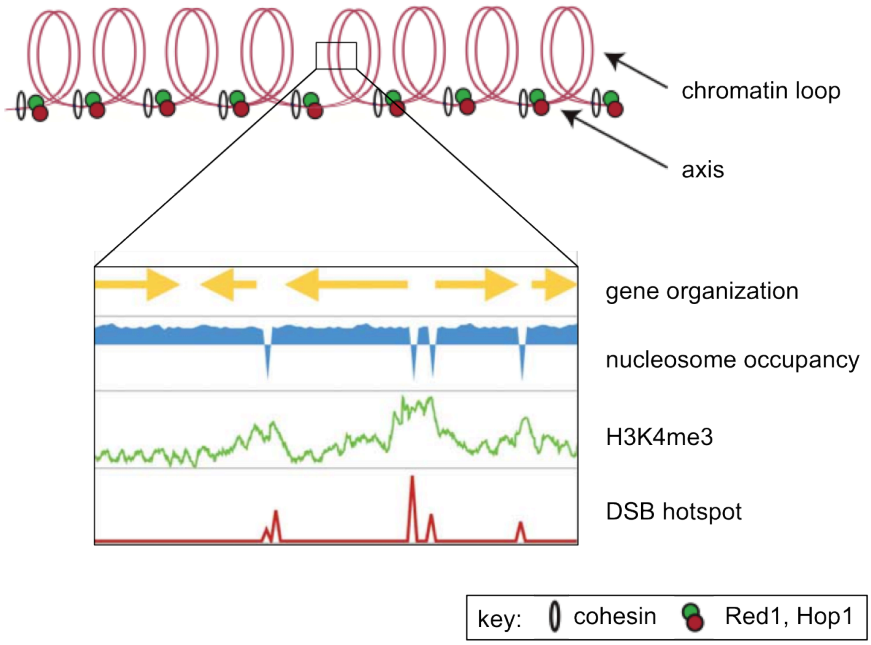

Figure 1-5 Meiotic DSB hot spot designation in budding yeast

The designation of meiotic DSB formation is dependent on chromosome and chromatin organization. Upon meiotic entry, chromosomes undergo structural changes and form loops that emerge from a proteinaceous axis (*e.g.* cohesin, Red1, Hop1). DSB formation frequently occurs within chromosomal loops (hot regions), whereas DNA breaks rarely form at the chromosomal axis (cold region). Within the loops, DSB formation is dependent on the underlying chromatin structure (*i.e.* gene organization, nucleosome occupancy and certain histone modifications such as trimethylation of lysine 4 of histone H3 (H3K4me3)). Figure is modified from Cooper et al. (2016).

On the contrary, cohesin, another axis-associated factor, was proposed to mediate inter-sister repair (Kim et al., 2010). The cohesin promoted inter-sister repair can be antagonized by the activity of Red1, Hop1 and Mek1 in some genomic regions, thereby ensuring inter-homolog repair (Kim et al., 2010). For inter-homolog repair, DSBs undergo either the CO or NCO recombination pathway. The choice of undergoing CO or NCO recombination involves an ensemble of meiosis-specific proteins, termed the ZMM proteins. The ZMM proteins promote the CO recombination pathway by stabilizing the strand invasion intermediate and ensuring their maturation into a double-Holliday junction (Allers and Lichten, 2001; Börner et al., 2004; Lynn et al., 2007; Schwacha and Kleckner, 1994). Moreover, a mechanism known as CO interference facilitates the spatial distribution of COs along chromosomes (Jones, 1984). Interference prevents that DSBs in close proximity to one another are all repaired as COs. This “interference” pathway ensures that one

DSB is repaired as a CO and the adjacent DSBs are processed into NCO recombination products. Another mechanism to distribute COs across the genome in budding yeast is termed CO homeostasis (Martini et al., 2006). Homeostasis ensures that the overall number of COs remains constant, although the amount of meiotic DSBs can vary from one cell to the other.

1.3 Centromeric and pericentromeric regions

As mentioned earlier, defined chromosomal loci upon which the kinetochore assembles are termed centromeres. In many species, centromeres are classified into regional and point centromeres (McKinley and Cheeseman, 2016). Regional centromeres are often made up of repetitive DNA elements (*e.g*. tandem repeats), which occupy large chromosomal regions in humans (up to 5 Mb), mice, flies, plants and fission yeast (up to 40-100 kb) (Fukagawa and Earnshaw 2014; McKinley and Cheeseman 2016; Musacchio and Desai 2017; Verdaasdonk and Bloom, 2011). In contrast to regional centromeres, point centromeres in budding yeast are short chromosomal regions (~125 bps) that include the three conserved centromere DNA elements (CDE) CDE I, a 8 bp sequence, CDE II, an AT-rich fragment of 79-88 bps, and CDE III, a 24 bp region (Hegemann and Fleig, 1993). Except for the conserved DNA elements CDE I-III of the budding yeast centromere (referred to as *CEN*), centromeric regions are epigenetically defined rather than by specific DNA sequences in most organisms. Most centromeres (with some exceptions (Drinnenberg et al. 2014) have one epigenetic marker in common: the histone H3 variant CENP-A, known as Cse4 in budding yeast. In comparison to human centromeres, which harbor several CENP-A proteins, budding yeast's *CEN*s contain only a single Cse4 protein that serves as the basis for kinetochore assembly.

Chromosomal regions surrounding centromeres are known as pericentromeres. In most organisms except for budding yeast, pericentromeric DNA is assembled into heterochromatin and contains H3K9 methylated histones (H3K9me3) (Almouzni and Probst, 2011; Déjardin, 2015). In *S. pombe,* pericentromeric heterochromatin forms at repetitive DNA elements at centromeres and is enriched in di- and trimethylation of histone H3 on lysine 9 (H3K9me2/3) (Grewal and Jia, 2007). In mice, pericentromeric heterochromatin comprises tandem arrays of AT-rich repeats (termed major satellites) characterized by hypoacetylation and H3K9 methylation (Almouzni and Probst, 2011; Vissel and Choo, 1989). *S. cerevisiae* lacks pericentromeric heterochromatin (Marston, 2015). However, there are some characteristics that

budding yeast and other organisms have in common at the pericentromere. These characteristics are described in the following sections (1.3.1 and 1.3.2).

1.3.1 Centromeres and pericentromeres are cold regions for meiotic DSB formation and recombination

In many eukaryotic systems, centromeres and pericentromeres are chromosomal cold regions for inter-homolog recombination during meiosis (Copenhaver et al., 1999; Ellermeier et al., 2010; Gore et al., 2009; Lambie and Roeder, 1986; Nakaseko et al., 1986; Mahtani and Willard, 1998; Puechberry et al., 1999; Saintenac et al., 2009; Tanksley et al., 1992). Improper placement of COs in the vicinity of centromeres is associated with unfaithful chromosome segregation that generates aneuploid/ inviable gametes (Hassold and Hunt, 2001; Koehler et al., 1996; Rockmill et al., 2006). Why pericentromeric CO recombination causes chromosome segregation defects is not entirely understood. However, there are two models proposing that CO formation close to centromeres might interfere with the function of cohesin around centromeres (Hassold and Hunt, 2001; Koehler et al., 1996; Rockmill et al., 2006). Under normal circumstances, CO formation and thus chiasmata establishment predominantly occur along chromosomal arms. Cohesin complexes on chromosomal arms, but not pericentromeres, are cleaved at the onset of anaphase I, which allows for the disjunction of the homologous chromosomes (Figure 1-6 A). One model proposes that chiasmata in the vicinity of centromeres are trapped by cohesin, which is protected from cleavage until anaphase II. This makes the homologous chromosomes difficult to separate and thus increases the likelihood of chromosome non-disjunction at meiosis I (Figure 1-6 B; Hassold and Hunt, 2001; Koehler et al., 1996; Lamb et al., 2005). The second model proposes that COs may disrupt pericentromeric cohesion, which would lead to precocious separation of sister chromatids (Figure 1-6 C) (Rockmill et al., 2006).

Careful control of meiotic DSB formation and recombination within centromere-proximal regions is required to avoid potential interference with meiotic chromosome segregation. Indeed, meiotic inter-homolog recombination in the vicinity of centromeres is mostly prevented in many species (Nambiar and Smith, 2016; Talbert and Henikoff, 2010). A reduction in CO recombination at the pericentromere was discovered for the first time in the fruit fly *Drosophila melanogaster* (*D. melanogaster*) carrying a translocated chromosome (Beadle, 1932; Dobzhansky, 1930; Mather, 1939). This chromosome was made up of a fragment of chromosome *III*, which was

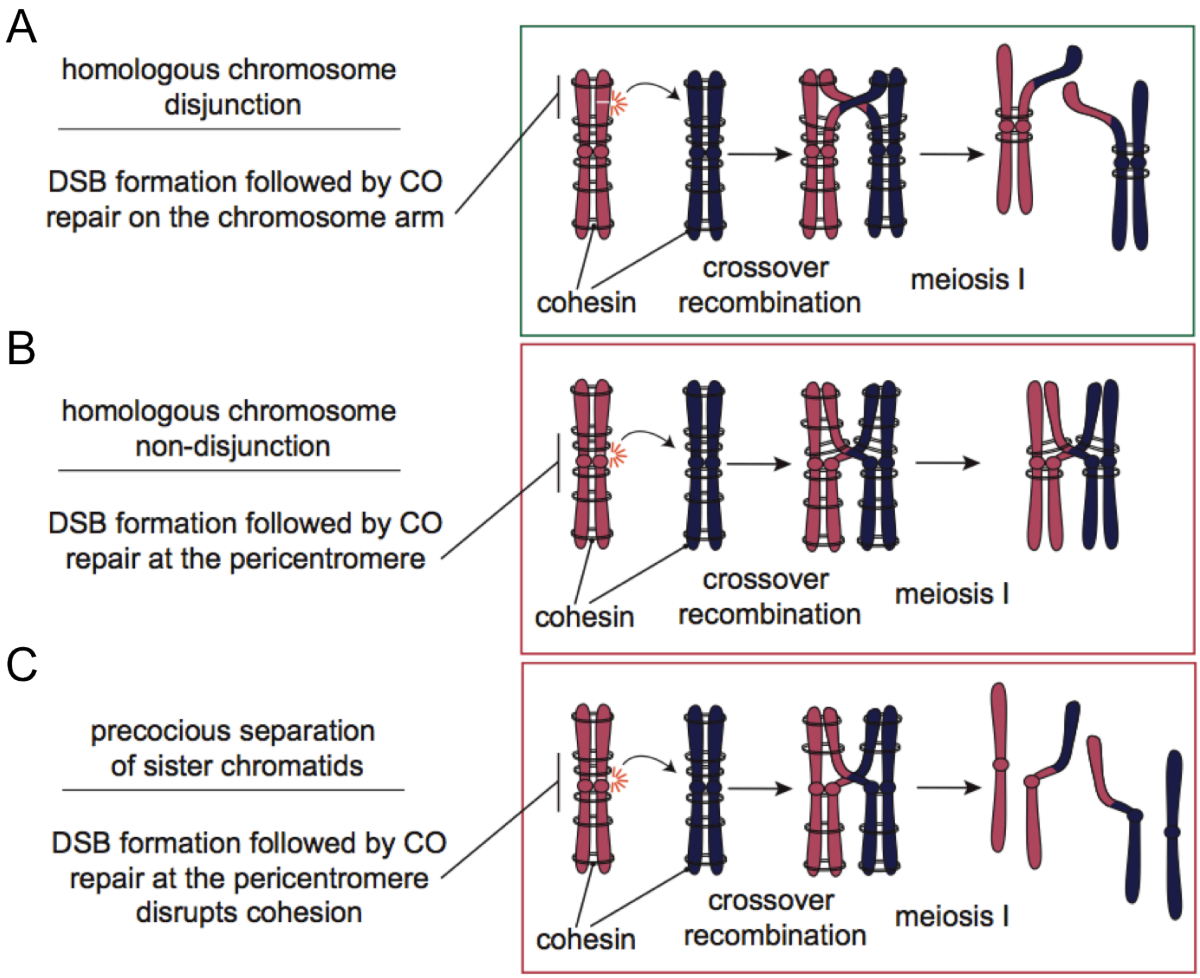

Figure 1-6 DSB formation followed by CO repair at the pericentromere is associated with chromosome mis-segregation during meiosis

A) Normal chromosome segregation at meiosis I: DSB formation followed CO repair at chromosomal arms enables disjunction of homologous chromosomes upon cohesin cleavage along chromosome arms. B) Model 1: Abnormal chromosome segregation at meiosis I. DSB formation followed by CO recombination in the vicinity of centromeres (*i.e.* pericentromeres) was proposed to cause non-disjunction of homologous chromosomes due to persisting cohesin. Homologous chromosomes are trapped through pericentromeric cohesin and not be separated at the first meiotic division. C) Model 2: Abnormal chromosome segregation at meiosis I. DSB formation followed by CO repair at pericentromeres was suggested to disrupt pericentromeric cohesion. Cohesin complexes along chromosome arms are removed at the onset of anaphase I (right before homologous chromosome segregation). Loss of cohesin at pericentromeres and chromosome arms might cause precocious separation of sister chromatids.

Centromeres are indicated as red and blue circles on the chromosomes.

placed in close proximity to the centromere of chromosome *IV*. The translocated fragment of chromosome *III* revealed reduced CO recombination frequency near the centromere. Since this observation in *D. melanogaster*, a decrease in homologous recombination close to centromeres was observed in several other organisms (Copenhaver et al., 1999; Ellermeier et al., 2010; Gore et al., 2009; Lambie and Roeder, 1986; Nakaseko et al., 1986; Mahtani and Willard, 1998; Puechberry et al., 1999; Saintenac et al., 2009; Tanksley et al., 1992). Evidence for reduced levels of inter-homolog recombination at chromosomal regions surrounding centromeres in budding yeast came from studies performed by Lambie and Roeder (1986, 1988). In these studies, it was shown that both types of recombination pathways, COs and NCOs, are decreased close to *CEN3* in *S. cerevisiae* (Lambie and Roeder, 1986, 1988). These findings were corroborated by recent genome-wide microarray analysis indicating that COs and NCOs are equally (~6 fold) reduced within a distance of 10 kb from centromeres as compared to chromosomal regions further than 10 kb away (Chen et al., 2008). In the fission yeast *S. pombe*, genetic maps of chromosome *II* unveiled that a ~50 kb region closely linked to the centromere is reduced in homologous recombination (Nakaseko et al., 1986). A decrease in homologous recombination within centromere-proximal regions was also found in other fungi such as *Neurospora crassa* (Davis et al., 1994) and *Aspergillus nidulans* (Aleksenko et al., 2001). In the plant *Arabidopsis thaliana,* the core centromere and pericentromere of chromosome *I* was shown to undergo infrequent formation of COs (Haupt et al., 2001). In *Homo sapiens,* meiotic recombination is at least 8-fold decreased near the centromere on the X chromosome relative to the average exchange level on this chromosome (Mahtani and Willard, 1998).

In budding yeast, it was demonstrated that the initiating event of meiotic recombination, DSB formation, is reduced close to centromeres (Blitzblau et al., 2007; Buhler et al., 2007; Gerton et al., 2000; Pan et al., 2011; Robine et al., 2006). The generation of genome-wide DSB maps based on microarray analyses revealed that meiotic DNA breaks are reduced within a window of 5-10 kb of centromeres (Blitzblau et al., 2007; Buhler et al., 2007). More recent nucleotide-resolution mapping (Pan et al., 2011) showed a ~2-3 fold decrease of meiotic DSB formation within ~5-10 kb surrounding centromeres and 7-fold less breaks within 1-3 kb on each side of centromeres relative to the genome average (Pan et al., 2011).

However, chromosomal features that control meiotic DSB formation and recombination in the vicinity of centromeres remain poorly understood (Nambiar and Smith, 2016; Talbert and Henikoff, 2010). In budding yeast, Chen et al. (2008) demonstrated that the major component of the synaptonemal complex, Zip1, plays a role in controlling both inter-homolog CO and NCO recombination near centromeres. An additional factor, the Bloom's helicase Sgs1, was shown to control meiotic recombination in the vicinity of centromeres (Rockmill et al., 2006). Both factors Zip1 and Sgs1 were proposed to act at a step after meiotic DSB formation (Rockmill et al., 2006; Chen et al., 2008). Studies performed in fission yeast and *D. melanogaster* showed that the integrity of pericentromeric heterochromatin prevents both the formation of DSBs and homologous recombination at centromere-proximal regions (Ellermeier et al., 2010; Westphal and Reuter, 2002). However, this explanation cannot account for budding yeast, which lacks heterochromatin (Marston, 2015). Alternatively, factors associated with centromeric and/ or pericentromeric regions might play a role in the local control of meiotic DSB formation and recombination. Robine et al. (2006) found that in budding yeast, the excision of *CEN3* relieves the suppression of meiotic DSB formation in the surrounding pericentromere, which might suggest that factors at the centromere control DNA breaks.
An overview of centromere- and pericentromere-associated factors is given in the following sections 1.3.2 and 1.4.

1.3.2 Centromere- and pericentromere-associated proteins

Kinetochores assemble onto centromeres. Despite the close proximity to centromeric regions, pericentromeres are thought not to directly interact with kinetochore proteins. An introduction about the budding yeast kinetochore is given in section 1.4.
In budding yeast and many other species, the pericentromere harbors a wide range of proteins that are involved in chromosome and/ or chromatin organization (Figure 1-7). Among these proteins are the "structural maintenance of chromosomes" (SMC) complexes cohesin, condensin and Smc5-Smc6 complex. The SMC complexes are multi-protein assemblies, which are evolutionary conserved from prokaryotes to eukaryotes (Harvey et al., 2002; Jeppsson et al., 2014; Uhlmann, 2016). In eukaryotes, each complex has at its core a ring-like structure, which is made up of a V-shaped Smc dimer and additional non-Smc subunits. The SMC complexes are crucial for the organization of chromosomal domains throughout both meiotic and mitotic programs. Among the complexes, cohesin is the most-studied multi-protein

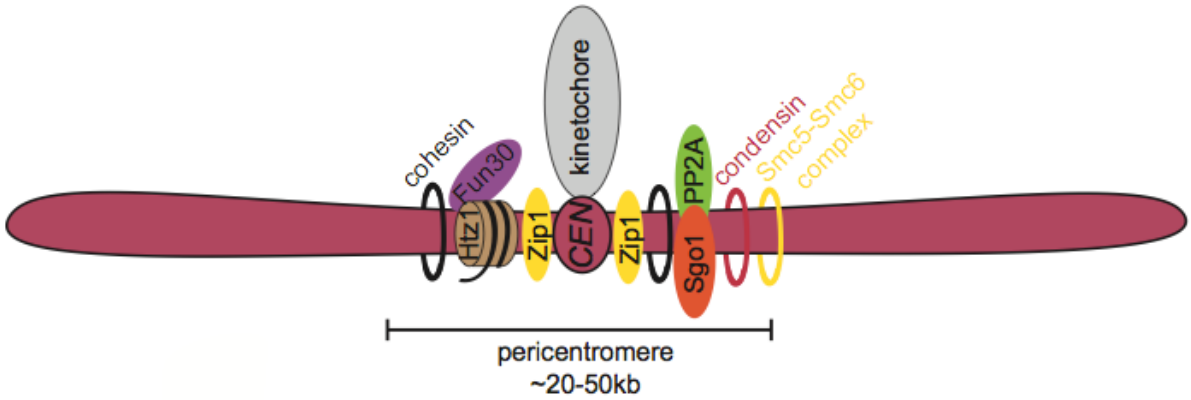

Figure 1-7 Scheme of centromere- and pericentromere-associated proteins in budding yeast meiosis

The assembly of the kinetochore is restricted to the point centromere (*CEN*) in budding yeast. Among other proteins, the pericentromere harbors the "structural maintenance of chromosomes" (SMC) complexes cohesin, condensin and Smc5-Smc6 complex, the Shugoshin (Sgo1)-PP2A (protein phosphatase 2A) complex, the synaptonemal complex protein Zip1 and chromatin-remodeling enzymes such as Fun30. In particular, the SMC complexes are highly enriched at centromeres and pericentromeres when compared to chromosome arms. Condensin and the Smc5-Smc6 complex associate with cohesin binding sites at pericentromeric regions, which span a distance of ~20-50 kb surrounding centromeres. Zip1 is recruited to cohesin-associated sites at centromeric- and pericentromeric regions in a manner dependent on Rec8 (meiosis-specific cohesin subunit) in early stages of meiosis.

assembly. In budding yeast, cohesin is composed of the two subunits Smc1 and Smc3 and the mitotic kleisin protein Scc1 (known as Rad21 in *S. pombe* and *H. sapiens*) and Scc3. In meiosis, Scc1 is replaced by the kleisin subunit Rec8 (Buonomo et al., 2000). As described earlier, cohesin complexes mediate cohesion between newly duplicated sister chromatids during S phase, which occurs via inter-chromosomal contacts (Michaelis et al., 1997; Uhlmann and Nasmyth, 1998). In addition, cohesin forms intra-chromosomal linkages via juxtaposing distant DNA elements for the purposes of transcriptional regulation and chromosome domain structure, which has recently received a significant amount of attention (Barrington et al., 2017; Fudenberg et al., 2016; Gassler et al., 2017; Haarhuis et al., 2017; Schalbetter et al., 2016). In mitosis, genome-wide studies of cohesin protein localization demonstrated that cohesin complexes are highly abundant within ~20-50 kb chromosomal regions surrounding centromeres (Megee et al., 1999; Glynn et al., 2004; Tanaka et al., 1999; Weber et al., 2004). Like cohesin, condensin, composed of the Smc2-Smc4 dimer and the three additional non-Smc proteins Ycs4, Ycs5 and

Brn1, serves as an intra-molecular linker to regulate chromosome condensation and disentanglement of sister chromatids (Hirano, 2012; Jeppsson et al., 2014; Uhlmann, 2016). The Smc5-Smc6 complex, built up of the Smc5-Smc6 dimer and at least four additional non-Smc subunits Nse1, Mms21, Nse3 and Nse4, is less understood. Previous studies indicated that the Smc5-Smc6 complex associates with DNA to maintain telomere homeostasis and ribosomal DNA stability and promotes DNA repair as well as the restart of stalled replication forks in mitotic cells (De Piccoli et al., 2009; Roy et al., 2015; Stöm and Sjögren, 2007). Both condensin and the Smc5-Smc6 complex were shown to associate with cohesin binding sites along chromosomes, including enhanced binding at pericentromeres (Copsey et al., 2013; D'Ambrosio et al., 2008).

The Shugoshins are other proteins that are highly enriched at pericentromeres in eukaryotic organisms (Clift and Marston, 2011; Kerrebrock et al., 1992; Marston 2015; Watanabe and Kitajima, 2005). In *S. cerevisiae* and *D. melanogaster*, a single Shugoshin protein has been identified and named Sgo1 and Mei-S332, respectively (Kerrebrock et al., 1992, 1995; Katis et al., 2004; Marston et al., 2004). Most other organisms, such as fission yeast, plants and mammals, harbor two Shugoshin-like proteins (Sgo1 and Sgo2) (Clift and Marston, 2011; Kitajima et al., 2004, Rabitsch et al., 2004). The canonical role of Shugoshin(s) is to protect pericentromeric cohesin from premature cleavage in meiosis and mitosis (Tang et al., 2006). During prophase I, the meiosis-specific kleisin subunit Rec8 of the cohesin complex is phosphorylated along the entire length of chromosomes for separase-mediated cleavage (Brar et al., 2006; Katis et al., 2010; Lee and Amon, 2003). Shugoshin counteracts the phosphorylation of Rec8 at pericentromeric regions. This is achieved by interactions between Shugoshin and the serine/ threonine protein phosphatase 2A (PP2A) at centromere-proximal regions (Ishiguro et al., 2010; Kitajima et al., 2006; Riedel et al., 2006; Xu et al., 2009). PP2A is a heterotrimeric enzyme that is composed of a structural subunit (A), a variable regulatory subunit (B) and a catalytic subunit (C) (Janssens and Goris, 2001). Budding yeast's Shugoshin, Sgo1, collaborates with PP2A containing the B subunit Rts1 to antagonize pericentromeric Rec8-cohesin phosphorylation (Riedel et al., 2006; Xu et al., 2009). Maintenance of pericentromeric cohesion by the Shugoshin-PP2A-B complex is similarly regulated in prophase of the mammalian mitotic cell cycle (McGuinness et al., 2005; Tang et al., 2006; Weizenegger et al., 2000). In addition to protecting pericentromeric cohesin during

meiosis and mammalian mitosis, Shugoshin(s) plays a role in promoting bi-orientation of sister chromatids (Indjeian et al., 2005; Kiburz et al., 2008). In budding yeast, it was demonstrated that the localization of Sgo1 at pericentromeres enables the recruitment of the SMC complex condensin, which in turn is required for chromosome bi-orientation in mitosis (Verzijlbergen et al., 2014).

An additional protein that is associated with centromeric and pericentromeric regions is the major component of the synaptonemal complex, Zip1 (Sym et al., 1993). Although Zip1 polymerises along whole chromosome axes later in prophase I, Zip1 was shown to associate with cohesin binding sites at centromeric and pericentromeric regions in a Rec8-cohesin dependent manner in early stages of meiosis (Bardhan et al., 2010).

Further factors that are associated with centromeric and pericentromeric regions are ATP-dependent chromatin remodeling complexes and histone-modifying enzymes. These factors alter the chromatin structure for critical cellular processes such as transcription, replication, recombination and repair of DNA (Clapier and Cairns, 2009). Chromatin remodeling complexes are protein families that hydrolyze ATP to drive sliding and unwrapping of nucleosomes, eviction of histones and exchange of histone variants (Gangaraju and Bartholomew, 2007). The families of chromatin remodelers are SWI/ SNF family, ISWI family, CHD family and INO80 family (Clapier and Cairns, 2009; Gangaraju and Bartholomew, 2007). An example for a chromatin-remodeling enzyme that shares sequence homology with the SWI/ SNF family is Fun30 (Clark et al., 1992; Flaus et al., 2006). Among other functions, Fun30 affects occupancy of the histone H2A variant Htz1 at pericentromeres in budding yeast, thereby supporting correct chromatin structure to ensure accurate chromosome separation (Durand-Dubief et al., 2012). Additional chromatin remodelers that are associated with the pericentromere are Isw1, a member of the ISWI family (Mellor and Morillon, 2004), and Arp8, a protein of the INO80 family (Shen et al., 2003). Isw1 and Arp8 were identified by a Sgo1-pulldown assay (performed in Adèle Marston's laboratory; personal communication) as factors that associate with pericentromeric regions. Isw1 can bind to Ioc3 (Isw One Complex protein 3) or Ioc2 and Ioc4 to form two distinct remodeling complexes, Isw1a and Isw1b respectively (Vary et al., 2003). It was proposed that Isw1 has nucleosome spacing activity (Ocampo et al., 2016), whereas Arp8 preferentially binds to histones H3 and H4 (Shen et al., 2003). As their name implies, histone-modifying enzymes mediate post-translational modifications of

histones including acetylation, phosphorylation, ubiquitination and methylation (Marmorstein and Trievel, 2009). For example, Irc20 is SWI/ SNF family ATPase domain-containing protein in budding yeast (Flaus and Owen-Hughes, 2011; Freemont, 2000). Irc20 was identified as a pericentromere-associated factor based on Sgo1-pulldown assay (performed in Adèle Marston's laboratory; personal communication). *In vitro*, Irc20 was shown to have E3 ligase activity (Richardson et al., 2013). An additional histone-modifying enzyme that was identified as a pericentromere-associated factor is Yta7 (Adèle Marston's laboratory; personal communication). Yta7 was shown to regulate transcription of histone genes (Gradolatto et al., 2008).

1.4 The kinetochore: Composition and function in *S. cerevisiae*

Both mitotic and meiotic cell divisions highly depend on the faithful transmission of duplicated genetic material into progeny cells to prevent aneuploidy, a cell state with an abnormal number of chromosomes (Orr et al. 2015; Potapova and Gorbsky 2017). Faithful chromosome segregation has at its heart a multi-protein machinery, termed the kinetochore (Musacchio and Desai, 2017). The kinetochore is a highly sophisticated and conserved structure found in organisms that range from unicellular eukaryotes, such as yeasts, to multicellular organisms, such as mammals, including humans. The kinetochore is known for its functions in connecting chromosomes to dynamic spindle microtubules, sensing microtubule attachments and regulating the transition from metaphase to anaphase via the SAC (Musacchio, 2011; Musacchio and Desai, 2017; Musacchio and Salmon, 2007; Santaguida and Musacchio, 2009).

The simplest kinetochore structures were identified in the budding yeast *S. cerevisiae* that bind only one microtubule (Figure 1-8 A) (McAinsh et al., 2003; Westermann et al., 2007). The budding yeast kinetochore is composed of approximately 40 proteins that assemble in a hierarchical fashion as distinct, interacting complexes. The protein complexes, named Cbf3, Ctf19, Mtw1, Ndc80, Spc105 and Dam1, are organized in inner, central and outer kinetochore layers, as defined by their relative position within the centromere-microtubule interface (Figure 1-8 B) (McAinsh et al., 2003; Westermann et al., 2007). Most of the kinetochore complexes (except for the Cbf3 and Dam1 complexes) are conserved from yeasts to humans (Cheeseman and Desai, 2008; Musacchio and Desai, 2017; Musacchio and Salmon, 2007).

The budding yeast kinetochore assembles onto ~125 bp point centromeres that contain the three DNA elements CDE I, CDE II and CDE III (Fitzgerald-Hayes et al.,

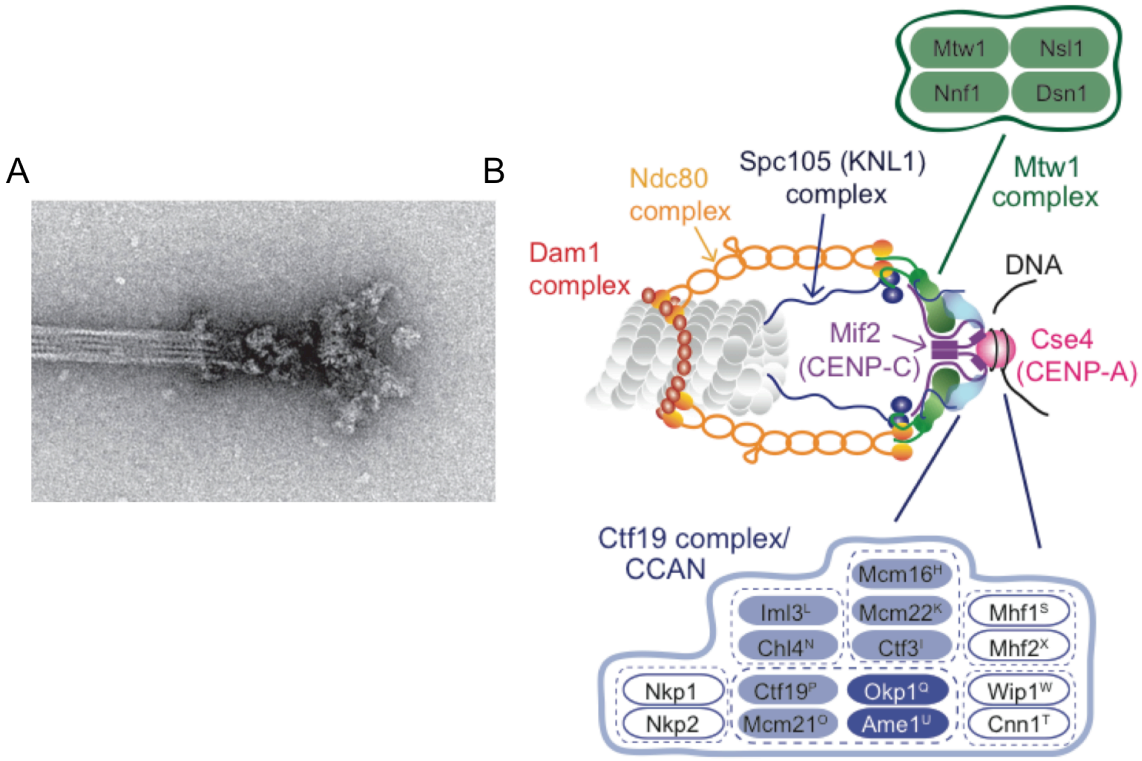

Figure 1-8 The budding yeast kinetochore.

A) Electron microscope image of purified budding yeast kinetochore particle attached to a single microtubule (Gonen et al., 2012). B) Illustration of the composition of the budding yeast kinetochore. Proteins of the conserved sub-complexes Ctf19/ CCAN and Mtw1/ Mis12/ MIND are highlighted in blue and green, respectively. Human "CENP" equivalents are indicated as superscript. Members of the Ctf19 complex essential for vegetative growth are shown in dark blue, whereas non-essential components are depicted in light blue. All proteins of the Mtw1 complex are essential for vegetative growth (modified from Vincenten et al., 2015).

1982; Hieter et al., 1985). Early events of budding yeast kinetochore assembly comprise the association of the centromere-binding factor 1 (Cbf1) and the four-protein Cbf3 complex (comprised of Cep3, Ctf13, Ndc10 and Skp1) with the DNA elements CDE I and CDE III, respectively (Connelly and Hieter, 1996; Yamagishi et al. 2014). In particular, the association of the Cbf3 complex with the centromere has been described as the primary determinant of kinetochore assembly, because all kinetochore proteins depend on the Cbf3 complex for the association with the centromere. Mutations in the Cbf3 complex cause a complete loss of the attachment between chromosomes and microtubules (He et al., 2001; Gardner et al., 2001; Goh and Kilmartin, 1993; Romao et al., 2008; Sorger et al., 1994). The Cbf3 complex mediates the association of Cse4 with the DNA element CDE II via a direct

interaction between Ndc10 and the chaperone Scm3 (Cho and Harrison, 2011; Stoler et al. 2007; Yamagishi et al. 2014). Cse4 (CENP-A in humans) is a specialized centromeric nucleosome that replaces the canonical histone H3 protein (Smith, 2002). The recognition of Cse4/ CENP-A depends on a signature motif in the protein Mif2 (CENP-C in humans) (Hornung et al., 2014; Kato et al., 2013). Mif2 in turn is required for the recruitment of the Ame1-Okp1 heterodimer (Hornung et al., 2014), a component of the Ctf19 complex (CCAN in humans) (Figure 1-8 B; De Wulf et al., 2003). Collectively, the Cbf3 complex, the histone H3 variant Cse4, Mif2 and the Ctf19 complex represent the inner layer of the budding yeast kinetochore.

The proteins Mif2 and Ame1 of the inner layer were shown to initiate the assembly of the outer budding yeast kinetochore via direct binding to the Mtw1 complex (Mis12 complex in humans) (Hornung et al., 2014). The Mtw1 complex is a subunit of the central layer of the budding yeast kinetochore that is composed of the four essential proteins Mtw1, Nnf1, Dsn1 and Nsl1 (Figure 1-8 B; Biggins, 2013; De Wulf et al., 2003). The proteins Mtw1 and Nnf1 as well as Dsn1 and Nsl1 form heterodimers (Hornung et al. 2011; Maskelll et al. 2010). All four proteins assemble in a 1:1:1:1 stoichiometry within the Mtw1 complex (Hornung et al. 2011). Based on quantitative fluorescence microscopy, it was suggested that six or seven copies of the Mtw1 complex assemble within a single budding yeast kinetochore (Joglekar et al. 2006). Within kinetochore assembly, the Mtw1 complex interacts with the outer kinetochore sub-complexes Ndc80 and Spc105 to form a larger entity of the kinetochore, termed the KMN network. The N-terminal domains of the complexes Ndc80 and Spc105 harbor microtubule-binding sites (Pagliuca et al., 2009; Powers et al., 2009). Within the KMN network, the Mtw1 complex is the only subunit that does not exhibit microtubule-binding activities (Cheeseman et al., 2006; Hornung et al. 2011).

The outermost component of the budding yeast kinetochore is the essential Dam1 complex, which is built up of the ten proteins Ask1, Dad1, Dad2, Dad3, Dad4, Dam1, Duo1, Hsk3, Spc19 and Spc34. Approximately sixteen Dam1 complexes associate in a ring-like structure that encircles the binding microtubule (Joglekar et al. 2006; Miranda et al., 2005; Westermann et al., 2005).

Previous studies demonstrated that the budding yeast kinetochore is stable throughout vegetative growth but it is restructured in meiosis. This means that some outer kinetochore components such as the whole Ndc80 complex and the protein

Hsk3, a member of the Dam1 complex, are absent from kinetochores upon meiotic entry (Miller et al. 2012). In contrast to these outer kinetochore complexes, the complexes Ctf19, Mtw1 and Spc105 are stably associated with centromeric chromatin during meiosis (Meyer et al. 2015; Miller et al. 2012). Dynamic changes in the kinetochore structure have also been reported in mammalian mitosis and meiosis (Dorn and Maddox 2012; Sun et al. 2011; Westhorpe and Straight 2013).

1.4.1 The Ctf19 complex

The Ctf19 complex (Ctf19-C) is an inner kinetochore subunit that is conserved among eukaryotes (Schleiffer et al., 2012), with the notable exception of certain organisms such as *D. melanogaster* and *C. elegans* (Drinnenberg et al., 2016). The Ctf19-C comprises the components Ctf19, Mcm21, Okp1, Ame1, Mcm22, Mcm16, Ctf3, Chl4, Iml3, Cnn1, Wip1, Nkp1 and Nkp2 (Figure 1-8 B) (Lampert and Westermann, 2011). With the exception of Nkp1 and Nkp2, all Ctf19-C proteins have corresponding counterparts in humans, in which they assemble in the constitutive centromere-associated network (CCAN, Figure 1-8 B) (McAinsh and Meraldi 2011; Westermann and Schleiffer 2013).

Ame1 and Okp1 are essential for yeast cell viability, whereas the other Ctf19-C components are non-essential. Within the Ctf19-C, the components form sub-complexes that assemble in a hierarchical fashion (Pekgöz Altunkaya et al. 2016; Schmitzberger et al., 2017). The core sub-complex of the Ctf19-C is composed of the proteins Ctf19, Okp1, Mcm21 and Ame1, termed COMA (De Wulf et al., 2003). Ame1 and Okp1 as well as Ctf19 and Mcm21 form heterodimers (Schmitzberger and Harrison, 2012). The Ame1-Okp1 heterodimer is required for the assembly of additional kinetochore components (Hornung et al., 2014; Pekgöz Altunkaya et al. 2016; Schmitzberger et al., 2017). Ame1 was shown to play a significant role in the recruitment of the central kinetochore (*i.e.* Mtw1 complex) together with Mif2 (Hornung et al. 2014), whereas Okp1 directly interacts with the inner kinetochore (*i.e.* Ctf19-Mcm21 and Nkp1-Nkp2 heterodimers) (Schmitzberger et al., 2017). A recent biochemical analysis of isolated Ctf19-C components when Ame1 served as bait for purification in a wild type strain and different deletion mutants demonstrated that the association of the Ctf19-Mcm21 heterodimer with Ame1-Okp1 enables the binding of three additional sub-complexes within the Ctf19-C (Pekgöz Altunkaya et al. 2016).

The Ctf19-Mcm21 heterodimer enables the association of the Iml3-Chl4 sub-complex, the three-subunit complex Ctf3 (Ctf3-Mcm16-Mcm22) and the Cnn1-Wip1 subunit (Pekgöz Altunkaya et al. 2016). Thus, the assembly of these three sub-complexes depends on the presence of COMA but not in reverse (Pekgöz Altunkaya et al. 2016). A recent study based on fluorescence microscopy revealed that the localization of the Iml3-Chl4 sub-complex to centromeres occurs in a manner dependent on a Ctf19-Mcm21 binding motif in Okp1 (and is thus dependent on Ctf19-Mcm21) (Schmitzberger et al., 2017). This study also demonstrated that the localization of the Ctf3 sub-complex occurs in a manner independent of the Ctf19-Mcm21 binding motif in Okp1 (and is thus independent of the Ctf19-Mcm21 heterodimer) (Schmitzberger et al., 2017), which is in contrast to findings by Pekgöz Altunkaya et al. (2016). Using quantitative fluorescence microscopy, it was revealed that two copies of the Ctf19-C incorporate into a single kinetochore (Joglekar et al. 2006).

The important role of the Ctf19-C in faithful chromosome segregation during mitosis and meiosis was demonstrated in several studies (Eckert et al. 2007; Fernius and Marston, 2009; Fernius et al. 2013; Ghosh et al. 2001; Hyland et al. 1999; Measday et al. 2002; Mehta et al. 2014; Marston et al. 2004; Ng et al., 2009; Natsume et al. 2013; Pot et al. 2003). In late G1 during vegetative growth, the Ctf19-C was shown to promote the enrichment of cohesin complexes containing the mitosis-specific subunit Scc1 at centromeric and pericentromeric regions, which is required for the establishment of robust sister chromatid cohesion (Eckert et al. 2007; Fernius and Marston, 2009). The Ctf19-C facilitates this via the recruitment of the Dbf4/ Cdc7 kinase to centromeres, which in turn leads to the association of the Scc2-Scc4 complex with centromeres (Fernius et al., 2013; Natsume et al., 2013). The Scc4 subunit contains a surface patch of conserved amino acids that targets both loader complex proteins Scc2 and Scc4 to centromeres (Hinshaw et al., 2015). The Scc2-Scc4 complex enables the loading of cohesin complexes at centromeres, which were proposed to move bidirectionally into the surrounding pericentromere (Fernius et al., 2013). Mutations in Ctf19-C components prevent cohesion establishment at centromeric and pericentromeric regions and consequently cause unfaithful chromosome segregation (Eckert et al. 2007; Fernius and Marston, 2009). The localization of cohesin at centromeric and pericentromeric regions was shown to

enable the association of the “cohesin protector”-protein Sgo1 with these regions (Kiburz et al., 2005; Verzijlbergen et al., 2014). It was suggested that Sgo1 recruitment to pericentromeres is indirectly dependent on the Scc2-Scc4 complex (Verzijlbergen et al., 2014). The localization of Sgo1 in turn was suggested to enable the association of the SMC complex condensin with pericentromeres (Verzijlbergen et al., 2014). Taken together, the Ctf19-C mediated recruitment of the Scc2-Scc4 complex to centromeres enables the association of certain factors (*e.g.* cohesin, Sgo1, condensin) with centromere-proximal regions, which was proposed to occur in a hierarchical fashion (Figure 1-9; Verzijlbergen et al., 2014). In addition, the association of the Smc5-Smc6 complex with chromosomal regions, including pericentromeres, occurs in a manner dependent on Scc2 (Betts Lindroos et al., 2006). Whether Scc2 (and by extension the Scc2-Scc4 complex) directly or indirectly enables the association of the Smc5-Smc6 complex with (peri)centromeres has not been shown yet. Nevertheless, it seems likely that the association of the Smc5-Smc6 complex with centromeric and pericentromeric regions is dependent on Ctf19-C function since it recruits the Scc2-Scc4 loader complex to centromeres (Figure 1-9). However, this has not been demonstrated yet. Furthermore, the Ctf19-C plays a role in the initiation of DNA replication at early origins around centromeres via the recruitment of the Dbf4/ Cdc7 kinase (Natsume et al. 2013). All in all, the Ctf19-C drives the loading and enrichment of pericentromere-associated proteins (*e.g.* cohesin, Sgo1, condensin and mostl ikely the Smc5-Smc6 complex) and promotes the initiation of DNA replication close to centromeres (Fernius and Marston, 2009; Fernius et al. 2013; Natsume et al. 2013). Although most studies that address the function of the Ctf19-C were performed in mitotically dividing cells, there are a few studies reporting on a pivotal role of the Ctf19-C during meiosis (Marston et al., 2004; Fernius and Marston 2009; Mehta et al. 2014). Along with Sgo1, the Ctf19-C components Iml3 and Chl4 were identified in a genome-wide screen as important proteins to retain centromeric cohesin complexes until the onset of anaphase II (Marston et al., 2004). Impaired Ctf19-C function leads to severe chromosome mis-segregation during meiosis and the production of inviable gametes (Mehta et al., 2014). These findings demonstrate the important role of the Ctf19-C in proper chromosome segregation during meiosis.

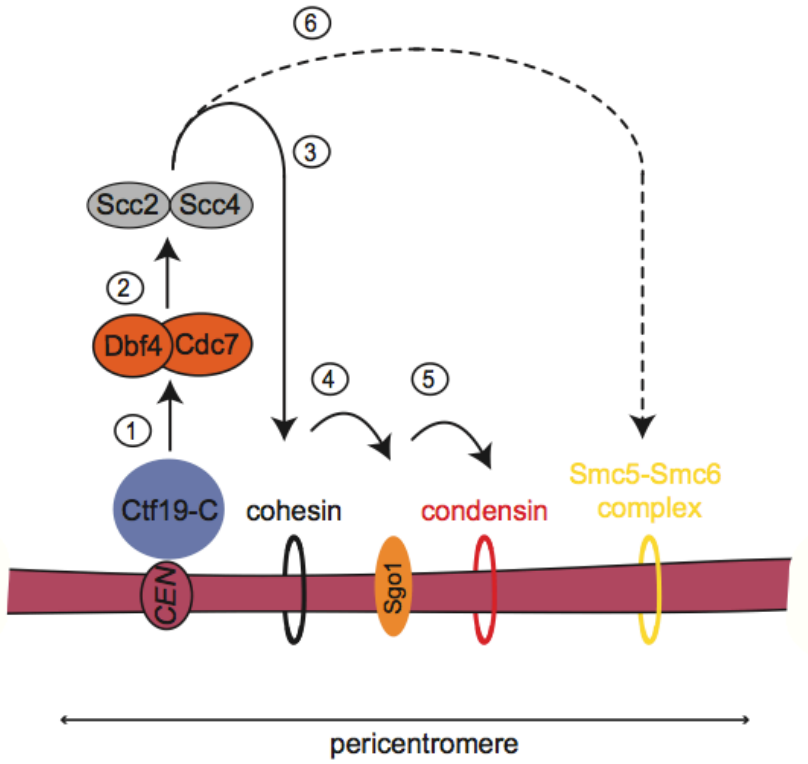

Figure 1-9 The Ctf19-C facilitates the association of certain factors with pericentromeres

Circuit 1+2: The Ctf19 complex (Ctf19-C) was shown to recruit the Dbf4/ Cdc7 kinase (also referred to as the Dbf4-dependent kinase, DDK) to centromeres, which is required for the recruitment of the Scc2-Scc4 loader complex. Circuit 3: The Scc2-Scc4 complex enables the loading of cohesin protein complexes at centromeres, from where the protein complexes are thought to translocate into the surrounding pericentromere. Circuit 4+5: The loading and enrichment of cohesin was proposed to allow for the recruitment of Shugoshin (Sgo1) and condensin. Circuit 6: The recruitment of the Smc5-Smc6 complex was shown to occur in a manner dependent on the Scc2-Scc4 loader complex.
This scheme combines findings by Betts Lindroos et al. (2006), Fernius et al. (2013), Natsume et al., (2013) and Verzijlbergen et al. (2014). *CEN* indicates the budding yeast centromere.

1.5 Objectives

Controlled DNA break formation followed by inter-homolog CO recombination is an essential part of gametogenesis. However, CO formation in chromosomal regions surrounding centromeres (*i.e.* pericentromeres) is associated with chromosome mis-segregation and aneuploid/ inviable gametes. Both DNA break formation and recombination (COs and NCOs) are mostly prevented in centromere-proximal

regions. However, chromosomal features that control meiotic DNA break formation and recombination at pericentromeres remain poorly understood. A promising candidate in controlling these events near centromeres is the kinetochore, a large multi-protein structure that assembles onto centromeres. Although progress has been made in understanding mechanisms of kinetochore assembly and microtubule attachment as well as the recruitment of the SAC machinery, it is not known whether the kinetochore is involved in controlling DNA break formation and recombination at centromere-proximal regions during meiosis. Therefore, this PhD thesis addresses the following questions:

1) Is there a role for the kinetochore in controlling meiotic DNA break formation and recombination at centromere-proximal regions?

If the kinetochore plays a role in controlling meiotic DSB formation and recombination close to centromeres, we want to understand:

2) How does the kinetochore control these events?
3) What is the molecular basis behind the kinetochore-driven control of meiotic DNA break formation and recombination at pericentromeres?

During meiotic G2/ prophase I, when recombination occurs, the inner and central kinetochore subunits Ctf19-C and Mtw1-C are assembled onto centromeres, whereas some outer kinetochore components are absent. Therefore, the focus of this study is on the Ctf19-C and Mtw1-C.

2 Materials and Methods

2.1 Materials

2.1.1 Chemicals and Reagents

All chemicals and reagents used in this study are listed in Table 2-1.

Table 2-1 Chemicals and Reagents.

Supplier	Chemicals and Reagents
Agilent Technologies, Santa Clara, USA	Salmon sperm DNA
Amresco, Solon, USA	Proteinase K
AppliChem, Darmstadt, Germany	Tween-20
Becton Dickinson, Franklin Lakes, USA	Agar, Bacto-Peptone, Difco yeast nitrogen base without AA, AS, Yeast Extract
Bio-Rad Laboratories, Hercules, USA	Precision Plus Protein™ Dual Color Standards
Carl Roth, Karlsruhe, Germany	Acrylamide, Agarose Standard, Ethanol (EtOH), Glycine, Milk powder blocking grade, Phenol/Chloroform/Isopropanol, Potassium acetate (KOAc), Sodium dodecryl sulfate (SDS), Tris-(hydroxymethyl)-aminomethane (Tris)
Fisher Scientific, Loughborough, UK	Hydrochloric acid (HCl)
Fermentas, St. Leon-Rot, Germany	DNA ladder GeneRuler ^{TM} 1kb
Gerbu Biotechnik, Heidelberg, Germany	Boric acid, Ethylenediaminetetraacetic acid (EDTA), Glycerol
Intron Biotechnology, Sungnam, Korea	RedSafe^{TM} Nucleic acid staining solution
Invitrogen, Carlsbad, USA	Dynabeads^{TM} Protein G
J.T.Baker Chemicals, Center Valley, USA	Isopropanol, Magnesium chloride (MgCl2), Potassium chloride (KCl)

Table 2-1 continued.

Supplier	Chemicals and Reagents
Life Technologies, Eugene, USA	SYTOX® Green nucleic acid stain
Lonza, Rockland, USA	SeaKem® LE Agarose
Merck, Darmstadt, Germany	Potassium dihydrogen phosphate (KH_2PO_4)
Nippon Genetics, Düren, Germany	Midori Green Advanced DNA stain
Polysciences, Warrington, USA	Formaldehyde, 10%, methanol free, Ultra Pure
Serva Electrophoresis, Heidelberg, Germany	Ammoniumperoxosulfate (APS), Ampicillin, β-Mercaptoethanol, Dimethylsulfoxide (DMSO), Dithiothreitol (DTT), N, N, N', N'-Tetramethylethylenediamine (TEMED), Phenylmethylsulfonyl fluoride (PMSF)
Roche Diagnostics, Mannheim, Germany	Proteinase K
Sigma-Aldrich, St. Louis, USA	Acetic acid, Bromophenol blue, D-Sorbitol, Dextran sulfate sodium salt, Lithium acetate dihydrate (LiAc), L-Tryptophan, Methanol (MeOH), Ponceau S solution, Polyethylene glycol (PEG) 3350, RNase A, Anti-FLAG® M2 Affinity Gel
VWR chemicals, Darmstadt, Germany	Sodium chloride (NaCl), Sodium hydroxide (NaOH)

2.1.2 Enzymes and commercially prepared master mixes

Enzymes and commercially prepared master mixes used in this study are listed in Table 2-2.

Table 2-2 Enzymes and commercially prepared master mixes.

Enzyme class	Name	Supplier
Restriction Endonuclease	AatII, DpnI, HindIII, BstZ17I	New England Biolabs, Ipswich, USA
Polymerase	TaKaRa Ex Taq®, Q5® High-Fidelity, LongAmp® *Taq*, Q5® High-Fidelity 2x Master Mix, VWR Taq, PerfeCTa® SYBR® Green FastMix®	Takara Bio, Kusatsu, Japan/ New England Biolabs, Ipswich, USA/ VWR, Radnor, USA/ Quantabio, Beverly, USA
Ligase	T4 DNA ligase, Gibson Assembly® Master Mix	New England Biolabs, Ipswich, USA
Lyticase, yeast lytic enzyme	Zymolyase ®T100	AMS Biotechnology, Abingdon, UK

2.1.3 Kits

Kits used in this study are listed in Table 2-3.

Table 2-3 Kits.

Supplier	Kits
Agilent Technologies, Santa Clara, USA	Prime-It RmT Random Primer Labeling Kit
GE Healthcare, Little Chalfont, UK	ECL™ Prime Western blotting Detection Reagent
Promega Corporation, Madison, USA	Wizard® SV Gel and PCR Clean-Up System
Qiagen, Hilden, Germany	QIAprep® Spin Miniprep Kit, QIAquick® Gel Extraction Kit, QIAquick® PCR Purification Kit

2.1.4. Laboratory instruments and supplies

Laboratory instruments and supplies used in this study are listed in Table 2-4.

Table 2-4 Laboratory instruments and supplies.

Method/ Application	Instruments and supplies	Supplier
Agarose gel electrophoresis	Agarose gel electrophoresis system	Carl Roth, Karlsruhe, Germany
	Owl™ A2-BP large gel system	Thermo Fisher Scientific, Waltham, USA
Cell density measurement	BioPhotometer®	Eppendorf AG, Hamburg, Germany
Cell lysis	FastPrep®-24	MP Biomedicals, Santa Ana, USA
	VXR basic Vibrax®	IKA® -Werke, Staufen, Germany
	Sonifier 450	Branson Ultrasonics Corporation, Danbury, USA
Centrifuge	Centrifuges 5424, 5424R, 5810R	Eppendorf AG, Hamburg, Germany
Flow cytometry	BD Accuri™ C6 Flow Cytometer	BD Biosciences, Franklin Lakes, USA
Incubators	Heraeus Instruments kelvitron®t B6030, Heratherm™ Microbiological Incubator, INCU-Line® IL23, Waterbath	Thermo Fisher Scientific, Waltham, USA VWR International, Radnor, USA, Memmert, Schwabach, Germany
Microscopy	Axio Vert.A1	Zeiss, Oberkochen, Germany
	DeltaVision Elite Imaging system microscope	GE Healthcare, Little Chalfont, UK

Table 2-4 continued.

Method/ Application	Instruments and supplies	Supplier
Microscopy	TDM Tetrad Dissection Microscope Ci-L	Nikon, Tokyo, Japan
Phosphorimaging	Typhoon TRIO+ Variable mode imager	GE Healthcare Life Sciences, Freiburg, Germany
	MP Imaging Plate Storage Phosphor Screen (20x 40 cm)	FujiFilm, Tokyo, Japan
	X-Ray Cassette (35x43 cm)	Kisker Biotech, Steinfurt, Germany
	LB 122 Contamination monitor equipment	Berthold Technologies, Bad Wildbad, Germany
Nucleic acid hybridization	HB-1000 Hybridizer hybridization oven	Analytik Jena AG, Jena, Germany
pH measurements	pH-Meter 766 Calimatic	Knick, Berlin, Germany
Polymerase chain reaction (PCR)	Thermocycler T3000	Biometra, Göttingen, Germany
	7500 Fast Real-Time PCR system	Applied Biosystems, Forster City, USA
Power supply	Power Source 300V	VWR International, Radnor, USA
Quantification of DNA	NanoDrop 2000 Spectrophotometer	Thermo Fisher Scientific, Waltham, USA

Table 2-4 continued.

Method/ Application	Instruments and supplies	Supplier
SDS-PAGE	Mini PROTEAN® Tetra Cell	Bio-Rad Laboratories, Hercules, USA
Shaker/ Mixer/ Rotator	Thermomixer comfort 5436	Eppendorf AG, Hamburg, Germany
	Minitron	INFORS AG, Bottmingen, Switzerland
	Innova™ 2000 Platform Shaker	New Brunswick Scientific, Edison, USA
	Stuart™ Scientific roller mixer SRT6	Bibby Scientific, Stone, UK
	See-saw rocker, SSL4	Bibby Scientific, Stone, UK
	Test-tube rotator	Labinco, Breda, Netherlands
Southern blot	Amersham Hybond™ – XL membrane	GE Healthcare Life Sciences, Freiburg, Germany
Western blot	BioTrace™ NT nitrocellulose transfer membrane	Pall Corporation, New York, USA
	Mini-PROTEAN® II Cell	Bio-Rad Laboratories, Hercules, USA
	ChemiDoc™ MP Imaging System	Bio-Rad Laboratories, Hercules, USA

2.1.5 Antibodies

All primary and secondary (HRP-conjugated) antibodies used in this study are summarized in Tables 2-5 and 2-6.

Table 2-5 Primary antibodies.

Immunogen	Source	Dilution	Supplier
α-Cas9 (7A9-3A3)	Mouse monoclonal	1: 1000	Abcam, Cambridge, UK
α-Flag	Mouse monoclonal	1: 1000	Sigma-Aldrich, St. Louis, USA
α-HA (Hemagglutinin)	Mouse Monoclonal	1: 1000	BioLegend, San Diego, USA
α-Pgk1	Mouse monoclonal	1: 1000	Life technologies, Carlsbad, USA

Table 2-6 HRP-conjugated antibodies.

Immunogen	Source	Dilution	Supplier
IgG α-mouse	sheep	1: 10000	GE Healthcare, Little Chalfont, UK

2.1.6 Buffers and solutions.

All buffers and solutions used in this study are listed in Table 2-7 with the corresponding method.

Table 2-7 Buffers and solutions.

Method	Buffer/ Solution	Composition	Final concentration
Agarose gel electrophoresis	10x DNA Loading Buffer	EDTA Bromophenol blue Xylencyanoblue Glycerol	1 mM 0.25% (w/v) 0.25% (w/v) 50% (v/v)
	10x TAE Buffer	Tris-base Glacial acetic acid EDTA	400 mM 200 mM 10 mM

Table 2-7 continued.

Method	Buffer/ Solution	Composition	Final concentration
Agarose gel electrophoresis	5x TBE Buffer	Tris-base Boric acid EDTA	445 mM 445 mM 10 mM
Co-Immunoprecipitation (Co-IP)	1x Phosphate Buffered Saline (PBS)	NaCl KCl Na_2HPO_4 KH_2PO_4	137 mM 2.7 mM 8 mM 2 mM
	2x Lysis Buffer	Hepes $MgCl_2$ NaCl Sorbitol Glycerol TritonX-100	20 mM 4 mM 500 mM 320 mM 4 % (v/v) 0.5 % (v/v)
	M2 Lysis Buffer	Tris-HCl (pH 7.4) NaCl Tritonx-100 EDTA	50 mM 150 mM 1 % (v/v) 1 mM
	TE/ 1% SDS Buffer	Tris (pH 8) EDTA (pH 8) SDS	50 mM 10 mM 1 % (w/v)
	10x Tris Buffered Saline (TBS)	Tris-base NaCl KCl	25 mM 150 mM 2 mM

Table 2-7 continued.

Method	Buffer/ Solution	Composition	Final concentration
Isolation of genomic DNA from yeast cells	DNA Breakage Buffer	Triton X-100 SDS NaCl Tris (pH 8) EDTA	2% (v/v) 1% (w/v) 100 mM 10 mM 1 mM
	Spheroplasting Buffer	Sorbitol K_2HPO_4 KH_2PO_4 EDTA	1M 42 mM 8 mM 5 mM
	Spheroplasting Solution	β-Mercaptoethanol Zymolyase in Spheroplasting buffer	 1% (v/v) 2.5% (v/v)
	Lysing Buffer	Tris (pH 8) EDTA	1M 500 mM
Hybridization and Washing (Southern blot)	20x SSC	NaCl $Na_3Citrate$	3M 300 mM
	Hybridization Buffer	Sodium phosphate (pH7.2) NaCl EDTA SDS Dextran sulphate	250 mM 250 mM 1mM 7% (w/v) 5% (w/v)
	Low Stringency Wash Buffer	SDS in 2x SSC	0.1% (w/v)

Table 2-7 continued.

Method	Buffer/ Solution	Composition	Final concentration
Hybridization and Washing (Southern blot)	High Stringency Wash Buffer	SDS in 0.1x SSC	0.1% (w/v)
Sample preparation for SDS-PAGE	Protein Breakage Buffer	Tris (pH 7.5) EDTA DTT	50 mM 1 mM 2.75 mM
SDS- PAGE	3x SDS Loading Buffer	Tris-acetate (pH6.8) β-Mercaptoethanol Glycerol SDS Bromophenol blue	190mM 6% (v/v) 30% (v/v) 9% (w/v) 0.05% (w/v)
	10 x SDS Running Buffer	Tris-base Glycine SDS	25mM 192mM 0.1% (w/v)
Southern blot	Sodium Phosphate Buffer (pH 7.2)	Na_2HPO_4 NaH_2PO_4	1M 1M
Western blot	10x Western Transfer Buffer	TRIZMA base Glycine SDS	3% (w/v) 14.4% (w/v) 0.2 % (w/v)
	Blocking Buffer	Milk powder in 1x PBS-T	4% (w/v)

2.1.7 Media.

Frequently used media for yeast and bacteria are summarized in Table 2-8. For the preparation of solid media, the media listed below were supplemented with either 2 % (w/v) agar for yeast plates or 1.5 % (w/v) agar for bacteria plates. Minimal (MIN) medium supplemented with various nutrients (amino acids, e.g. tryptophan, histidine, leucine, arginine, lysine, and nucleotide precursors, e.g. uracil, adenine) was used to select for auxotrophic yeast strains. For the selection of drug-resistant mutants, the antibiotics Geneticin (0.2 mg/ml) and Hygromycin B (50 mg/ml) were added to yeast extract peptone dextrose (YPD) medium for yeast or Ampicillin (100 μg/ml) to bacterial Luria-Bertani (LB) medium.

Table 2-8 Frequently used media.

Liquid medium	Microorganism	Composition	Final concentration
Buffered YTA (BYTA)	*Saccharomyces cerevisiae*	Yeast extract Bactotryptone KAc Potassium phthalate	1 % (w/v) 2 % (w/v) 1 % (w/v) 50 mM
Luria-Bertani (LB)	*Escherichia coli*	Tryptone Yeast extract NaCl	0.5 % (w/v) 1 % (w/v) 0.5 % (w/v)
Minimal (MIN)	*Saccharomyces cerevisiae*	Difco yeast nitrogen without AA, AS Ammonium sulfate Inositol D-Glucose	0.15 % (w/v) 0.5 % (w/v) 2 mM 2 % (w/v)
Sporulation (SPO)	*Saccharomyces cerevisiae*	KAc Acetic acid	0.3% (w/v) 5% (v/v)

Table 2-8 continued.

Liquid medium	Microorganism	Composition	Final concentration
Yeast extract peptone dextrose (YPD)	*Saccharomyces cerevisiae*	Bacto peptone Yeast extract L-Tryptophan D-Glucose	2 % (w/v) 1 % (w/v) 0.015 % (w/v) 2 % (w/v)/ 4 % (w/v)
Yeast peptone glycerol (YPG)	*Saccharomyces cerevisiae*	Bacto peptone Yeast extract L-Tryptophan Glycerol	2 % (w/v) 1 % (w/v) 0.015 % (w/v) 3 % (v/v)

2.1.8 Yeast strains.

Yeast strains used in this study are listed in Table 7-1.

2.1.9 Synthetic oligonucleotides.

Synthetic oligonucleotides were used for Polymerase Chain Reaction (PCR), real-time quantitative Polymerase Chain Reaction (qPCR), cloning (Gibson assembly) and sequencing. Synthetic oligonucleotides were purchased from Sigma-Aldrich. A list of synthetic oligonucleotides used for qPCR and cloning (Gibson assembly) can be found in Table 7-2.

2.1.10 Plasmids.

Plasmids used for CRISPR/ dCas9-based approaches are the following:

The plasmids used for the expression of individual kinetochore proteins fused to 3xFlag-dCas9 are pHOP1-3xFLAG-DCAS9-p11, pHOP1-CTF19-3xFLAG-DCAS9-p11 and pHOP1-IML3-3xFLAG-DCAS9-p11. These plasmids were cloned via Gibson assembly. For transformation, the plasmids were digested with *BstZ17I* and integrated at the budding yeast *TRP1* locus.

The plasmids used for the expression of single guide RNAs are pSNR52-sgRNA-VIII-p83, pSNR52-sgRNA-III-p83 and pSNR52-sgRNA-mock-p83. These plasmids contain single guide RNA expression cassettes that were cloned according to

Laughery et al. (2015). The single guide RNA expression cassettes harbor a 20 bp target specific sequence. The DNA sequences of the single guide RNA expression cassettes can be found in the appendix. For transformation, the plasmids were digested with *NdeI* and integrated at the budding yeast *URA3* locus.

2.1.11 Online Tools.

Online tools used in this study are listed in Table 2-9.

Table 2-9 Online Tools.

Online Tool	Website
Saccharomyces GENOME DATABASE	http://www.yeastgenome.org
Reverse complement	http://reverse-complement.com
Oligonucleotide Properties Calculator	http://biotools.nubic.northwestern.edu/OligoCalc.html
Fisher's exact test calculator	http://www.socscistatistics.com/tests/fisher/Default2.aspx

2.1.12 Software

Software used in this study is listed in Table 2-10.

Table 2-10 Software.

Software	Supplier
Illustrator CS4	Adobe, San Josè, USA
ImageJ	National Institutes of Health, Rockville, USA
Photoshop	Adobe, San Josè, USA
ApE- A plasmid Editor	M. Wayne Davis
Enzyme X	Nucleobytes, Aalsmeer, Netherlands
Excel	Microsoft, Redmond, USA

Table 2-10 continued.

Software	Supplier
Word	Microsoft, Redmond, USA
G*Power	Heinrich-Heine University Düsseldorf, Dusseldorf, Germany
FlowJo®	FlowJo, LLC, Ashland, USA
7500 Software v2.06	Applied Biosystems, Forster City, USA

2.2 Methods

2.2.1 Growth and maintenance of *S. cerevisiae*

2.2.1.1 Growth conditions of yeast strains

Depending on the experimental procedure, yeast strains were grown in either liquid medium or on solid agar plates. To grow the strains on solid medium, 2% agar was added to the medium. Yeast extract peptone dextrose (YPD) medium (Table 2-8) was commonly used to grow the yeast cells under nonselective conditions. Yeast cells were grown on minimal medium (MIN) agar plates (Table 2-8) for testing the mating type using specific mating type tester strains (known *MATa* and *MATalpha)*. MIN medium supplemented with defined nutrients (*e.g.* mixtures of amino acids) was employed to select for yeast cells containing specific nutritional markers. YPD medium containing antibiotics such as hygromycin B or geneticin was used to select for yeast containing drug resistance markers *HPH* (confers resistance to hygromycin B) or *KAN* (confers resistance to geneticin). Before and after storing yeast at -80 °C, the cells were grown on yeast peptone glycerol (YPG) agar plates (Table 2-8). Diploid yeast cells were sporulated in liquid nitrogen-deficient sporulation medium (SPO) supplemented with acetate as a non-fermentable carbon source (Table 2-8).
Liquid yeast cultures were grown in a shaking incubator Multitron® (Infors AG, Bottmingen, Switzerland) or Innova™ 2000 (New Brunswick Scientific, Edison, USA) at 180 rpm. Growth on solid agar plates was carried out in an incubator Heratherm™ (Thermo Fisher Scientific, Waltham, USA) without shaking. Both liquid and solid yeast cultures were grown at 30 °C, unless otherwise mentioned.

2.2.1.2 Meiotic cell cycle synchronization

Diploid yeast cells were thawed on YPG agar plates for 16 hours at 30 °C and then grown on 4% YPD agar plates for 24 hours at 30 °C in an incubator Heratherm™. The cells were then grown to saturation in liquid YPD medium for 24 hours at room temperature, 180 rpm on a platform shaker Innova™ 2000 before being diluted into buffered YTA (BYTA) medium (1% yeast extract, 2% bactotryptone, 1% potassium acetate, 50 mM potassium phthalate) to an optical density at 600 nm (OD_{600}) of 0.3. BYTA cultures were incubated for 16 hours at 30 °C, 180 rpm in an incubator shaker Multitron ®. Following two washes in sterile distilled water, cells were resuspended in

SPO medium at an OD_{600} of 1.9 and induced to undergo synchronous meiosis with shaking (180 rpm) at 30 °C.

2.2.1.3 Yeast stock preservation

Yeast strains were grown on YPG agar plates overnight at 30 °C in a Heratherm™ incubator and then scraped up with sterile toothpicks and suspended in 1 ml of sterile 15 % glycerol solution. Yeast cells were then frozen at -80 °C for long-term storage.

2.2.1.4 Yeast cell growth assay

Yeast cells from a fresh YPD agar plate were inoculated in a pre-culture of 15 ml YPD medium and grown overnight at 30 °C, 180 rpm in an incubator shaker Multitron®. Next, cells of the pre-culture were diluted into fresh YPD medium to an OD_{600} of 0.4 and incubated for 4.5 hours at 30 °C, 180 rpm. A culture of 5 ml was then harvested and centrifuged for 2 min at 2000 rpm. Cell pellet was suspended in 500 μl of sterile water and six fold serial dilutions were generated (10^{-1}, 10^{-2}, 10^{-3}, 10^{-4}, 10^{-5} and 10^{-6}). 5-10 μl of the six dilutions were spotted onto appropriate plates. YPD agar plates supplemented with and without rapamycin (10 μg/ ml) were used for the growth assay in this study. Cells were grown for 48 hours and photographs were taken.

2.2.2 Construction of yeast strains

2.2.2.1 Competent yeast cells

A pre-culture of 50 ml YPD medium with yeast cells from a fresh YPD agar plate was inoculated and then incubated overnight at 30 °C, 180 rpm in an incubator shakerMultitron ®. The next morning, cells of the pre-culture were diluted into 50 ml of fresh YPD medium to an optical density at 600nm (OD_{600}) of 0.15 and grown with shaking (180 rpm) for 4 hours at 30 °C. Cells of the 50 ml YPD culture were then harvested in a falcon tube by centrifugation for 5 min at room temperature, 3000 rpm (Centrifuge 5810 R, Eppendorf AG, Hamburg, Germany). Supernatant was removed and cell pellet was resuspended in 1 ml of 0.1 M lithium acetate (LiAc) and then transferred to a 1.5 ml microfuge tube. Cells were spun down for 2 min at room temperature, 3000 rpm in a tabletop centrifuge (Centrifuge 5424, Eppendorf AG,

Hamburg, Germany) and cell pellet was resuspended in about 4 volumes of 0.1 M LiAc. At that time, yeast cells were competent and ready to use for transformation.

2.2.2.2 Yeast transformation

Transformation of either PCR-amplified DNA or plasmid DNA into competent yeast cells was based on a protocol published by Agatep et al., 1998.

As a reagent for the transformation mix, single-stranded carrier DNA was obtained from salmon sperm DNA that has been boiled for 5 min at 95 °C and then chilled on ice. The transformation mix was composed of 240 µl of polyethylene glycol (PEG3350; 50 % w/v), 36 µl of 1 M LiAc, 10 µl of single-stranded carrier DNA, 50 µl DNA from PCR reaction (200 µl reaction precipitated and dissolved in 50 µl sterile distilled water) or 10 µl digested plasmid DNA from a heat inactivated digestion mix and sterile distilled water was added to a final volume of 360 µl of transformation mix. A volume of 50 µl of competent cell suspension was added to 360 µl of transformation mix and vortexed vigorously. After an incubation time of 30 min at 30 °C on a rotating rack, cells were heat shocked for 15 min at 42 °C in a water bath (Memmert, Schwabach, Germany). Cells were pelleted for 2 min at 3000 rpm in a tabletop centrifuge and transformation mixture was removed. Cell pellet was resuspended in 300 µl of sterile distilled water and plated onto appropriate selective medium. Plates were incubated for 2 to 4 days at 30 °C in a Heratherm™ incubator until colonies were grown. Positive transformants were then tested by PCR.

2.2.2.3 Diploid yeast strain creation

Diploid yeast strains were created by mating two haploid strains of the opposite mating types (*MATa* and *MATalpha*) on YPD agar plates overnight at 30 °C. This mixture was then streaked onto solid YPD medium covered by alpha-factor (10 µg/ ml) to select for diploid yeast cells and haploid cells (*MATalpha*). Following an incubation of 48 hours at 30 °C, single colonies were picked and streaked onto a new YPD agar plate. Diploid strains were selected by replica plating onto MIN agar plates with mating type tester strains.

2.2.3 Methods of DNA analysis

2.2.3.1 Polymerase Chain Reaction (PCR)

PCR was used in this study to amplify plasmid or genomic DNA templates for Gibson cloning, genotyping and transformation of *S. cerevisiae* and *E. coli*. PCR reactions were performed in a T3000 Thermocycler (Biometra). An example for a PCR reaction mix and a standard PCR program are shown in Tables 2-11 and 2-12, respectively.

Table 2-11 Example of the composition of a 20 µl PCR reaction.

Component	20 µl reaction
DNA template	1 µl
20 µM forward primer	1 µl
20 µM reverse primer	1 µl
10xExTaq buffer	2 µl
dNTPs	1.6 µl
TaKaRa Ex Taq®	0.16 µl
sterile water	13.24 µl

Table 2-12 Example of a standard PCR program.

Reaction step	Temperature (°C)	Time	Cycles
Initial Denaturation	94	2 min	1
Denaturation Primer Annealing Elongation	94 50 72	1 min 30 sec 2 min 30 sec	2x30
Final Elongation	72	10 min	1
Hold	4	∞	

2.2.3.2 Agarose gel electrophoresis

Agarose gel electrophoresis was performed in this study to separate DNA molecules by size. Depending on their molecular weight, PCR-based DNA products, plasmid DNA and digested DNA were loaded onto 0.8-1.2 % standard agarose gels and separated at 100-130 V in an agarose gel system (Carl Roth, Karlsruhe, Germany) using 1x TAE buffer.

Prior to Southern blot analysis, restricted genomic DNA was separated on a 0.6 % SeaKem® LE agarose (Lonza, Rockland, USA) gel for 16 hours at 70 V in an Owl™ A2-BP large gel system (Thermo Fisher Scientific, Waltham, USA) containing 1x TBE buffer. Separated DNA bands were visualised by UV light after staining the gel in a RedSafe™ bath (1 ml/ 1 L H_2O; iNtRON Biotechnology, Sungnam, Korea) for 30 min at room temperature, 35 rpm on a platform shaker Innova™ 2000 (New Brunswick Scientific, Edison, USA).

2.2.3.3 DNA extraction and purification

DNA fragments were extracted and purified from agarose gels using a gel extraction kit (Qiagen) according to the manufacturer's instructions.

2.2.3.4 Gibson assembly

Gibson assembly is an alternative strategy for the traditional cloning to combine multiple fragments together in one vector without the need to use restriction enzymes (Gibson et al., 2009). In this study, Gibson cloning was used for the construction of kinetochore components fused to deactivated Cas9 (dCas9). These constructs were placed under a meiosis-specific promoter (construct: *pHOP1-kinetochore protein-3xFLAG-DCAS9;* Figure 3-17). Following DNA extraction and purification of the PCR products, the Gibson assembly reaction mix was incubated for 1 hour at 50 °C and then transformed into competent bacteria cells. 5 µl of the reaction mix were used for transformation. The composition of the Gibson cloning reaction mix is shown in Table 2-13.

Table 2-13 Gibson cloning procedure.

Component	20 μl reaction
DNA template	5 μl
Gibson Assembly® Master Mix	15 μl

2.2.3.5 Transformation of plasmid DNA into competent bacteria cells

For plasmid transformation, 150 μl of frozen *E.coli* competent cells were thawed on ice and 1-5 μl of DNA was added. The suspension was gently mixed by flicking the tube. After an incubation of 30 min on ice, the cells were heat-shocked at 42 °C for 45 sec and subsequently chilled on ice for 2 min. 300 μl of LB medium were added to the mixture and incubated on a rotating rack for 20-40 min at 37 °C. The transformation mixture was platted onto a LB agar plate with antibiotic for selection and incubated at 37 °C overnight.

2.2.3.6 Colony PCR

Following bacterial transformation, colony PCR was conducted to confirm the successful of the Gibson cloning. Individual transformants were picked with a pipet tip and dipped into 20 μl of a PCR reaction mix containing primers, water, dNTPs and LongAmp® *Taq* polymerase. The remaining cells on the tip were dipped into a culture of 5 ml LB medium and incubated at 37 °C overnight.

2.2.3.7 Isolation of plasmid from *Escherichia coli*

Colonies from a fresh overnight LB agar plate were picked and grown in a culture of 5 ml LB medium with the appropriate antibiotic at 37 °C, 180 rpm overnight in a Minitron incubator shaker (Infors HT). Plasmid DNA from *E. coli* overnight cultures was isolated using the miniprep kit (Qiagen) according to the manufacturer's instructions.

2.2.3.8 Determination of DNA concentration

The concentration of DNA samples was determined by measuring the absorbance at 260 nm with a NanoDrop 2000 spectrophotometer (Thermo Scientific, Waltham, USA).

2.2.3.9 Sequencing

Plasmids obtained from successful Gibson assemblies were submitted for Sanger sequencing to the company Genewiz, Takeley, UK.

2.2.3.10 Real time quantitative PCR (qPCR)

Following chromatin immunoprecipitation (ChIP, described in 2.2.4.5), real time quantitative PCR (qPCR) was conducted in a 7500 Fast Real-Time PCR System (Applied Biosystems, Forster City, USA) to quantify specific target sequences in input and ChIP DNA samples. At every PCR cycle the amount of amplicon is detected by the accumulation of a fluorescence signal. In this study, a master mix (PerfeCTa® SYBR® Green FastMix®, Quantabio, Beverly, USA) containing SYBR-Green as fluorescent dye that intercalates to DNA was used. The threshold cycle number (C_t value) of a fast 2-Step cycling program for product detection was used to normalize the ChIP-qPCR data according to the Percent Input method. Statistical significance was evaluated using unpaired t test. The composition of a 20 μl qPCR reaction mix and the procedure of the fast 2-step cycling program are shown in Tables 2-14 and 2-15, respectively.

Table 2-14 Composition of a 20 μl qPCR reaction mix.

Component	20 μl reaction
DNA template	5 μl
2x master mix	10 μl
20 mM forward primer	0.025 μl
20 mM reverse primer	0.025 μl
Sterile water	4.5 μl

Table 2-15 Fast 2-Step cycling procedure.

Step	Temperature (°C)	Time
Initial Denaturation	95	30 sec
PCR cycling (30-45 cycles)	95	3-5 sec
Collect data at end of extension step	60	20-30 sec

2.2.3.11 Southern Blot

Southern blot analysis was conducted to detect the presence of DNA double-strand breaks at specific chromosomal loci in meiotic yeast cells. The protocol for Southern blotting used in this study is described in the following sections (according to Vader et al., 2011).

2.2.3.11.1 Isolation of genomic DNA from meiotic yeast cells for Southern blot analysis

Samples for Southern blotting were harvested at time points 0, 3, 5, and 8 hours after synchronous induction of meiosis. While harvesting, cells of 10 ml meiotic cultures were killed by addition of sodium azide (final concentration 0.1 %), centrifuged for 3 min at 4 °C, 3000 rpm in a tabletop centrifuge (Centrifuge 5810 R, Eppendorf, Hamburg, Germany) and stored at -20 °C.

A sufficient amount of genomic DNA of meiotic cells, which is suitable for digestion by restriction endonucleases and for Southern blot analysis, was isolated as follows: Cells were thawed on ice, suspended in 1 ml of pre-chilled TE buffer, transferred to a 1.5 ml microfuge tube and centrifuged. Cell pellet was resuspended in 500 µl of freshly prepared spheroplasting solution (spheroplasting buffer, 1/100 volume of β-mercaptoethanol, 1/40 volume of the zymolyase stock) and incubated for 45 min at 37 °C on a rotating rack until spheroplasting was complete. The spheroplasted cells were then lysed by adding 100 µl preheated lysing buffer and 15 µl proteinase K (Roche Diagnostics, Mannheim, Germany) and incubated for 2 hours at 65 °C. Afterwards, lyses of spheroplasts was further facilitated by addition of 150 µl of 5 M potassium acetate and incubated for approximately 30 min on ice until tube content became semi-solid. At the end of incubation, lysed cells were centrifuged for 20 min

at 4 °C, 15 000 rpm in a tabletop centrifuge (Centrifuge 5424 R, Eppendorf AG, Hamburg, Germany) and 600 µl of the clear lysate was transferred to a clean 2 ml microfuge tube containing 750 µl of absolute ethanol. Tube content was mixed by inverting a few times and incubated on ice for 10 min. Precipitated DNA was pelleted by centrifugation for 10 min at 4 °C, 15 000 rpm in a tabletop centrifuge. Pellet was dissolved in 750 µl of a freshly prepared TE buffer-RNase A (50 µg/ml; 1: 600 stock solution; Sigma-Aldrich, St. Louis, USA) solution (1:600 stock solution) for 1 hour at 37 °C. The microfuge tube was stored at 4 °C overnight.

The next day, 500 µl of a phenol/chloroform/isopropanol solution (Carl Roth, Karlsruhe, Germany) was added to the tube, which was gently mixed by inverting 60 times. After sitting for a few minutes, microfuge tube was inverted another 60 times and then centrifuged for phase separation for 10 min at 4 °C, 15 000 rpm in a tabletop centrifuge. 750 µl of isopropanol and 600 µl of the DNA-containing upper phase was transferred into a clean 2 ml tube. The solution was inverted 10 times and incubated for 10 min at 4 °C. The DNA was recovered by centrifugation for 10 min at 4 °C, 15 000 rpm. The recovered DNA pellet was washed in 1 ml of 70% ethanol and centrifuged for 5 min at 4 °C, 15 000 rpm. The supernatant was removed and the pellet was dissolved in 125 µl of TE buffer over night. On the next morning, themicrofuge tube was gently tapped 3-4 times in order to mix the tube content and the isolation of genomic DNA from meiotic cells was completed.

2.2.3.11.2 Digestion of genomic DNA

For Southern blot analysis, isolated genomic DNA from meiotic yeast cultures was digested with appropriate restriction enzymes (HindIII digestion for DNA break hotspot *YCR047C*; AatII digestion for *CEN1*) for 4 hours at 37 °C. Digestion was carried out in a 300 µl reaction volume and composed of 35 µl of genomic DNA, 30 µl of 10x NEB buffer, 2.5 µl NEB restriction enzyme and 232.5 µl of sterile distilled water. Once digestion was completed, fragmented DNA was precipitated by addition of 25 µl of 3 M sodium acetate, pH 5.5 and 650 µl of absolute ethanol and stored at -20 °C for at least 30 min. DNA was then pelleted for 10 min at 4 °C, 15 000 rpm in a tabletop centrifuge (Centrifuge 5424 R, Eppendorf, Hamburg, Germany) and supernatant was discarded. Pellet was air-dried for 15 min and resuspended in 15 µl of TE buffer. For the following agarose gel electrophoresis, 5 µl of loading buffer

(1 ml loading buffer contains 400 µl of 10x NEB3 buffer and 600 µl of 10x loading buffer) were added.

2.2.3.11.3 Southern blotting procedure

Prior to transferring separated DNA fragments from the agarose gel onto a Amersham Hybond™–XL membrane, gel was first incubated with 0.25 M hydrochloric acid (HCl) in a clean plastic dish for 40 min with gentle shaking in order to depurinate the DNA. After pouring off HCl and rinsing gel briefly with 1 L distilled water, DNA was denatured with 0.4 M sodium hydroxide (NaOH) for 35 min with gentle shaking in order to yield single strands that can bind to the membrane.

For the following transfer, a Whatman filter paper wick (20 x 35 cm) was placed on an inverted gel tray in the Owl™ A2-BP large gel system (Thermo Fisher Scientific, Waltham, USA). The wick was wetted with 0.4 M NaOH + 0.6 M NaCl and dipped into NaOH + NaCl, which has been poured into the system to create a reservoir. Two gel-size pieces of Whatman paper were placed on top of the wick and soaked with NaOH + NaCl. The gel was laid on the wet blotting papers and covered with a pre-soaked (distilled water) membrane. Two additional gel-sized Whatman papers were wetted with distilled water and placed on top of the membrane. While assembling the stack, the potential air bubbles between the layers were avoided by rolling a glass tube over the surfaces. The top filter paper was surrounded by Parafilm M® (Bemis, Neenah, USA). Finally, a pile of dry paper towels was laid on top to draw the liquid and transfer the DNA to the membrane by gravity flow of buffer. To ensure good contact between gel and membrane during the blotting process, pressure was applied by placing a 1 kg weight on top of the stack. Sufficient transfer of the DNA from the gel to the membrane was achieved overnight.

The following day, the transfer set-up was disassembled and the membrane was rinsed for at least 30 min in 1 L of 50 mM sodium phosphate buffer, pH 7.2 and stored at -20 °C.

2.2.3.11.4 Southern blot hybridization and washing

Prior hybridization, Southern blot membranes were thawed in 50 mM sodium phosphate buffer in a plastic dish at room temperature. Blots were then pre-hybridized in pre-warmed glass bottles filled with 20 ml of hybridization solution and 300 µl of denatured salmon sperm DNA as blocking reagent for at least 30 min at 65 °C in an HB-1000 hybridization oven (Analytik, Jena, Germany).

In the meantime, DNA probes *CEN1* (SGD coordinates: chromosome *I*, 145305-145650) and *YCR047C* (SGD coordinates: chromosome *III*, 209361-210030) were labeled with [α-^{32}P]dCTP using the Prime-It RmT Random Primer Labeling Kit (Agilent Technologies) according to the manufacturer's protocol. Labeled probes were then purified from unincorporated labeled nucleotides using an illustra ProbeQuant G-50 Micro column (GE Healthcare, Little Chalfont, UK), denatured for 10 min at 95 °C and chilled on ice. Denatured probes were added to 5 ml of pre-warmed hybridization solution and mix was poured into the glass bottles, followed by incubation at 65 °C overnight.

The next day, membranes were first washed twice with 120 ml of pre-warmed low stringency buffer for 15 min at 65 °C and then washed two more times in 120 ml of pre-warmed high stringency buffer for 30 min at 65 °C.

2.2.3.11.5 Phosphorimaging

Freshly washed membranes were covered with saran wrap and placed in an X-ray cassette. An X-ray film was exposed to the membranes for 7 days at room temperature. The film was scanned using Typhoon TRIO imager (GE Healthcare, Little Chalfont, UK). DNA double-strand break intensities were determined using ImageJ.

2.2.3.12 Genomic DNA preparation from yeast for PCR-based genotyping

The following protocol for genomic DNA extraction of yeast cells for routine PCR-based genotyping was used in this study:

A toothpick worth of cells was scraped off from a yeast agar plate and suspended in 500 µl of sterile filtered TE buffer in a 2 ml microfuge tube. Cells were pelleted for 15 sec at full speed in a tabletop centrifuge (Centrifuge 5424, Eppendorf, Hamburg, Germany) and supernatant was removed. Lysis of cells was achieved by addition of 200 µl of DNA breakage buffer, 0.3 g glass beads (Carl Roth, Karlsruhe, Germany) and 200 µl of phenol/chloroform/isopropanol (Carl Roth, Karlsruhe, Germany). The mixture was vigorously mixed on a VXR basic Vibrax® (IKA®-Werke, Staufen, Germany) for 6 min and then centrifuged for phase separation in a tabletop centrifuge for 5 min at full speed. After centrifugation, 100 µl of the DNA containing upper layer was carefully transferred to a clean 1.5 ml microfuge tube containing 1 ml of absolute, cold ethanol. To recover precipitated DNA, sample was centrifuged for 5

min at full speed and supernatant was discarded. DNA pellet was air-dried for 15 min at room temperature and dissolved in 50 µl of sterile distilled water.

2.2.3.13 Analysis of the meiotic program by flow cytometry

The DNA content of cells of meiotic cultures was measured by flow cytometry to assess meiotic progression. As cells underwent meiosis, samples were taken and processed for flow cytometric analysis as described in the following (according to Vader et al., 2011):

For each time point (0, 3, 5 and 8 hours), cells from 150 µl of sporulation culture were fixed for 2 hours at 4 °C in 350 µl of absolute ethanol. Cells were pelleted for 1 min at 7000 rpm in a tabletop centrifuge (Centrifuge 5424, Eppendorf, Hamburg, Germany) and then resuspended in 500 µl of 50 mM sodium citrate supplemented with 0.7 µl RNase A (30 mg/ml; Sigma-Aldrich, St. Louis, USA). Following 2 hours of incubation at 50 °C, cells were deproteinated with proteinase K (20 mg/ml; Amresco Inc, Solon, USA) for 2 hours at 50 °C. To stain the DNA, 500 µl of 50 mM sodium citrate containing 0.2 µl of the nucleic acid dye SYTOX® Green (Life Technologies, Eugene, USA) was added to the cells. Cell preparation was completed by brief sonication at low power. The DNA content of cells was measured using BD Accuri™ C6 (BD Biosciences, Franklin Lakes, USA) flow cytometer and DNA histograms were analysed by the FlowJo Software (FlowJo LLC, Ashland, USA).

2.2.4 Methods of protein analysis

2.2.4.1 Western blot

Proteins from yeast whole cell extracts were denatured and separated via SDS-PAGE and then transferred to a nitrocellulose membrane. A protein of interest was detected on the membrane using primary and secondary antibodies and a chemiluminescent reagent.

2.2.4.2 Yeast whole cell extract for Western blotting using trichloroacetic acid

At appropriate time points, cells from 5 ml meiotic cultures were collected by centrifugation for 3 min at 4 °C, 3000 rpm in a tabletop centrifuge (Centrifuge 5810 R, Eppendorf, Hamburg, Germany). Cell pellets were resuspended in 5 ml of 5% trichloroacetic acid (TCA) and incubated for 10 min on ice. Precipitated proteins were pelleted by centrifugation for 3 min at 4 °C, 3000 rpm. After washing with 1 ml of

acetone at room temperature, pellets were air-dried for at least 2-3 hours in the hood and then resuspended in 100 µl of protein breakage buffer (4 ml of TE (50 mM Tris pH 7.5, 1 mM EDTA), 11 µl of 1 M DTT). One volume of glass beads was added to the mixture and cells were disrupted using FastPrep®-24 machine (MP Biomedicals, Santa Ana, USA) twice at speed 6 for 1 min. Samples were chilled on ice for 5 min in-between runs. Protein extracts were resolved by SDS-PAGE and then transferred to a membrane by Western blotting.

2.2.3.4 Sodium dodecyl sulfate-polyacrylamide gel electrophoresis (SDS-PAGE)

SDS-PAGE is a method that involves the denaturation of proteins with the detergent sodium dodecyl sulfate (SDS) and the separation of the proteins according to their molecular weight by polyacrylamide gel electrophoresis (PAGE) (Smith, 1984). Prior to loading proteins onto a polyacrylamide gel, 50 µl of 5x SDS buffer was added to TCA extraced samples which were boiled for 5 min at 95 °C. Boiling with SDS gives the proteins a negative charge in proportion to their molecular weight (Smith, 1984). The negatively charged proteins migrated through a polyacrylamide gel in a Mini PROTEAN® Tetra Cell (Bio-Rad, Hercules, USA) with SDS running buffer for 60-120 min at 100 V. Low molecular weight proteins travel faster through the pores of the gel than high molecular weight proteins. The chemical composition of a polyacrylamide gel is shown in Table 2-16.

Table 2-16 Chemical composition of polyacrylamide gels used in this study. Volume (ml) of components required to cast two 1.5 mm gels.

Solution	Stacking gel (5%) Volume 5 ml	Running gel (10%) Volume 20 ml	Running gel (12%) Volume 20 ml
sterile water	3.4 ml	7.9 ml	6.6 ml
acrylamide mix (30%)	0.83 ml	6.7 ml	8.0 ml
1 M Tris (pH 6.8)	0.63 ml	----	----
1.5 M Tris (pH 8.8)	----	5.0 ml	5.0 ml
SDS (10%)	0.05 ml	0.2 ml	0.2 ml
ammonium persulfate (10%)	0.05 ml	0.2 ml	0.2 ml
TEMED	0.005 ml	0.008 ml	0.008 ml

2.2.4.4 Western blotting procedure

Separated proteins were transferred from a polyacrylamide gel onto a BioTrace™ NT nitrocellulose transfer membrane (Pall Corporation, New York, USA) using a Mini-PROTEAN® II Cell (Bio-Rad, Hercules, USA). After transfer, the Ponceau S staining solution was used to visualize proteins loaded onto the membrane. The staining was removed by washing the membrane once with PBST buffer for 5 min. The membrane was blocked with PBST buffer supplemented with 4% (w/v) milk powder for 30-60 min at room temperature on a rocking platform See-saw SSL4 (Bibby Scientific, Stone, UK). After blocking, the membrane was rinsed with PBST buffer for 5 min. This was followed by incubation with one of the following primary antibodies (α-Cas9, α-HA, α-Flag and α-Pgk1) diluted in 1x PBST supplemented with 4% (w/v) milk powder at 4 °C overnight. The next morning, the membrane was washed three times with 1xPBST buffer for 5 min at room temperature and then incubated with the secondary HRP-conjugated antibody diluted in 1x PBST supplemented with 4% (w/v) milk powder for 1 hour at room temperature on a rocking platform. After three washes

with 1x PBST, 500-1000 µl of ECL detection solution was added on the membrane and respective proteins were visualized using ChemiDoc™ MP Imaging System.

2.2.4.5 Chromatin immunoprecipitation

Chromatin immunoprecipitation (ChIP) was performed for Flag-tagged and HA-tagged proteins. Cells of 100 ml sporulation culture (collected in two 50 ml falcon tubes) were harvested 4.5 hours after meiosis induction and crosslinked with 1% formaldehyde for 15 min at room temperature. Cross-linking was quenched for 5 min at room temperature by adding glycine solution to a final concentration of 125 mM. After quenching, cells were pelleted for 3 min at 4 °C, 3000 rpm in a tabletop centrifuge (Centrifuge 5810 R, Eppendorf AG, Hamburg, Germany) and washed once with 20 ml ice-cold 1x TBS buffer. Cells were transferred to two screw cap tubes. The following steps were performed on ice to avoid protein degradation. To every tube, 200 µl of pre-chilled M2 lysis buffer supplemented with 1 mM PMSF, 1x SERVA and Complete protease inhibitor cocktail tablet (without EDTA, Roche) was added as well as an equal volume of glass beads (Carl Roth, Karlsruhe, Germany). Cells were then lysed using FastPrep®-24 machine (MP Biomedicals, Santa Ana, USA) twice at speed 4.5 for 1 min. Afterwards, cell lysates were mixed on a VXR basic Vibrax® (IKA® -Werke, Staufen, Germany) for 2 min at 1500 rpm. Lysates of both screw cap tubes (initially originated from the same sporulation culture) were pooled and transferred into a fresh Eppendorf tube. The chromatin was then fragmented by sonication using Branson Sonifier 450 at output control 2, constant cycle three times for 15 sec. In between runs, samples were kept on ice for 2 min. After fragmentation of the chromatin, cellular debris was pelleted for 10 min at 4 °C, 15 000 rpm and the crude lysate was collected in a new Eppendorf tube. As Input sample, 50 µl of the crude lysate was added to 200 µl of 1x TE/ 1% SDS buffer and stored at 4 °C until reversal of crosslinking.

For Flag-tagged chromatin immunoprecipitation (ChIPs), 500 µl of the crude lysate was incubated with 40 µl of 50 % slurry of anti-FLAG® M2 beads (Sigma-Aldrich, St. Louis, USA) previously washed three times with 1 ml of ice-cold 1X TBS buffer on a rotating rack at 4 °C. After an incubation time of 2 hours, ChIPs were washed four times with 500 µl of ice-cold M2 buffer and once with 500 µl of M2 buffer without detergent on a rotating rack at 4 °C for 2 min. After washing, protein-DNA complexes were eluted from the beads by adding 200 µl of ice-cold M2 buffer without detergent

containing FLAG peptides to a final concentration of 150 ng/ µl to every ChIP sample and rotated at 4 °C for 30 min. The beads were pelleted in a refrigerated centrifuge for 30 sec at 9000 rpm and the supernatant containing the protein-DNA complexes was transferred to a new tube. This elution step was repeated one more time and 800 µl of 1x TE/ 1% SDS buffer was added to the eluate.

For chromatin immunoprecipitation (ChIP) of HA-tagged proteins, 500 µl of the crude lysate was incubated with 1µl of anti-HA antibody (BioLegend, San Diego, USA) for 2-3 hours at 4 °C on a rotating rack. After incubation, 35 µl of a 50% slurry of Dynabeads™ protein G (Invitrogen, Carlsbad, USA) was added to lysate. Following incubation on a rotating rack overnight at 4 °C, the beads were coupled to the HA-tagged proteins bound to the anti-HA antibody and washed four times with ice-cold M2 buffer without inhibitors. Following one more wash with ice-cold M2 buffer without detergent, the supernatant was removed and beads were resuspended in 200 µl of 1x TE/ 1% SDS buffer.

The formaldehyde cross-links of both Input and ChIP samples were reversed by incubation of the samples at 65 °C for 18 hours. Next, 5 µl of glycogen (stock 20 mg/ ml) and 5 µl of proteinase K (20 mg/ ml) were added to the samples and incubated at 37 °C for 2 hours. Afterwards, ChIP samples were split up into two screw cap tubes and 68.7 µl of 3 M LiCl and 1 ml of ethanol was added to the Input and ChIP samples. To precipitate the DNA, samples were stored at – 20 °C overnight.

The DNA of both Input and ChIP samples was pelleted at 15 000 rpm for 10 min in a refrigerated table top centrifuge and washed once with 1 ml of 75% ethanol. The final DNA pellets were resuspended in 50 µl of TE containing RNAse A (1 µl / 100 µl) and incubated at 37 °C for 30 min. ChIP analysis was coupled to real time quantitative PCR (qPCR) described in section 2.2.3.10.

2.2.4.6 Co-Immunoprecipitation

For Co-Immunoprecipitation (Co-IP) experiments, cells from 100 ml cultures were harvested 4.5 hours after being induced to synchronously undergo meiosis and washed once with pre-chilled 1x PBS. Cells of the same sporulation culture were distributed into two screw cap tubes, snap-frozen with the aid of liquid nitrogen and stored at -80 °C. Unless otherwise noted, all subsequent steps were performed on ice. Cells were resuspended in 150 µl of ice-cold IP buffer (20 mM Hepes, pH 7.5, 4 mM MgCl2, 500 mM NaCl, 0.32 M Sorbitol, 4% Glycerol (v/v), 0.5 % Triton X-100

(v/v)) supplemented with 1 mM PMSF and Complete protease inhibitor cocktail tablet (without EDTA, Roche) and an equal volume of glass beads (Carl Roth, Karlsruhe, Germany) was added. Afterwards, cells were broken by three 45 sec cycles at power 6 in a FastPrep®-24 machine (MP Biomedicals, Santa Ana, USA) with dry ice by three 45 sec cycles at power 6. Tubes were pierced with a hot needle and the cell lysates were spun down at 3000 rpm for 5 min and transferred into fresh Eppendorf tubes. Cell lysates from two screw cap tubes (originated from the same sporulation culture) were then pooled, sonicated two times for 15 sec and centrifuged for 15 min at 4 °C, 15 000 rpm. As Input sample (control), 50 µl of the lysate was precipitated with 5 µl of TCA for 30 min on ice. Following centrifugation for 30 min at 4 °C, 15 000 rpm, the pellet was washed once with 500 µl of ice-cold acetone and air-dried for 30 min. The pellet was then resuspended in 40 µl of TCA resuspension buffer with urea (2% SDS, 50 mM Tris, pH 7.5, 6 M Urea) and vigorously mixed. 10 µl of 2x Laemmli loading buffer (127 mM Tris-acetate, pH 6.8, 4% β-Mercaptoethanol, 20% Glycerol, 6% SDS, 0.03% Bromophenol Blue) was added to the input sample and boiled at 95 °C for 5 min. The input sample was stored at -20 °C until analysis by SDS PAGE and Western blot. For IP samples, 35 µl of a 50% slurry of Dynabeads™ protein G (Invitrogen, Carlsbad, USA) coupled to either anti-Flag or anti-HA antibodies (depending on the IP) were added to the remaining 500 µl of the lysate. Following incubation on a rotating rack overnight, the beads coupled to either anti-Flag or anti-HA antibody were bound to the Flag-tagged proteins and HA-tagged proteins, respectively, and washed three times with 1x IP buffer. Each wash step was conducted for 10 min. Finally, the beads were eluted in 50 µl of 2x Laemmli loading buffer, boiled for 5 min and frozen at -20 °C. To detect immunoprecipitated and coimmunoprecipitated proteins and their binding proteins, Input and IP samples were loaded onto SDS-PAGE gels and subsequently analyzed by Western blot (described in sections 2.2.4.3 and 2.2.4.4).

2.2.5 Meiotic recombination, DNA double-strand breaks and spore analyses

2.2.5.1 Live cell reporter assay

For the Live Cell Recombination assay, cells were employed that contain fluorescent markers (tdTomato (RFP), green fluorescent protein (GFP), m-Cerulean (CFP)) integrated into different chromosomal loci on the homologous chromosomes *VIII*

were employed based on Thacker et al., 2011 (and Vincenten et al., 2015). Cells were induced to synchronously undergo meiosis and harvested after 24 hours. Images of the tetrads were taken in three channels (RFP, GFP, CFP) on a DeltaVision Elite High Resolution Microscope (GE Healthcare) using a 40x objective. Images were processed and analyzed using ImageJ software. This assay can reports only on crossover recombination between homologous chromosomes VIII when chromosomes are faithfully segregated during the meiotic divisions. Therefore, only tetrads with four CFP (blue) fluorescence spores were included in the final analysis. Tetrads composed of less than four blue spores are the outcome of mis-segregated chromosomes VIII and were not considered in the analysis. Recombination frequency, expressed as centiMorgans, and standard error were calculated using Perkins formulas (based on the online tool http://elizabethhousworth.com/StahlLabOnlineTools/EquationsMapDistance.html).
G*Power analysis was performed to determine the sample size that needs to be analyzed for >0.80 confidence in comparison to wild type cells. Statistical significance was evaluated using the Fisher's exact test (using the online tool http://www.socscistatistics.com/tests/fisher/Default2.aspx).

2.2.5.2 Sporulation efficiency and spore viability

To assess sporulation efficiency and spore viability, cells were induced to synchronously undergo meiosis and harvested after 24 hours. For sporulation efficiency, 200 cells per culture were scored and the number of tetrads, dyads, monads and no spores were determined using the Axio Vert.A1 microscope. To determine the spore viability, 150 µl of each culture was digested with 150 µl zymolyase solution (1 mg/ ml in 1M sorbitol) for 15 min at 37 °C. Following digestion, 300-400 µl of sterile water was added to each culture and at least 65 tetrads were dissected on plates containing appropriate medium using TDM Tetrad Dissection Microscope Ci-L (Nikon, Tokyo, Japan). After an incubation of 48 hours at 30 °C, spore viability was evaluated.

2.2.5.3 Genome-wide analysis of meiotic recombination and DNA double-strand breaks

Single nucleotide polymorphisms in a diploid hybrid yeast strain and DNA double-strand breaks were identified by high throughput sequencing as described in Vincenten et al., (2015).

3 Results

Controlled DNA double-strand break (DSB) formation followed by inter-homolog crossover (CO) recombination is required for the faithful chromosome segregation during meiosis. However, the formation of COs in chromosomal regions surrounding centromeres, called pericentromeres, is associated with chromosome segregation defects and aneuploid inviable gametes in diverse eukaryotic organisms, including humans (Hassold and Hunt, 2001; Koehler et al., 1996; Rockmill et al., 2006). In budding yeast, meiotic recombination (*i.e.* COs and non-crossovers (NCOs)) is suppressed within centromere-proximal regions (~6-fold within 10 kb of centromeres) (Chen et al., 2008) and DSB formation, the initiating event of meiotic recombination, occurs at reduced levels at pericentromeric regions compared to chromosomal arms (Blitzblau et al., 2007; Buhler et al., 2007; Gerton et al., 2000; Pan et al., 2011; Robine et al., 2006). DSB formation is ~2-3-fold reduced within a 5-10 kb distance from centromeres as compared to chromosomal regions greater than 10 kb away (Blitzblau et al., 2007; Buhler et al., 2007; Pan et al., 2011). The formation of DSBs is even more decreased (~7-fold) within a narrower domain of 1-3 kb on both sides of centromeres (Pan et al., 2011). However, the chromosomal features that control meiotic DSB formation and recombination at centromere-proximal regions remain poorly understood. A promising candidate in controlling these events is a multi-protein complex that assembles onto centromeres, termed the kinetochore. In meiotic G2/ prophase I, when recombination occurs, the Ctf19 complex (Ctf19-C) and Mtw1 complex (Mtw1-C) of the budding yeast kinetochore are assembled onto centromeres, while other subunits are absent (Meyer et al., 2015; Miller et al., 2015). In this PhD study, we investigate whether there is a role for the Ctf19-C and Mtw1-C in controlling meiotic DSB formation and recombination at centromere-proximal regions. If so, we want to understand how these complexes regulate meiotic DNA break formation and recombination and what the molecular basis behind this control is.

3.1 The Ctf19-C plays a role in controlling meiotic homologous recombination at pericentromeres

To investigate whether there is a role for the Ctf19-C in controlling meiotic homologous recombination in chromosomal regions surrounding centromeres, we analyzed the effect of deletion mutants of the Ctf19-C on CO recombination at a

defined pericentromeric region using a live cell fluorescent reporter assay (Thacker et al., 2011; Vincenten et al., 2015). The live cell reporter assay was established to measure CO recombination rates within an interval close to the centromere on chromosome *VIII* (*CEN8*) (Figure 3-1 D; Vincenten et al., 2015). This interval comprises a tdTomato (RFP) marker inserted adjacent to *CEN8* into one of the two homologous chromosomes *VIII* and a green fluorescent protein (GFP) reporter integrated into a chromosomal position within a 10 kb distance from *CEN8* in the other homologous chromosome *VIII*. The fluorescent protein markers were placed under the control of a promoter, which is active upon spore formation (Thacker et al., 2011). Therefore, this assay allows for measuring CO recombination rates in the four products of budding yeast meiosis. (The final outcome of a single meiosis in budding yeast is a tetrad containing four haploid spores.) A single CO event within the 10 kb range between the RFP and GFP reporters of the homologous chromosomes yields tetrads composed of two different parental class spores (containing either RFP or GFP) and two different recombinant class spores. One of the two recombinant spores contains none of the two reporters and the other recombinant spore inherited both markers RFP and GFP generating a yellow signal (Figure 3-1 A, B). To ensure that the two recombinant class spores were produced through a CO event rather than chromosome mis-segregation, another marker, m-Cerulean (CFP), was integrated at a chromosomal locus 50 kb away from the centromere into both homologous chromosomes *VIII*. CFP produces a blue signal. In case of mis-segregation of chromosome *VIII*, less than four spores containing a blue signal are visible. Tetrads composed of spores in which chromosome mis-segregation occurred were not included in this analysis. As opposed to tetrads with a single CO, tetrads containing four haploid cells of the parental class (two red spores and two green products) are generated when no CO event occurs within the interval at *CEN8* (Figure 3-1 C). As a control, we determined CO frequency within an interval on chromosome arm *VIII*, which is, different from the pericentromere, permissive for CO recombination (Figure 3-1 D; Vincenten et al., 2015). The interval on arm *VIII* is of equivalent size as the interval close to *CEN8* (10 kb) and also flanked by RFP and GFP reporters.

In collaboration with Adèle Marston and colleagues, we first determined CO frequency close to *CEN8* and, as a control, on the chromosome arm *VIII* in cells lacking the synaptonemal complex protein Zip1, which was shown to affect

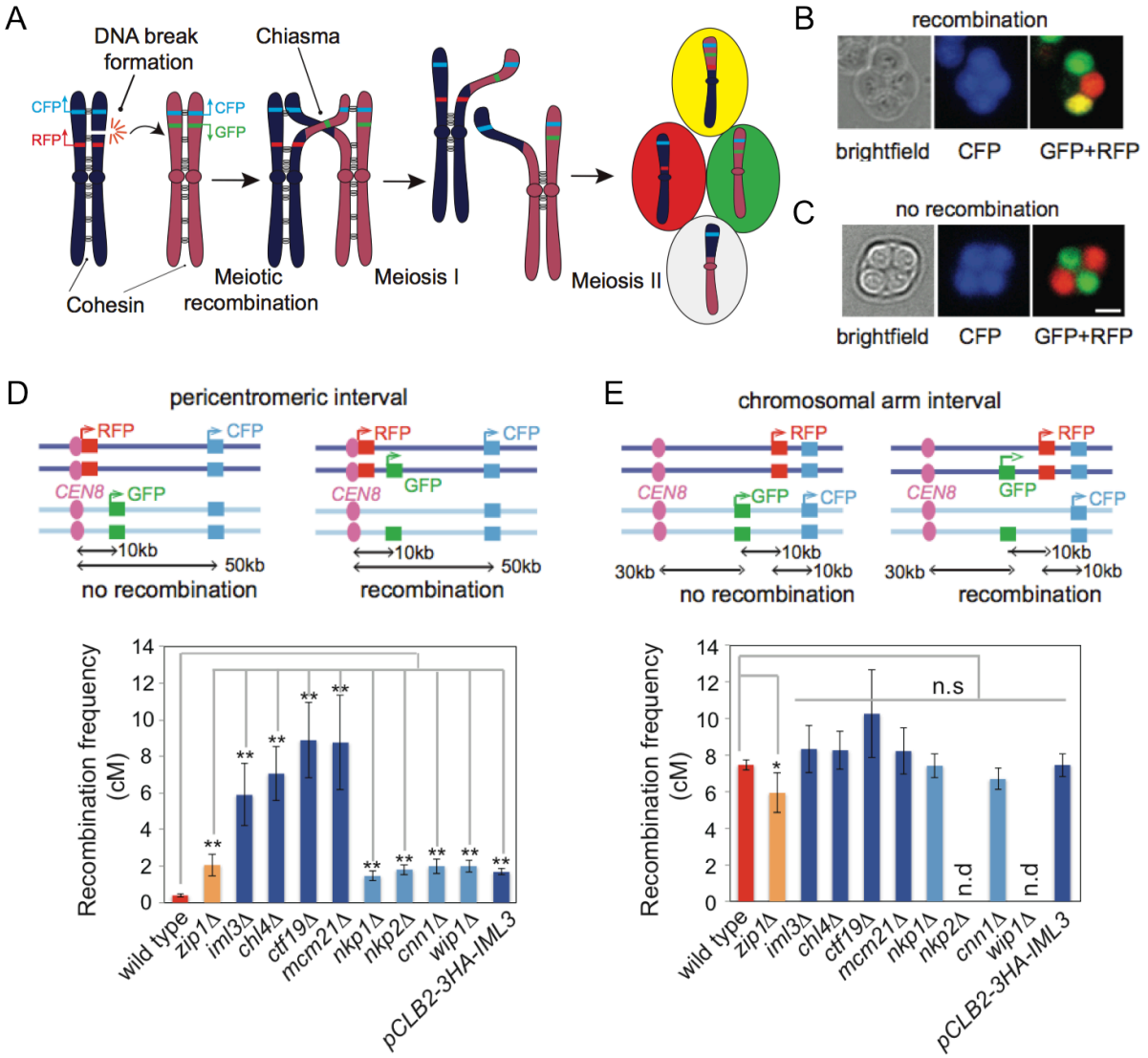

Figure 3-1 The Ctf19-C suppresses meiotic homologous CO recombination at *CEN8*

A-E) Scheme of the live cell fluorescent reporter assay used to measure CO recombination frequency within a pericentromeric interval at *CEN8* (D) and as a control on a chromosomal arm region (E) in a wild type strain and deletion mutants of non-essential components of the Ctf19-C. Both pericentromeric (D) and chromosomal arm (E) intervals span a distance of 10 kb flanked by tdTomato (RFP) and Green fluorescent protein (GFP) reporters. The control reporter m-Cerulean (CFP) is localized within a 50 kb distance from *CEN8* (A-E). Expression patterns of the RFP and GFP reporters differ in spores when CO recombination (A, B) or no recombination (C) occurred in meiosis as illustrated in the images of live tetrads (B, C). CO rates at *CEN8* (D) and within the chromosomal arm interval (E), represented as map distances (centiMorgans (cM)), and standard error bars were obtained based on Perkins equation (described in Materials and Methods). p values were determined using Fisher's exact test (* $p<0.05$; ** $p<0.0001$). n.s., not significant; n.d., not determined. Experiments shown in B-E were performed by Adèle Marston and colleagues; modified from Vincenten et al., 2015.

pericentromeric recombination (Chen et al., 2008). Indeed, map distance, a measure of CO frequency, increased from 0.41 centiMorgans (cM) at *CEN8* in the wild type to 2.06 cM at *CEN8* in *zip1Δ* cells when assessed by the live cell reporter assay (Figures 3-1 D). By contrast, CO recombination rates showed only a modest decrease on the chromosome arm *VIII* in *zip1Δ* cells compared to the wild type (Figure 3-1 E). These results are in agreement with previous observations (Chen et al., 2008). Thus, the live cell reporter assay can be used as a system to measure pericentromeric CO recombination frequency.

We next analyzed CO rates at *CEN8* and the chromosome arm *VIII* in deletion mutants of non-essential components of the Ctf19-C. We found significantly increased levels of *CEN8*-proximal COs in cells lacking Iml3, Chl4, Mcm21 and Ctf19 when compared to the wild type (Figure 3-1 D; Vincenten et al., 2015). Map distances were 5.9 cM and 7.06 cM in *iml3Δ* and *chl4Δ* cells, respectively. However, the strongest effects on CO levels close to *CEN8* were observed in *mcm21Δ* and *ctf19Δ* cells as the map distances were 8.76 cM and 8.89 cM, respectively. Other Ctf19-C mutants such as *nkp1Δ, nkp2Δ, cnn1Δ* and *wip1Δ* had only a minor effect on CO recombination at *CEN8* in comparison to wild type cells (1.47 cM in *nkp1Δ,* 1.81 cM in *nkp2Δ*, 2 cM in *cnn1Δ* and 2 cM in *wip1Δ* cells). Based on these results, we conclude that the Ctf19-C suppresses meiotic CO recombination close to *CEN8*. This effect of the Ctf19-C seems to be spatially restricted to the pericentromere as no significant changes in CO formation were observed on the chromosomal arm *VIII* (Figure 3-1 E; Vincenten et al., 2015).

The data of the live cell reporter assay were extended through investigations on genome-wide repair products of COs and NCOs in the spores of a hybrid yeast strain of *pCLB2-3HA-IML3*, a meiosis-specific depletion allele of the Ctf19-C component Iml3. This allele was generated by the substitution of the promoter of *IML3* with the *CLB2* promoter (Lee and Amon, 2003). *CLB2* is exclusively expressed in mitosis (Grandin and Reed, 1993). A meiosis-specific depletion allele was employed for this analysis as poor spore viability (less than 30%) precluded us from using deletion mutants of Ctf19-C components. After the hybrid *pCLB2-3HA-IML3* strain was induced to undergo meiosis, DNA from eight tetrads containing four viable spores was isolated and CO and NCO recombination products were determined by high throughput sequencing to identify single-nucleotide polymorphisms (Figure 3-2 A;

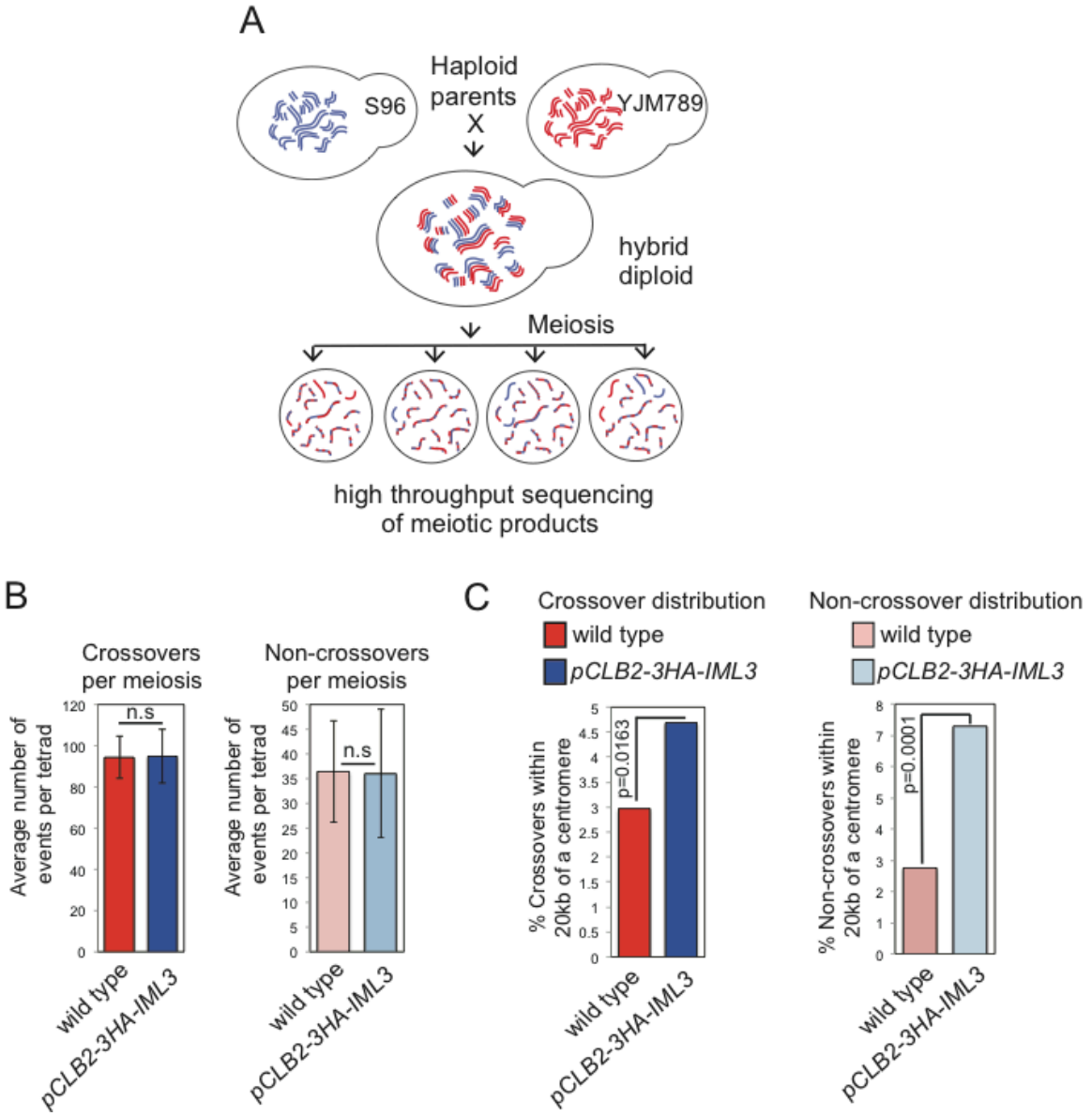

Figure 3-2 The Ctf19-C prevents meiotic CO and NCO recombination at pericentromeres

A) To assess whether the Ctf19-C plays a role in global CO and NCO recombination events, the DNA of the meiotic products of a diploid hybrid strain (*pCLB2-3HA-IML3*) was isolated and sequenced to identify single-nucleotide polymorphisms. B) The sequencing analysis revealed no significant changes in the average number of COs (left panel) and NCOs (right panel) per tetrad between wild type and *pCLB2-3HA-IML3* cells. Error bars represent standard deviation. A two-tailed t test showed non-significance ($p>0.05$). C) The distribution of COs (left panel) and NCOs (right panel) within ~20 kb of centromeres is significantly increased in *pCLB2-3HA-IML3* cells compared to the wild type. Data for wild type was obtained from Oke et al. (2014). 8 tetrads composed of four viable spores were analyzed from the hybrid *pCLB2-3HA-IML3* strain and 52 tetrads from the wild type. p values were determined using chi-square test with Yates correction. Experiments shown in A-C were performed by Jennifer Fung and colleagues; modified from Vincenten et al., 2015.

Anderson et al., 2011; Oke et al., 2014; Vincenten et al., 2015). In collaboration with Jennifer Fung and colleagues, we found that the total number of COs and NCOs genome-wide was not significantly affected in the *pCLB2-3HA-IML3* mutant compared to the wild type (~90 COs and ~35 NCOs in both wild type and *pCLB2-3HA-IML3*) (Figure 3-2 B; Vincenten et al., 2015). However, the sequencing data showed a significant increase in COs and NCOs within 40 kb chromosomal regions surrounding all centromeres (20 kb on each side of centromeres) in cells depleted for Iml3 and revealed thus a change in the distribution of homologous recombination profiles at pericentromeres (Figure 3-2 C; Vincenten et al., 2015). These results indicate that the Ctf19-C prevents meiotic homologous recombination at pericentromeres.

In collaboration with Adèle Marston and colleagues, we also employed the hypomorphic *pCLB2-3HA-IML3* mutant to measure CO rates at *CEN8* and, as a control, on the chromosome arm *VIII* by the live cell reporter assay (Figure 3-1 D, E). We measured a CO frequency of 1.69 cM at the *CEN8*-proximal region in *pCLB2-3HA-IML3* cells. Thus, this analysis revealed only a mild effect on pericentromeric COs in the hypomorphic *pCLB2-3HA-IML3* mutant as compared to cells deleted for *IML3* (5.9 cM in *iml3Δ*) (Figure 3-1 D). This indicates that the analysis of the *pCLB2-3HA-IML3* mutant likely underestimates the role of the Ctf19-C in preventing homologous recombination at pericentromeres. By contrast, we did not observe any significant changes in CO rates within the interval on chromosome arm *VIII* in *pCLB2-3HA-IML3* compared to *iml3Δ* cells (Figure 3-1 E).

In conclusion, the results of the live cell reporter assay (Figure 3-1) and the high throughput sequencing analysis (Figure 3-2) unveil a novel role for the Ctf19-C in controlling meiotic homologous recombination at centromere-proximal regions.

3.2 The Ctf19-C minimizes meiotic DSB formation at pericentromeres

We next wanted to understand how the Ctf19-C prevents meiotic recombination at pericentromeres. Homologous recombination events are initiated by the formation of DSBs via the activity of the enzyme Spo11 (Keeney et al., 1997). DSB formation occurs at reduced levels in close proximity to centromeres when compared to chromosomal arms (Blitzblau et al., 2007; Buhler et al., 2007; Gerton et al., 2000; Pan et al., 2011). To investigate whether the Ctf19-C affects pericentromeric DSB formation, we, in collaboration with Scott Keeney and colleagues, generated genome-wide DSB maps from a population of cells lacking the Ctf19-C component

Mcm21 by high throughput sequencing analysis of Spo11-oligo complexes (Pan et al., 2011; Vincenten et al., 2015). This method is based on sequencing of short DNA fragments covalently attached to Spo11 after enzymatic cleavage from chromosomes (so-called Spo11-oligos). The Spo11-oligos serve as tags that allow for the precise detection of DNA breakage in the budding yeast genome (Figure 3-3 A; Pan et al., 2011). This, in turn, enables the generation of genome-wide meiotic DSB maps. The sequencing analysis of Spo11-oligo complexes revealed a genome-wide increase of meiotic DSBs of ~6 kb surrounding centromeres (~3 kb on each side of centromeres) in *mcm21Δ* cells compared to the wild type (Figure 3-3 B). These results are in line with previous findings by Pan et al. (2011). Increased levels of pericentromeric DSB formation in cells lacking Mcm21 and the genome average (dotted lines, Figure 3-3 C) were similar, suggesting that there is no residual DNA break reduction in *mcm21Δ* cells. These observations demonstrate that the Ctf19-C plays a general role in minimizing meiotic DSB formation in the direct vicinity of centromeres.

It is striking that the Ctf19-C minimizes meiotic DSB formation within a narrower domain of ~6 kb surrounding centromeres (Figure 3-3 B), whereas CO recombination is prevented within a broader region of ~40 kb of centromeres (Figure 3-2 C). These findings might imply that the Ctf19-C mediated reduction in DSB formation is not the sole cause for decreased levels of pericentromeric COs. To compare the effect of the Ctf19-C on DSBs and COs more directly, we analyzed meiotic DSB formation within the intervals on chromosome arm *VIII* (Figure 3-1 D, E) in *mcm21Δ* and wild type cells. As expected, we found an increase in DSB formation at the *CEN8*-proximal interval in which we also observed elevated levels of COs in *mcm21Δ* cells compared to the wild type when assessed by the live cell reporter assay (Figure 3-3 D). However, we observed only a ~5-fold increase in *CEN8*-proximal DSBs in *mcm21Δ* cells compared to the wild type, whereas COs at the same interval were ~21-fold increased (Figure 3-3 E, F). Based on these findings, we conclude that the Ctf19-C partially prevents CO recombination at the pericentromere by minimizing meiotic DSB formation.

Moreover, we found that DSB formation at pericentromeres was not equally affected in *mcm21Δ* cells because the fold change of Spo11-oligos at some centromere-proximal regions was higher than in others (Figure 3-3 D). We assume that distinct effects on pericentromeric DSB formation of the chromosomes are dictated by the underlying chromosomal structure (*i.e.* promoter regions, nucleosome-depleted

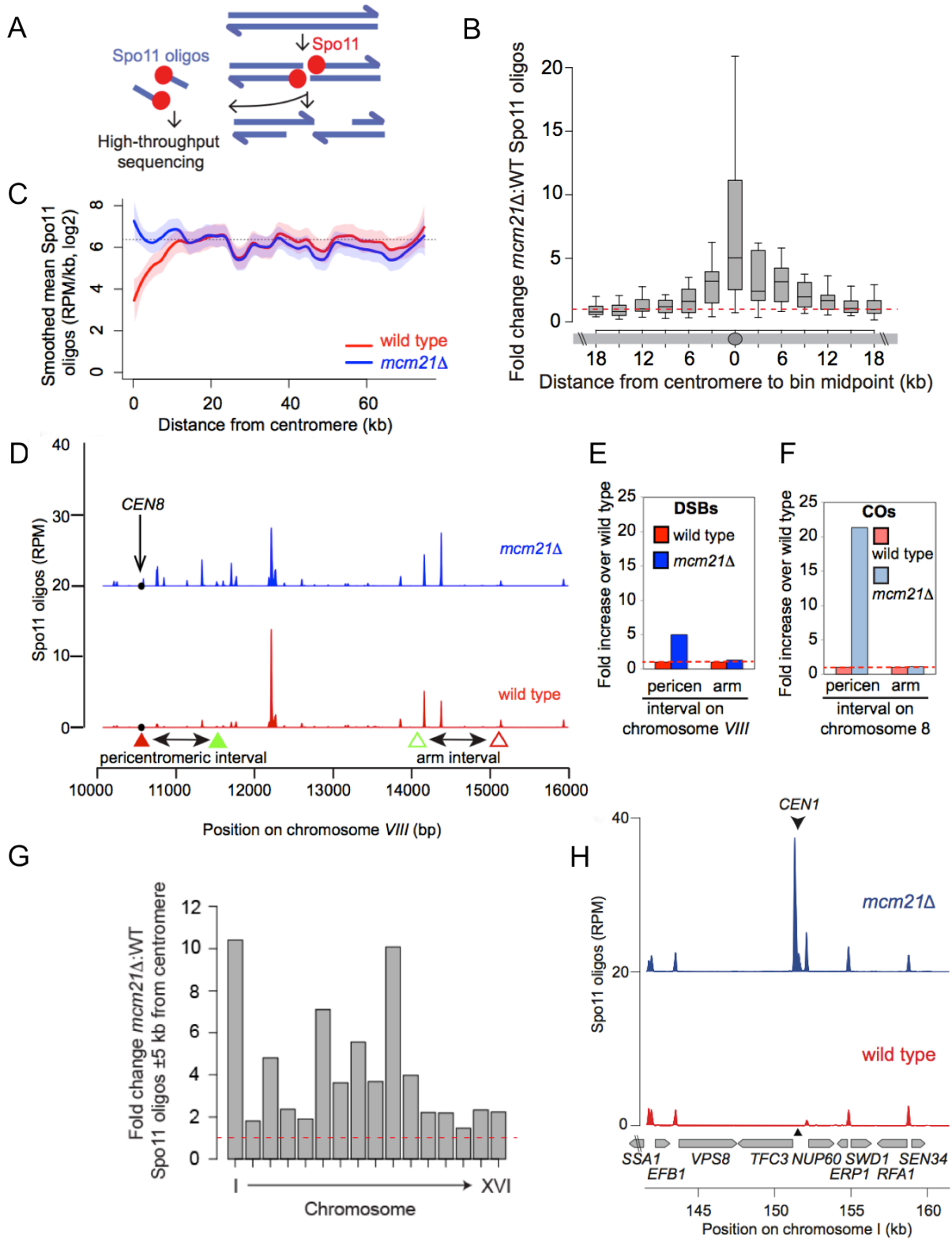

Figure 3-3 The Ctf19-C minimizes meiotic DSB formation at pericentromeres

A) High throughput sequencing of Spo11-oligo complexes was used to detect the genome-wide distribution of meiotic DSBs. B) Fold change of Spo11-oligos surrounding all 16 centromeres in 3kbsegments in *mcm21Δ* cells compared to the wild type. Boxes show median and interquartile range. Red dashed line indicates a fold change of one. C) Smoothed mean of Spo11-oligos in a distance of

Figure 3-3 continued

up to 75kb from the centromere in the wild type (red line) and *mcm21Δ* (blue line) (shading indicates the 95% confidence interval). Spo11-oligo density was measured within 500bp bins starting from the centromere across the 32 chromosome arms. The horizontal dotted line represents the genome average. D) DSB formation in the intervals on chromosome *VIII* analyzed in the live cell reporter assay (Figure 3-1 D, E). Spo11 oligo counts smoothed with a 201 bp window are shown. The black circle represents the centromere. The filled triangles indicate the midpoints of coordinates where RFP (red) and GFP (green) reporters were integrated for the *CEN8*-proximal analysis by the live cell reporter assay. The open triangles indicate the positions of the reporters integrated for the chromosome arm *VIII* analysis. E and F) Fold change in the number of DSBs (E) and COs (F) in the same (pericentromere and arm) intervals used for the live cell reporter assay (Figure 3-1 D, E) in wild type and *mcm21Δ* cells. G) Whole-chromosome view of the change of Spo11-oligos in *mcm21Δ* vs. wild type in 5kb bins from the centromere of all 16 chromosomes. Red dashed line, fold change of one. H) Zoom-in of the fold change of Spo11-oligo density (reads per million mapped (RPM) per kb) close to the centromere on chromosome *I* in *mcm21Δ* (blue) and wild type (red). Below wild type, chromosomal organization of the genes on chromosome *I.* Triangle indicates the position of the centromere (*CEN1*).
Experiments shown in A-H were performed by Scott Keeney and colleagues; modified from Vincenten et al., 2015.

areas). The pericentromeric region on chromosome *I*, in particular, manifested the strongest effect on DSB formation in *mcm21Δ* cells compared to the wild type (Figure 3-3 D-E). This strong break hotspot was detected in the divergent promoter region of the genes *TFC3* and *NUP60* (Figure 3-3 E; Vincenten et al., 2015). Indeed, DSB hotspots are often found in divergent promoter regions (Blitzblau et al., 2007; Pan et al., 2011).

Data from Spo11-oligo complex sequencing in cells lacking Mcm21, performed by Scott Keeney and colleagues, are in accord with earlier studies that were conducted in our laboratory. We used established microarray analysis (Blitzblau et al., 2007) to specifically measure Spo11-dependent DSBs by detecting single-stranded DNA that naturally accumulates at DSB sites. For microarray analysis, we used a temperature-sensitive mutant of Ndc10 (*ndc10-1*), an essential kinetochore component of the yeast-specific Cbf3 complex. Cells carrying *ndc10-1* exhibit increased chromosome segregation defects (Goh and Kilmartin, 1993). The severe phenotype of *ndc10-1* is thought to reflect impaired kinetochore assembly as no kinetochore components can associate with centromeric DNA in the absence of the Cbf3 complex (Gardner et al.,2001; Goh and Kilmartin, 1993). We found a genome-wide increase of DSB

formation within pericentromeres at 34°C in *ndc10-1* cells compared to the wild type when assessed by microarray analysis (Figure 7-1 A). In agreement with the strong break hotspot close to the centromere on chromosome *I* in *mcm21Δ* cells (Figure 3-3 D-E), we also detected the highest peaks of single-stranded DNA and thus meiotic DSBs in the centromere-proximal region on chromosome *I* in *ndc10-1* cells by microarray analysis (Figure 7-1 B).

3.3 *CEN1*-proximal DSB formation is reduced by the Ctf19-C

To examine a role for additional components of the Ctf19-C in controlling pericentromeric DSB formation, we systematically tested the effect of deletion mutants of non-essential components of the sub-assemblies COMA (Mcm21 and Ctf19), Iml3-Chl4, Ctf3 (Ctf3-Mcm16-Mcm22) and Nkp1-Nkp2 as well as Cnn1 on DSB formation by Southern blot analysis. For Southern blotting, cells were induced to synchronously undergo meiosis and collected at different time points. Total genomic DNA of the cells was isolated, digested with appropriate restriction enzymes and separated according to size by gel electrophoresis. The separated DNA molecules were transferred to a membrane and hybridized with radioactively labeled probes. We used a probe that specifically hybridizes within the centromere-proximal region on chromosome *I* (*CEN1*) (Figure 3-4 B) as we found the strongest effect on DSB formation at this region in *mcm21Δ* (Figure 3-3 E) and *ndc10-1* (Figure 7-1 B) cells. As a positive control for DSB formation, we utilized a probe that hybridizes at the prominent DSB hotspot *YCR047c* on chromosome *III* (Baudat and Nicolas, 1997). For Southern blot analyses, we employed yeast strains that are deleted for the gene *DMC1* (*i.e*. *dmc1Δ* cells). The gene *DMC1* encodes a meiosis-specific recombinase required for DSB repair (Bishop et al., 1992). A deletion of *DMC1* leads to the accumulation, hyperresection and persistence of DSBs and arrest of the meiotic program at prophase I (Bishop et al., 1992; Masson and West, 2001). Thus, meiotic DSBs are permanently detectable upon their formation in cells deleted for *DMC1* via Southern blot analysis. Blitzblau et al. (2007) revealed that a deletion of *DMC1* generally does not affect DSB patterns when assessed by genome-wide microarray analysis.

First, we examined DSB formation at *CEN1* in *ndc10-1* cells by Southern blotting to confirm the appearance of the strong DSB hotspot in the direct vicinity of the centromere on chromosome *I,* which we found through microarray analysis (Figure 7-1 B). Indeed, Southern blot analysis revealed elevated *CEN1*-proximal DSB

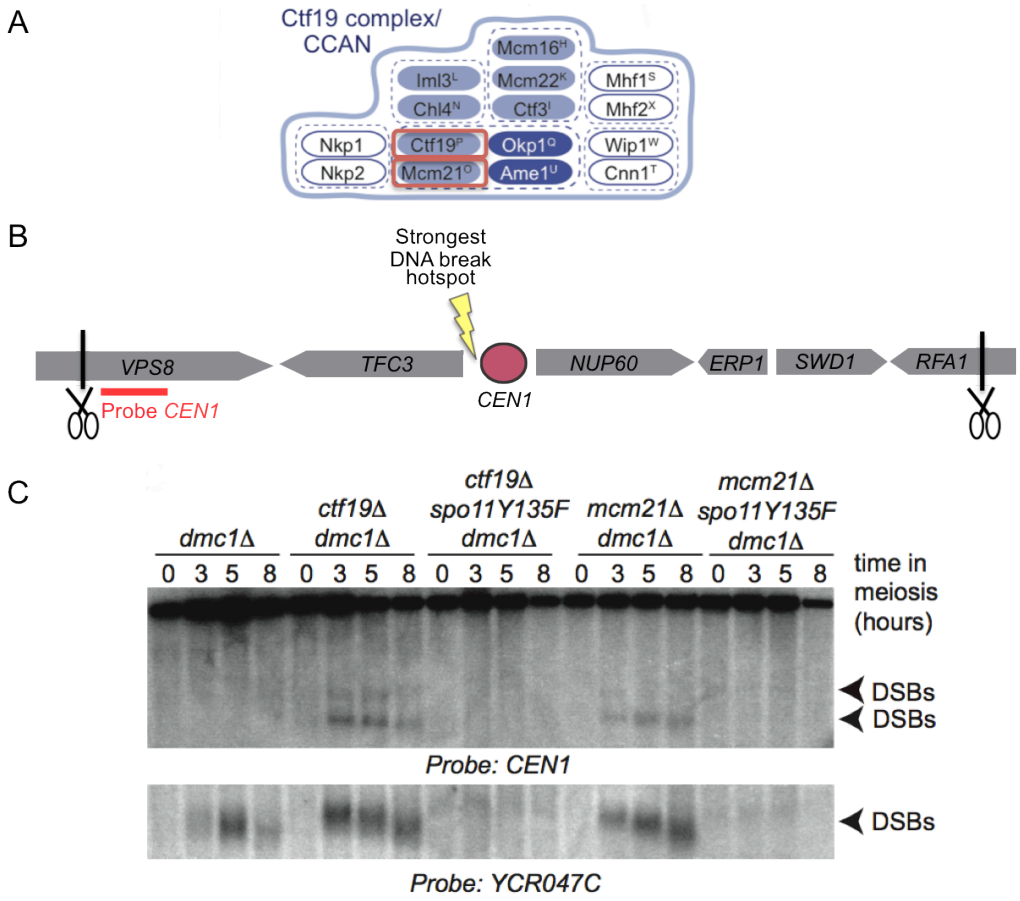

Figure 3-4 The COMA components Ctf19 and Mcm21 minimize Spo11-dependent DSB formation at *CEN1*.

A) The COMA proteins Ctf19 and Mcm21 (highlighted in red) were tested for a role in controlling centromere-proximal DNA break formation. B) Illustration of the chromosomal organization (genes and centromere position) of the region surrounding the centromere on chromosome *I*. The yellow "lightning" points at the position of the strongest DNA break hotspot based on the data from Spo11-oligo complex sequencing (Figure 3-3 E). Scissors indicate restriction sites. Radioactively labeled probe *CEN1* hybridizes at gene *VPS8* in close proximity to the break hotspot. C) DNA breakage close to *CEN1* in cells lacking either Ctf19 (*ctf19Δ*) or Mcm21 (*mcm21Δ*) was monitored by conventional Southern blot analysis. *CEN1*-proximal DSB formation in *ctf19Δ* and *mcm21Δ* cells was analyzed for dependency on Spo11 activity (*ctf19Δ spo11Y135F* and *mcm21Δ spo11Y135F*). Cells carrying the background mutation *dmc1Δ* accumulate meiotic DNA breaks allowing their detection via Southern blot analysis. DSBs were analyzed at *CEN1* and the control hotspot *YCR047c*. Cells were induced to synchronously undergo meiosis and harvested at time points 0, 3, 5 and 8 hours after induction. Arrowheads indicate the position of DSB formation.

formation at 34°C in *ndc10-1* cells compared to the wild type (Figure 7-1 C). DNA breaks were detectable 3, 5 and 8 hours after *ndc10-1* cells were induced to synchronously undergo meiosis. We then analyzed meiotic DSB formation at *CEN1* in cells lacking the COMA components Ctf19 and Mcm21 (Figure 3-4 A). By Southern blot analysis, we found increased levels of *CEN1*-proximal DNA breaks at time points 3, 5 and 8 hours in *ctf19Δ* and *mcm21Δ* cells relative to the wild type (Figure 3-4 C). To assess whether the increase in *CEN1*-proximal DSB formation in *ctf19Δ and mcm21Δ* cells was dependent on the activity of the enzyme Spo11, we examined the effect of the double mutants *ctf19Δ spo11Y135F* and *mcm21Δ spo11Y135F* on meiotic DNA breakage. The *spo11Y135F* mutant is a catalytic inactive form of Spo11 (Bergerat et al., 1997). Indeed, DNA breaks were undetectable at *CEN1* (and the control hotspot *YCR047c*) in *ctf19Δ spo11Y135F* and *mcm21Δ spo11Y135F* cells when assessed by Southern blot analysis (Figure 3-4 C). This result confirms the dependency of Spo11 activity on DSB formation in cells lacking Ctf19 and Mcm21 (Figure 3-4 C). The Spo11-dependent increase in DSB formation at *CEN1* in cells lacking Mcm21 is in agreement with the sequencing data of the Spo11-oligo complexes (Figure 3-3 D, E). Based on these findings, we conclude that the COMA components Ctf19 and Mcm21 are required to reduce Spo11-dependent DSB formation at *CEN1*.

Next, we investigated whether the Iml3-Chl4 sub-complex influences the formation of pericentromeric DNA breaks (Figure 3-5 A). Recent biochemical analyses demonstrated that the Iml3-Chl4 sub-complex only associates with the COMA component Ame1 when the proteins Ctf19 and Mcm21 are present (Pekgöz Altunkaya et al., 2016). Moreover, fluorescence microscopy studies of living mitotically cycling cells showed that Iml3 and Chl4 localize to centromeres in a manner depend on the Ctf19-Mcm21 binding motif in Okp1 (Schmitzberger et al., 2017). Thus, the assembly of the Iml3-Chl4 sub-complex onto centromeres requires the presence of COMA components. For this study, we induced cells lacking Iml3 and Chl4 to synchronously undergo meiosis and analyzed meiotic DSB profiles near *CEN1* by Southern blotting. We observed enhanced *CEN1*-proximal DSB formation in *iml3Δ* and *chl4Δ* cells compared to the wild type (Figure 3-5 B). These findings demonstrate that the Iml3-Chl4 sub-complex prevents centromere-proximal DSB formation.

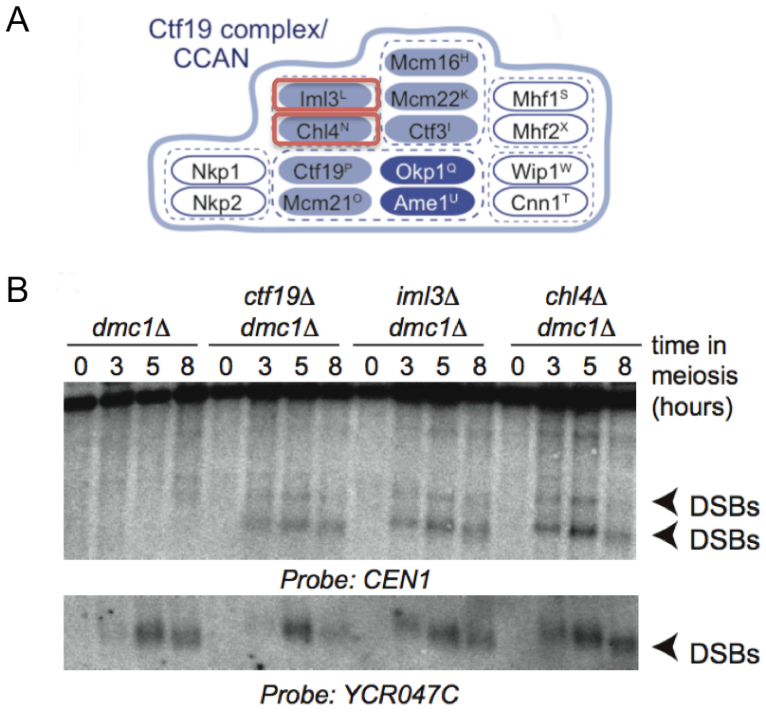

Figure 3-5 The Iml3-Chl4 sub-complex prevents *CEN1*-proximal DSB formation.

A) The proteins Iml3 and Chl4 (highlighted in red) were analyzed in affecting the formation of pericentromeric DSBs. B) Meiotic DSB profiles at *CEN1* and *YCR047c* were analyzed in wild type, *ctf19Δ* (positive control), *iml3Δ* and *chl4Δ* cells. Yeast cells with unrepaired DNA breaks (*dmc1Δ*) were collected after 0, 3, 5 and 8 hours after induction of meiosis. Triangles point at the chromosomal position with increased DNA breakage.

We then examined whether the proteins Ctf3, Mcm16 and Mcm22 of the Ctf3 sub-complex affect centromere-proximal DSB profiles (Figure 3-6 A). It was shown that the association of the Ctf3 sub-complex with Ame1 as bait depends on the presence of the Ctf19-Mcm21 heterodimer and the Iml3-Chl4 sub-complex in soluble extracts (Pekgöz Altunkaya et al., 2016). Live cell fluorescence microscopy studies revealed that mitotic centromere localization of the proteins Ctf3, Mcm16 and Mcm22 does not depend on the Ctf19-Mcm21 binding motif in Okp1 and thus on Ctf19-Mcm21and Iml3-Chl4 (Schmitzberger et al., 2017). In this study, we found increased DSB formation at *CEN1* in *ctf3Δ* cells relative to the wild type (Figure 3-6 B). By contrast, we were unable to observe *CEN1*-proximal DSB formation in the *ctf3Δ spo11Y135F* double mutant. These findings indicate that increased DSB formation at *CEN1* in *ctf3Δ* cells is dependent on Spo11 activity. Furthermore, we detected an elevation in DSB formation at *CEN1* in cells lacking the proteins Mcm16 and Mcm22 when

compared to the wild type (Figure 3-6 C). These results reveal that the Ctf3 sub-complex suppresses *CEN1*-proximal DSB formation.

We next tested whether the Ctf19-C protein Cnn1 plays a role in controlling pericentromeric DNA break formation (Figure 3-7 A). Cnn1 is recruited to centromeres in a manner dependent on the Ctf3 sub-complex (Pekgöz Altunkaya et al., 2016). Biochemical reconstitution experiments indicated that Cnn1 forms a stable assembly with Wip1 and the Ctf3 sub-complex (Pekgöz Altunkaya et al., 2016). By Southern blot analysis, we were unable to detect *CEN1*-proximal DSB formation in cells lacking Cnn1 (Figure 3-7 B). This result demonstrates that Cnn1 is not required for pericentromeric DSB control. Moreover, we examined whether the Ctf19-C members Nkp1 and Nkp2 control meiotic DSB formation (Figure 3-7 A). It was recently shown that the association of Nkp1-Nkp2 with the Ctf19-C depends on Ame1-Okp1 (Schmitzberger et al., 2017). Southern blot analysis revealed no detectable changes in *CEN1*-proximal DSB formation in cells lacking Nkp1 and Nkp2 relative to the wild type (Figure 3-7 C), suggesting that Nkp1-Nkp2 are not involved in controlling pericentromeric DSB formation.

In summary, the findings described here in this section reveal that the COMA components Ctf19 and Mcm21, the Iml3-Chl4 sub-complex and the Ctf3 sub-assembly play a role in controlling pericentromeric DSB formation. By contrast, the Ctf19-C components Cnn1, Nkp1 and Nkp2 are dispensable for DSB control (Figure 3-7 D).

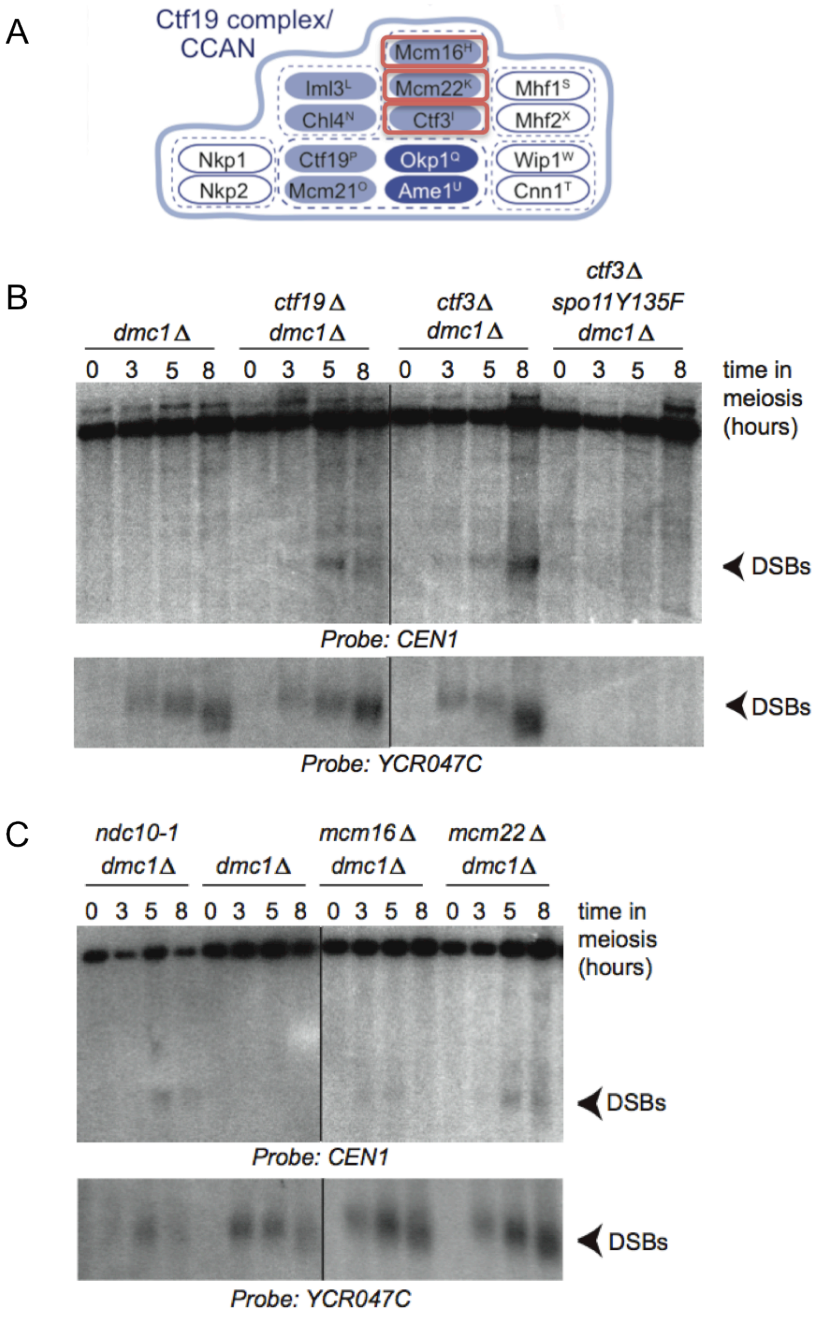

Figure 3-6 The Ctf3 sub-complex reduces levels of *CEN1*-proximal DSBs

A) Deletion mutants of the non-essential components Ctf3, Mcm16 and Mcm22, highlighted in red, of the Ctf3 complex were used for Southern blot analysis shown in B) and C). B-C) DSB patterns in close proximity to *CEN1* and the DNA break hotspot *YCR047c* were detected at appropriate time points in a wild type yeast strain and in cells lacking the genes *CTF19* (positive control), *CTF3* (B), *MCM16* and *MCM22* (C). A double mutant of *ctf3Δ spo11Y135F* was tested for Spo11-dependent *CEN1*-proximal DSB formation in B). The temperature-sensitive mutant *ndc10-1* served as a positive control in C).

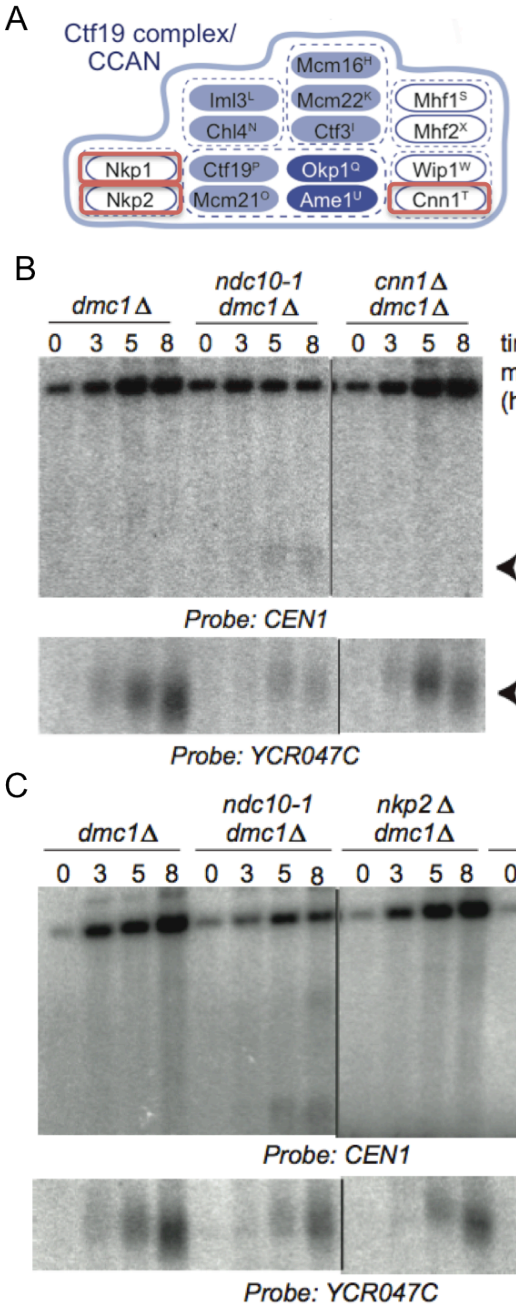

D

kinetochore component (allele)	DSB at *CEN1*
ndc10-1	Yes
ctf19Δ	Yes
mcm21Δ	Yes
chl4Δ	Yes
iml3Δ	Yes
nkp1Δ	No
nkp2Δ	No
cnn1Δ	No
ctf3Δ	Yes
mcm16Δ	Yes
mcm22Δ	Yes

Figure 3-7 Neither Cnn1 nor the Nkp1-Nkp2 complex affect DSB formation at *CEN1*

A) The Ctf19-C proteins Cnn1, Nkp1 and Nkp2 were tested for a role in controlling meiotic *CEN1*-proximal DNA break formation. B-C) Wild type, *ndc10-1*, *cnn1Δ, nkp1Δ* and *nkp2Δ* cells were collected after 0, 3, 5 and 8 hours in the meiotic program and analyzed for DSB formation at *CEN1* by Southern blotting. DNA breakage was also monitored at the control hotspot *YCR047c*. Arrow heads indicate the region of DNA break formation. D) Summary of all tested Ctf19-C components in meiotic DSB formation at *CEN1* by Southern blot analysis.

3.4 The Mtw1-C plays a role in controlling pericentromeric DSB formation

For this study, we also aimed to investigate whether there is a role for the kinetochore component Mtw1-C in controlling homologous recombination at pericentromeres. Together with the Ctf19-C, the Mtw1-C is assembled onto centromeres when recombination events occur in meiotic G2/ prophase I, while other kinetochore members such as the Ndc80/ Dam1 complexes are absent from centromeres upon meiotic entry (Meyer et al., 2015; Miller et al., 2012). Recent biochemical and genetic experiments showed that the Mtw1-C incorporates into kinetochores via direct binding to Mif2 and the COMA protein Ame1 (Hornung et al., 2014). To gain more insights into the assembly of the Mtw1-C and Ctf19-C onto centromeres, Adèle Marston and colleagues performed chromatin immunoprecipitation (ChIP) coupled to quantitative real-time PCR (qPCR) to analyze the association of the Mtw1-C subunit Dsn1 with a centromeric region and, as a negative control, a chromosomal arm region in prophase I arrested *mcm21Δ* and wild type cells (Figure 3-8 B; Vincenten et al., 2015). They found that the signal of Dsn1 (C-terminally fused to Flag) at the centromere on chromosome *IV* (*CEN4*) is reduced by approximately 50% in cells lacking Mcm21 when compared to the wild type. As expected, no signal of Dsn1-Flag was observed on the chromosome arm (arm1) in *mcm21Δ* and wild type cells. These results suggest that the Ctf19-C protein Mcm21 is required for proper levels of Dsn1 at the centromere during prophase I. In addition, Adèle Marston and colleagues determined levels of Mcm21 enrichment at *CEN4* cells depleted for the Mtw1-C components Dsn1 and Mtw1 and the wild type (Figure 3-8 C). Because the Mtw1-C is essential for cell viability, we employed yeast strains containing the meiosis-specific depletion alleles *pCLB2-3HA-DSN1* and *pCLB2-3HA-MTW1* for this work (Figure 3-8 A). In these strains, the genes *DSN1* and *MTW1* were placed under the control of the promoter of *CLB2* (*pCLB2*) (Lee and Amon, 2003), which is active only during mitotic growth (Grandin and Reed, 1993). ChIP-qPCR analysis revealed no significant changes in the accumulation of Mcm21 (C-terminally fused to GFP) at *CEN4* in *pCLB2-3HA-DSN1* cells relative to the wild type (Figure 3-8 C). However, an increase in the Mcm21-GFP localization at *CEN4* was observed in *pCLB2-3HA-MTW1* cells. These findings indicate that the Mtw1-C partially affects levels of Mcm21 at the centromere during prophase I.

Unfortunately, we were unable to examine the requirement for the Mtw1-C in pericentromeric CO recombination, because *pCLB2-3HA-MTW1 and pCLB2-3HA-*

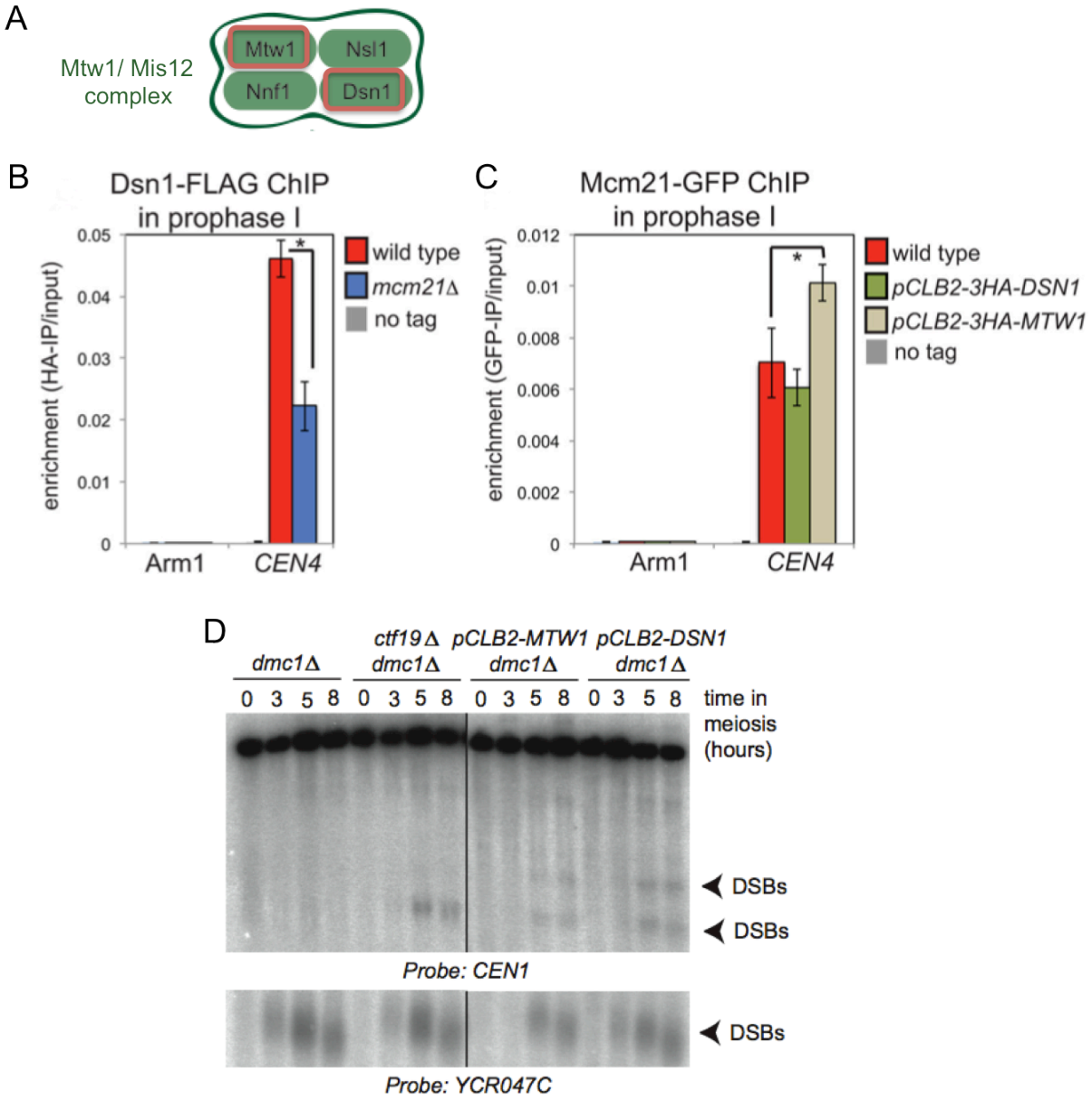

Figure 3-8 The Mtw1-C partially depends on the Ctf19-C and reduces *CEN1*-proximal DSB formation

A) Meiosis-specific depletion alleles of the conserved components Mtw1 and Dsn1 of the Mtw1-C (highlighted in red) were employed for ChIP analysis coupled to qPCR (C) and Southern blot analysis (D). B) The Ctf19-C component Mcm21 has an effect on the enrichment of the Mtw1-C protein Dsn1 at *CEN4* in meiosis. Wild type (*DSN1-6HIS-3FLAG, ndt80Δ*), *mcm21Δ* (*DSN1-6HIS-3FLAG, mcm21Δ, ndt80Δ*) and no tag cells (*DSN1, ndt80Δ*) were induced to undergo meiosis and arrested at prophase I. Cells were collected 5 hours after induction and Dsn1 levels were analyzed at *CEN4* and a chromosomal arm region (arm1 as negative control) by ChIP-qPCR. C) Effect of depleting the Mtw1-C subunit Mtw1 and Dsn1 on Mcm21 levels at *CEN4*. Wild type (*MCM21-yeGFP, ndt80Δ*), *pCLB2-3HA-MTW1* (*pCLB2-3HA-MTW1, MCM21-yeGFP, ndt80Δ*), *pCLB2-3HA-DSN1* (*pCLB2-3HA-DSN1,*

Figure 3-8 continued

MCM21-yeGFP, *ndt80Δ*) and no tag cells (*MCM21, ndt80Δ*) were harvested 5 hours in the meiotic program. Levels of Mcm21 at *CEN4* and a chromosome arm (arm1 as negative control) were determined by ChIP-qPCR. D) Southern blot analysis of meiotic DNA break formation in wild type, *ctf19Δ*, *pCLB2-3HA-MTW1* and *pCLB2-3HA-DSN1* cells. These cells are insufficient to repair accumulated DSBs as they carry a deletion of *DMC1* (*dmc1Δ*). Radioactively labeled probes were used to specifically anneal at either *CEN1* or *YCR047c*. Yeast strains were induced to synchronously undergo meiosis and collected at 0, 3, 5 and 8 hours after induction. Arrowheads indicate the position of meiotic DNA breakage.
ChIP, chromatin immunoprecipitation; qPCR, quantitative polymerase chain reaction. Experiments shown in (B) and (C) were conducted by Adèle Marston and colleagues; modified from Vincenten et al., 2015.

DSN1 cells did not accurately execute the meiotic divisions and tetrad formation (Vincenten et al., 2015). Alternatively, we induced *pCLB2-3HA-MTW1 and pCLB2-3HA-DSN1* cells to synchronously undergo meiosis and arrested the cells in prophase I to analyze meiotic DSB formation by Southern blotting. We observed increased *CEN1*-proximal DSB formation in *pCLB2-3HA-MTW1 and pCLB2-3HA-DSN1* cells relative to the wild type (Figure 3-8 C). These findings indicate that the Mtw1-C plays a role in controlling pericentromeric DSB formation.

3.5 The Ctf19-C regulates meiotic DSB formation and CO recombination at pericentromeres through independent mechanisms

In section 3.1, we uncovered a novel role for the Ctf19-C in controlling meiotic CO recombination at pericentromeres. We showed that the Ctf19-C partially suppresses pericentromeric CO recombination by reducing the initiating event of meiotic recombination, DSB formation (sections 3.2-3.3). Intriguingly, the Ctf19-C controls DSB formation over a narrower domain of ~6 kb surrounding centromeres (section 3.2) and CO recombination within a broader region of ~40 kb of centromeres (section 3.1), although the binding of the Ctf19-C is restricted to the 125 bp point centromere in budding yeast. Thus, the Ctf19-C controls DSBs within chromosomal regions 50 times larger than that occupied by the centromere and CO recombination at regions 320 times larger. This raised the question of how does the Ctf19-C control meiotic DSB formation and recombination over such distances. One possibility is that the Ctf19-C controls factors located at centromere-proximal regions to reduce both levels of DSB formation and CO recombination. This idea is supported by studies demonstrating that the Ctf19-C enables the recruitment of factors, such as the conserved multi-subunit cohesin complex, to pericentromeres required for faithful chromosome segregation (Eckert et al., 2007; Fernius and Marston, 2009; Fernius et al., 2013; Hinshaw et al., 2015, 2017; Kogut et al., 2009; Ng et al., 2009). In the following sections (3.5.1- 3.5.5), we focused on factors located within centromere-proximal regions and analyzed the effect of mutating these factors on DSB formation and CO recombination.

3.5.1 The Ctf19-C controls meiotic DSB formation regardless of its role in promoting pericentromeric Rec8-cohesin enrichment

To analyze whether the Ctf19-C minimizes meiotic DSB formation by controlling factors located within pericentromeric regions, we first focused on the multi-subunit cohesin complex. In budding yeast, cohesin complexes are highly enriched within ~20-50 kb regions surrounding centromeres when compared to chromosomal arms (Glynn et al., 2004; Lengronne et al., 2006; Weber et al., 2004). It was shown that the Ctf19-C enables the enrichment of pericentromeric cohesin complexes by recruiting the Scc2-Scc4 loader complex to centromeres in late G1 (Eckert et al., 2007; Fernius and Marston, 2009; Fernius et al., 2013; Hinshaw et al., 2015, 2017; Kogut et al., 2009; Ng et al., 2009). It is thought that the Scc2-Scc4 complex facilitates the loading

of cohesin proteins at the centromere, which then spread bidirectionally into the surrounding pericentromere (Fernius et al., 2009). Cohesin complexes were implicated in playing a dual role along chromosomes. One role of cohesin complexes is to mediate inter-molecular contacts to establish robust sister chromatid cohesion, a process coupled to DNA replication in S phase (Lengronne et al., 2006; Nasmyth, 2001; Uhlmann and Nasmyth, 1998). Studies revealed that deleting any of several Ctf19-C components leads to impaired centromeric cohesion and chromosome mis-segregation (Eckert et al., 2007; Fernius and Marston, 2009; Hu et al., 2011; Ng et al., 2009). Another role of cohesin complexes is to operate intra-molecular contacts to juxtapose distant DNA fragments, thereby forming DNA loops (Fudenberg et al., 2016; Barrington et al., 2017; Gassler et al., 2017; Schalbetter et al., 2016).

Adèle Marston and colleagues found that the enrichment of cohesin complexes containing the meiosis-specific subunit Rec8 at centromeric and pericentromeric regions in prophase I arrested cells also depends on a functional Ctf19-C when assessed by ChIP analysis coupled to genome-wide sequencing (Vincenten et al., 2015). These findings raised the question of whether pericentromeric Rec8-cohesin establishment by the Ctf19-C is involved in controlling meiotic DSB formation. To test this possibility, we analyzed the effect of deleting the meiosis-specific cohesin subunit Rec8 (*rec8Δ*) on DSB formation at the *CEN1*-proximal region by Southern blotting. We observed no detectable changes in DSB profiles at *CEN1* in *rec8Δ* cells compared to the wild type (Figure 3-9). By contrast, we found increased levels of DSB formation at *CEN1* in cells lacking both Rec8 and the Ctf19-C component Mcm21 (*rec8Δ mcm21Δ*). These results suggest that the Ctf19-C controls meiotic DSB formation independently of its function in promoting the loading and enrichment of Rec8-cohesin at pericentromeres.

To further examine that the Ctf19-C dependent Rec8-cohesin establishment is dispensable for meiotic DSB control, we uncoupled Ctf19-C function from pericentromeric cohesin enrichment by employing a specific allele of the loader complex subunit Scc4 (*scc4-m35*, Hinshaw et al., 2015). The *scc4-m35* allele was generated by substitution of 5 amino acids (*scc4*$^{F324A;\ K327A;\ K331A;\ K541A;\ K542A}$) in a conserved patch of Scc4 (Hinshaw et al., 2015). In mitotic cells, the *scc4-m35* mutation impairs the localization of Scc2 to centromeres and specifically decreases levels of centromeric and pericentromeric cohesin containing the Scc1 subunit (Hinshaw et al., 2015). In meiotic cells, the *scc4-m35* mutation reduces both levels at

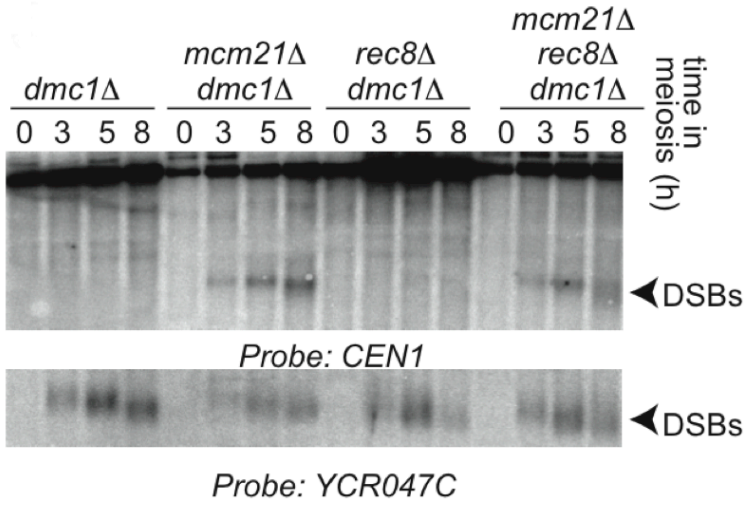

Figure 3-9 Loss of the meiosis-specific cohesin subunit Rec8 does not affect DSBs at *CEN1*

Detection of *CEN1*-proximal DSB formation in *mcmc21Δ, rec8Δ and mcm21Δ rec8Δ* cells. The background mutation *dmc1Δ* was used to accumulate DNA breaks, allowing their detection by Southern blot analysis. The DSB hotspot *YCR047c* serves as positive control. Cells synchronously entered the meiotic program and were collected at time points 0, 3, 5, and 8 hours. Arrowheads point at DSB positions.

centromeric/ pericentromeric regions and chromosome arms (Vincenten et al., 2015). Thus, utilizing the *scc4-m35* allele allows us to analyze the effect of preventing the loading and enrichment of Rec8-cohesin complexes at pericentromeres (and arms) without impairing Ctf19-C function on meiotic DSB formation. By Southern blot analysis, we found no detectable changes in *CEN1*-proximal DSB patterns in *scc4-m35* cells when compared to the wild type (Figure 3-10). This finding demonstrates that Rec8-cohesin is not implicated in meiotic DSB control at the pericentromere.

To provide more evidence that Rec8-cohesin is not involved in controlling meiotic DSB formation, we applied the anchor-away system to functionally deplete the Ctf19-C component Ctf19 from the nucleus by binding it to a receptor protein localized in the cytoplasm (Haruki et al., 2008). In this approach, a fusion protein of Ctf19 coupled to the human Frb domain and GFP (Ctf19-Frb-GFP) served as the target for a receptor protein, which is composed of the ribosomal subunit Rpl13A and the human FKBP12 domain (Rpl13A-2xFKBP12). Adding rapamycin to the cells enables functional depletion of Ctf19 from the nucleus of a cell as target and receptor proteins with rapamycin form a tight ternary complex when the ribosomal flow goes through the nucleus (Figure 3-11 A). Utilizing the anchor-away system allows us to

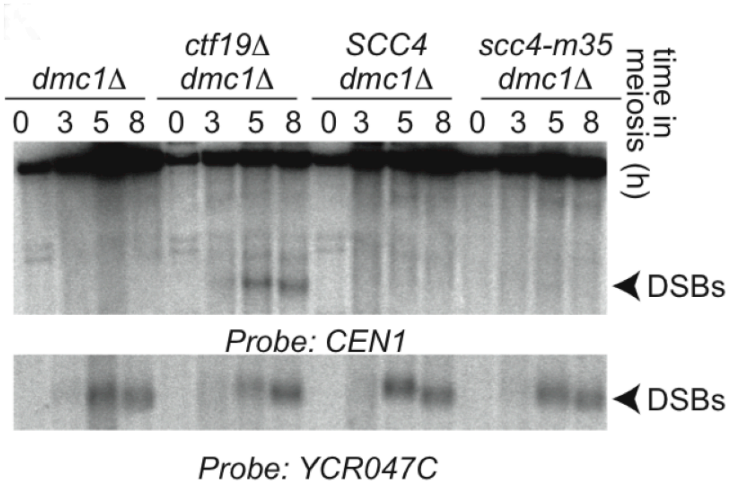

Figure 3-10 Preventing pericentromeric Rec8-cohesin enrichment without impairing Ctf19-C function through the *scc4-m35* mutant does not affect *CEN1*-proximal DSBs.

The mutant of *scc4-m35,* which specifically prevents centromere-proximal cohesin establishment (Hinshaw et al., 2015; Vincenten et al., 2015), was employed to study the effect on *CEN1*-DNA breakage after 0, 3, 5 and 8 hours in meiosis by Southern blot analysis. Additionally, DSB formation was also monitored in the strains wild type and *ctf19Δ* as well as a control *SCC4* replacement strain. As a DSB control hotspot, a radioactively labeled probe that anneals at *YCR047c* was used. Arrowheads indicate meiosis-specific broken DNA fragments.

examine the effect of uncoupling Ctf19-C function from pericentromeric Rec8-cohesin enrichment via timed addition of rapamycin on meiotic DSB formation.

We first performed a yeast cell growth assay with six fold serial dilutions of cells spotted on solid YPD medium supplemented with or without rapamycin (concentration: 10 ug/ml) to test the functional and conditional depletion of Ctf19-Frb-GFP. We combined a strain carrying *CTF19-FRB-GFP, RPL13A-2xFKBP12, tor1-1, fpr1Δ* with a deletion of the spindle assembly checkpoint component Mad2 (*mad2Δ*) to induce synthetic lethality when grown on solid YPD medium containing rapamycin (Pangilinan and Spencer, 1996; Wang and Burke, 1995). Synthetic lethality between two mutants occurs when either mutation individually generates viable cells but both mutations together cause compromised growth or lethality of the cells (Daniel et al., 2006). Although neither *CTF19* nor *MAD2* is essential for cell viability, mutations in these genes increase the rate of chromosome loss (Li and Murray, 1991; Ortiz et al., 1999). Hence, we expect that cells depleted for Ctf19-Frb-GFP via the anchor away system are either compromised in growth or inviable when combined with a deletion of *MAD2*. Indeed,

we observed inviability of cells containing *CTF19-FRB-GFP, RPL13A-2xFKBP12, tor1-1, fpr1Δ, mad2Δ* when spotted on solid YPD medium supplemented with rapamycin, whereas the cells are viable when grown on solid YPD medium without rapamycin (Figure 3-11 B). This observation confirms functional and conditional depletion of Ctf19-Frb-GFP using the anchor away system. The yeast cell growth assay revealed that wild type cells and cells harboring *CTF19-FRB-GFP, RPL13A-2xFKBP12, tor1-1, fpr1Δ* are viable when spotted on solid YPD medium supplemented with and without rapamycin (Figure 3-11 B). As a positive control for this assay, we employed cells containing *ORC2-FRB*, *RPL13A-2xFKBP12, tor1-1, fpr1*. Orc2 is a subunit of the origin recognition complex and required for replication initiation in eukaryotic cells (Bell et al., 1993; Bell, 2002). Cells defective in Orc2 function trigger mitotic cell cycle arrest and loose viability (Bell et al., 1993). Thus, depletion of Orc2 via the anchor away system is lethal to cells. As expected, we observed inviability of *ORC2-FRB*, *RPL13A-2xFKBP12, tor1-1, fpr1Δ* cells when spotted on solid YPD medium supplemented with rapamycin, whereas the cells are viable when spotted on solid YPD medium without rapamycin. In addition to the yeast cell growth assay, we induced Ctf19-Frb-GFP cells and wild type cells to synchronously undergo meiosis when either rapamycin or DMSO was added to the cultures and analyzed sporulation efficiency and spore viability. DMSO was used as a negative control for Ctf19-Frb-GFP depletion. Analyzing the effect of a protein of interest on sporulation efficiency and spore viability when it is absent or mutated gives important insights into the meiotic functions of the protein (Börner and Cha, 2015). Although most proteins of the Ctf19-C are non-essential for cell viability, the Ctf19-C is crucial for faithful chromosome segregation during meiosis and thus for the generation of viable spores (Marston et al., 2004; Mehta et al., 2014). Hence, we expect that depletion of Ctf19-Frb-GFP via the anchor away system severely affects sporulation efficiency and spore viability. Indeed, we found that levels of sporulation efficiency of *CTF19-FRB-GFP, RPL13A-2xFKBP12, tor1-1, fpr1Δ* cells (31 % tetrads) were reduced in comparison to the wild type (83 % tetrads) when rapamycin was added to the cultures (Figure 3-11 C). By contrast, levels of sporulation efficiency of *CTF19-FRB-GFP, RPL13A-2xFKBP12, tor1-1, fpr1Δ* cells were similar to the wild type when DMSO was added to the cultures (both 92% tetrads). These findings provide more evidence that the anchor away system can be used to functionally and conditionally deplete Ctf19-Frb-GFP. Moreover, spore viability was dramatically

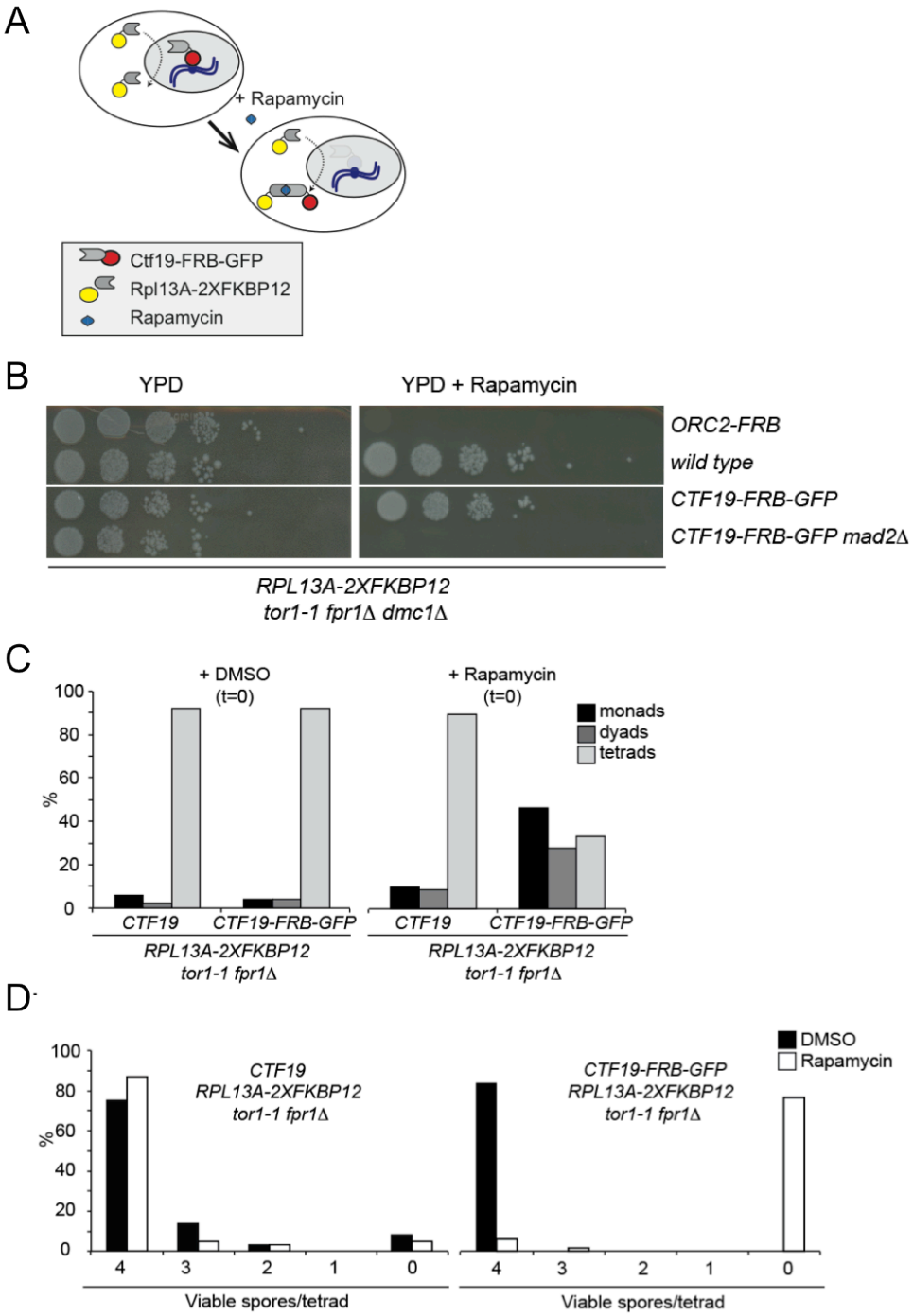

Figure 3-11 The anchor away system enables functional depletion of Ctf19

A) The anchor away system allows functional depletion of a protein of interest localized in the nucleus by tethering to a receptor component localized in the cytoplasm upon addition of rapamycin (Haruki et al., 2008). B) Yeast cell growth assay with six fold serial dilutions of wild type, *ORC2-FRB*, *CTF19-FRB-GFP* and *CTF19-FRB-GFP mad2Δ* cells, grown on solid YPD medium supplemented with and without rapamycin (10 ug/ml). C) Sporulation efficiency analysis of wild type (*CTF19*, *RPL13A-2xFKBP12, tor1-1, fpr1Δ*) and Ctf19-FRB-GFP (*CTF19-FRB-GFP, RPL13A-2xFKBP12, tor1-1, fpr1Δ*) cells exposed to either DMSO or rapamycin (both added at time point 0 hours). Percentage of monads, dyads and tetrads in these strains was determined. 200 cells per strain and condition (DMSO

Figure 3-11 continued

and rapamycin) were counted. D) Spore viability (in %) of wild type (*CTF19*, *RPL13A-2xFKBP12, tor1-1, fpr1Δ*) and Ctf19-FRB-GFP (*CTF19-FRB-GFP, RPL13A-2xFKBP12, tor1-1, fpr1Δ*) tetrads was investigated. While undergoing meiosis, DMSO or rapamycin was added to the cultures.

decreased in *CTF19-FRB-GFP, RPL13A-2xFKBP12, tor1-1, fpr1Δ* cells as compared to the wild type when rapamycin was added to the cultures (Figure 3-11 D). We found that 88% of tetrads produced from the wild type were composed of four viable spores, whereas only 6% of tetrads originated from *CTF19-FRB-GFP, RPL13A-2xFKBP12, tor1-1, fpr1Δ* cells contained four viable when rapamycin was added to the cultures (Figure 3-11 D). In contrast to this, levels of spore viability of *CTF19-FRB-GFP, RPL13A-2xFKBP12, tor1-1, fpr1Δ* cells and the wild type were comparable when DMSO was added to the cultures. These results confirm functional and conditional depletion of Ctf19-Frb-GFP using the anchor away system in meiotically dividing cells.

We then investigated the effect of uncoupling Ctf19-C function from pericentromeric Rec8-cohesin enrichment on meiotic DSB formation when we “anchored away” the protein Ctf19 before and after pre-meiotic S phase via timed addition of rapamycin. For this, the experimental set-up was the following (Figure 3-12 A): We induced *CTF19-FRB-GFP, RPL13A-2xFKBP12, tor1-1, fpr1Δ* cells to synchronously undergo meiosis and added rapamycin either after 0 hours (before S phase) or after 3 hours (after S phase) to the cultures. As a negative control for Ctf19-Frb-GFP depletion, we added DMSO to another culture 0 hours after *CTF19-FRB-GFP, RPL13A-2xFKBP12, tor1-1, fpr1Δ* cells entered the meiotic program. In addition, we also induced *CTF19*, *RPL13A-2xFKBP12, tor1-1, fpr1Δ, dmc1Δ* cells to synchronously undergo meiosis and added both rapamycin and DMSO after 0 hours to the cultures. To confirm depletion of Ctf19-Frb-GFP upon addition of rapamycin, we performed ChIP analysis coupled to qPCR (Figure 3-12 B). For this, we analyzed the enrichment of Ctf19-Frb-GFP at the centromeric region 4 (*CEN4*) and, as a negative control, at a chromosomal arm region (arm2). We observed significantly decreased levels Ctf19-Frb-GFP enrichment at *CEN4* in cells treated with rapamycin at time points 0 and 3 hours when compared to cells treated with DMSO. As expected, we were unable to observe an accumulation of Ctf19-Frb-GFP at arm2 in cells treated with rapamycin and DMSO. Based on these findings, we conclude that Ctf19-Frb-GFP is depleted

upon addition of rapamycin. Next, we aimed to prevent Ctf19-C dependent pericentromeric Rec8-cohesin establishment by depleting Ctf19-Frb-GFP before pre-meiotic S phase, thereby resembling a *ctf19Δ* mutant (Fernius et al., 2009). It was shown that the Ctf19-C promoted loading and enrichment of pericentromeric cohesin is coupled to late G1/ early S phase (Fernius et al., 2013; Natsume et al., 2013). By ChIP-qPCR analysis, we confirm that depletion of Ctf19-Frb-GFP before S phase mostly impairs the accumulation of centromeric cohesin as levels of the meiosis-specific cohesin subunit Rec8 at *CEN4* were significantly reduced in cells treated with rapamycin at 0 hours when compared to cells treated with DMSO (Figure 3-12 C). We observed that levels of Rec8 accumulation at *CEN4* were increased in Ctf19-Frb-GFP cells treated with rapamycin at 3 hours as compared to cells treated with rapamycin at 0 hours. This observation indicates that depleting Ctf19-Frb-GFP after S phase enables the loading and enrichment of centromeric Rec8-cohesin complexes. However, we noticed that levels of Rec8 accumulation at *CEN4* in Ctf19-Frb-GFP cells treated with rapamycin at 3 hours are reduced compared to Ctf19-Frb-GFP cells treated with DMSO. This result might suggest that depletion of Ctf19-Frb-GFP after S phase enables the loading and enrichment of S phase-associated Rec8-cohesin, which is known to be required for the establishment of robust sister chromatid cohesion. Cohesion establishment between sister chromatids is coupled to DNA replication (Uhlmann and Nasmyth, 1998). Therefore, Rec8-cohesin complexes loaded after S phase were mostly not considered in this analysis. We then performed Southern blot analysis to examine the effect of depleting Ctf19-Frb-GFP before and after S phase on pericentromeric DSB formation. As expected, we found increased levels of DSB formation at *CEN1* in *CTF19-FRB-GFP, RPL13A-2xFKBP12, tor1-1, fpr1Δ* cells and *ctf19Δ* cells when treated with rapamycin at 0 hours compared to *CTF19, RPL13A-2xFKBP12, tor1-1, fpr1Δ* cells (Figure 3-12 D). Quantification analysis showed that meiotic DSB profiles in cells depleted for Ctf19-Frb-GFP at 0 hours were comparable to the timing and intensity of those in *ctf19Δ* cells (Figure 3-12 E). Interestingly, we also detected *CEN1*-proximal DSBs in *CTF19-FRB-GFP, RPL13A-2xFKBP12, tor1-1, fpr1Δ* cells treated with rapamycin at 3 hours (Figure 3-12 D). This result suggests that the Ctf19-C promoted establishment of S phase-associated Rec8-cohesin does not play a role in controlling pericentromeric DSB formation. Flow cytometry analysis confirmed that the DNA content of Ctf19-Frb-GFP cells was doubled (4N) when treated with rapamycin 3 hours after meiotic entry

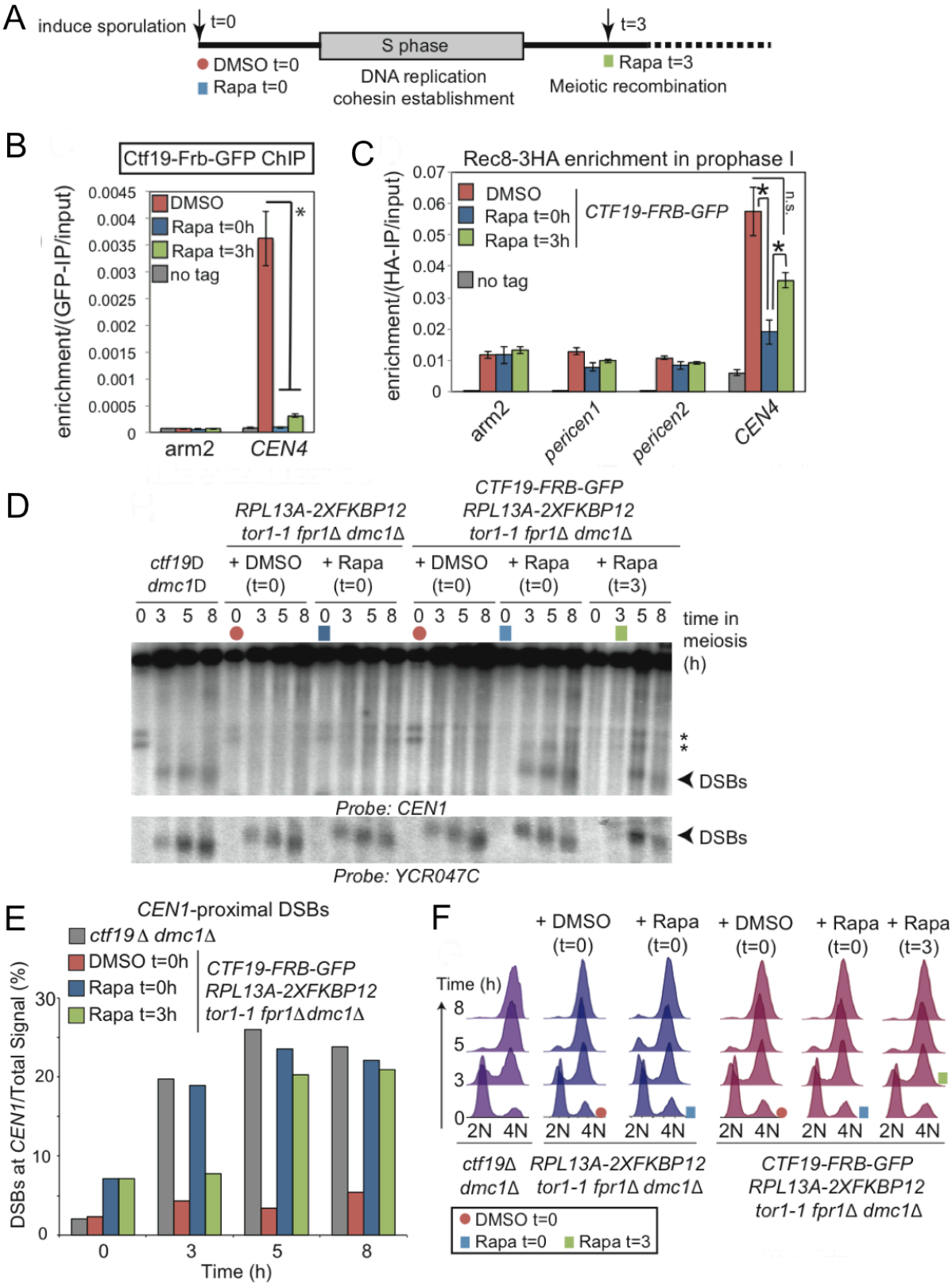

Figure 3-12 The Ctf19-C minimizes DSB formation in a manner independent of Rec8-cohesin establishment in S phase

A) Experimental set-up for the functional depletion of Ctf19-Frb-GFP before (Rapa t=0) and after (Rapa t=3) pre-meiotic S phase. Addition of DMSO (t=0) serves as a negative control. B) Depletion of

Figure 3-12 continued

Ctf19-Frb-GFP from the nucleus after addition of rapamcin (t=0 and t=3) was confirmed byChIP-qPCR analysis. Addition of DMSO at t=0 served as a control as well as a “no tag” strain. Cells used for ChIP-qPCR analysis were arrested in prophase I (*ndt80Δ*) and harvested after 5 hours in meiosis. Primer sets that amplify *CEN4* and a chromosomal arm region (arm2) were used for qPCR. Error bars represent standard error of n=4 biological replicates. *p<0.05, paired t-test. C) Analysis of Rec8-3HA enrichment (in prophase I) at indicated chromosomal sites in three different culutures (addition of DMSO at t=0, rapamycin at t=0 and t=3) of *CTF19-FRB-GFP* cells by anti-HA ChIP-qPCR. Error bars represent standard error of n=4 biological replicates. *p<0.05, paired t-test D) *CEN1*-proximal DSB analysis in *ctf19Δ dmc1Δ*, *CTF19 RPL13A-2xFKBP12 tor1-1 fpr1Δ dmc1Δ* and *CTF19-FRB-GFP, RPL13A-2xFKBP12, tor1-1, fpr1Δ dmc1Δ* cells by Southern blotting. Ctf19-Frb-GFP was anchored away before (Rapa t=0) and after (Rapa t=3) S phase. Addition of DMSO (t=0) serves as negative control. Cells were induced to synchronously undergo meisois and harvested at time points 0, 3, 5 and 8 hours after induction. Arrowheads indicate the position of DNA breakage. E) Quantification analysis of DSBs shown in (D). F) Analysis of the DNA content (2N/ 4N) in *ctf19Δ*, wild type (*CTF19*, *RPL13A-2xFKBP12, tor1-1, fpr1Δ*) and Ctf19-Frb-GFP (*CTF19-FRB-GFP, RPL13A-2xFKBP12, tor1-1, fpr1Δ*) cells by flow cytometry. Samples were taken after 0, 3, 5 and 8 hours after induction of meiosis. Anchoring away Ctf19-Frb-GFP was conducted before (Rapa t=0) and after (Rapa t=3) pre-meiotic S phase. As a control, DMSO was added at time point=0 hours.
ChIP, chromatin immunoprecipitation; qPCR, quantitative polymerase chain reaction. Experiments shown in (B) and (C) were performed by Adèle Marston and colleagues; modified from Vincenten et al., 2015.

(Figure 3-12 F).

Taken together, the results described here suggest that the Ctf19-C controls meiotic DSB formation at pericentromeres independently of its role in promoting the establishment of S phase-associated Rec8-cohesin.

3.5.2 The Ctf19-C mediated establishment of Rec8-cohesin is required to suppress CO recombination at the pericentromere

Our next approach was to test the requirement for the Ctf19-C mediated establishment of Rec8-cohesin in CO suppression at the pericentromere. Although we demonstrated in section 3.5.1 that there is presumably no role for the (S phase-associated) Rec8-cohesin in controlling the initiating event of meiotic homologous recombination, DSB formation, it might be possible that cohesin acts at a step after DSB formation to suppress CO recombination near centromeres. To test this possibility, in collaboration with Adèle Marston and colleagues, we analyzed the effect of preventing Rec8-cohesin establishment without affecting Ctf19-C function on

pericentromeric CO recombination. For this, we measured CO frequency at *CEN8* and, as a control, on chromosomal arm *VIII* in the *scc4-m35* mutant (described in section 3.5.1; Hinshaw and Harrison, 2015) and wild type as well as *SCC4* cells (as controls) using the live cell reporter assay. (The live cell reporter assay has been described in section 3.1.) Interestingly, we found significantly increased levels of *CEN8*-proximal COs in *scc4-m35* cells compared to the wild type and a *SCC4* replacement strain (Figure 3-13 A; Vincenten et al., 2015). Map distance was 2.44 cM in *scc4-m35* cells, whereas map distances were 0.41 cM and 0.49 cM in wild type and *SCC4* cells, respectively. These findings indicate that Rec8-cohesin plays a role in suppressing pericentromeric CO recombination. By contrast, we were unable to observe any significant changes in CO formation within the interval on chromosomal arm *VIII* in *scc4-m35* cells compared to wild type and *SCC4* cells (Figure 3-13 B; Vincenten et al., 2015), indicating that the role of Rec8-cohesin in suppressing CO recombination is specific to the pericentromere.

To provide more evidence that Rec8-cohesin is involved in controlling meiotic CO recombination, we analyzed the effect of depleting the protein Ctf19 before and after pre-meiotic S phase via the anchor away system on pericentromeric CO recombination. (The anchor away system has been described in section 3.5.1.) For this analysis, the same experimental set-up shown in Figure 3-12 A was used. As mentioned in section 3.5.1, Adèle Marston and colleagues found that depletion of Ctf19-Frb-GFP before pre-meiotic S phase (addition of rapamycin at 0 hours) more greatly reduces centromeric Rec8-cohesin levels rather than after pre-meiotic S phase (addition of rapamycin at 3 hours) when analyzed by ChIP-qPCR (Figure 3-12 C; Vincenten et al., 2015). This result suggests that depletion of Ctf19-Frb-GFP after pre-meiotic S phase allows for the Ctf19-C dependent pericentromeric Rec8-cohesin establishment required robust sister chromatid cohesion. Using the live cell reporter assay, we observed increased levels of *CEN8*-proximal COs in Ctf19-Frb-GFP cells treated with rapamycin at 0 hours compared to cells treated with DMSO (Figure 3-13 C; Vincenten et al., 2015). Map distance was 6.36 cM in Ctf19-Frb-GFP cells treated with rapamycin at 0 hours, whereas map distance was only 0.47 cM in Ctf19-Frb-GFP cells treated with DMSO. This observation demonstrates that preventing the Ctf19-C mediated establishment of Rec8-cohesin leads to an increase in pericentromeric CO recombination. On the contrary, the live cell reporter assay revealed only a modest effect on CO levels at *CEN8* in Ctf19-Frb-GFP cells treated

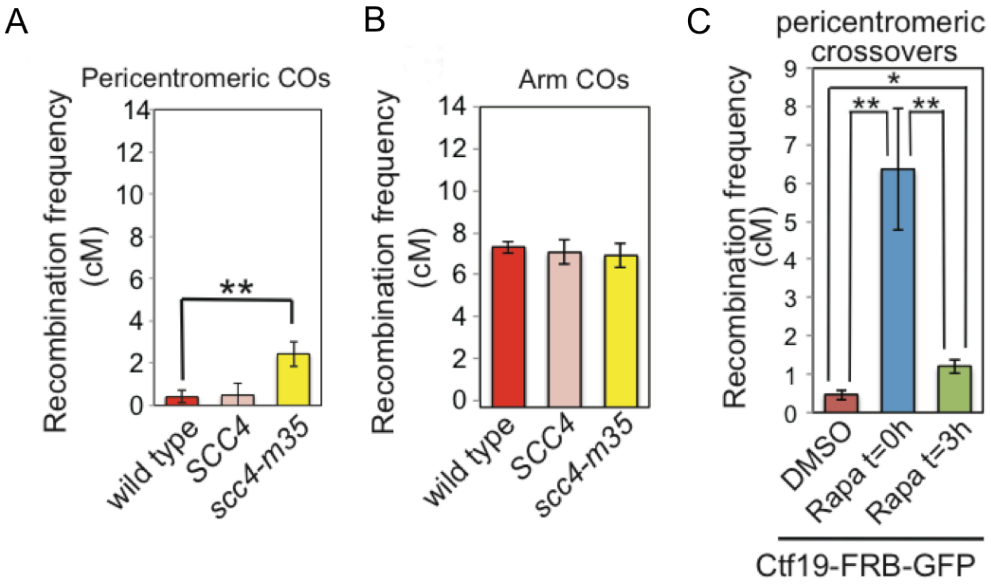

Figure 3-13 Pericentromeric Rec8-cohesin establishment by the Ctf19-C is required to prevent CO recombination

A-B) CO recombination rates, in centiMorgans (cM), at pericentromeric (A) and chromosomal arm (B) intervals in wild type, *SCC4* and *scc4-m35* cells were determined using the live cell reporter assay. The live cell reporter assay has been described in section 3.1. C) Removal of Ctf19-Frb-GFP from the nucleus after pre-meiotic S phase (Rapa t=3) via the anchor away system (described in section 3.5.1). leads only to a modest increase in pericentromeric CO frequency (cM). *CEN8*-proximal CO recombination rates in the "anchor away" strain Ctf19-Frb-GFP were also measured when either DMSO or rapamycin was added before S phase (t=0).
Experiments shown in A-C were conducted by Adèle Marston and colleagues; modified from Vincenten et al., 2015.

with rapamycin at 3 hours (1.2 cM) compared to cells treated with DMSO. This result suggests that the S phase-associated Rec8-cohesin is involved in suppressing pericentromeric CO recombination.

Taken together, the findings described here suggest that the Ctf19-C mediated establishment of Rec8-cohesin is a safeguarding mechanism to channel residual centromere-proximal DSBs towards repair pathways that do not promote CO formation.

3.5.3 Rec8-cohesin establishment by the Ctf19-C directs Zip1 association to suppress pericentromeric CO recombination, but not DSB formation

The major component of the synaptonemal complex, Zip1, localizes to centromeric and pericentromeric regions in a Rec8-dependent manner to mediate homology-independent pairing of homologous chromosomes in early stages of meiosis

(Tsubouchi and Roeder, 2005; Bardhan et al., 2010). Because a requirement for Zip1 in CO control at centromere-proximal regions was demonstrated in earlier studies (Chen et al., 2008), we asked whether pericentromeric cohesin establishment by the Ctf19-C recruits Zip1 to suppress pericentromeric CO recombination. In collaboration with Adèle Marston and colleagues, we showed that levels of Zip1 enrichment were significantly reduced at centromeric and pericentromeric regions (and chromosome arm) in prophase I arrested *scc4-m35* cells compared to the wild type when assessed by ChIP-qPCR (Figure 3-14 A; Vincenten et al., 2015). This confirms that association of Zip1 with core centromeres and pericentromeres (and arms) depends on Rec8-cohesin. Consequently, Zip1 association must also depend on the Ctf19-C since Rec8-cohesin loading and enrichment at pericentromeres requires a functional Ctf19-C (Vincenten et al., 2015). Indeed, levels of Zip1 enrichment were significantly reduced at centromeric and pericentromeric regions in prophase I arrested cells lacking the Ctf19-C components Ctf19, Mcm21, Iml3 and Chl4 compared to the wild type when analyzed by ChIP-qPCR (Figure 3-14 B; Vincenten et al., 2015). These data indicate that the Ctf19-C is required for Zip1 association with core centromeres and pericentromeres. Using the live cell reporter assay (described in section 3.1), we found that pericentromeric CO frequencies were comparable in *zip1Δ* (2.06 cM) and *scc4-m35* (2.44 cM) cells (Figure 3-14 C; Figure 3-13 A). Together, these data suggest that the Ctf19-C promoted establishment of Rec8-cohesin directs Zip1 association to prevent pericentromeric CO recombination. By contrast, Zip1 is dispensable for controlling pericentromeric DSB formation as we were unable to detect any changes DSB patterns at *CEN1* in *zip1Δ* cell compared to the wild type (Figure 3-14 D). This observation is in agreement with a previous study (Chen et al., 2008).

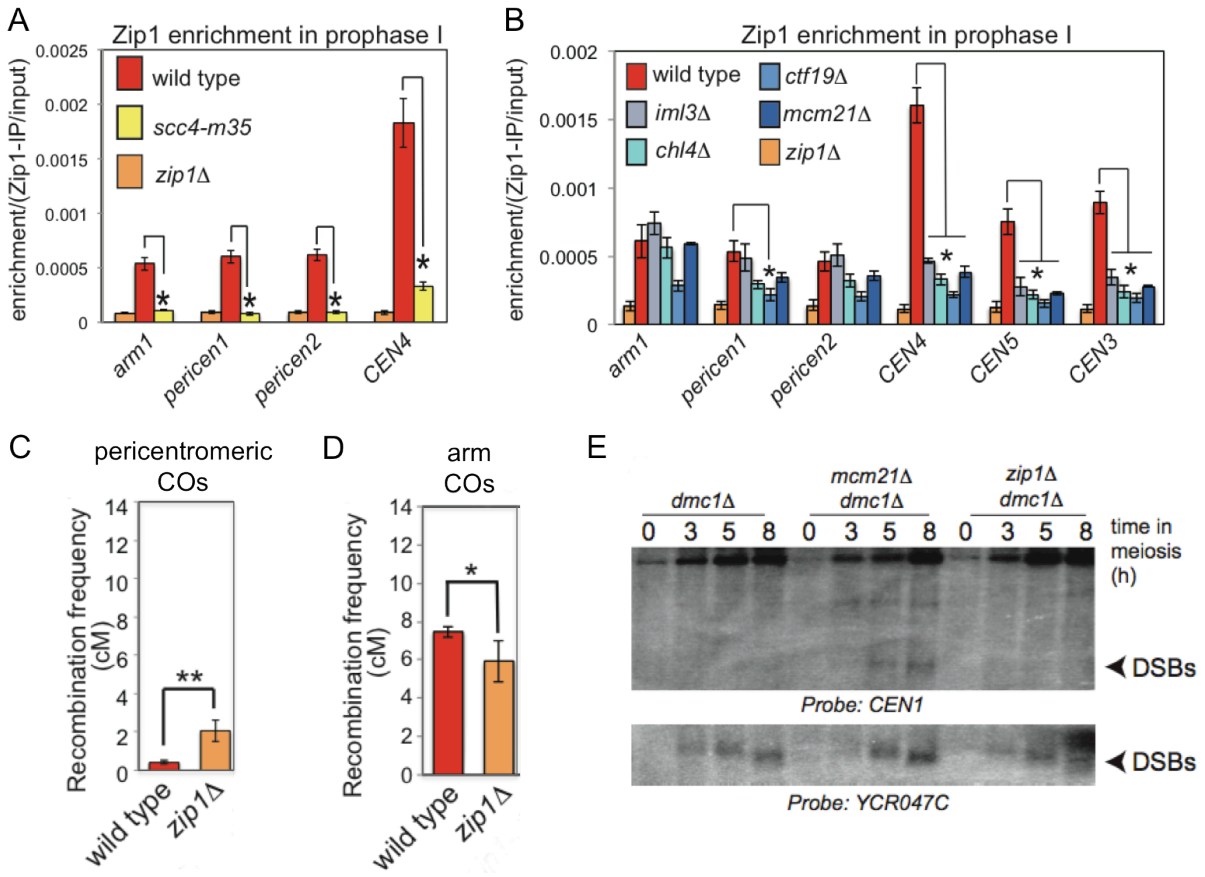

Figure 3-14 The Ctf19-C promoted establishment of Rec8-cohesin directs Zip1 association to suppress pericentromeric CO recombination, but not DSB formation

A) Wild type, *scc4-m35* and *zip1Δ* cells carrying *ndt80Δ* were induced to synchronously undergo meiosis and collected after 5 hours (prophase I arrest) for anti-Zip1 ChIP-qPCR. Error bars represent standard error (n=4 biological replicates). p<0.05, paired t-test. B) Wild type, *iml3Δ, chl4Δ, ctf19Δ, mcm21Δ* and *zip1Δ* cells harboring *ndt80Δ* were induced to synchronously undergo meiosis and harvested after 5 hours (prophase I arrest) for anti-Zip1 ChIP-qPCR. Error bars represent standard error (n=3 biological replicates). p<0.05, paired t-test.C-D) Pericentromeric (C) and chromosomal arm (D) COs were measured in wild type and *zip1Δ* cells using the traffic light assay described in section 3.1. The unit of CO frequency is represented as map distance, in centiMorgans (cM). E) Analysis of DSB formation at *CEN1* and, as a positive control, at *YCR047c* in wild type, *mcm21Δ* and *zip1Δ* cells by Southern blotting. Cells were harvested 0, 3, 5 and 8 hours upon meiotic entry. Positions of meiotic DNA breakage are marked by arrowheads. ChIP, chromatin immunoprecipitation; qPCR, quantitative polymerase chain reaction. Experiments shown in A-D were performed by Adèle Marston and colleagues; modified from Vincenten et al., 2015.

3.5.4 The Shugoshin1-protein phosphatase 2A complex does not play a role in controlling *CEN1*-proximal DSB formation

To analyze additional factors that might be involved in the Ctf19-C mediated control of meiotic DSB formation at pericentromeres, we focused on the Shugoshin1 (Sgo1)-protein phosphatase 2A (PP2A) complex. Sgo1 localizes to the pericentromere in a manner dependent on the Ctf19-C proteins Iml3-Chl4, the multi-subunit complex cohesin and phosphorylation of histone 2A on residue S121 by the kinetochore-associated kinase Bub1 (Kawashima et al., 2010; Kiburz et al., 2005; Liu et al., 2013). Sgo1 serves as an adaptor protein that recruits PP2A to promote accurate chromosome segregation in mitosis and meiosis (Eshleman and Morgan, 2014; Ishiguro et al., 2010; Kitajima et al., 2006; Liu et al., 2013; Nerusheva et al., 2014; Riedel et al., 2006; Verzijlbergen et al., 2014; Xu et al., 2009). PP2A is a serine/ threonine phosphatase that is composed of a scaffold subunit (A), a regulatory subunit (B) and a catalytic subunit (C). Although multiple sub-families of the PP2A regulatory subunit exist (B, B', B'', B''') (Janssens and Goris, 2001; Lechward et al., 2001), Sgo1 interacts with PP2A containing the B' subunit (termed Rts1) in budding yeast (Kitajima et al., 2006; Riedel et al., 2006). In meiosis, Sgo1 protects pericentromeric Rec8-cohesin from premature cleavage by separase in meiosis I by recruiting PP2A-Rts1, which counteracts Rec8 phosphorylation and thereby making it a poor substrate for separase (Kitajima et al., 2004; Marston et al., 2004; Rabitsch et al., 2004; Kitajima et al., 2006; Riedel et al., 2006; Clift and Marston, 2011). Based on the findings that the Sgo1-PP2A complex recruitment to pericentromeres is dependent on the Ctf19-C (Kiburz et al., 2005; Verzijlbergen et al., 2014) and that the complex plays a crucial role in accurate chromosome segregation (Clift and Marston, 2011), we examined whether Sgo1 and PP2A containing the B' subunit Rts1 are implicated in controlling meiotic DSB formation at centromere-proximal regions (Figure 3-15 A). For this study, we employed *sgo1* and *rts1* null cells (*sgo1Δ* and *rts1Δ*) as well as the *sgo1-3A* mutant. The *sgo1-3A* mutant was generated by alanine substitutions of three surface residues of Sgo1 to disrupt the binding site of Sgo1 for PP2A-Rts1 without affecting pericentromeric localization of Sgo1 (Xu et al., 2009). By Southern blot analysis, we found that none of the three mutants (neither *sgo1Δ*, *sgo1-3A* nor *rts1Δ*) show an effect on *CEN1*-proximal DSB formation when compared to the wild type (Figure 3-15 B). These data reveal that the Sgo1-PP2A complex does not play a role in controlling pericentromeric DSB formation in meiosis.

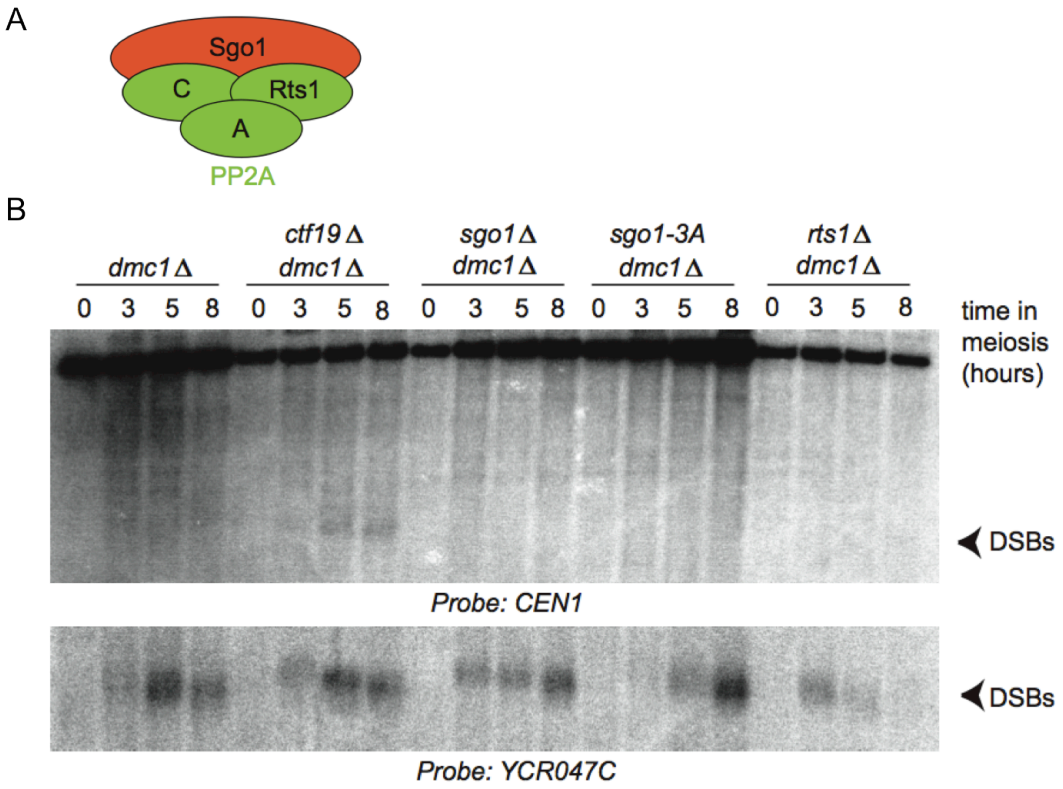

Figure 3-15 The Sgo1-PP2A complex does not play a role in controlling DSB formation at *CEN1*

A) The Sgo1-PP2A complex was tested in controlling centromere-proximal DSB formation in meiosis. B) Southern blot analysis was used to detect DSBs at *CEN1* and *YCR047c* (positive control for meiotic DSB formation) at time points 0, 3, 5 and 8 hours after induction of meiosis in a wild type strain and *sgo1Δ*, *sgo1-3A* and *rts1Δ* cells. Arrowheads point at the position of meiotic DNA breakage.

3.5.5 Neither local chromatin remodelers nor histone modifiers are involved in controlling pericentromeric DSB formation

The investigations described in sections 3.5.1-3.5.4 revealed that neither cohesin, Zip1 nor the Sgo1-PP2A complex are implicated in pericentromeric DSB formation. We realized that these factors are located within ~20-50 kb chromosomal regions surrounding centromeres, whereas the Ctf19-C exerts DSB suppression within a narrower domain of ~6 kb of centromeres (Figure 3-3). We therefore speculate that the Ctf19-C might suppress DSBs by altering local chromosome structure, thereby creating an environment that does not promote Spo11 activity. The placement of meiotic DNA breaks depends on features of the underlying chromatin structure. For example, it is well established that DSBs preferentially form within nucleosome-depleted promoter-regions (Pan et al., 2011) and at chromosomal regions with certain histone modifications such as H3K4me3 (Tischfield and Keeney, 2012). For

this study, we asked whether local chromatin remodelers and/ or histone modifiers are involved in suppressing meiotic DSB formation at pericentromeres. In budding yeast, the chromatin remodeling enzyme Fun 30, a conserved SWI/ SNF-like protein, was shown to affect occupancy of the histone H2A variant Htz1 at pericentromeres, thereby supporting correct chromatin structure to ensure accurate chromosome separation (Durand-Dubief et al., 2012). The remodelers Isw1, a member of the ISWI family (Mellor and Morillon, 2004), and Arp8, a protein of the INO80 family (Shen et al., 2003), are additional factors localized at pericentromeric regions (based on Sgo1 pulldown assay performed in Adèle Marston's laboratory; personal communication). It was proposed that Isw1 has nucleosome spacing activity (Ocampo et al., 2016). The INO80 complex member Arp8 (Shen et al., 2000) was shown to preferentially bind to histones H3 and H4 (Shen et al., 2003). In this study, we observed no detectable changes in DSB formation at *CEN1* at time points 0, 5 and 8 hours in cells lacking Fun30, Isw1, Arp8 and Htz1 (*fun30Δ*, *isw1Δ*, *arp8Δ* and *htz1Δ*) relative to the wild type when analyzed by Southern blotting (Figure 3-16). These results demonstrate that none of these chromatin remodelers plays a role in meiotic DSB formation at the pericentromere.

The histone modifiers Irc20, a ubiquitin ligase (Richardson et al., 2013), and Yta7, which plays a role in histone gene expression (Gradolatto et al., 2008) are additional factors localized at pericentromeres (based on Sgo1 pulldown assay performed in Adèle Marston's laboratory; personal communication). Southern blot analysis revealed no detectable changes in *CEN1*-proximal DSB formation in *irc20Δ* and *yta7Δ* cells compared to wild type cells (Figure 3-16), indicating that neither Irc20 nor Yta7 is implicated in meiotic DSB control at the pericentromere.

Based on these data, we conclude that the chromatin remodelers and histone modifiers, tested in this study, do not play a role in controlling centromere-proximal DSB formation. However, we cannot rule out a role for other, here untested, factors that were identified in Sgo1 pull-down experiments in DSB suppression.

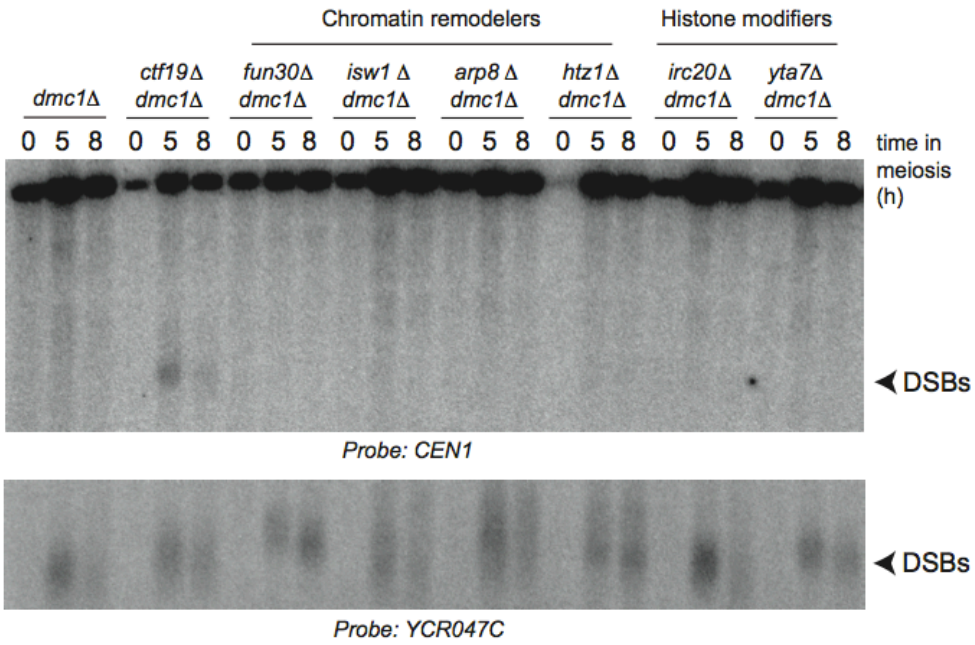

Figure 3-16 Local chromatin remodelers and histone modifiers are not involved in controlling meiotic DSB formation at *CEN1*

Pericentromeric chromatin remodelers and histone modifiers were screened for controlling meiotic DNA break formation at *CEN1*-proximal region by Southern blot analysis. For the screen, cells containing the chromatin remodeler mutants *fun30Δ*, *isw1Δ*, *arp8Δ* and *htz1Δ* and the histone modifier alleles *irc20Δ* and *yta7Δ* were transferred to sporulation medium and collected 0, 5 and 8 hours after induction of meiosis. Probes that specifically anneal at *CEN1* and *YCR047c* were used. Arrowheads indicate the position of DNA breaks.

3.6 Ectopic targeting of individual Ctf19-C components to a non-centromeric region via a developed CRISPR/ dCas9-driven system

In the previous sections, we identified the Ctf19-C of the budding yeast kinetochore as a major factor in controlling meiotic recombination (*i.e* COs and NCOs) within chromosomal regions of ~40 kb surrounding centromeres (section 3.1). We demonstrated that the Ctf19-C partially prevents homologous recombination by reducing local levels of DSB formation (~6 kb surrounding centromeres; sections 3.2-3.3). In addition, we found that the Ctf19-C mediated establishment of Rec8-cohesin at centromeric and pericentromeric regions directs Zip1 association to suppress CO recombination (sections 3.5.2- 3.5.3).

Our next aim was to understand molecular details of the Ctf19-C-driven control of pericentromeric CO recombination. So far, we manipulated kinetochore function by either gene deletion for non-essential proteins or promoter replacement technique (mitosis-specific *pCLB2*-promoter, Lee and Amon, 2003) for essential kinetochore subunits. However, this has the disadvantage that other proteins in the kinetochore might also be affected. This constraint makes it difficult to define on a molecular level the contribution of individual kinetochore components in centromere-proximal CO suppression. We therefore developed a system that allows for the molecular dissection of kinetochore function in CO control by targeting individual Ctf19-C proteins to ectopic chromosomal sites without manipulating the native kinetochore.

3.6.1 Development of a CRISPR/ dCas9-driven kinetochore targeting system

To establish an efficient and reliable system that allows for the ectopic targeting of individual components of the kinetochore to a defined chromosomal region, we used CRISPR-dCas9 (clustered regularly interspaced short palindromic repeat-deactivated Cas9). While CRISPR-Cas9 is widely used as a mechanism for genome editing, the CRISPR-dCas9 system finds its application in genome regulation, such as controlling the activation and repression of the transcription of genes (Qi et al., 2013; Dominguez et al., 2015). The difference between Cas9 and dCas9 is that mutations in both nuclease domains, RuvC1 and HNH, of Cas9 cause a loss of nuclease function and thus generate a catalytic dead form of Cas9, termed dCas9. Despite a lack of nuclease function, dCas9 retains its ability to bind to DNA through

guidance of an engineered single guide RNA molecule (sgRNA) (Gasiunas et al., 2012; Jinek et al., 2012). Thus, this entity can be utilized to target proteins to desired chromosomal positions located upstream of a proto-spacer adjacent motif (PAM; sequence: NGG) (Figure 3-17 A).

For our “CRISPR/ dCas9-driven kinetochore targeting system”, we employed the Ctf19-C components Ctf19 and Iml3. In section 3-1, we showed that the COMA proteins Ctf19 and Mcm21 as well as the Iml3-Chl4 sub-complex exert the strongest effect on pericentromeric CO suppression when compared to other Ctf19-C components, although Iml3 and Chl4 affect CO frequency less strongly than the COMA members (Figure 3-1 A; Vincenten et al., 2015). Therefore, the proteins Ctf19, Mcm21, Iml3 and Chl4 are promising candidates in analyzing CO recombination at a non-(peri)centromeric region when they are ectopically targeted via the CRISPR/ dCas9 system. For this study, we designed the constructs *pHOP1-CTF19-3xFLAG-DCAS9* and *pHOP1-IML3-3xFLAG-DCAS9* as well as *pHOP1-3xFLAG-DCAS9* and integrated them at the *TRP1* locus (Figure 3-17 B). We want to point out that *pHOP1-3xFLAG-DCAS9* was used as a control as it does not contain any kinetochore component. Expression of the constructs was placed under the control of the promoter of the protein Hop1 (p*HOP1*). The *HOP1* gene, which encodes a component of the synaptonemal complex, is repressed in mitotically growing cells, but its transcription is induced shortly after cells enter the meiotic program (Vershon et al., 1992). We chose *pHOP1* for early, meiosis-specific expression of the constructs and to avoid potential interference with chromosome segregation during mitosis. By anti-Cas9 Western blot analysis, we were able to detect the fusion proteins Ctf19-3xFlag-dCas9 and Iml3-3xFlag-dCas9 3 and 5 hours after cells were induced to undergo meiosis (Figure 3-17 C). Ctf19-3xFlag-dCas9 and Iml3-3xFlag-dCas9 were stable for at least up to 5 hours in the meiotic program despite their high molecular weight (Ctf19-3xFlag-dCas9: ~200 kDa and Iml3-3xFlag-dCas9: ~190 kDa). We also detected the control protein 3xFlag-dCas9 (without fusion to any kinetochore component; molecular weight: ~160 kDa) 3 and 5 hours upon meiotic entry (Figure 3-17 C). In addition, we observed expression of Ctf19-3xFlag-dCas9, Iml3-3xFlag-dCas9 and 3xFlag-dCas9 3 and 5 hours after cells were induced to undergo meiosis when an antibody against Flag was used (data not shown). We conclude that the fusion proteins Ctf19-3xFlag-dCas9, Iml3-3xFlag-dCas9 and

3xFlag-dCas9 are expressed in early stages of meiosis and can thus be used for our CRISPR/ dCas9-based analyses.

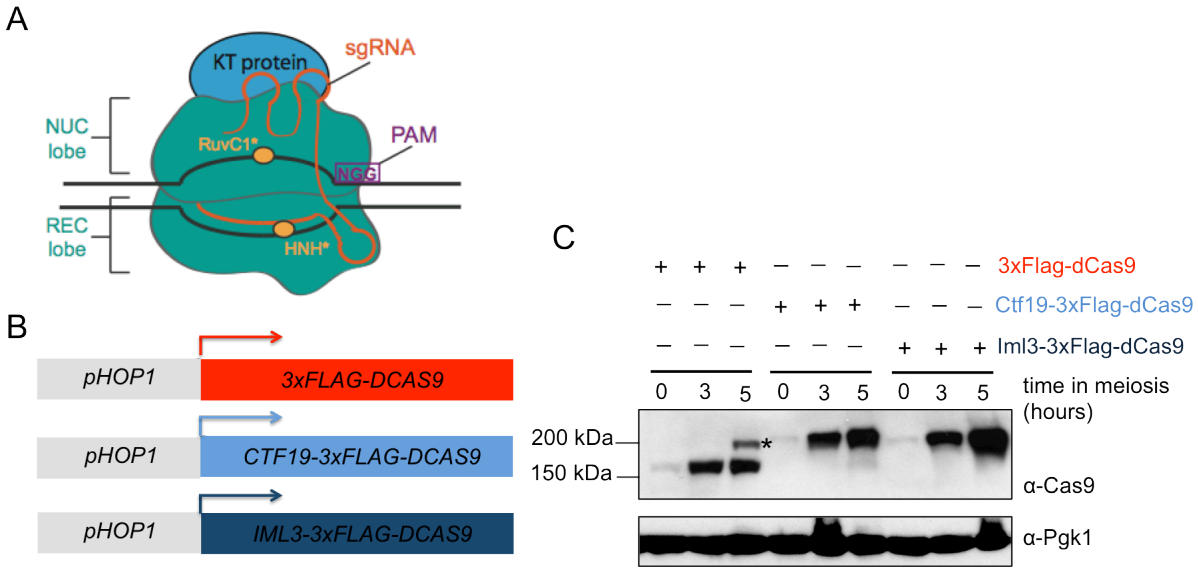

Figure 3-17 CRISPR/ dCas9-based constructs to target Ctf19-C components to specific chromosomal sites

A) The CRISPR-dCas9 system is based on the nuclease-deficient mutant of Cas9 (dCas9) that binds to a DNA target specific sequence (usually 20 bps) through guidance of a single guide RNA (sgRNA) molecule and a proto-spacer adjacent motif (PAM) adjacent to the dCas9 binding site. B) Illustration of kinetochore protein-dCas9 constructs used in this study. *CTF19* and *IML3* were C-terminally fused to *3xFLAG-DCAS9* and driven by p*HOP1*. Another construct, *3xFLAG-DCAS9* was employed as a control. C) Meiosis-specific expression of the fusion proteins Ctf19-3xFlag-dCas9 and Iml3-3xFlag-dCas9, as well as 3xFlag-dCas9, confirmed by Western blot analysis when detected with a Cas9 antibody. Protein extracts probed with an antibody against Pgk1 served as loading control. Samples for Western blotting were collected 0, 3 and 5 hours after cells were induced to undergo meiosis. Asterisk indicates a non-specific band.

3.6.2 Fusion proteins Ctf19-3xFlag-dCas9 and Iml3-3xFlag-dCas9 can functionally replace the native kinetochore components Ctf19 and Iml3

Our initial attempt was to assess whether the fusion proteins Ctf19-3xFlag-dCas9 and Iml3-3xFlag-dCas9 can functionally replace their endogenous counterparts Ctf19 and Iml3, respectively, in meiosis. For this, we analyzed the effect of Ctf19-3xFlag-dCas9 and Iml3-3xFlag-dCas9 expression in the absence of the native proteins Ctf19 and Iml3, respectively, on sporulation efficiency and spore viability. Analyzing sporulation efficiency and spore viability is a powerful tool to gain important insights

into the meiotic function(s) of a protein of interest when it is absent or mutated (Börner and Cha, 2015).

To determine whether Ctf19-3xFlag-dCas9 can functionally replace the native kinetochore component Ctf19, we induced *pHOP1-CTF19-3xFLAG-DCAS9*, *ctf19Δ* cells to synchronously undergo meiosis along with wild type, *ctf19Δ* and *pHOP1-CTF19-3xFLAG-DCAS9*, *CTF19* cells (Figure 3-18). Analysis of sporulation efficiency revealed that 88% tetrads were generated in the wild type strain, whereas only 53% tetrads were produced in the *ctf19Δ* mutant (Figure 3-18 A). This result demonstrates that Ctf19 is required for the proper execution of the meiotic nuclear divisions, which is in agreement with earlier observations (Fernius and Marston, 2009; Mehta et al., 2014). We observed that sporulation efficiency in *pHOP1-CTF19-3xFLAG-DCAS9, CTF19* cells (79% tetrads) was similar to the wild type (Figure 3-18 A), indicating that expressing Ctf19-3xFlag-dCas9 in addition to endogenous Ctf19 does not negatively influence the execution of the meiotic divisions. Moreover, we found that levels of sporulation efficiency in *pHOP1-CTF19-3xFLAG-DCAS9*, *ctf19Δ* cells (72% tetrads) were nearly restored to wild type levels (Figure 3-18 A). This observation demonstrates that Ctf19-3xFlag-dCas9 can functionally replace endogenous Ctf19. We next found that levels of spore viability were dramatically decreased in the *ctf19Δ* mutant compared to the wild type (Figure 3-18 B). Only 2% of tetrads produced from *ctf19Δ* cells were composed four viable spores, whereas 90% of wild type-tetrads were comprised of four viable spores. This finding indicates that loss of Ctf19 causes meiotic chromosomes mis-segregation and thus generates inviable spores, which is in line with previous studies (Fernius and Marston, 2009; Mehta et al., 2014). We observed that levels of spore viability in *pHOP1-CTF19-3xFLAG-DCAS9, CTF19* and wild type cells were similar as approximately 90% of the tetrads were composed of four viable spores (Figure 3-18 B). This result reveals that accurate meiotic chromosome segregation occurred in the presence of both the fusion Ctf19-3xFlag-dCas9 and endogenous Ctf19. Levels of spore viability were increased in *pHOP1-CTF19-3xFLAG-DCAS9*, *ctf19Δ* cells (62% of tetrads were composed of four viable spores) when compared to the *ctf19Δ* mutant (Figure 3-18 B). This result confirms that Ctf19-3xFlag-dCas9 can functionally replace the native Ctf19 protein. By Western blot analysis, we demonstrated early expression of Ctf19-3xFlag-dCas9 in meiosis (Figure 3-18 C). Based on the findings described here, we conclude that Ctf19-3xFlag-dCas9 performs meiotic function(s) of the native Ctf19.

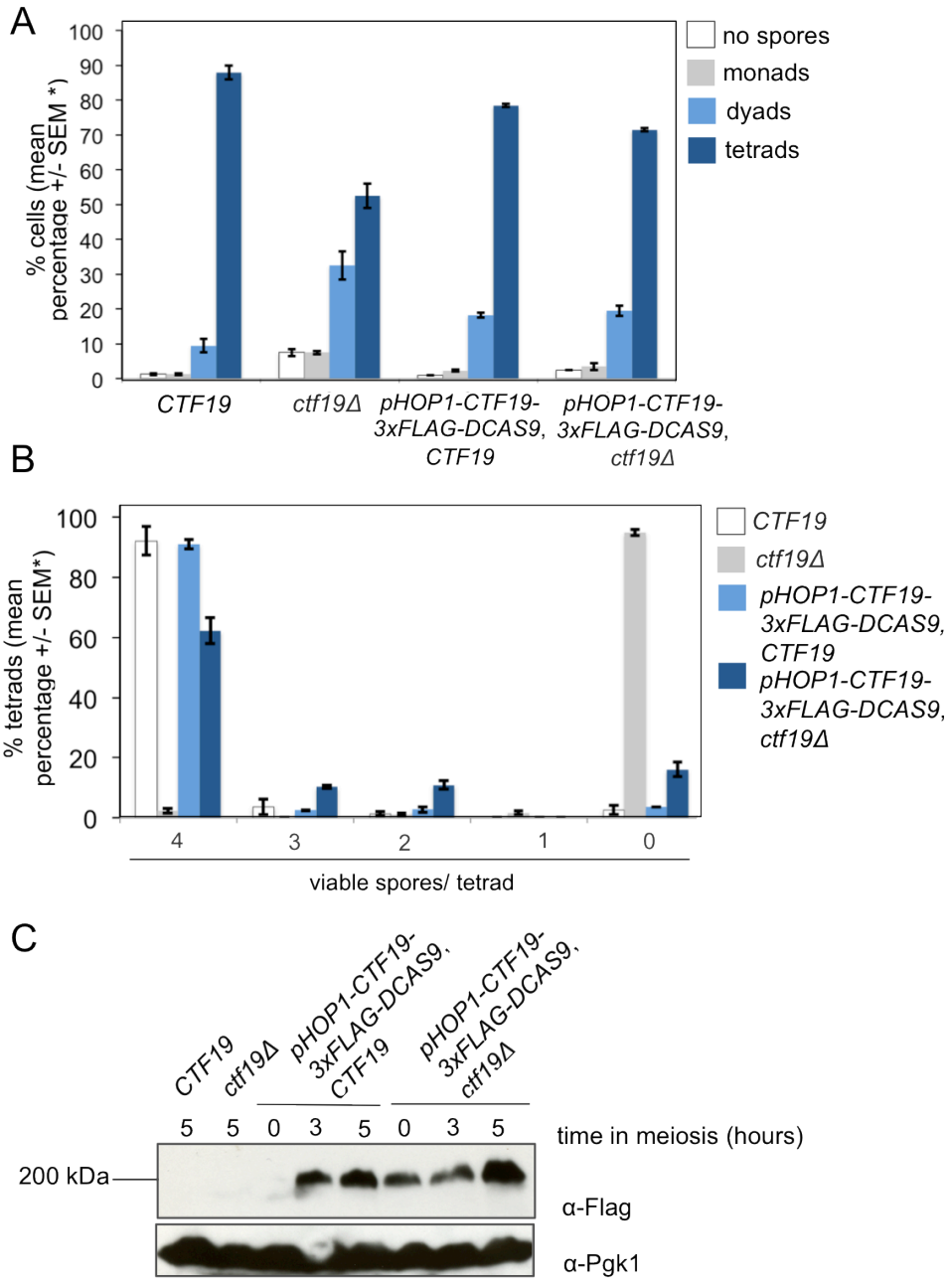

Figure 3-18 Fusion protein Ctf19-3xFlag-dCas9 rescues the phenotype of *ctf19Δ* cells

A) Yeast strains wild type (*CTF19*), *ctf19Δ*, *CTF19-3xFLAG-DCAS9 CTF19* and *CTF19-3xFLAG-DCAS9 ctf19Δ* were analyzed for sporulation efficiency. Two hundred cells for each strain were counted and numbers of tetrads, dyads, monads and no spores were determined. *Mean percentage and standard error of the mean (SEM) of two independent experiments. B) Spore viability analysis of yeast strains mentioned in (A) after growth on glucose-rich medium for 48 hours at 30°C. At least 65 tetrads of each strain were dissected. Asterisk indicates mean percentage and standard error of the mean (SEM) of two independent experiments. C) Detection of Ctf19-3xFlag-dCas9 after 0, 3 and 5 hours in the meiotic program in wild type (*CTF19*), *ctf19Δ*, *CTF19-3xFLAG-DCAS9 CTF19* and

Figure 3-18 continued

CTF19-3xFLAG-DCAS9 ctf19Δ cells by Western blot analysis. Protein extracts were probed with antibodies against Flag and Pgk1 (control).

We then assessed whether the fusion protein Iml3-3xFlag-dCas9 can functionally replace the native kinetochore component Iml3. Analysis of sporulation efficiency revealed that levels in *iml3Δ* cells were reduced when compared to the wild type strain (58% tetrads in *iml3Δ,* 83% tetrads in the wild type; Figure 3-19 A). This finding indicates that Iml3 is required for the proper execution of the nuclear divisions in meiosis, which is in agreement with previous studies (Fernius and Marston, 2009; Marston et al., 2004). We observed that levels of sporulation efficiency in *pHOP1-IML3-3xFLAG-DCAS9*, *IML3* cells (82% tetrads) were similar to the wild type (Figure 3-19 A), demonstrating that expressing Iml3-3xFlag-dCas9 does not interfere with the meiotic divisions when endogenous Iml3 is present. Levels of sporulation efficiency in *pHOP1-IML3-3xFLAG-dCAS9*, *iml3Δ* cells (78% tetrads) were nearly restored to wild type levels (Figure 3-19 A), revealing that Iml3-3xFlag-dCas9 can functionally replace endogenous Iml3. In line with earlier observations (Fernius and Marston, 2009; Marston et al., 2004), analysis of spore viability showed a dramatic decrease in *iml3Δ* cells when compared to the wild type (Figure 3-19 B). We observed that less than 1% of tetrads generated from *iml3Δ* cells were composed of four viable spores, whereas 94% of tetrads originated from the wild type strain were comprised of four viable spores. This result demonstrates that loss of Iml3 causes unfaithful meiotic chromosome segregation and consequently generates inviable spores (Fernius and Marston, 2009; Marston et al., 2004). Furthermore, we found that 90% of tetrads produced from *pHOP1-IML3-3xFLAG-DCAS9*, *IML3* cells were composed of four viable spores, thereby resembling the wild type strain (Figure 3-19 B). Levels of spore viability in *pHOP1-IML3-3xFLAG-dCAS9*, *iml3Δ* cells (81% of tetrads were comprised of four viable spores) were nearly restored to wild type levels (Figure 3-19 B). This finding provides more evidence that Iml3-3xFlag-dCas9 can functionally replace native Iml3. By anti-Cas9 Western blot analysis, we showed expression of Iml3-3xFlag-dCas9 in early stages of meiosis (Figure 3-19 C). The results described here allow us to conclude that the fusion protein Iml3-3xFlag-dCas9 performs meiotic function(s) of its endogenous counterpart.

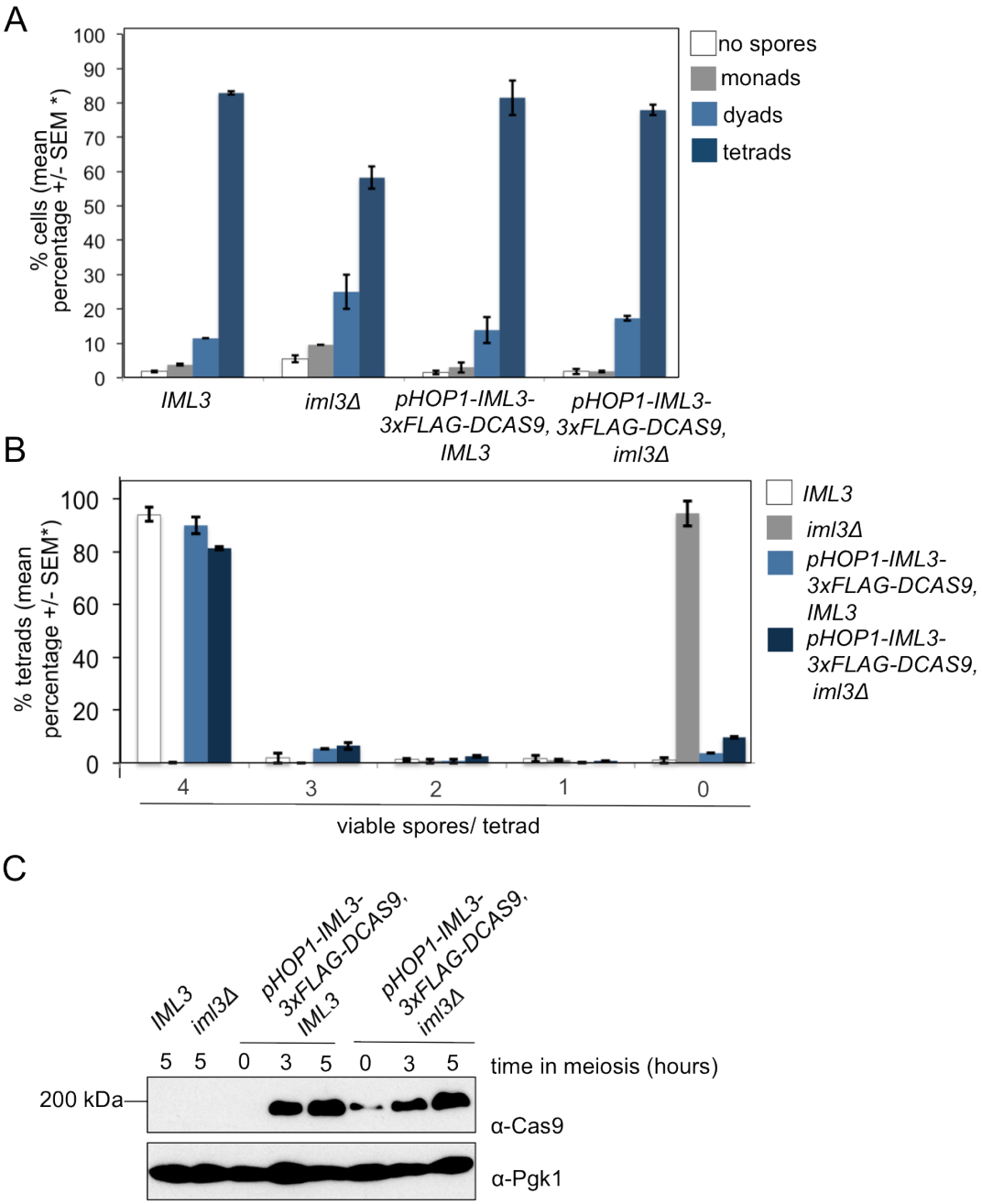

Figure 3-19 Iml3-3xFlag-dCas9 mimics meiotic function(s) of endogenous *IML3*

A) Analysis of sporulation efficiency in *IML3*, *iml3Δ*, *pHOP1-IML3-3xFLAG-DCAS9 IML3* and *pHOP1-IML3-3xFLAG-DCAS9 iml3Δ* cells. Two hundred cells for each strain were counted and numbers of tetrads, dyads, monads and no spores were determined. *Mean percentage and standard error of the mean (SEM) of two independent experiments. B) Viability of spores in yeast strains described in (A) was examined. At least 65 tetrads were dissected. Asterisk indicates mean percentage and standard error of the mean (SEM) of two independent experiments. C) Meiosis-specific expression of Iml3-3xFlag-dCas9 at time points 0, 3 and 8 hours was monitored in cells mentioned in (A) by Western blotting. Antibodies against Cas9 and Pgk1 (control) were used.

3.6.3 CRISPR/ dCas9-driven ectopic targeting of kinetochore components is sufficient to locally control CO recombination

Next, we aimed to examine whether the kinetochore components Ctf19 and Iml3 can mimic pericentromeric CO suppression when ectopically targeted to a non-centromeric region via our developed CRISPR/ dCas9-driven system. As a non-centromeric region, we used the interval on chromosome arm *VIII* from the live cell reporter assay, which has been described in section 3.1. We ectopically targeted the fusion proteins Ctf19-3xFlag-dCas9 and Iml3-3xFlag-dCas9 as well as the protein 3xFlag-dCas9 to a defined position within this interval via a sgRNA molecule. The sgRNA molecule was expressed from a guide RNA expression cassette that we integrated at the *URA3* locus. The guide RNA expression cassette is composed of a 20-nt target-specific complementary region, a Cas9-binding hairpin and the *SUP4* terminator (Figure 3-20 A; Laughery et al., 2015). The constitutive promoter *SNR52* drives expression of the sgRNA molecule (Laughery et al., 2015). We utilized a cassette, which expresses a sgRNA molecule that specifically targets the fusion proteins to a chromosomal position upstream of a PAM sequence between the genes *YHR020w* and *YHR021c* within the 10 kb interval flanked by GFP and RFP on the chromosome arm *VIII* (Figure 3-20 B). Given that we observed a ~6 kb sized DSB effect surrounding centromeres, we chose a target position within a distance of ~2.5 kb from the actual DNA break hotspot, which was found in the divergent promoters of the genes *YHR019c* and *YHR020w* (Pan et al., 2011). It is important to not directly recruit the fusion proteins to the DSB site in order to circumvent indirect effects. We termed the sgRNA molecule "sgRNA-*VIII*". In addition, we used a sgRNA molecule that lacks the 20-nt target sequence, called "sgRNA-mock", and another sgRNA molecule, named "sgRNA-*III*", which directs the proteins to a locus between the genes *YCR045c* and *YCR046c* on chromosome *III*. Both sgRNA-mock and sgRNA-*III* served as negative controls in this analysis. The target regions of the molecules sgRNA-*VIII* and sgRNA-*III* are specifically located in intergenic regions to prevent potential interference with the expression of the adjacent genes. We first performed anti-Flag ChIP-qPCR to analyze the enrichment of the fusion proteins at the target sites when guided via the sgRNA molecules. For qPCR, we used primer sets that amplify the target site *YHR020w-YHR021c* on chromosome *VIII*, the centromeric region 3 (*CEN3*) and the chromosomal region *YCR045c-YCR046c* on chromosome *III*. We found an enrichment of the fusion proteins Ctf19-3xFlag-dCas9,

Iml3-3xFlag-dCas9 and 3xFlag-dCas9 at the locus *YHR020w-YHR021c* on chromosome arm *VIII* when guided via sgRNA-*VIII* (Figure 3-20 C, middle panel). By contrast, we were unable to detect any signals for the same proteins in combination with either sgRNA-mock or sgRNA-*III* at *YHR020w-YHR021c* on arm *VIII.* These results confirm ectopic targeting of the fusion proteins to the target site *YHR020w-YHR021c* on arm *VIII* through the corresponding sgRNA molecule (sgRNA-*VIII*). However, we noticed that levels of 3xFlag-dCas9 at *YHR020w-YHR021c* on arm *VIII* and *YCR045c-YCR046c* on arm *III* were increased as compared to levels of Ctf19-3xFlag-dCas9 and Iml3-3xFlag-dCas9 at the same target loci. We speculate that increased levels of 3xFlag-dCas9 were the consequence of the Flag antibody-based ChIP analysis. The protein dCas9 is N-terminally tagged with 3xFlag, whereas the kinetochore proteins are linked to dCas9 via 3xFlag-tag. Hence, the Flag-antibody used for ChIP can efficiently bind to the "free" 3xFlag-tag of dCas9 but is constrained in its accessibility to 3xFlag of the kinetochore-dCas9 fusions. It therefore seems possible that using anit-Flag ChIP underestimates the binding profiles of the fusion proteins Ctf19-3xFlag-dCas9 and Iml3-3xFlag-dCas9 at the target loci. In addition, we observed an enrichment of Ctf19-3xFlag-dCas9, Iml3-3xFlag-dCas9 and 3xFlag-dCas9 at the control site *YCR045c-YCR046c* on chromosome *III* when targeted through the corresponding sgRNA molecule (sgRNA-*III*, Figure 3-20 C, right panel). On the contrary, binding of the fusion proteins at chromosome *III* was not detectable when guided via sgRNA-mock and sgRNA-*VIII*. These observations confirm ectopic targeting of the fusion proteins to the control locus *YCR045c-YCR046c* on chromosome *III*. Furthermore, ChIP-qPCR analysis revealed an enrichment of Ctf19-3xFlag-dCas9 and Iml3-3xFlag-dCas9 at the control locus *CEN3* regardless of the sgRNA molecule (sgRNA-mock, sgRNA-*VIII* and sgRNA-*III*) (Figure 3-20 C, left panel), indicating that Ctf19-3xFlag-dCas9 and Iml3-3xFlag-dCas9 assemble at the native kinetochore. These results were expected as we demonstrated in section 3.6.2 that the fusion proteins Ctf19-3xFlag-dCas9 and Iml3-3xFlag-dCas9 can functionally replace their endogenous counterparts Ctf19 and Iml3. Unlike Ctf19-3xFlag-dCas9 and Iml3-3xFlag-dCas9, we did not detect any signals for 3xFlag-dCas9 at *CEN3* when directed by any of the three sgRNAs. Taken together, these results confirm target-specific guidance of the fusion proteins through the corresponding sgRNA molecules.

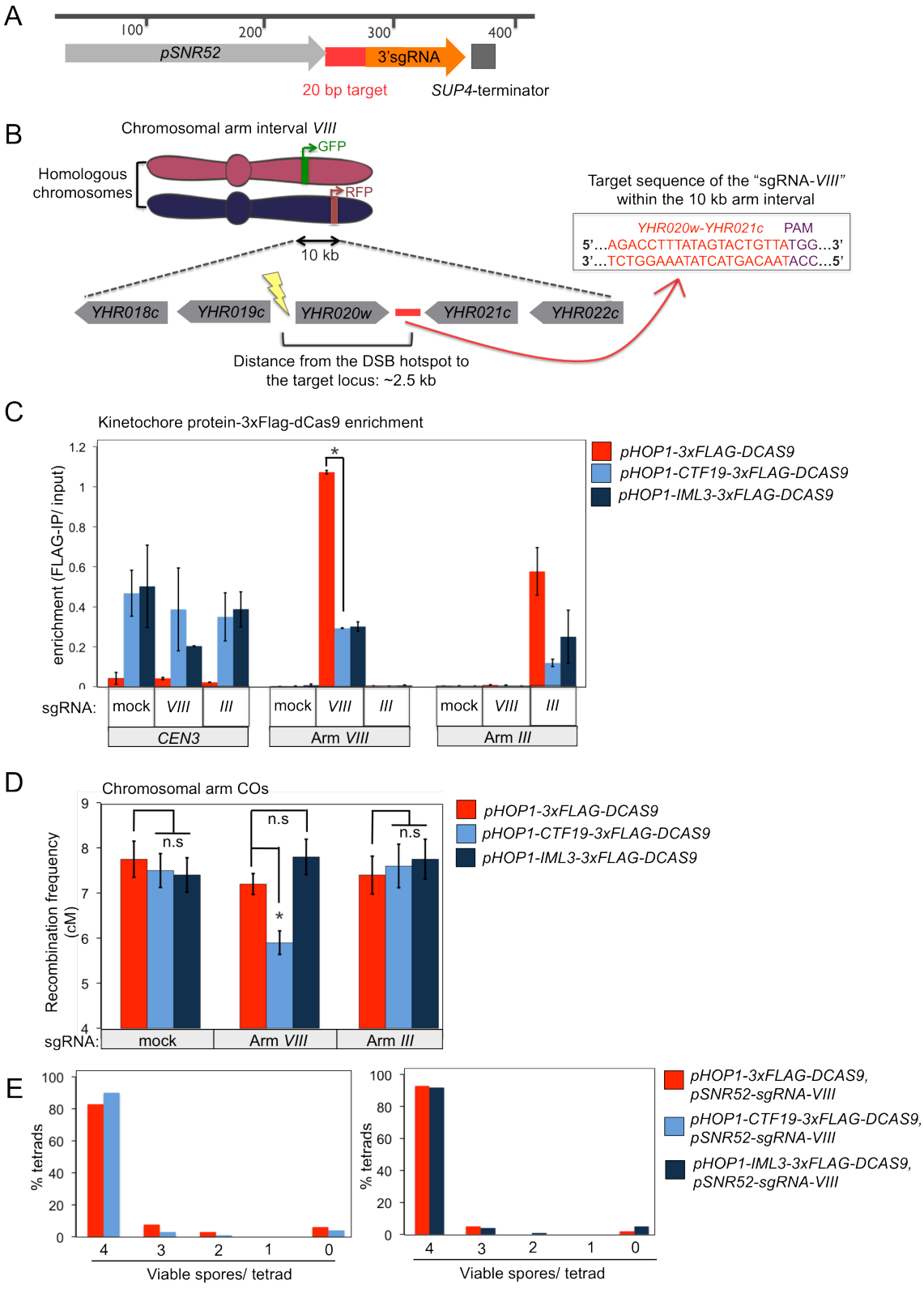

Figure 3-20 CRISPR/dCas9-driven targeting of the protein Ctf19 is sufficient to reduce local CO recombination at chromosome arm *VIII*, but Iml3 is not

A) Illustration of the guide RNA expression cassette used in this study. The cassette is composed of

Figure 3-20 continued

the *SNR52* promoter, a 20 bp target sequence, 3' end of the sgRNA and *SUP4* terminator (adapted from Laughery et al., 2015) B) Within the 10 kb chromosomal arm interval *VIII* flanked by tdTomato (RFP) and green fluorescent protein (GFP) markers, a 20-nt sequence located in an intergenic region between the genes *YHR020w* and *YHR021c* upstream of a proto-spacer adjacent motif (PAM) serves as the targeting site for dCas9-fusion proteins in this study when guided via a sgRNA-*VIII***,** which contains a complementary target-specific sequence of "*YHR020w-YHR021c".* Importantly, the target locus for the fusion proteins is ~2.5 kb away from the DSB hotspot (depicted by the yellow "lightning") to prevent indirect effects. C) Cells co-expressing a fusion protein (either Ctf19-3xFlag-dCas9, Iml3-3xFlag-dCas9 or 3xFlag-dCas9) and any of the three sgRNA molecules mock, *VIII* or *III* were collected 4.5 hours after induction of meiosis. The sgRNA molecules mock, which does not contain a 20-nt target sequence, and *III*, which ectopically targets the fusion proteins to the intergenetic regions between the genes *YCR045c* and *YCR046c* on chromosome *III*, were used as controls. Levels of enrichment of the fusion proteins Ctf19-3xFlag-dCas9 and Iml3-3xFlag-dCas9, as well as 3xFlag-dCas9, at chromosomal regions *CEN3*, *YHR020w-YHR021c* on chromosome *VIII* and *YCR045c-YCR046c* on chromosome *III* were analyzed by ChIP-qPCR. Error bars represent standard error of n=2 biological replicates. *p<0.05, unpaired t-test. D) Map distances (in centiMorgans (cM)) were calculated for a 10 kb chromosomal arm interval *VIII* in cells expressing the fusion proteins 3xFlag-dCas9, Ctf19-3xFlag-dCas9 and Iml3-3xFlag-dCas9 when directed by the sgRNAs mock, *VIII* and *III* using the live cell reporter assay described in Figure 3-1 D. The sgRNA molecules mock and *III* were utilized as controls. Standard error bars were determined based on Perkins equation (described in Materials and Methods). p values were obtained using Fisher's exact test (*p<0.05). E) Viability analysis of spores originated from cells expressing Ctf19-3xFlag-dCas9, sgRNA-*VIII* (left chart) and Iml3-3xFlag-dCas9, sgRNA-*VIII* (right chart). The protein 3xFlag-dCas9 guided through sgRNA-*VIII* was used as a control. At least 65 tetrads of each strain were dissected.
ChIP, chromatin immunoprecipitation; qPCR, quantitative polymerase chain reaction.

We then analyzed the effect of ectopic targeting Ctf19-3xFlag-dCas9, Iml3-3xFlag-dCas9 and, as a control, 3xFlag-dCas9 to the locus *YHR020w-YHR021c* on arm *VIII* on local CO recombination. We measured a CO frequency of 7.2 cM within the interval on arm *VIII* in *pHOP1-3xFLAG-DCAS9, pSNR52-sgRNA-VIII* cells using the live cell reporter assay (Figure 3-20 D, middle panel). This result is in line with findings earlier in this study when we showed that map distance was 7.4 cM on arm *VIII* in wild type cells (Figure 3-1 D; Vincenten et al., 2015). We conclude that ectopic targeting of 3xFlag-dCas9 alone (without any kinetochore protein) to chromosome arm *VIII* yields CO frequency comparable to the wild type and thus does not interfere with meiotic processes. The live cell reporter assay revealed that levels of arm *VIII*-proximal CO formation were significantly decreased in *pHOP1-CTF19-3xFLAG-*

DCAS9, *pSNR52-sgRNA-VIII* cells when compared to *pHOP1-3xFLAG-DCAS9, pSNR52-sgRNA-VIII* cells (Figure 3-20 D, middle panel). Map distance was 5.9 cM in *pHOP1-CTF19-3xFLAG-DCAS9*, *pSNR52-sgRNA-VIII* cells. This result indicates that ectopic targeting of the Ctf19-C component Ctf19 to a non-centromeric region via our developed CRISPR/ dCas9 targeting system is sufficient to mimic pericentromeric CO suppression at this region. We found that the effect of ectopic targeting Ctf19 to arm *VIII* on CO suppression is locally restricted as no changes in CO frequency within the arm interval *VIII* were observed when Ctf19-3xFlag-dCas9 was guided to either no defined chromosomal position (sgRNA-mock) or arm *III* (sgRNA-*III*) (Figure 3-20 D, left and right panels). Using the live cell reporter assay, we did not observe any significant changes in CO rates on arm *VIII* in *pHOP1-IML3-3xFLAG-DCAS9*, *pSNR52-sgRNA-VIII* cells relative to *pHOP1-3xFLAG-DCAS9, pSNR52-sgRNA-VIII* cells (Figure 3-20 D, middle panel). Map distance was 7.4 cM in *pHOP1-IML3-3xFLAG-DCAS9*, *pSNR52-sgRNA-VIII* cells. This observation reveals that ectopic targeting of the Ctf19-C protein Iml3 to a non-centromeric region via the CRISPR/ dCas9-driven system is insufficient to suppress CO recombination on this region.

We then analyzed the viability of spores generated from cells expressing the fusion proteins Ctf19-3xFlag-dCas9, Iml3-3xFlag-dCas9 and, as a control, 3xFlag-dCas9 in combination with sgRNA-*VIII* to assess whether targeting of these proteins assembles an entire synthetic kinetochore. Assembly of another functional kinetochore on chromosome arm *VIII* would generate a di-centric chromosome, which would interfere with meiotic chromosome segregation and thus produce aneuploid/ inviable gametes. We found that levels of spore viability were similar in all tested strains as 80-90 % of tetrads were composed of four viable spores (Figure 3-20 E, 3xFlag-dCas9, sgRNA-*VIII* and Ctf19-3xFlag-dCas9, sgRNA- sgRNA-*VIII*: left chart; 3xFlag-dCas9, sgRNA-*VIII* and Iml3-3xFlag-dCas9, sgRNA-*VIII*: right chart). These data demonstrate that neither Ctf19-3xFlag-dCas9 nor Iml3-3xFlag-dCas9 assembles an entire synthetic kinetochore on chromosome arm *VIII*.

3.6.4 The Ctf19 protein co-recruits Mcm21 to the ectopic site

In section 3.6.3, we showed that ectopic targeting of the Ctf19-C protein Ctf19 to a defined position on chromosome arm *VIII* via our developed CRISPR/ dCas9-driven system enables local CO suppression (Figure 3-20 D). Within native kinetochores, the Ctf19 protein functions within a tetrameric complex, termed COMA, together with Mcm21, Ame1 and Okp1 (De Wulf et al., 2003). The assembly of additional Ctf19-C

proteins at kinetochores depends on COMA (Pekgöz Altunkaya et al., 2016; Schmitzberger et al., 2017). To explore whether ectopic targeting of Ctf19 co-recruits other kinetochore components to the target site or whether Ctf19 alone is sufficient to suppress local CO formation, we performed co-immunoprecipitation (Co-IP) and ChIP-qPCR analyses. We found that the fusion protein Ctf19-3xFlag-dCas9 co-immunoprecipitates with Mcm21-3HA when probed with antibodies against Cas9 and HA, respectively, after HA-based Co-IP analysis (Figure 3-21 A). This finding is in accord with studies that demonstrate that Ctf19 forms a heterodimer with the protein Mcm21 (Schmitzberger and Harrison, 2012). Furthermore, we were able detect Chl4-3HA when probed with an antibody against HA following Flag-based Co-IP of cells co-expressing Chl4-3HA and Ctf19-3xFlag-dCas9 (Figure 3-21 B). This result is line with previous findings revealing that the Iml3-Chl4 sub-complex assembles in the presence of Ctf19-Mcm21 (Pekgöz Altunkaya et al., 2016; Schmitzberger et al., 2017). Taken together, these data indicate that the Ctf19-C proteins Mcm21 and Chl4 associate with the fusion protein Ctf19-3xFlag-dCas9. By HA antibody-based ChIP-qPCR analysis, we observed increased levels of Mcm21-3HA enrichment at the target locus *YHR020w-YHR021c* on arm *VIII* in *MCM21-3HA, pHOP1-CTF19-3xFLAG-DCAS9, pSNR52-sgRNA-VIII* cells when compared to *MCM21-3HA, pHOP1-3xFLAG-DCAS9, pSNR52- sgRNA-VIII* cells (Figure 3-21 C, middle panel). This result reveals that ectopic targeting of Ctf19 to arm *VIII* co-recruits Mcm21. On the contrary, we did not observe any significant changes in Chl4-3HA accumulation at the target locus on arm *VIII* in *CHL4-3HA, pHOP1-CTF19-3xFLAG-DCAS9, pSNR52-sgRNA-VIII* cells relative to *CHL4-3HA, pHOP1-3xFLAG-DCAS9, pSNR52-sgRNA-VIII* cells (Figure 3-21 C, middle panel). This finding demonstrates that ectopic targeting of Ctf19 does not co-recruit Chl4. As a positive control for Mcm21 and Chl4 localization, we examined levels of Mcm21-3HA and Chl4-3HA enrichment at the centromeric region 3 (*CEN3*) by anti-HA ChIP-qPCR analysis. As expected, we found increased levels of Mcm21-3HA and Chl4-3HA enrichment at *CEN3* in cells containing *MCM21-3HA, pSNR52-sgRNA-VIII* combined with either *pHOP1-CTF19-3xFLAG-DCAS9* or *pHOP1-3xFLAG-DCAS9* and in cells harboring *CHL4-3HA, pSNR52-sgRNA-VIII* combined with either *pHOP1-CTF19-3xFLAG-DCAS9* or *pHOP1-3xFLAG-DCAS9* when compared to no tag strains (*pHOP1-CTF19-3xFLAG-DCAS9, pSNR52-sgRNA-VIII* and *pHOP1-3xFLAG-DCAS9, pSNR52-sgRNA-VIII*) (Figure 3-21 C, left panel), demonstrating that Mcm21-

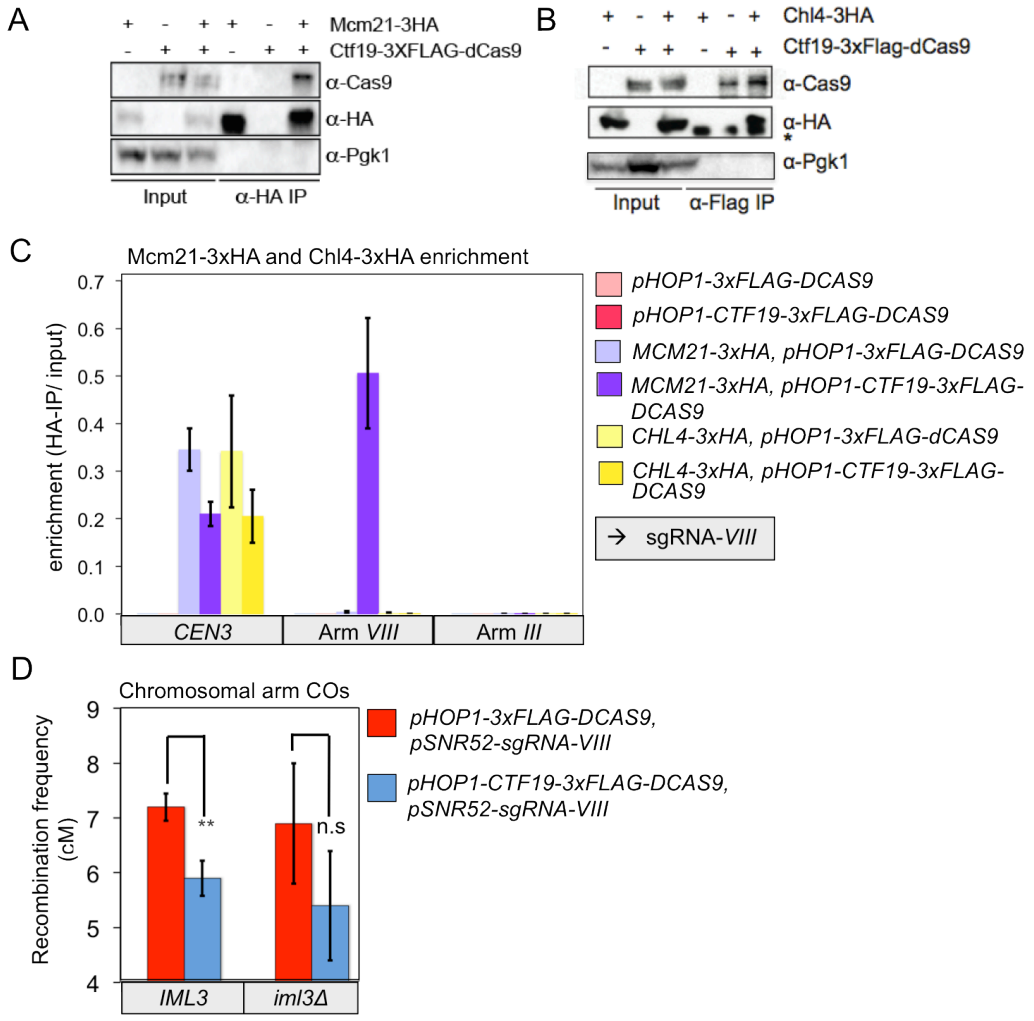

Figure 3-21 Ectopic targeting of Ctf19 co-recruits Mcm21, but not Chl4.

A) HA-based co-immunoprecipitation (Co-IP) of Mcm21-3HA and Ctf19-3xFlag-dCas9 from cells sporulated for 4.5 hours. The antibodies Cas9 and HA were used to detect Ctf19-3xFlag-dCas9 and Mcm21-3HA, respectively. Probing with an antibody against Pgk1 was utilized as a control. B) Flag- IP was conducted to detect association of Ctf19-3xFlag-dCas9 with Chl4-3HA after 4.5 hours in meiosis when probed with antibodies against Cas9 and HA. Using an antibody against Pgk1 served as a control. C) Cells expressing the fusion proteins 3xFlag-dCas9 or Ctf19-3xFlag-dCas9 in combination with either Mcm21-3HA or Chl4-3HA were collected 4.5 hours after sporulation. The fusion proteins were guided through the molecule sgRNA-*VIII* to the target locus *YHR020w-YHR021c* on chromosome *VIII*. HA-ChIP followed by qPCR was performed to analyze levels of Mcm21-3HA and Chl4-3HA enrichment at the chromosomal regions *CEN3*, *YHR020w-YHR021c* on chromosome *VIII* and *YCR045c-YCR046c* on chromosome *III* by qPCR. Strains expressing either 3xFlag-dCas9 or Ctf19-3xFlag-dCas9 alone served as no tag controls for the HA-ChIP. Error bars represent standard error of n=2 biological replicates. D) The live cell reporter assay was utilized to measure map distances (in centiMorgans (cM)) for a 10 kb chromosomal arm interval *VIII* in cells expressing the fusion proteins 3xFlag-dCas9, sgRNA-*VIII* and Ctf19-3xFlag-dCas9, sgRNA-*VIII* in a background of

Figure 3-21 continued

wild type Iml3 (*IML3*) and deletion of Iml3 (*iml3Δ*). Standard error bars were determined based on Perkins equation (described in Materials and Methods). p values were obtained using Fisher's exact test (*p<0.05).
ChIP, chromatin immunoprecipitation; qPCR, quantitative polymerase chain reaction.

3HA and Chl4-3HA assemble at native kinetochores. As a negative control for Mcm21 and Chl4 localization, we determined levels of Mcm21-3HA and Chl4-3HA enrichment at *YCR045cYCR046c* on chromosome *III* by anti-HA ChIP-qPCR analysis. As expected, we were unable to detect any signals for Mcm21-3HA and Chl4-3HA on chromosome *III* in cells containing *MCM21-3HA, pSNR52-sgRNA-VIII* combined with either *pHOP1-CTF19-3xFLAG-DCAS9* or *pHOP1-3xFLAG-DCAS9* and in cells harboring *CHL4-3HA, sgRNA-VIII* combined with either *pHOP1-CTF19-3xFLAG-DCAS9* or *pHOP1-3xFLAG-DCAS9* when compared to no tag strains (*pHOP1-CTF19-3xFLAG-DCAS9, pSNR52-sgRNA-VIII* and *pHOP1-3xFLAG-DCAS9, pSNR52-sgRNA-VIII*) (Figure 3-21 C, right panel). Taken together, these results allow us to conclude that ectopic targeting of the Ctf19-C component Ctf19 to the target locus on chromosome arm *VIII* co-recruits Mcm21, but not Chl4. This conclusion is in line with findings of spore viability analysis, demonstrating that ectopic targeting of Ctf19-3xFlag-dCas9 to arm *VIII* is not sufficient to restore complete kinetochore assembly (Figure 3-20 E).

Based on the data described in this section, we predict that the effect of ectopic targeting Ctf19 (and consequently Mcm21) to arm *VIII* on CO frequency should not change in cells lacking the Iml3-Chl4 sub-complex. Indeed, CO frequency remained the same in *pHOP1-CTF19-3xFLAG-DCAS9, pSNR52-sgRNA-VIII, IML3* cells and *pHOP1-CTF19-3xFLAG-DCAS9, pSNR52-sgRNA-VIII, iml3Δ* cells when analyzed by the live cell reporter assay (Figure 3-21 D). These findings suggest that the Ctf19-Mcm21 heterodimer has a specific function in local CO suppression.

4 Discussion

A key event of meiosis is the programmed formation of DNA double-strand breaks (DSBs) to initiate the reciprocal exchange of DNA fragments between homologous chromosomes, known as inter-homolog crossover (CO) recombination. The final outcome of inter-homolog CO recombination, a structure termed chiasma, is essential for the proper execution of meiosis I (Gray and Cohen, 2016; Hochwagen, 2008; Marston and Amon, 2004). Improper placement of COs in some chromosomal regions such as the surroundings of centromeres, also referred to as pericentromeres, is strongly associated with meiotic chromosome mis-segregation and developmental aneuploidy (*e.g.* Trisomy 21 in humans) (Hassold and Hunt, 2001; Koehler et al., 1996; Rockmill et al., 2006). In budding yeast, CO recombination is suppressed close to centromeres (Chen et al., 2008) and although DNA breaks occur at pericentromeric regions, there is a general suppression of the total amount at these chromosomal regions when compared to genome-wide levels (Blitzblau et al., 2007; Buhler et al., 2007; Gerton et al., 2000; Pan et al., 2011). However, the chromosomal features that locally control meiotic DNA break formation and recombination at pericentromeres remain mostly unexplored. Here, we identified the macromolecular structure that assembles onto the centromere, termed the kinetochore, as a major factor in controlling meiotic DNA break formation and recombination at pericentromeric regions in budding yeast.

4.1 Kinetochore-driven control of meiotic DNA break formation and recombination at centromere-proximal regions

The observation that centromere-adjacent regions cross over less frequent than centromere-distal regions was made for the first time in the early 1930s. Analysis of CO recombination frequency in the fruit fly *Drosophila melanogaster* (*D. melanogaster*) carrying translocation of chromosome *III-IV* led to the suggestion that the centromere exerts inhibition on meiotic recombination in the surrounding chromosomal areas (Beadle, 1932; Dobzhansky, 1930). In the following decades, reduction in CO recombination in the vicinity of centromeres was demonstrated in many other species, including humans (Chen et al., 2008; Copenhaver et al., 1999; Ellermeier et al., 2010; Gore et al., 2009; Lambie and Roeder, 1986; Mahtani and Willard, 1998; Nakaseko et al., 1986; Puechberty et al., 1999; Saintenac et al., 2009; Tanksley et al., 1992). In budding yeast, it was shown that both inter-homolog

recombination pathways COs and non-crossovers (NCOs) (*i.e.* gene conversion) are strongly inhibited close to centromeres (~6-fold within 10 kb of centromeres) (Chen et al., 2008; Lambie and Roeder, 1986, 1988). DSBs that act as initiators of meiotic recombination occur at centromere-proximal regions but there is a general suppression of the total amount at these genomic regions (Blitzblau et al., 2007; Buhler et al., 2007; Gerton et al., 2000; Pan et al., 2011). DNA break formation is ~2-3-fold suppressed within a 5-10 kb distance from centromeres as compared to chromosomal regions greater than 10 kb away (Blitzblau et al., 2007; Buhler et al., 2007; Pan et al., 2011). DNA breaks are even more suppressed (~7-fold) within a narrower domain of 1-3 kb on both sides of centromeres (Pan et al., 2011). Although a suppression of meiotic DNA break formation and recombination at pericentromeric regions was discovered decades ago, chromosomal features that control these events remain poorly understood (Chao, 1998; Nambiar and Smith, 2016; Talbert and Henikoff, 2010).

Here, we provide the first direct evidence that the kinetochore, the multi-subunit protein assembly nucleated onto the centromere, controls meiotic DNA break formation and recombination at centromere-proximal regions in budding yeast (Figure 4-1; Vincenten et al., 2015). In particular, a subunit of the inner kinetochore, the Ctf19 complex (Ctf19-C), was central to this investigation. We revealed that the Ctf19-C suppresses meiotic recombination (*i.e.* COs and NCOs) within ~40 kb chromosomal regions surrounding all centromeres (~20 kb on each side of centromeres) (Figure 4-1 A). This study demonstrated that the Ctf19-C exerts meiotic CO suppression at centromere-proximal regions through a multi-layered mechanism (Figure 4-1 B). One layer by which the Ctf19-C suppresses CO recombination is the inhibition of Spo11-dependent DNA break formation, the initiating event of meiotic recombination, over a narrower domain of ~3 kb on each side of the centromeres (~6 kb in total surrounding centromeres) (Figure 4-1 A, B). In addition, we found that the Ctf19-C provides an additional layer for CO suppression that involves the loading and enrichment of the conserved multi-protein cohesin complex containing the meiosis-specific subunit Rec8 at centromeric and pericentromeric regions by the recruitment of the Scc2-Scc4 loader complex. The enrichment of cohesin complexes generally expands over a broader domain of ~20-50 kb surrounding centromeres (Tanaka et al., 1998; Glynn et al., 2004; Weber et al., 2004). We demonstrated that the Ctf19-C promoted establishment of Rec8-cohesin is required to suppress

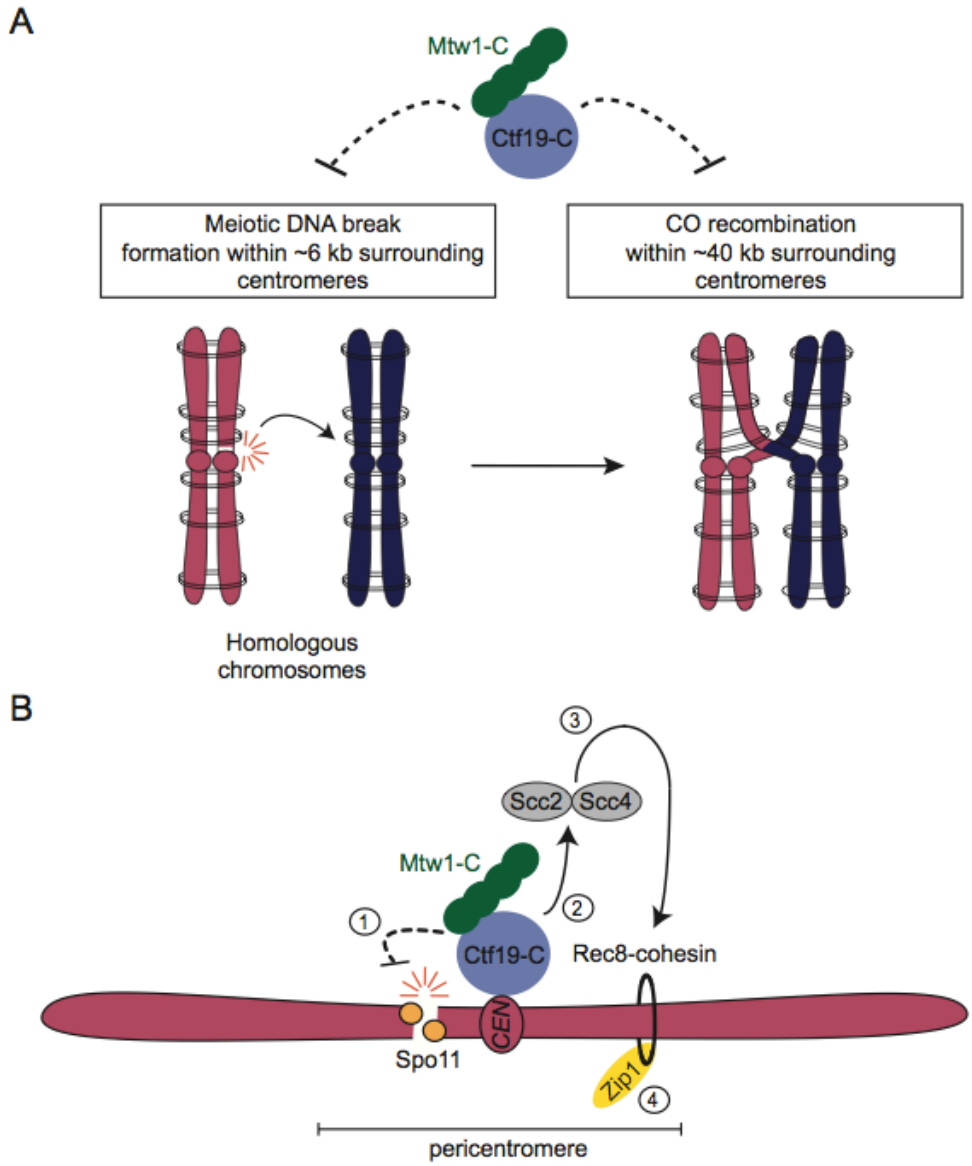

Figure 4-1 Model for the kinetochore-driven control of meiotic DNA break formation and recombination at centromere-proximal regions.

A) The inner and central subunits of the budding yeast kinetochore Ctf19 complex (Ctf19-C) and Mtw1 complex (Mtw1-C), respectively, play a role in suppressing meiotic DNA break formation close to centromeres. In particular, the Ctf19-C was shown to suppress DNA breaks within a ~6 kb chromosomal region surrounding centromeres (~3 kb on both sides of centromeres) and CO recombination with ~40 kb of centromeres (~20 kb on each side of centromeres). B) The Ctf19-C exerts CO suppression through a multi-layered mechanism. Circuit 1: The Ctf19-C minimizes the initiating event of meiotic recombination, DSB formation, in the direct vicinity of centromeres. Another kinetochore subunit, the Mtw1-C was also shown to suppress centromere-proximal DNA breaks. Circuit 2: The Ctf19-C recruits the Scc2-Scc4 loader complex to centromeres. Circuit 3: The Scc2-Scc4 complex enables the loading and enrichment of Rec8-cohesin at centromeric and pericentromeric regions. Cohesin complexes expand over ~20-50 kb chromosomal regions surrounding centromeres. Circuit 4: The establishment of Rec8-cohesin at centromeric and

Figure 4-1 continued.

pericentromeric regions directs the association of Zip1 with these regions to suppress CO recombination. Meiotic recombination (*i.e.* COs and NCOs) is prevented within ~40 kb chromosomal domains of centromeres (~20 kb on each side of centromeres).
For simplicity, only one homologous chromosome, Ctf19-C, Mtw1-C, Rec8-cohesin complex and Zip1 are shown in B). *CEN* indicates the budding yeast centromere.

pericentromeric CO recombination. We also showed that the Ctf19-C promoted establishment of Rec8-cohesin directs the association of the major component of the synaptonemal complex, Zip1, to centromeric and pericentromeric regions to suppress CO recombination. Our data showed that both Rec8-cohesin and Zip1 act at a step after meiotic DSB formation. The finding that Zip1 is required for pericentromeric CO suppression but dispensable for DNA break control is in agreement with previous studies (Blitzblau et al., 2007; Chen et al., 2008). We suggest that the Ctf19-C promoted establishment of Rec8-cohesin and Zip1 at centromere-proximal regions is a safeguarding mechanism to impede residual DNA breaks from undergoing a repair pathway that uses the homologous chromosome as the repair template.
In addition to the Ctf19-C, we showed that a subunit of the central layer of the kinetochore, the Mtw1 complex (Mtw1-C), is also involved in the suppression of centromere-proximal DNA break formation (Figure 4-1). However, the exact role of the Ctf19-C and Mtw1-C in meiotic DSB control at pericentromeric regions remains elusive and will be discussed in sections 4.2 and 4.4.

4.2 The Ctf19-C minimizes meiotic DNA break formation at centromere-proximal regions

The genome-wide distribution of meiotic DNA breaks is tightly regulated through different levels of chromosome organization. On a large scale, chromosome organization comprises the “architecture” of the chromosomes. Upon meiotic entry, chromosomes undergo condensation through which chromosomal loops emerge from a proteinaceous axis composed of Rec8-cohesin (Klein et al., 1999), the axial element proteins Red1 and Hop1 (Hollingsworth et al., 1990; Smith and Roeder, 1997), components of the DSB machinery (Panizza et al., 2011) and other factors. The establishment of this “loop-axis” organization of chromosomes was proposed to be a prerequisite for meiotic DSB formation (Klein et al., 1999; Panizza et al., 2011).

Chromosomal loops, which are known as “hot regions”, frequently undergo meiotic DSB formation. By contrast, axis-associated sites are cold regions as they rarely create breaks (Blat et al., 2002; Ito et al., 2014; Panizza et al., 2011). On a small scale of chromosome organization, meiotic DSB formation is dependent on nucleosome occupancy, gene organization and sequence composition in the loops. For example, nucleosome-depleted regions (*i.e.* often promoters), GC-rich areas and regions near histone modifications such as trimethylation of lysine 4 of histone 3 (H3K4me3) are permissive for DNA break formation (Cooper et al., 2016; Tischfield and Keeney, 2012). Chromosomal regions such as repetitive DNA arrays, telomeres and pericentromeres are DSB “cold domains” (Blitzblau et al., 2007; Buhler et al., 2007; Gerton et al., 2000; Pan et al., 2011). Often, cold domains are at-risk during DNA break repair. For example, in some eukaryotic systems, DNA break formation followed by inter-homolog CO recombination at pericentromeres is strongly associated with chromosome mis-segregation and aneuploid inviable gametes (Hassold and Hunt, 2001; Koehler et al., 1996; Rockmill et al., 2006).

In this study, we revealed that the inner (*i.e.* Ctf19-C) and central (*i.e.* Mtw1-C) subunits of the budding yeast kinetochore play a role in controlling meiotic DNA break formation at pericentromeric regions (Figures 3-3, 3-4, 3-5, 3-6, 3-7 D, 3-8). More specifically, the Ctf19-C was shown to suppress Spo11-dependent DSB formation within ~6 kb chromosomal regions surrounding all centromeres (~3 kb on both sides of all centromeres; Figures 3-3). The chromosome organization of these regions is not obviously different from the rest of the chromosomes (*e.g.* same density of genes), which would be expected to be permissive for Spo11-dependent DNA breakage. Indeed, the strongest DNA break hotspot was found within the divergent promoter region of the genes *TFC3* and *NUP60* close to the centromere on chromosome *I* (*CEN1*) in cells lacking Ctf19-C function (Figure 3-3 H). Divergent promoters are DNA break “hot spot”-associated regions (Blitzblau et al., 2007). We speculate that the role of the Ctf19-C in controlling meiotic DNA break formation is to overcome the underlying chromatin features at centromere-proximal regions (*e.g.* a divergent promoter close to *CEN1*), although the binding of the kinetochore and thus the Ctf19-C is restricted to the ~125 bp budding yeast point centromere. A way by which the Ctf19-C might accomplish this is to control factors located at centromere-proximal regions, which interfere with chromosome organization. Here, we tested the requirement for cohesin, a highly conserved “structural maintenance of

chromosomes" (SMC) multi-protein complex (Jeppsson et al., 2014; Uhlmann, 2016), in controlling meiotic DNA break formation at pericentromeric regions (Figures 3-9, 3-10, 3-12). In late G1, the Ctf19-C enables the loading and enrichment of cohesin complexes at centromeric and pericentromeric regions by the recruitment of the Scc2-Scc4 loader complex to centromeres (Fernius and Marston, 2009; Fernius et al., 2013; Hinshaw et al., 2015; Natsume et al., 2013; Vincenten et al., 2015). Cohesin complexes are highly enriched within ~20-50 kb genomic regions surrounding centromeres (Glynn et al., 2004; Lengronne et al., 2004; Weber et al., 2004). Primarily, cohesin is known for its function in facilitating inter-chromosomal contacts via the establishment of sister chromatid cohesion (*trans*-interaction), a process coupled to DNA replication in S phase (Nasmyth, 2001; Uhlmann and Nasmyth, 1998). Maintenance of sister chromatid cohesion at centromeres during meiosis I is essential for faithful segregation of sister chromatids during meiosis II (Marston and Amon, 2004). Manipulation of Ctf19-C function leads to impaired centromeric cohesion and causes meiotic chromosome mis-segregation (Eckert et al., 2007; Fernius and Marston, 2009; Hu et al., 2011; Ng et al., 2009). Another role of the ring-shaped cohesin complexes goes beyond encircling juxtaposed sister chromatids. A number of studies provided evidence that cohesin complexes operate intra-chromosomal contacts through placing distant DNA fragments next to each other (*cis*-interaction), thereby organizing higher-order chromosome structures. These higher-order structures culminate in the formation of chromosomal loops (domains) (Barrington et al., 2017; Fudenberg et al., 2016; Gassler et al., 2017; Schalbetter et al., 2016). Because the Ctf19-C promotes the loading and enrichment of cohesin at centromere-proximal regions and because cohesin organizes higher-order chromosome structures, it seems possible that cohesin containing the meiosis-specific subunit Rec8 is involved in controlling DNA break formation near centromeres. However, our data argue against a role for Rec8-cohesin in suppressing meiotic DSBs at pericentromeres. By Southern blot analysis, we were unable to detect *CEN1*-proximal DNA break formation in prophase I-arrested cells deleted for *REC8*, unless a component of the Ctf19-C was also absent (Figure 3-9). Moreover, we observed no detectable changes in pericentromeric DSB formation in prophase I-arrested cells containing *scc4-m35* cells compared to the wild type (Figure 3-10). The *scc4-m35* allele expresses a mutated version of the cohesin loader subunit Scc4, which contains 5 amino acid substitutions (*scc4*$^{F324A; K327A; K331A;}$

$^{K541A;\ K542A}$) in a conserved surface patch (Hinshaw et al., 2015). In mitosis, the mutated version of Scc4 (*scc4-m35*) eliminates the localization of Scc2 to centromeres and specifically reduces levels of centromeric and pericentromeric Scc1-cohesin (Hinshaw et al., 2015). In the meiotic program, the Scc4 mutant (*scc4-m35*) disrupts the association of the cohesin subunit Rec8 with centromeric and pericentromeric areas as well as chromosomal arms (Vincenten et al., 2015). In another approach, we found increased *CEN1*-proximal DNA break formation in both cells depleted for the Ctf19 protein before and after pre-meiotic S phase (Figure 3-12 D). Similar to a *ctf19Δ* mutant (Fernius et al., 2009; Marston et al., 2005), depletion of Ctf19 before S phase mostly impaired pericentromeric Rec8-cohesin establishment. By contrast, depletion of Ctf19 after S phase allowed for Rec8-cohesin establishment close to centromeres (Figure 3-12 C; Vincenten et al., 2015). These findings suggest that the Ctf19-C promoted establishment of S phase-associated Rec8-cohesin required for robust sister chromatid cohesion does not play a role in centromere-proximal DSB control. In conclusion, the Ctf19-C suppresses DNA break formation in a manner independent of Rec8-cohesin establishment. In addition to cohesin, we examined whether the major protein of the synaptonemal complex, Zip1, is involved in controlling centromere-proximal DNA break formation. Our data demonstrated that Zip1, whose association with centromeric and pericentromeric regions is dependent on the Ctf19-C promoted establishment of Rec-cohesin (Figure 3-14 A, B; Vincenten et al., 2015), does not affect pericentromeric DSB patterns (Figure 3-14 E, Blitzblau et al., 2007; Chen et al., 20008). As another approach, we investigated whether the Shugoshin1 (Sgo1)-phosphatase 2A (PP2A) complex, whose association with pericentromeric regions is dependent on the Ctf19-C (Kiburz et al., 2005; Verzijlbergen et al., 2014), is involved in DSB control near centromeres. This study, however, unveiled that pericentromeric DSB patterns are not affected when the function of the Sgo1-PP2A complex is impaired (Figure 3-15). In conclusion, the Ctf19-C suppresses meiotic DSB formation close to centromeres in a manner independent of the SMC complex Rec8-cohesin, the synaptonemal complex protein Zip1 and the Sgo1-PP2A complex.

It remains to be explored whether other, here untested, factors are involved in the kinetochore-driven suppression of meiotic DNA breaks at centromere-proximal regions. For example, in addition to cohesin, there are two other SMC complexes termed condensin and Smc5-Smc6 complex (Jeppsson et al., 2014; Uhlmann, 2016),

which could potentially be investigated. Like cohesin (Glynn et al., 2004; Lengronne et al., 2004; Weber et al., 2004), condensin and the Smc5-Smc6 complex are highly enriched throughout the pericentromere (Copsey et al., 2013; D'Ambrosio et al., 2008). Condensin, which primarily operates intra-chromosomal contacts, is required for chromosome compaction and proper chromosome segregation during mitosis and meiosis (Chan et al., 2004; Hirano, 2005; Yu and Koshland, 2003). Studies revealed that condensin organizes higher-order chromosome structure in two specific chromosomal regions, at centromeres and adjacent to the rDNA, in mitotically dividing budding yeast cells (Freeman et al., 2000; Schalbetter et al., 2016; Stephens et al., 2011). The Smc5-Smc6 complex also plays a crucial role in accurate chromosomes segregation during mitosis and meiosis (De Picolli et al., 2009; Copsey et al., 2013; Farmer et al., 2011). Among other functions, the Smc5-Smc6 complex was proposed to form intermolecular contacts between newly synthesized sister chromatids to promote the resolution of replication-induced DNA supercoiling (Kegel et al., 2011). Based on the findings that condensin and the Smc5-Smc6 complex are enriched at pericentromeres and organize higher-order chromosome structures, it seems reasonable to test a role for these SMC complexes in controlling meiotic DSB formation. However, like cohesin, studies proposed that the loading of condensin and the Smc5-Smc6 complex onto chromosomes occurs in a manner dependent on the Scc2-Scc4 complex (Betts Lindroos et al., 2006; Verzijlbergen et al., 2014). We therefore speculate that utilizing the *scc4-m35* loader mutant, which diminishes the association of cohesin at centromeric and pericentromeric regions in mitosis and meiosis (Hinshaw et al., 2015; Vincenten et al., 2015), might also interfere with the enrichment of condensin and the Smc5-Smc6 complex at these regions. To test this possibility, we can analyze the localization of condensin and Smc5-Smc6 complex at centromere-proximal regions in *scc4-m35* cells through chromatin immunoprecipitation (ChIP) coupled to real time quantitative PCR (qPCR) or deep sequencing (seq). If the *scc4-m35* allele reduces the accumulation of condensin and the Smc5-Smc6 complex at centromeric and pericentromeric regions, we predict that condensin and the Smc5-Smc6 complex are dispensable for meiotic DSB suppression near centromeres. This prediction takes into account that our work clearly showed that *CEN1*-proximal DSB formation is unaffected in *scc4-m35* cells (Figure 3-10). Moreover, Copsey et al. (2013) revealed that the Scm5-Smc6 complex is essential for meiotic chromosome segregation only after DSB formation in budding

yeast. Similarly, Yu and Koshland (2003) demonstrated that condensin plays a role in the proper processing but not formation of meiotic DNA breaks. These finds support our hypothesis that condensin and the Smc5-Smc6 complex may be dispensible for meiotic DSB control.

As an alternative to the SMC complexes, we envision that the meiosis-specific proteins Red1 and Hop1 might be involved in controlling DSB formation close to centromeres. As mentioned earlier, among other factors, Red1 and Hop1 are involved in setting up the chromosomal axes from which chromosomal loops emerge upon cells commit to the meiotic program (Hollingsworth et al., 1990; Smith and Roeder, 1997). Red1 and Hop1 physically interact (de los Santos and Hollingsworth, 1999) and are essential factors in meiotic DSB formation (Panizza et al., 2011). It was demonstrated that Red1 and Hop1 are required for the correct localization of the DSB machinery component Mer2 to chromosomal sites (Panizza et al., 2011). At these sites, Mer2 is phosphorylated by the kinase complexes Cdc28-Clb5 and Cdc28-Clb6 as well as the Dbf4-dependent kinase Cdc7 (Henderson et al., 2006; Murakami and Keeney 2008; Wan et al. 2008). Phosphorylation of Mer2 leads to the association of the DSB factors Rec114 and Mei4 with Mer2. These proteins (Mer2, Rec114 and Mei4) were shown to form a sub-complex required for the binding of the enzyme Spo11 to chromosomal sites of DNA cleavage (Li et al., 2006; Sasanuma et al., 2007). Thus, Red1 and Hop1 act as “initiators” of meiotic DSB formation. Importantly, both Red1 and Hop1 are required for wild type levels of DSBs as absence of either protein impairs Mer2 localization and consequently meiotic DNA break formation (Panizza et al., 2011). Insights into the assembly of the axis-associated proteins Red1 and Hop1 were recently given by Sun et al. (2015). The study demonstrated that Red1 recruitment to chromosomal axis sites is regulated through three ways (Sun et al., 2015). First, Red1 localizes to cohesin binding sites along chromosomes in a Rec8-dependent manner. Red1 in turn recruits Hop1 to chromosomes (Smith and Roeder, 1997; Woltering et al., 2000). Second, Red1 localization to chromosomes is also mediated via Hop1, which occurs in a Rec8-independent fashion. Third and most intriguingly, Hop1 down-regulates the Rec8-dependent accumulation of Red1 at some chromosomal regions such as the close vicinity of centromeres. Based on these observations, we hypothesize the following (Figure 4-2): In a wild type strain, the Ctf19-C recruits the Scc2-Scc4 complex to centromeres, which in turn allows for the loading of Rec8-cohsin. Upon loading,

Rec8-cohesin complexes translocate into the surrounding pericentromere. This in turn leads to the Rec8-dependent localization of Red1 to cohesin-associated sites within the pericentromere. Red1 might recruit Hop1 to these sites. Hop1 in turn may counteract Red1 accumulation to mostly prevent the deposition of DSB machinery factors in the direct vicinity of centromeres. Preventing the localization of DSB inducing factors would be an efficient way to guard against meiotic DSB formation. If this hypothesis is true, it means that Hop1 plays an active role in pericentromeric DSB suppression close to centromeres (via counteracting Red1 and consequently preventing the deposition of DSB factors). This role of Hop1 near centromeres would stand in contrast to its function as a DSB “initiator” at the rest of the chromosomes (Figure 4-2 A). In contrast to the wild type, the Scc2-Scc4 complex is not recruited and consequently the loading and enrichment of Rec8-cohesin complexes at pericentromeres is prevented when Ctf19-C function is impaired (*ctf19Δ* mutant). In the absence of Rec8-cohesin, Red1 and Hop1 might localize to pericentromeric regions as a complex and promote the localization of DSB machinery factors, which in turn may lead to the Spo11-depent DSB formation near centromeres. Thus, we suggest that in the absence of the Ctf19-C and consequently Rec8, Red1 and Hop1 cooperate/ act in concert to promote meiotic DSB induction (Figure 4-2 B). In addition to Red1 and Hop1, we include another factor in our model. This factor is a widely conserved hexameric AAA+ ATPase, called Pch2 (San-Segundo and Roeder, 1999). Among other functions (Vader, 2015), Pch2 is known for its role in removing Hop1 from chromosomes upon the assembly of the synaptonemal complex (Subramanian et al., 2016) and for suppressing meiotic DNA break formation at the edges of the repetitive ribosomal DNA array in budding yeast (Vader et al., 2011). These findings were expanded by a recent study, which revealed that Pch2 plays a crucial role at centromeres (Subramanian et al., 2017). In this study, it was suggested that Pch2 is required to remove Hop1 from pericentromeres in order to prevent DSB activity in late prophase. Based on these data, we expand our model and propose that the Ctf19-C might enable the recruitment of Pch2 to centromeres. Pch2 in turn removes Hop1 from the immediate vicinity of centromeres, which is required to suppress meiotic DSB around centromeres (in late prophase) (Figure 4-2). To test such as a model, in the future we will analyze whether the localization of Red1, Hop1 and Pch2 near centromeres is affected in cells lacking Ctf19-C components.

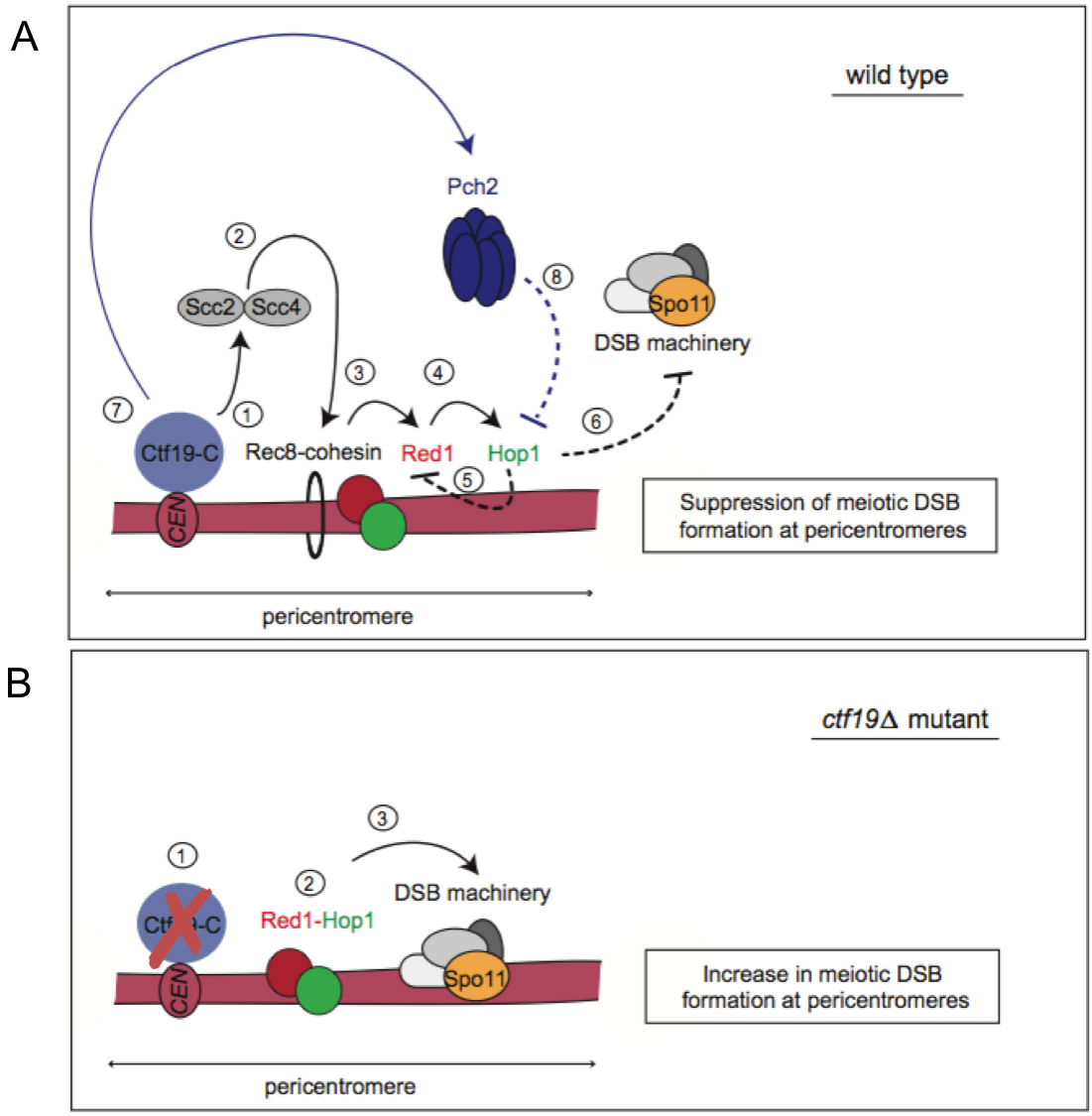

Figure 4-2 Hypothesis: A role for the meiosis-specific proteins Red1, Hop1 and Pch2 in the Ctf19-C driven control of DSB formation near centromeres?

A) In the wild type: Reducing the accumulation of Red1 and Hop1 to prevent the localization of the DSB machinery close to centromeres. Circuit 1: The Ctf19 complex (Ctf19-C) recruits the Scc2-Scc4 complex to centromeres. Circuit 2: The Scc2-Scc4 complex in turn enables the loading and enrichment of Rec8-cohesin complexes at centromeric and pericentromeric regions. Circuit 3: Rec8 recruits Red1 to cohesin-binding sites. Circuit 4: Red1 in turn recruits Hop1 to these sites. Circuit 5: Hop1 near centromeres antagonizes Red1 accumulation (which stands in contrast to the function of Hop1 at other chromosomal regions). Circuit 6: Antagonizing Red1 accumulation by Hop1 would prevent the deposition of DSB inducing factors near centromeres. Circuit 7: The Ctf19-C promotes the recruitment of Pch2 to centromeric regions. Circuit 8: Pch2 removes Hop1 from chromosomal regions near centromeres, which in turn prevents DSB activity (mostly in late prophase). B) In the *ctf19Δ* mutant: Accumulation of Red1-Hop1 near centromeres leads to the localization of the DSB machinery. Circuit 1: Impaired Ctf19-C function prevents the loading and enrichment of Rec8-cohesin near centromeres. Circuit 2+3: Rec8-independent localization of Red1-Hop1 to pericentromeric regions

Figure 4-2 continued.

enables the deposition of DSB inducing factors (DSB machinery), which in turn leads to increased DNA break formation.

For simplicity, only one copy of each factor (homologous chromosome, Ctf19-C, Rec8-cohesin complex, Red1, Hop1, Pch2 and DSB machinery) is shown. *CEN* indicates the budding yeast centromere.

This model is based on findings by Sun et al. (2015), Subramanian et al. (2017) and ours and needs to be tested in the future.

Alternatively, we imagine that factors that organize chromatin structure play a role in the kinetochore-driven suppression of meiotic DSBs. More precisely, the Ctf19-C might alter local chromatin structure by affecting the localization of chromatin remodeling complexes and/ or histone modifiers to prevent accessibility of DNA for the Spo11. However, in this PhD study, we found that neither the chromatin remodelers Fun30, Isw1, Arp8 and Htz1 nor the histone modifiers Irc20 and Yta7 are involved in controlling DSBs at the pericentromere (Figure 3-16). The chromatin remodelers and histone modifiers tested in this study were identified as pericentromere-associated factors through Sgo1-pulldown experiments (Adèle Marston, personal communication). It remains to be tested whether other factors found via Sgo1-pulldown assays play a role in DSB suppression. (In agreement with Subramanian et al., 2017, Pch2 was also found as a pericentromere-associated factor in the Sgo1-pulldown assays (Adèle Marston, personal communication).)

4.3 The Ctf19-C promoted Rec8-cohesin establishment directs Zip1 association to prevent CO recombination at pericentromeres

In meiosis, there is a bias for DSB repair pathways that favor the homologous chromosome as a repair template rather than the sister chromatid to ensure the establishment of chiasmata (physical connections between homologs), which is required for faithful chromosome segregation (Hollingsworth, 2010; Humphryes and Hochwagen, 2014). However, chromosomal regions surrounding centromeres are exceptions for inter-homolog repair (COs and NCOs) in diverse eukaryotic organisms (Chen et al., 2008; Copenhaver et al., 1999; Ellermeier et al., 2010; Gore et al., 2009; Lambie and Roeder, 1986; Mahtani and Willard, 1998; Nakaseko et al., 1986; Puechberty et al., 1999; Saintenac et al., 2009; Tanksley et al., 1992). In budding yeast, we demonstarted that the Ctf19-C promoted establishment of Rec8-cohesin at

centromeric and pericentromeric regions directs the association of Zip1 with these regions (Figures 3-14 A, B; Vincenten et al., 2015). The recruitment of both factors Rec8-cohesin and Zip1 is required to suppress CO recombination close to centromeres (Figures 3-13, 3-14; Vincenten et al., 2015). We assume that the establishment of Rec8-cohesin and Zip1 enriched zones surrounding centromeres by the Ctf19-C directs residual DNA breaks into a pathway that favors the sister chromatid as a repair template rather than the homologous chromosome. The assumption that cohesin and Zip1 promote inter-sister repair is in agreement with various studies (Chen et al., 2008; Kadyk and Hartwell, 1992; Kim et al., 2010; Sjögren and Nasmyth, 2001; Ström et al., 2004).

How the Ctf19-C promoted establishment of Rec8-cohesin and Zip1 near centromeres prevents inter-homolog repair remains an open question. As mentioned earlier, a number of studies proposed that the cohesin complex regulates both inter-chromosomal contacts for the establishment of sister chromatid cohesion (*trans*-interaction) (Nasmyth, 2001) and intra-chromosomal contacts through placing distant DNA fragments next to each other (*cis*-interaction), thereby organizing higher-order chromosome structures. These higher-order structures culminate in the formation of chromosomal domains. The mechanism of how cohesin promotes chromosomal domain formation has recently received a significant amount of attention (Fudenberg et al., 2016; Barrington et al., 2017; Gassler et al., 2017; Haarhuis et al., 2017). A model termed the “loop extrusion” model (Nasmyth, 2001; Alipour and Marko, 2012) was proposed as a potential mechanism for cohesin-mediated domain organization. The loop extrusion model proposes that the formation of chromatin loops is promoted by loop extruding factors (LEFs). The idea is that LEFs translocate along DNA, thereby extruding a loop, until their translocation is blocked by boundary elements (BEs) (Barrington et al., 2017). In mammalian systems, it was shown that loop extrusion of interphase chromosomes is mediated by cohesin complexes as LEFs and CTCF-binding factor as BE proteins (Fudenberg et al., 2016). A powerful tool to study chromosome architecture (such as cohesin-mediated loop formation) is the Hi-C method, which allows for the generation of genome-wide interaction maps (Belton et al., 2012; van Berkum et al., 2010). Using Hi-C analysis, Rao et al. (2017) showed that all chromatin loops are lost when the cohesin proteins are degraded in human cells, which demonstrates the significant role of cohesin in the formation of chromatin loops. A higher-order structure of chromosome organization in chromatin

loop formation via cohesin activity was also indicated in mitotic budding yeast cells when assessed by Hi-C analysis (Schalbetter et al., 2016). Although a role for cohesin in organizing chromatin loops (*cis*-interaction) of meiotic chromosomes in budding yeast has not been described yet, it seems likely that cohesin operates intra-molecular contacts of chromosomes upon meiotic entry (after S phase). This hypothesis takes into account that chromosomes undergo structural changes when they enter the meiotic program (*i.e.* formation of chromosomal loops that emanate from proteinaceous axes) (Blat et al., 2002; Klein et al., 1999). Our data might argue for a role of Rec8-cohesin in suppressing CO recombination through inter-chromosomal contacts. We showed that depletion of Ctf19 before pre-meiotic S phase leads to a significant increase in CO formation near *CEN8* (Figure 3-13 C). On the contrary, depletion of Ctf19 after pre-meiotic S phase had only a mild effect on *CEN8*-proximal CO formation. We demonstrated that depleting Ctf19 before S phase mostly abolishes Rec8-cohesin association with the centromeric region, whereas depletion of Ctf19 after S phase mostly enabled Rec8 accumulation at centromeric und pericentromeric sites (Figure 3-12 C). We suggest that depletion of Ctf19 after S phase allows for the Ctf19-C promoted loading and enrichment of Rec8-cohesin within pericentromeric regions required for the establishment of robust sister chromatid cohesion (which is coupled to DNA replication (Uhlmann and Nasmyth, 1998)) (Vincenten et al., 2015). Based on these findings, we hypothesize that the cohesin mediated inter-chromosomal contacts (*trans*-interactions) required for the establishment of sister chromatid cohesion in S phase might be involved in controlling meiotic CO recombination close to centromeres rather than cohesin regulated intra-molecular contacts (*cis*-interactions; *i.e.* loop formation). One possibility to test whether cohesin mediated inter-molecular contacts play a role in CO suppression is to analyze the architecture of meiotic chromosomes via Hi-C analysis when the protein Ctf19 is depleted from centromeres before and after pre-meiotic S phase. We predict that depleting Ctf19 before pre-meiotic S phase abolishes cohesin-dependent inter-molecular contacts (required for sister chromatid cohesion establishment in S phase) and intra-molecular contacts (that might contribute to the chromosomal loop-axis formation upon meiotic entry) near centromeres, thereby relieving pericentromeric CO suppression. By contrast, depleting Ctf19 after pre-meiotic S phase might enable cohesin-dependent inter-molecular contacts but may prevent intra-molecular contacts and thus suppressing

pericentromeric CO fromation. As an alternative to this approach, we can analyze the effect of depleting the Scc2-Scc4 cohesin loader complex before and after pre-meiotic S phase without impairing Ctf19-C function on pericentromeric CO formation. We predict that depleting Scc2-Scc4 before S phase, thereby diminishing Rec8-cohesin association with centromeric and pericentromeric regions (Vincenten et al., 2015), prevents both intra- and inter-molecular contacts. Abolishing the association of Rec8-cohesin with centromeric and pericentromeric regions using the cohesin loader mutant *scc4-m35* leads to increased *CEN8*-proximal CO formation (Figure 3-13 A). On the contrary, depleting the Scc2-Scc4 complex after S phase might allow for cohesin-dependent inter-molecular contacts but may prevent intra-molecular contacts upon meiotic entry. This prediction is based on the finding that the Scc2-Scc4 complex has another function in cohesin biology, in addition to its canonical role in cohesin loading onto chromosomes. The Scc2-Scc4 complex was shown to promote loop extrusion in human cells (Haarhuis et al., 2017). Whether the Scc2-Scc4 complex also promotes chromosomal loop formation in budding yeast needs to be tested. If so, the prediction would be that depleting Scc2-Scc4 after S phase impairs chromosomal loop extrusion upon meiotic entry.

Like cohesin, the mechanism by which Zip1 suppresses inter-homolog repair remains to be investigated. We envision that Zip1 might be required to remove or inactivate factors located near centromeres, which promote a DSB repair pathway that uses the homologous chromosome. An example for such factors is the serine/ threonine kinase Mek1 (Bailis and Roeder, 1998; de los Santos and Hollingsworth, 1999), which is known to promote a bias for inter-homolog repair (Niu et al., 2005; Subramanian et al., 2016, 2017; Wu et al., 2010). Mek1 is activated upon meiotic DSB formation and forms a complex with the meiosis-specific axis proteins Red1 and Hop1 to ensure that crossovers are formed between homologous chromosomes rather than sister chromatids (Wan et al., 2004; Niu et al., 2005). Moreover, Mek1 was suggested to antagonize the Rec8 promoted inter-sister bias (Kim et al., 2010). A recent study reported that Mek1 is enriched around centromeres when meiotic recombination occurs (Subramanian et al., 2017), although the kinase (as mentioned above) was suggested to not promote inter-sister repair (Niu et al., 2005; Subramanian et al., 2016, 2017; Wu et al., 2010). Interestingly, the ATPase Pch2 was also found close to centromeres (Subramanian et al., 2017; Adèle Marston, personal communication). Work by Subramanian et al. (2016) demonstrated that on

synapsed chromosomes Zip1 recruits Pch2, which in turn removes Mek1 and Hop1. Since both Pch2 and Mek1 are present at centromeres, this Zip1-dependent function does not seem to count for centromere-proximal regions. In particular, Pch2 was shown to suppress DSB formation, the initiating event of meiotic recombination, (Subramanian et al., 2017) but does not affect CO formation near centromeres (Chakraborty et al., 2017). We can therefore envision that the role of Zip1 in pericentromeric CO suppression might be that it is required to inactivate Mek1 rather than removing it from centromeres.

Based on our data and the findings described above, we propose the following model for the role of Rec8-cohesin and Zip1 in the Ctf19-driven suppression of inter-homolog repair at pericentromeres (Figure 4-3): In the first step, the Ctf19-C enables the loading and enrichment of Rec8-cohesin by the recruitment of the Scc2-Scc4 complex. The establishment of the Ctf19-C dependent Rec8-cohesin is required for robust sister chromatid cohesion at pericentromeres. Rec8 in turn directs the association of Zip1 with cohesin-associated sites at and around centromeres. The high accumulation of Rec8-cohesin within pericentromeric regions (as compared to chromosome arms) and the cohesin-dependent inter-molecular contacts (sister chromatid cohesion establishment in S phase) might be required to turn the sister chromatid into the preferred DSB repair template rather than the more distant homolog. The role of Zip1 in CO suppression may be that it inactivates Mek1 kinase to prevent Mek1-promoted inter-homolog bias.

In this model, we also propose that both factors Rec8-cohesin and Zip1 might be equally essential for the pericentromeric of CO suppression. This hypothesis takes into account that we observed an equal increase in *CEN8*-proximal CO formation in *scc4-m35* (Figure 3-13 A) and *zip1Δ* (Figures 3-14 C) cells. Because Zip1 recruitment is dependent on Rec8-cohesin localization but not in reverse (Bardhan et al., 2010), we assume that Rec8-cohesin is associated with centromeres and pericentromers in *zip1Δ* cells but Rec8-cohein alone (without Zip1) is not sufficient to suppress CO recombination.

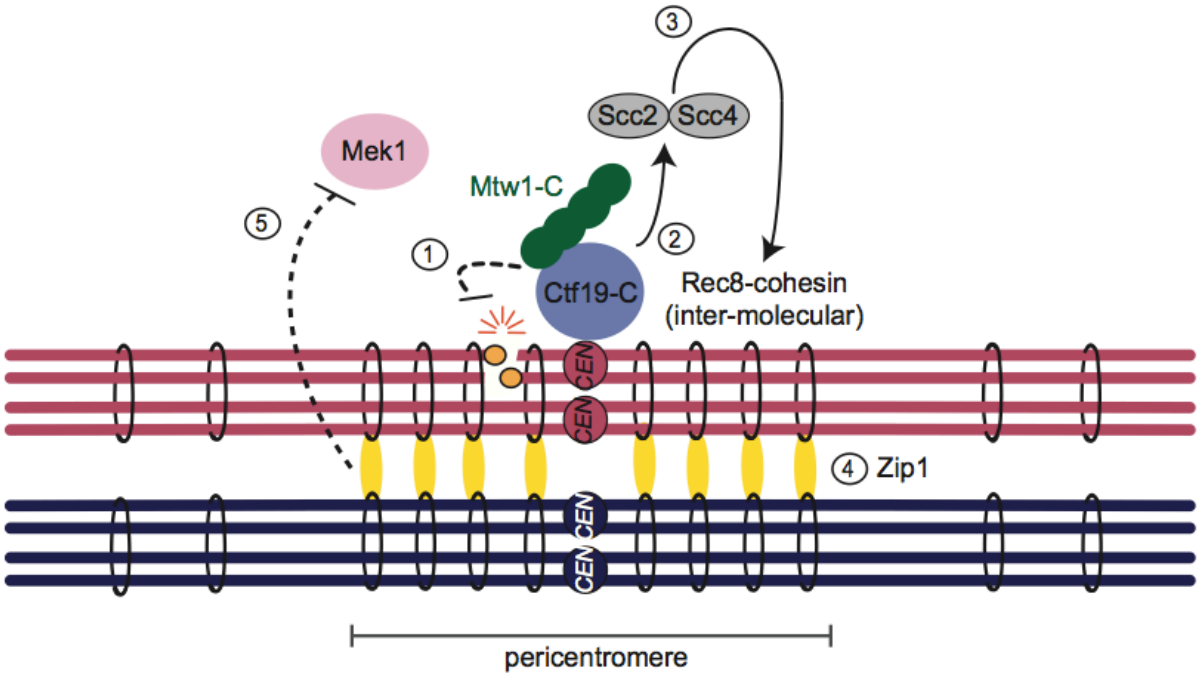

Figure 4-3 Hypothesis: The role of Rec8-cohesin and Zip1 in the kinetochore-driven suppression of CO recombination at pericentromeres.

The inner and central kinetochore subunits Ctf19 complex (Ctf19-C) and Mtw1 complex (Mtw1-C), respectively, minimize DSB formation, the initiating event of meiotic recombination. However, the kinetochore-driven suppression of DSBs is not absolute (Circuit 1). To channel residual DNA breaks into a pathway that avoids the homologous chromosome as a repair template, the Ctf19-C promotes the enrichment of Rec8-cohesin at cenromeric and pericentromeric regions (Circuit 2-3), which is required to direct Zip1 association with these sites (Circuit 4). The enrichment of Rec8-cohesin and the cohesin-dependent inter-molecular contacts required for the establishment of robust sister chromatid cohesion at pericentromeres might turn residual breaks into inter-sister repair pathway (Circuit 3). Zip1 might promote inter-sister repair by inactivation of the kinase Mek1, which was shown to promote inter-homolog bias (Circuit 5). For simplicity, only one copy of each kinetochore subunit is shown. *CEN* indicates the budding yeast centromere.

4.4 The Mtw1-C controls centromere-proximal DSB formation

The Mtw1-C, Ndc80 complex (Ndc80-C) and Spc105 complex (Spc105-C) form a larger conserved network, called KMN, within kinetochores that contains the core microtubule-binding activitiy (Cheeseman et al., 2006). Although the Mtw1-C does not directly bind to microtubules (Cheeseman et al., 2006; Hornung et al., 2011), it is essential for faithful chromosome disjunction. The Mtw1-C serves as a linker between inner-layer kinetochore components, Mif2 and COMA, and outer-layer components, Ndc80-C and Spc105-C (De Wulf et al.,2003; Pinsky et al., 2003; Biggins, 2013; Hornung et al., 2011; Dimitrova et al., 2016). In G2/ prophase I, when

meiotic recombination occurs, the inner and central kinetochore subunits Ctf19-C and Mtw1-C, respectively, are anchored to centromeric chromatin (Miller et al., 2012; Meyer et al., 2015). By contrast, some outer kinetochore components such as the Ndc80-C are not assembled onto centromeres when meiotic recombination occurs (Miller et al., 2012; Meyer et al., 2015). This may suggest that the Mtw1-C fulfills a centromeric function(s) during this meiotic stage that does not involve the bridging of inner and outer kinetochore subunits. Indeed, this work revealed that the Mtw1-C plays a role in controlling DSB formation, the initiating event of meiotic recombination, close to the centromere (Figure 3-8). Hence, we discovered a new function of the central-layer kinetochore component Mtw1-C during meiosis. In addition to the Mtw1-C, our study also showed that the Ctf19-C is involved in pericentromeric DSB control (Figures 3-3- 3-7). How these kinetochore subunits suppress DSB formation near centromeres remains to be tested. Due to the highly cooperative nature of kinetochore assembly (Musacchio and Desai, 2017), we can envision that the Ctf19-C and Mtw1-C are not directly involved in DSB suppression. Instead, we hypothesize that these subunits might interact with other kinetochore factors to control meiotic DSB formation near centromeres. Based on our current understanding of budding yeast kinetochore assembly, the Mtw1-C associates with centromeric chromatin through direct binding of Mif2 and the COMA component Ame1 (Hornung et al., 2014). Apart from Ame1, no other Ctf19-C components have been implicated in direct interactions with the Mtw1-C. Size exclusion chromatography performed by Hornung et al. (2014) revealed that the Ame1-Okp1 heterodimer directly binds to the Mtw1-C, whereas the Ctf19-Mcm21 heterodimer is insufficient to interact with the Mtw1-C. However, Hornung et al. (2014) did not exclude a role for the Ctf19-C components Ctf19 and Mcm21 in Mtw1-C binding in the context of the full COMA assembly (Ame1, Okp1, Ctf19, Mcm21). Our study revealed that the enrichment of the Mtw1-C component Dsn1 is reduced by half at the centromere in prophase I when Mcm21 is absent (Figure 3-8 B; Vincenten et al., 2015), suggesting that Mcm21 is required for proper levels of Dsn1 at centromeres. On the contrary, depletion of Dsn1 and Mtw1 did not reduce levels of Mcm21 accumulation at the centromere (Figure 3-8 C; Vincenten et al.,2015). These findings might imply that the recruitment of the Mtw1-C onto centromeres also depends on other Ctf19-C components (in addition to Ame1 and Mif2) during meiosis. By contrast, the recruitment of the Ctf19-C onto centromeres may not depend on the

Mtw1-C during meiosis. If this is the case, it seems likely that the role of the Ctf19-C in controlling pericentromeric DSB formation is to direct the recruitment of the Mtw1-C. The Mtw1-C in turn might regulate other kinetochore factors to suppress DSBs. In this study, we found that *CEN1*-proximal DSB formation is increased when the Ctf19-C subunits Ctf19, Mcm21, Iml3, Chl4, Ctf3, Mcm16 and Mcm22 are absent (Figure 3-7 D). Thus, this might suggest that the Mtw1-C contacts Ctf19, Mcm21, the Iml3-Chl4 sub-complex and the Ctf3 sub-complex (in addition to Mif2 and Ame1) during meiosis. To test whether Ctf19, the Iml3-Chl4 sub-complex and the Ctf3 sub-complex are required for Mtw1-C recruitment during meiosis, we can analyze the levels of Mtw1-C enrichment at centromeres by ChIP-qPCR when these Ctf19-C components are absent. If the hypothesis is true that the Ctf19-C controls DSB formation via directing the recruitment of the Mtw1-C, the increase in pericentromeric DNA break formation in Ctf19-C mutants may be the result of reduced levels of Mtw1-C accumulation (and potentially other kinetochore factors) at centromeres. Taken together, our hypothesis is the following (Figure 4-4 A): The recruitment of the Mtw1-C onto centromeres occurs via the direct binding to Mif2 and Ame1 (based on findings by Hornung et al. (2014)) and through contacts with the Ctf19, Mcm21, the Iml3-Chl4 sub-complex and the Ctf3 sub-complex. The Mtw1-C in turn might interact with other kinetochore factors such as the Spc105-C to suppress DSB formation near centromeres. Meyer et al. (2015) showed that, in addition to the Ctf19-C and Mtw1-C, the Spc105-C is assembled onto centromeres throughout prophase I. To test whether the Spc105-C plays a role in controlling meiotic DSB formation, we can analyze the effect of impairing Spc105-C function on pericentromeric DNA break formation. If the Spc105-C is involved in DSB control, we can go one step further and speculate that there might be a role for further factors such as kinases in controlling meiotic DSB formation near centromeres. For example, the Spc105-C is target of the conserved protein kinase Mps1 that regulates chromosome segregation and the spindle checkpoint (London et al., 2012).

As an alternative, we envision that the assembly of the Mtw1-C onto centromeres primarily depends on the direct binding to Mif2 and Ame1 (based on findings by Hornung et al. (2014)) and partially depends on the presence of Mcm21 based on our finding (Figure 3-8 B)) during meiosis and that the Mtw1-C and Ctf19-C have distinct roles in pericentromeric DSB control (Figure 4-4 B). The distinct roles of these kinetochore subunits might be equally important for DSB control. Thus,

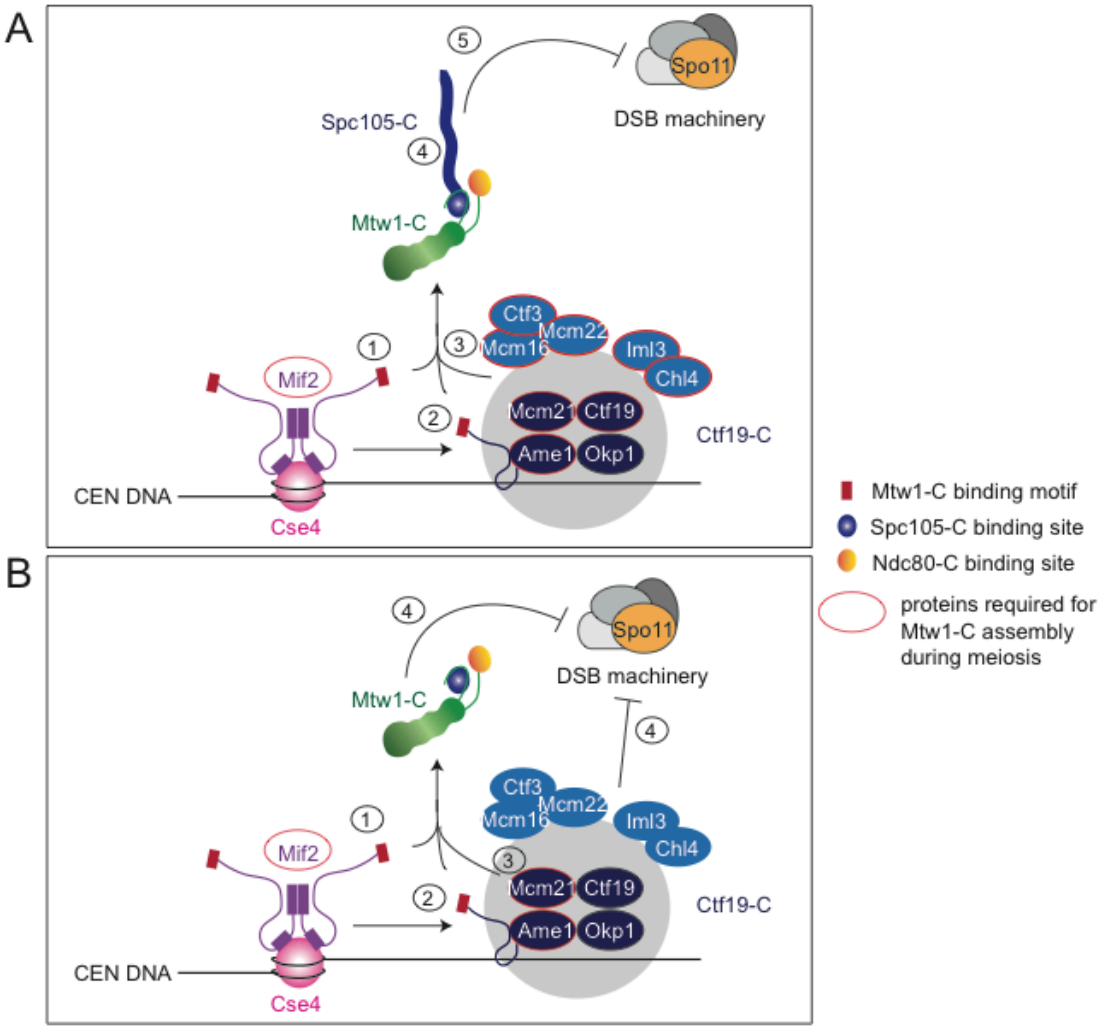

Figure 4-4 Hypothesis: The role of the Ctf19-C and Mtw1-C in pericentromeric DSB suppression during meiosis.

A) The Ctf19 complex (Ctf19-C) is required for Mtw1 complex (Mtw1-C) assembly, which in turn might interact with other kinetochore factors such as the Spc105-C to suppress meiotic DSB formation near centromeres. Circuit 1+2: Mif2 and Ame1 represent a binding platform for the Mtw1-C (based on Hornung et al., 2014). Circuit 3: The Ctf19-C proteins Mcm21, Ctf19, Iml3, Chl4, Ctf3, Mcm16 and Mcm22 are required for Mtw1-C assembly onto centromeres during meiosis. Circuit 4+5: The Mtw1-C interacts with the Spc105-C, which in turn is required to suppress meiotic DSB formation near centromeres. B) The assembly of the Mtw1-C onto centromeres depends on Mif2 and Ame1 as well as Mcm21 but the Mtw1-C and Ctf19-C perform distinct functions to suppress meiotic DSB formation close to centromeres. Circuit 1+2: Mif2 and Ame1 represent a binding platform for the Mtw1-C (based on Hornung et al., 2014). Circuit 3: The Ctf19-C proteins Mcm21 is required for Mtw1-C assembly during meiosis. Circuit 4: Both kinetochore subunits Ctf19-C and Mtw1-C have distinct roles in pericentromeric DSB suppression. The distinct roles of the Ctf19-C and Mtw1-C are equally important to prevent meiotic DSBs.

absence of either Mtw1-C or Ctf19-C would relieve DSB suppression in the vicinity of centromeres. To define the contribution of the Mtw1-C and Ctf19-C in DSB control, we will isolate individual components of both subunits from kinetochores through a synthetic targeting system and analyze the effect of targeting these components to a native DSB hotspot (such as *YCR047c* on chromosome *III* (Baudat and Nicolas, 1997)) on meiotic DNA break formation.

4.5 Molecular dissection of kinetochore function during meiotic CO recombination

4.5.1 Using CRISPR/ dCas9-based technology for the ectopic targeting of kinetochore components to defined chromosomal regions

In this study, we demonstrated that the kinetochore controls meiotic DNA break formation and CO recombination at centromere-proximal regions (Figures 3-1; 3-2; 3-3; 3-7D; 3-8). However, exact molecular details behind these kinetochore-driven processes remain completely unclear. We showed that manipulation of kinetochore components either through gene deletion for non-essential proteins or promoter replacement technique (mitosis-specific *pCLB2*-promoter; Lee and Amon, 2003) for essential kinetochore subunits has the disadvantage that other proteins in the kinetochore might also be affected. This constraint makes it difficult to define on a molecular level the contribution of individual kinetochore components in controlling meiotic DNA break formation and CO recombination. To overcome this constraint, we developed a “CRISPR/ dCas9-driven kinetochore targeting system” that allows us to uncouple individual kinetochore proteins from their native chromosomal position, the centromere, by targeting these proteins to an ectopic chromosomal site, a non-centromeric region, without manipulating native kinetochore function (Figure 3-17). This system is based on the clustered regularly interspaced short palindromic repeats (CRISPR)/ deactivated CRISPR associated protein 9 (dCas9) technique, which is an adaptation of CRISPR/ Cas9 (Dominguez et al., 2015). CRISPR/ Cas9 is an RNA-mediated system that was discovered in bacteria and archaea, in which it servers as a defense mechanism to protect from invading foreign DNA molecules (Barrangou et al., 2007; Bhaya et al., 2011; Wiedenheft et al., 2012). The CRISPR/ Cas9 system uses a single guide RNA (sgRNA) to direct the endonuclease Cas9 to a

sequence-specific target site, which is located upstream of a protospacer adjacent motif (short: PAM; sequence: NGG). Cas9 contains two distinct endonuclease domains (HNH and RuvC) to cleave the two DNA strands at the target site. Using CRISPR/ Cas9 as a kinetochore targeting system would have the disadvantage that Cas9 induces a DSB at the target site, which would interfere with meiotic DNA breaks and recombination at this site. Therefore, we employed a catalytically deactivated version of Cas9, referred to as dCas9, in which amino acid substitutions in the two active domains RuvC1 (D10A) and HnH (H840A) cause a loss of endonuclease function (Jinek et al., 2012; Gasiunas et al., 2012). However, loss of endonuclease activity does not disable dCas9 to target desired chromosomal regions adjacent to a PAM when guided through a sgRNA molecule (Jinek et al., 2012). As an alternative to the CRISPR/ dCas9-based targeting strategy, we could potentially employ the widely used repressor/ operator system including *lac* repressor (LacI)-*lac* operator (LacO) (Belmont and Straight, 1998; Belmont, 2001) and *tet* repressor (TetR)-*tet* operator (TetO) (Michaelis et al., 1997). Targeting a protein of interest fused to any of the two repressors (LacI or TetR) to a desired chromosomal position depends on the integration of an array of corresponding operator repeats (LacO or TetO). These approaches have successfully been utilized for the ectopic targeting of kinetochore proteins to explore their assembly and function (Kiermaier et al., 2009; Lacefield et al., 2009; Ho et al., 2014). However, we suspected that integrating operator repeats into chromosomes interferes with the recombination landscape, including formation and repair of meiotic DNA breaks. An example for altering DSB patterns on a chromosomal region as a consequence of integrating ectopic DNA sequences is the well-characterized *HIS4-LEU2* locus (Cao et al., 1990). Thus, the advantage of the CRISPR/ dCas9-based targeting system compared to the repressor/ operator technique is that altering the underlying DNA composition by integration of an operator array is unnecessary. Another reason why we favored CRISPR/ dCas9 as a targeting system for this study rather than the repressor/ operator methods is the high number of repeats contained within an operator array. A small operator array is made up of eight repeats (Lacefield et al., 2009). As one operator repeat binds a dimer of repressor fused to a protein of interest, sixteen copies of the protein can be recruited to a small array. However, the focus of this investigation was on the Ctf19-C. Based on our current understanding of budding yeast kinetochore composition, there is only two copies of the Ctf19-C assembled

onto centromeres (Joglekar et al., 2006). Thus, a number of sixteen Ctf19-C proteins might cause unwanted effects. In contrast to the repressor/ operator technique, our developed CRISPR/ dCas9-driven system allows for ectopic targeting of one copy of the kinetochore protein.

In this study, we demonstrated functionality and efficiency of our developed CRISPR/ dCas9-driven kinetochore targeting system. First, we observed expression of the fusion proteins Ctf19-3xFlag-dCas9, Iml3-3xFlag-dCas9 and 3xFlag-dCas9 when analyzed by Western blotting (Figure 3-17 C). Second, by ChIP-qPCR analysis, we found that the fusion proteins associate with the target sites *YHR020w-YHR021c* on chromosome *VIII* and *YCR045c-YCR046c* on chromosome *III* when directed via the corresponding sgRNAs (sgRNA-*VIII* and sgRNA-*III*) (Figure 3-20 C). By contrast, proteins guided with a control sgRNA (sgRNA-mock), which does not contain any complementary target-specific sequence, did not accumulate at the target sites on chromosomes *VIII* and *III*. Importantly, ectopic targeting of the fusion proteins to the target sites did not interfere with meiotic chromosome segregation and the production of viable gametes (Figure 3-20 E). Thus, we conclude that our developed CRISPR/ dCas9-driven system can be used to target kinetochore components to defined (non-centromeric) regions during meiosis.

4.5.2 The Ctf19 protein plays a specific role in pericentromeric CO suppression during meiosis

In this study, we analyzed the effect of ectopic targeting individual kinetochore components to a non-centromeric region via our developed CRISPR/ dCas9-based system on local CO formation to define the contribution of these components in controlling meiotic recombination. For this, we chose the Ctf19-C proteins Ctf19 and Iml3 because they (along with their binding partners Mcm21 and Chl4, respectively) exert the strongest effect on pericentromeric CO suppression (Figure 3-1 A). As a non-centromeric region, we chose a defined site within the interval on chromosome arm *VIII* used for the live cell reporter assay (Figure 3-20 B). We demonstrated that targeting Ctf19 to this site on chromosome arm *VIII* is sufficient to suppress local CO formation (Figure 3-20 D). On the contrary, targeting Iml3 to the same site did not affect CO patterns. These results indicate that Ctf19 has a specific function in controlling CO recombination.

However, we noticed that the effect of targeting Ctf19 to arm *VIII* on local CO formation is not as penetrant as it is at the chromosomal region close to *CEN8*. We observed an increase in CO frequency at the *CEN8*-proximal region from 0.4 centiMorgan (cM) in wild type cells to 8.9 cM in *ctf19Δ* cells (Figure 3-1 D). By contrast, we found a decrease in CO rates on the chromosome arm *VIII* from 7.2 cM in 3xFlag-dCas9 cells to 5.9 cM in Ctf19-3xFlag-dCas9 cells (Figure 3-20 D). Thus, targeting Ctf19 to arm *VIII* shows only a mild effect on local CO suppression when compared to the pericentromere. One explanation for the Ctf19 mediated mild effect on CO suppression at the ectopic locus could be due to limitations of the CRISPR/ dCas9-driven targeting system. Our current CRISPR/ dCas9-driven system allows for targeting of a single copy of Ctf19 to a defined chromosomal locus. However, studies demonstrated that two copies of the Ctf19-C are incorporated into the native kinetochore (Joglekar et al., 2006). Thus, recruiting only one copy of Ctf19 to chromosome arm *VIII* might not be sufficient enough to mimic pericentromeric CO suppression. Adapting the current CRISPR/ dCas9-driven system to enable the targeting of more than one protein via a multiplexed system would overcome this limitation. For the multiplexed system, it would be ideal to target two copies of the Ctf19 protein in close proximity to each other on chromosome arm *VIII* by co-expressing two sgRNAs with different target sequences (examples for multiplexed CRISPR/Cas9 systems: Cong et al., 2013; Kabadi et al., 2014). However, the choice of CRISPR/ dCas9 target sites within the chromosomal arm interval is limited due to the requirement for a PAM sequence adjacent to the sgRNA target sequence. For this reason, artificial integration of short arrays of sgRNA sequences on the chromosome arm (maximum distance of ~3 kb between DSB hotspot and target locus) would allow for targeting of multiple proteins in juxtaposition with each other. These sgRNA arrays need to be designed in such a way that they solely contain the sgRNA target complementary sequence and the PAM sequence (20 nt for sgRNA and 3 nt for the PAM sequence) without additional markers to prevent potential interference with the local meiotic recombination landscape. The multiplexed CRISPR/ dCas9-driven targeting system would allow us to examine the effect of targeting more than one Ctf19 protein to chromosome arm *VIII* on CO formation.

Another reason for the mild effect on CO suppression on arm *VIII* when Ctf19 is ectopically targeted might be that tetrads were included in the analysis in which the CRISPR/ dCas9-driven targeting system was not functional or efficient. Although

ChIP-qPCR analysis revealed that the overall targeting strategy for the fusion proteins to the target sites was efficient (Figure 3-20 C), we cannot rule out the possibility that the artificial recruitment does not work in every single cell. Hence, it might be possible that in some tetrads used for this analysis the CRISPR/ dCas9-driven system was not efficient enough to ectopically target the protein to the target site. If so, this analysis might underestimate the effect of targeting Ctf19 to arm *VIII* on CO suppression.

A further explanation for the modest effect of targeting Ctf19 to chromosome arm *VIII* on local CO formation could be that other factors, in addition to Ctf19, are required to exert complete CO suppression. It seems likely that the Ctf19 protein cooperates with other kinetochore components and/ or non-kinetochore factors to establish an environment surrounding centromeres that is not permissive for CO formation. Such factors might be absent from the target site when Ctf19 is synthetically recruited. This hypothesis takes into account that Ctf19 can co-recruit Mcm21 to the target site on arm *VIII*, but not Chl4 (Figure 3-21 C). Moreover, we demonstrated that targeting Ctf19 to arm *VIII* does not lead to meiotic chromosome segregation defects and the production of aneuploid inviable gametes, which would be expected as a consequence of the formation of di-centric chromosomes due to complete kinetochore restoration at the target site (Figure 3-20 E). Thus, we hypothesize that some currently undefined kinetochore factors are absent from the site on arm *VIII* when Ctf19 is targeted, which might explain the mild effect on CO suppression. Such factors might be factors involved in the Ctf19-C promoted loading and enrichment of Rec8-cohesin surrounding centromeres, which is required for CO suppression. To test whether the mild effect of targeting Ctf19 to chromosome arm *VIII* on CO suppression is due to the absence of factors required for Rec8-cohesin establishment, we will expand on recent work by Hinshaw et al. (2017). This work revealed the molecular mechanism of the Ctf19-C promoted loading and enrichment of cohesin at and around centromeres in mitotically dividing cells. This mechanism involves the phosphorylation of nine defined serine/ threonine residues within the unstructured N-terminal tail of the COMA protein Ctf19 drives the recruitment of the Scc2-Scc4 loader complex to centromeres. This phosphorylation depends on the activity of the Dbf4/ Cdc7 kinase (also referred to as the Dbf4-dependent kinase; DDK), which is directed to centromeres by Ctf3, another Ctf19-C component. The Ctf19 mediated recruitment of Scc2-Scc4 to centromeres in turn enables the

enrichment of cohesin at centromeric and pericentromeric regions. The molecular mechanism described by Hinshaw et al. (2017) might present a rationale for how exactly the Ctf19-C promotes Rec8-cohesin establishment at pericentromeres to suppress meiotic CO recombination. Based on our work and the findings by Hinshaw et al. (2017), we propose the following model for the role of the Ctf19-C in CO suppression (Figure 4-5): Within kinetochore assembly, the sub-complexes COMA, Iml3-Chl4 and Ctf3 may be the most important components for CO suppression at centromere-proximal regions. The presence of COMA onto centromeres seems to be required for the assembly of the Iml3-Chl4 sub-complex (Pekgöz Altunkaya et al., 2016; Schmitzberger et al., 2017). The Iml3-Chl4 complex in turn might be required for the incorporation of the Ctf3 sub-complex within kinetochores (Pekgöz Altunkaya et al., 2016), although there is evidence that this might occur in a manner independent of COMA and the Iml3-Chl4 sub-complexes (Schmitzberger et al., 2017). The Ctf3 protein recruits DDK to centromeres, which in turn phosphorylates nine defined serine/ threonine residues within the unstructured N-terminal tail of the Ctf19 protein. Phosphorylation of the N-terminal tail of Ctf19 allows for the recruitment of the Scc2-Scc4 complex to centromeres. The Scc2-Scc4 complex in turn enables the loading of Rec8-cohesin complex at centromeres, which spread into the adjacent pericentromere. The loading and enrichment of Rec8-cohesin promotes the association of Zip1 with cohesin-associated sites within the pericentromere. As suggested in section 4.3, both factors Rec8-cohesin and Zip1 might be equally essential for the suppression of pericentromeric COs.

In addition to our current understanding of the hierarchical assembly of the Ctf19-C (Pekgöz Altunkaya et al., 2016; Schmitzberger et al., 2017), the hypothesis that the sub-complexes COMA, Iml3-Chl4 and Ctf3 may be the most important kinetochore factors in CO suppression takes into account that we found increased pericentromeric CO formation in cells lacking Ctf19, Mcm21, Iml3 and Chl4, whereas CO rates were not affected in cells lacking other Ctf19-C components such as Nkp1, Nkp2, Cnn1 and Wip1 (Figure 3-1 D). A requirement for the Ctf3 sub-complex in pericentromeric CO control was not tested in this study. Alternatively, we observed increased pericentromeric DSB formation in cells lacking Ctf3, Mcm16 and Mcm22 (Figure 3-6), indicating a role for the Ctf3 sub-complex in controlling the initiating event of meiotic recombination. Since the Ctf3 protein is required for the recruitment of DDK to centromeres (Hinshaw et al., 2017), we predict that pericentromeric CO

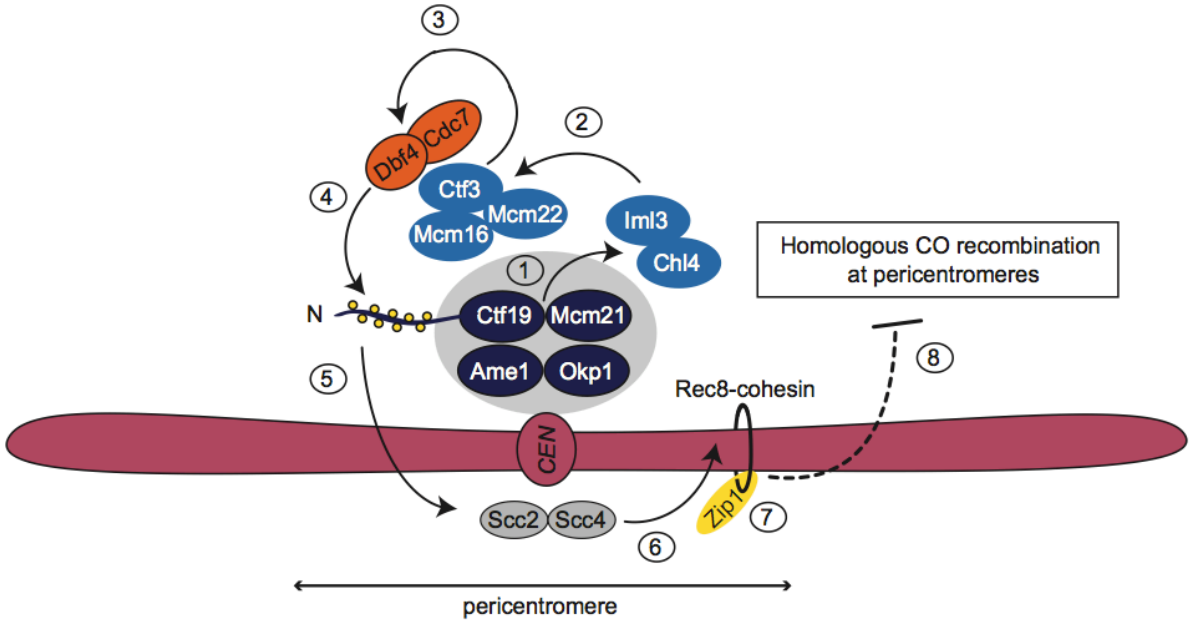

Figure 4-5 Model for the role of the Ctf19-C in controlling CO recombination at pericentromeres during meiosis.

Circuit 1: COMA (composed of the proteins Ctf19, Okp1, Mcm21 and Ame1) recruits the Iml3-Chl4 sub-complex to centromeres (Pekgöz Altunkaya et al., 2016 and Schmitzberger et al., 2017). Circuit 2: The assembly of COMA and the Iml3-Chl4 sub-complex is required for the assembly of the Ctf3 sub-complex (Pekgöz Altunkaya et al., 2016). Circuit 3: The Ctf3 protein recruits the Dbf4/ Cdc7 kinase (also referred to as the Dbf4-dependent kinase, DDK) to centromeres (Hinshaw et al., 2017). Circuit 4+5: The Dbf/ Cdc7 kinase phosphorylates nine defined serine/ threonine residues within the unstructured N-terminal tail of the Ctf19 protein, which in turn leads to the recruitment of the Scc2-Scc4 complex to centromeres (Hinshaw et al., 2017). Circuit 6: The Scc2-Scc4 complex enables the loading and enrichment of Rec8-cohesin. Circuit 7: Rec8-cohesin directs the association of Zip1 with cohesin-associated sites within centromere-proximal regions. Circuit 8: Both factors Rec8-cohesin and Zip1 are required for the suppression of CO recombination near centromeres.
For simplicity, only one chromosome and one copy of each kinetochore subunit are shown. *CEN* indicates the budding yeast centromere.

rates would increase in cells lacking the Ctf3 sub-complex. Without the Ctf3 sub-complex DDK might not efficiently be recruited to centromeres, which in turn would diminish/ prevent phosphorylation of the N-terminal tail of Ctf19 and thus abolish the loading and enrichment of Rec8-cohesin (and consequently Zip1). Thus, we hypothesize that the Ctf3 sub-complex might be involved in controlling CO recombination at centromere-proximal regions.

In the future, we will address this model via different approaches: We will analyze the effect of ectopic targeting different Ctf19 proteins containing mutations in the DDK

target residues within the N-terminal region to chromosome arm *VIII* on local CO formation. As a Ctf19 mutant, we will employ a phosphonull version of Ctf19, in which the nine serine/ threonine target residues of DDK in the N-terminus are mutated to alanine (*ctf19-9A*; Hinshaw et al., 2017). Hinshaw et al. (2017) demonstrated that the *ctf19-9A* mutant leads to reduced levels of the cohesin loader subunit Scc2 at centromeres and impairs cohesion. Targeting the *ctf19-9A* allele to the target site on arm *VIII* would allow us to determine whether the DDK-dependent phosphorylation of the N-terminal tail of Ctf19 (and thus cohesin enrichment) is required for the suppression in local CO formation. In addition to the *ctf19-9A* allele, we will use a phosphomimetic form of Ctf19, in which the nine serine/ threonine target residues of DDK are substituted by glutamate (*ctf19-9E*). As opposed to the *ctf19-9A* mutant, we expect that targeting the *ctf19-9E* mutant to the target site on arm *VIII* might cause enhanced binding of Rec8-cohesin complexes at this site and thus exert a stronger effect on CO suppression. Another possibility to test whether the Ctf19 (and Mcm21) mediated effect on CO suppression on arm *VIII* is dependent on DDK activity is to co-target the Ctf19-C proteins Ctf19 and Ctf3 to the target site via a multiplexed CRISPR/ dCas9-driven system. The prediction of co-targeting both Ctf19 and Ctf3 would be that Ctf3 recruits DDK to the target site to phosphorylate the nine residues of the N-terminal tail of Ctf19. This in turn might promote an enrichment of Rec8-cohesin complexes at the target locus and potentially exert a stronger effect on CO suppression on arm *VIII*. Alternatively, examining the effect of targeting Ctf19 in combination with DDK, instead of Ctf3, to the target site on local CO formation would also contribute to a better understanding of how exactly the Ctf19-C controls meiotic CO recombination.

4.6 Perspectives

As mentioned earlier, in diverse sexually reproducing organisms, homologous CO recombination at centromere-proximal regions is associated with meiotic chromosome segregation defects and the production of aneuploid/ inviable gametes (Hassold and Hunt, 2001; Koehler et al., 1996; Rockmill et al., 2006). In humans, CO formation in the vicinity of centromeres is associated with the incidence of Trisomy 21 (Down's syndrome) (Hasslod and Hunt, 2001). This PhD work contributes to a better understanding of how potentially dangerous homologous recombination events are prevented in genomic regions surrounding centromeres. We found that in budding yeast, the kinetochore, more specifically the Ctf19-C, suppresses both programmed

DNA break formation, the initiating event of meiotic recombination, and inter-homolog repair (COs and NCOs) near centromeres during meiosis. Although we showed that impaired Ctf19-C function leads to an increase in pericentromeric DSBs and COs, the impact of this phenotype on meiotic chromosome segregation is currently unknown. A characteristic feature of Ctf19-C mutants is chromosome non-disjunction in meiosis II, although some mutants of the Ctf19-C also exhibit chromosomes mis-segregation in meiosis I (Fernius and Marston, 2009; Adèle Marston, personal communication). In the future, it is therefore important to examine whether the chromosome segregation defects observed in Ctf19-C mutants are the result of misplaced meiotic DSBs and inter-homolog repair (COs) within centromere-proximal regions. Moreover, it is crucial to corroborate our findings and further define on a molecular level the Ctf19-C mediated mechanisms to suppress homologous CO recombination around centromeres.

The Ctf19-C is a conserved kinetochore subunit in eukaryotes, with the notable exception of certain organisms such as *D. melanogaster* and *C. elegans* (Drinnenberg et al., 2016). However, suppression of CO formation in the surroundings of centromeres is a common feature in diverse eukaryotic systems, including *D. melanogaster* (Beadle, 1932; Dobzhansky, 1930). Therefore, it would be interesting to investigate whether, if at all, other kinetochore subunits are involved in controlling CO recombination at pericentromeric regions in organisms whose kinetochores lack Ctf19-C function. On the contrary, in organisms that contain a Ctf19-C (for example, CCAN in humans), it would be exciting to determine whether the role of the Ctf19-C in controlling meiotic CO recombination at pericentromeres is conserved.

5 Summary

Controlled DNA double-strand break formation followed by homologous crossover recombination is essential to link homologous chromosomes and drive faithful chromosome segregation during meiosis. However, the formation of crossovers in the chromosomal regions surrounding the centromeres, also referred to as pericentromeres, is associated with meiotic chromosome mis-segregation and developmental aneuploidy in diverse eukaryotic organisms. In humans, crossover formation at pericentromeres is associated with the incidence of Trisomy 21 (Down's syndrome). In this study, we demonstrated that the multi-protein complex that assembles onto centromeres, the kinetochore, actively suppresses meiotic crossover recombination at pericentromeric regions in the budding yeast *Saccharomyces cerevisiae*. Within kinetochore assembly, we identified the conserved Ctf19 complex as the major factor in suppressing crossover formation close to centromeres. We revealed that the Ctf19 complex provides a multi-layered mechanism to exert crossover suppression. One layer of Ctf19 complex mediated crossover suppression is the inhibition of DNA break formation in the direct vicinity of centromeres. In addition to the Ctf19 complex, we showed that the Mtw1 complex, another conserved subunit of the budding yeast kinetochore, inhibits meiotic DNA break formation close to centromeres. However, this inhibition is not absolute as meiotic DNA breaks occur within centromere-proximal regions, although the overall amount is reduced. To channel residual DNA breaks away from a pathway that uses the homologous chromosome as a repair template, the Ctf19 complex provides another layer of suppression. This layer involves the Ctf19 complex promoted establishment of cohesin containing the meiosis-specific Rec8 subunit at centromeres and pericentromeres. The establishment of Rec8-cohesin in turn directs the association of the synaptonemal complex protein Zip1 with centromeric and pericentromeric regions. Both proteins Rec8-cohesin and Zip1 are required to suppress crossover recombination near centromeres. To understand the molecular basis of the Ctf19 complex-driven control of meiotic crossover recombination, we developed a synthetic targeting system, based on CRISPR/ dCas9 technology, that allows us to isolate components of the Ctf19 complex from kinetochores. Using this system, we directed Ctf19 complex proteins to an ectopic site, a non-centromeric region, and revealed sufficiency of a specific protein (called Ctf19) in the local control of crossover recombination. The role of the Ctf19-C in controlling crossover recombination near

centromeres might represent a rationale of how the incidence of meiotic chromosome segregation defects and the generation of aneuploid gametes is prevented.

6 Zusammenfassung

Während der Meiose ist die kontrollierte Bildung von DNA Doppelstrangbrüchen und die darauf folgende homologe Crossover Rekombination essentiell, um homologe Chromosomen zu verbinden und akkurat zu trennen. Die Entstehung von Crossovern in chromosomalen Regionen um die Centromere, auch als Pericentromere bezeichnet, ist allerdings mit Chromosomenfehlverteilung und Aneuploidie in diversen eukaryotischen Organismen verbunden. Bei Menschen ist die Entstehung von Crossovern in Pericentromeren mit Trisomie 21 (Down Syndrom) assoziiert. In dieser Studie demonstrierten wir, dass der Multiproteinkomplex der sich auf Centromeren zusammensetzt, genannt das Kinetochore, Crossover Recombination in pericentromeren Regionen der Hefe *Saccharomyces cerevisiae* aktiv unterdrückt. Innerhalb des Kinetochores identifizierten wir den konservierten Ctf19 Komplex als einen Hauptfaktor in der Unterdrückung von Crossover Bildung in der Nähe von Centromeren. Wir offenbarten, dass der Ctf19 Komplex einen mehrschichtigen Mechanismus zur Verfügung stellt, um Crossover-Unterdrückung zu gewährleisten. Eine Schicht, der vom Ctf19 Komplex ausgehenden Crossover Unterdrückung, stellt die Inhibierung von DNA Doppelstrangbrüchen in direkter Nachbarschaft von Centromeren dar. Zusätzlich zu dem Ctf19 Komplex zeigten wir, dass der Mtw1 Komplex, eine weitere konservierte Untereinheit des Hefe-Kinetochores, die Bildung von Doppelstrangbrüchen in der Nähe von Centromeren inhibiert. Diese Inhibierung ist allerdings nicht vollständig, obwohl die Gesamtanzahl von DNA Brüchen, die in der Centromere-Region enstehen, reduziert ist. Um verbleibende DNA Brüche von einem Pfad, der homologe Chromosomen als Reparaturvorlage benutzt, abzulenken, stellt der Ctf19 Komplex eine weitere Schicht zur Unterdrückung bereit. Diese Schicht beinhaltet die vom Ctf19 Komplex geförderte Anreicherung von Cohesin mit der meiose-spezifischen Rec8 Untereinheit bei Centromeren und Pericentromeren. Die Anreicherung von Rec8-Cohesin steuert wiederum die Assoziierung des Proteins Zip1 des synaptonemalen Komplexes mit centromerischen und pericentromerischen Regionen. Sowohl Rec8-cohesin als auch Zip1 sind benötigt um Crossover Recombination in der Nähe con Centromeren zu unterdrücken. Um die molekulare Basis des Ctf19 Komplexes in der Kontrolle von Crossover Recombination zu verstehen, entwickelten wir ein synthetisches System, basierend auf CRISPR/ dCas9 Technologie, dass uns ermöglichte Komponenten des Ctf19 Komplexes vom Kinetochore zu isolieren. Durch Anwendung dieses Systems lenkten wir Proteine des

Ctf19 Komplexes zu einer ektopischen Stelle, eine nicht-centromere Region, und offenbarten, dass das Protein Ctf19 ausreichend ist um Crossover Recombination zu unterdrücken. Die Funktion des Ctf19 Komplexes in der Unterdrückung von Crossover Recombination in der Nähe von Centromeren könnte ein Grundprinizip darstellen, wie meiotische Chromosomenfehlverteilungen und die Entstehung von aneuploidien Gameten verhindert werden.

7 Appendices

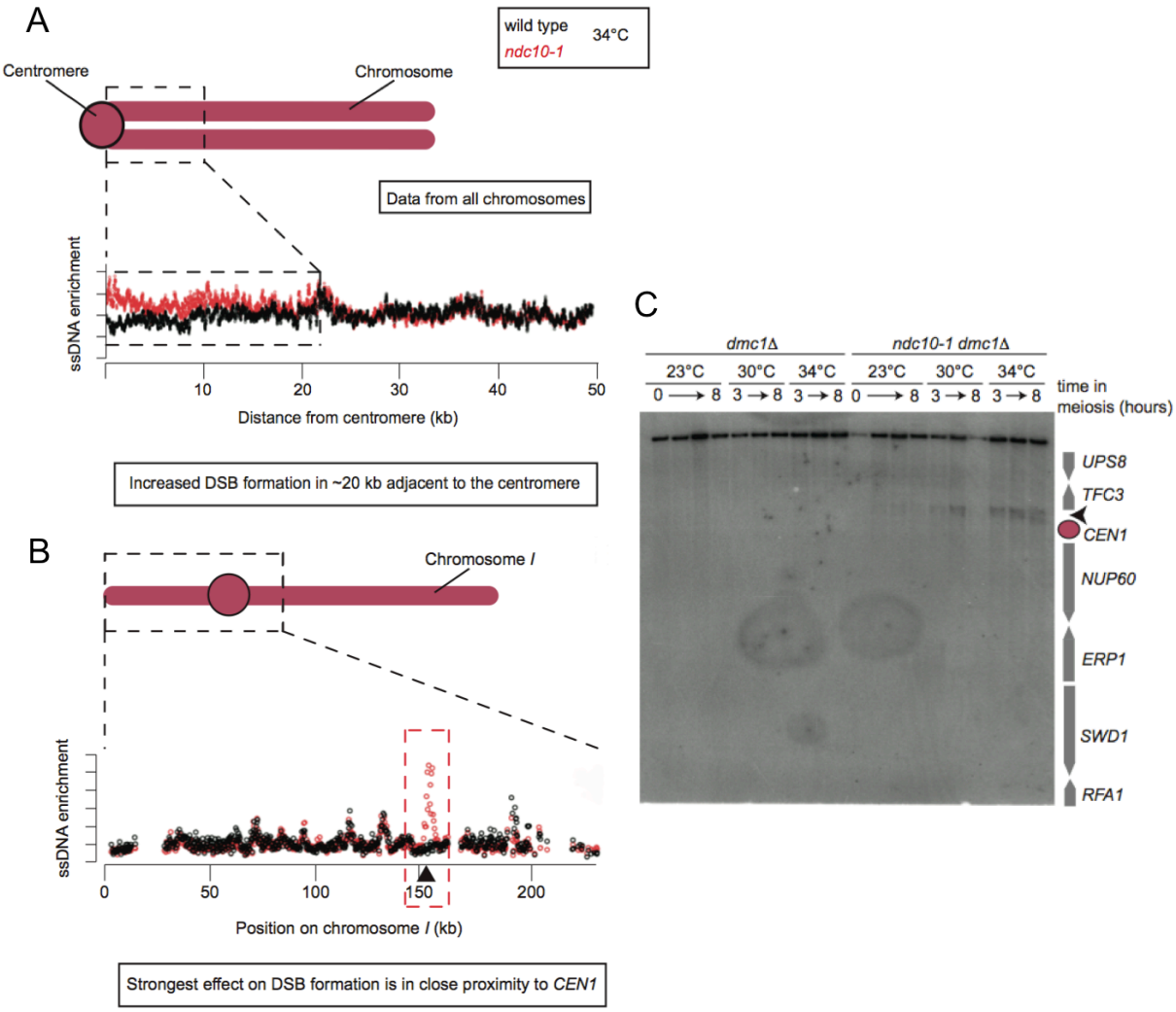

Figure 7-1 Impaired kinetochore function causes increased pericentromeric DSB formation

A) Measurement of ssDNA enrichment of all pericentromeres (~50 kb region surrounding the yeast centromere) at 34^{0}C in wild type (*dmc1Δ*) and *ndc10-1* (*ndc10-1 dmc1Δ*) cells. The mutation *dmc1Δ* is used to trigger meiotic arrest and accumulate DNA breaks allowing the mapping of ssDNA that naturally occurs on DNA break sites. This mutation does not affect meiotic DSB patterns when compared to wild type cells. B) Zoom in of ssDNA profile surrounding the centromere (*CEN1*) on chromosome *I* at 34^{0}C in wild type (*dmc1Δ*) and *ndc10-1* (*ndc10-1 dmc1Δ*) cells. C) Southern blot analysis of meiotic DNA breaks in region surrounding *CEN1* at 23^{0}C, 30^{0}C and 34^{0}C in wild type (*dmc1Δ*) and *ndc10-1* (*ndc10-1 dmc1Δ*) cells. Illustration of the chromosomal organization (genes and centromere position) of the region surrounding the centromere on chromosome *I*. Arrowhead indicates DSBs.

Table 7-1: Yeast strains used in this study.

Strain	Genotype	Reference	Figure
AM 10658	*MATa/MATα ndt80Δ::LEU2/ndt80Δ::LEU2 chl4Δ::KanMX6/chl4Δ::KanMX6*	Marston laboratory	3-14 B
AM 10660	*MATa/MATα ndt80Δ::LEU2/ndt80Δ::LEU2 ctf19Δ::KanMX6/ctf19Δ::KanMX6*	Marston laboratory	3-14 B
AM 10664	*MATa/MATα ndt80Δ::LEU2/ndt80Δ::LEU2 mcm21Δ::KanMX6/mcm21Δ::KanMX6*	Marston laboratory	3-14 B
AM 10686	*MATa/MATα ndt80Δ::LEU2/ndt80Δ::LEU2 iml3Δ::KanMX6/iml3Δ::KanMX6*	Marston laboratory	3-14 B
AM 10913	*MATa/MATα ndt80Δ::LEU2/ndt80Δ::LEU2 zip1Δ::HIS3/zip1Δ::HIS3*	Marston laboratory	3-14 A, B
AM 11633	*MATa/MATα ndt80Δ::LEU2/ndt80Δ::LEU2*	Marston laboratory	3-14 A, B
AM 13408	*MATa/MATα THR1::pYKL050c-CFP::TRP/THR1::pYKL050c-CFP::TRP CEN8::pYKL050c-RFP::LEU/+ SGD.115024-115572::pYKL050c-GFP*::URA/+ iml3Δ::KanMX6/iml3Δ::KanMX6*	Marston laboratory	3-1 D
AM 13410	*MATa/MATα THR1::pYKL050c-CFP::TRP/THR1::pYKL050c-CFP::TRP CEN8::pYKL050c-RFP::LEU/+ SGD.115024-115572::pYKL050c-GFP*::URA/+ chl4Δ::KanMX6/chl4Δ::KanMX6*	Marston laboratory	3-1 D

Table 7-1 continued.

Strain	Genotype	Reference	Figure
AM 13413	*MATa/MATα THR1::pYKL050c-CFP::TRP/THR1::pYKL050c-CFP::TRP CEN8::pYKL050c-RFP::LEU/+ SGD.115024-115572::pYKL050c-GFP*::URA/+ mcm21Δ::KanMX6/mcm21Δ::KanMX6*	Marston laboratory	3-1 D
AM 13964	*MATa/MATα THR1::pYKL050c-CFP::TRP/THR1::pYKL050c-CFP::TRP CEN8::pYKL050c-RFP::LEU/+ SGD.115024-115572::pYKL050c-GFP*::URA/+ zip1Δ::HIS3/zip1Δ::HIS3*	Marston laboratory	3-1 D, 3-14 C
AM 14087	*MATa/MATα THR1::pYKL050c-CFP::TRP/THR1::pYKL050c-CFP::TRP ARG4::pYKL050c-GFP*::URA/+ SGD.150521-151070::pYKL050c-RFP::LEU/+*	Marston laboratory	3-1 E
AM 14235	*MATa/MATα THR1::pYKL050c-CFP::TRP/THR1::pYKL050c-CFP::TRP ARG4::pYKL050c-GFP*::URA/+ SGD.150521-151070::pYKL050c-RFP::LEU/+ mcm21Δ::KanMX6/mcm21Δ::KanMX6*	Marston laboratory	3-1 E
AM 14237	*MATa/MATα THR1::pYKL050c-CFP::TRP/THR1::pYKL050c-CFP::TRP ARG4::pYKL050c-GFP*::URA/+ SGD.150521-151070::pYKL050c-RFP::LEU/+ chl4Δ::KanMX6/chl4Δ::KanMX6*	Marston laboratory	3-1 E

Table 7-1 continued.

Strain	Genotype	Reference	Figure
AM 14239	*MATa/MATα THR1::pYKL050c-CFP::TRP/THR1::pYKL050c-CFP::TRP ARG4::pYKL050c-GFP*::URA/+ SGD.150521-151070::pYKL050c-RFP::LEU/+ ctf19Δ::KanMX6/ctf19Δ::KanMX6*	Marston laboratory	3-1 E
AM 14243	*MATa/MATα THR1::pYKL050c-CFP::TRP/THR1::pYKL050c-CFP::TRP ARG4::pYKL050c-GFP*::URA/+ SGD.150521-151070::pYKL050c-RFP::LEU/+ iml3Δ::KanMX6/iml3Δ::KanMX6*	Marston laboratory	3-1 E
AM 14247	*MATa/MATα THR1::pYKL050c-CFP::TRP/THR1::pYKL050c-CFP::TRP ARG4::pYKL050c-GFP*::URA/+ SGD.150521-151070::pYKL050c-RFP::LEU/+ zip1Δ::HIS3/zip1Δ::HIS3*	Marston laboratory	3-1 E, 3-14 D
AM 17554	*MATa/MATα THR1::pYKL050c-CFP::TRP/THR1::pYKL050c-CFP::TRP ARG4::pYKL050c-GFP*::URA/+ SGD.150521-151070::pYKL050c-RFP::LEU/+ iml3::pCLB2-3HA-IML3::KanMX6/iml3::pCLB2-3HA-IML3::KanMX6*	Marston laboratory	3-1 E

Table 7-1 continued.

Strain	Genotype	Reference	Figure
AM 17700	*MATa/MATα THR1::pYKL050c-CFP::TRP/THR1::pYKL050c-CFP::TRP CEN8::pYKL050c-RFP::LEU/+ SGD.115024-115572::pYKL050c-GFP*::URA/+ nkp1Δ::KanMX6/nkp1Δ::KanMX6*	Marston laboratory	3-1 D
AM 17702	*MATa/MATα THR1::pYKL050c-CFP::TRP/THR1::pYKL050c-CFP::TRP CEN8::pYKL050c-RFP::LEU/+ SGD.115024-115572::pYKL050c-GFP*::URA/+ cnn1Δ::KanMX6/cnn1Δ::KanMX6*	Marston laboratory	3-1 D
AM 17809	*MATa/MATα THR1::pYKL050c-CFP::TRP/THR1::pYKL050c-CFP::TRP CEN8::pYKL050c-RFP::LEU/+ SGD.115024-115572::pYKL050c-GFP*::URA/+ wip1Δ::NAT/wip1Δ::NAT*	Marston laboratory	3-1 D
AM 18054	*MATa/MATα THR1::pYKL050c-CFP::TRP/THR1::pYKL050c-CFP::TRP ARG4::pYKL050c-GFP*::URA/+ SGD.150521-151070::pYKL050c-RFP::LEU/+ cnn1Δ::KanMX6/cnn1Δ::KanMX6*	Marston laboratory	3-1 E

Table 7-1 continued.

Strain	Genotype	Reference	Figure
AM 18881	*MATa/MATα ndt80Δ::LEU2/ndt80Δ::LEU2 scc4-m35::HIS3/scc4-m35::HIS3*	Marston laboratory	3-14 A
AM 20078	*MATa/MATα ndt80Δ::LEU2/ndt80Δ::LEU2 DSN1-6HIS-3FLAG::URA3/ DSN1-6HIS-3FLAG::URA3*	Marston laboratory	3-8 B
AM 20080	*MATa/MATα ndt80Δ::LEU2/ndt80Δ::LEU2 DSN1-6HIS-3FLAG::URA3/ DSN1-6HIS-3FLAG::URA3 mcm21Δ::KanMX6/mcm21Δ::KanMX6*	Marston laboratory	3-8 B
AM 20294	*MATa/MATα mtw1::pCLB2-3HA-MTW1::KanMX6/mtw1::pCLB2-3HA-MTW1::KanMX6 ndt80Δ::LEU2/ndt80Δ::LEU2 MCM21-yEGFP::KanMX6/MCM21-yEGFP::KanMX6*	Marston laboratory	3-8 B
AM 20295	*MATa/MATα dsn1::pCLB2-3HA-DSN1::KanMX6/dsn1::pCLB2-3HA-DSN1::KanMX6 REC8-3HA::URA3/- ndt80Δ::LEU2/ndt80Δ::LEU2 MCM21-yEGFP::KanMX6/MCM21-yEGFP::KanMX6*	Marston laboratory	3-8 B
AM 20296	*MATa/MATα ndt80Δ::LEU2/ndt80Δ::LEU2 MCM21-yEGFP::KanMX6/MCM21-yEGFP::KanMX6*	Marston laboratory	3-8 B
GV 8	*MATa/ MATalpha, ho::LYS2, lys2, ura3, leu2::hisG, his3::hisG, trp1::hisG*	This study	3-18, 3-19

Table 7-1 continued.

Strain	Genotype	Reference	Figure
GV 48	*MATa/ MATalpha, ho::LYS2, lys2, leu2::hisG, his4X::LEU2-URA3, ura3, arg4-Bgl2, dmc1D::ARG4, arg4-nsp*	This study	3-4 C, 3-5 B, 3-6 B, C, 3-7 B, C, 3-8 D, 3-9, 3-10, 3-14 E, 3-15 B, 3-16, 7-1
GV 1819	*MATa/ MATalpha, ho::LYS2, lys2, ura3, leu2::hisG, his3::hisG, TRP1, his4X::LEU2-URA3, ndc10-1::KanMX, dmc1::ARG4, trp1::hisG, arg4-nsp*	This study	3-6 C, 3-7 B, C, D, 7-1
GV 1853	*MATa/ MATalpha, ho::LYS2, lys2, ura3, leu2::hisG, his3::hisG, trp1::hisG, RPL13A-2XFKBP12::TRP1, fpr1::KanMX4, tor1-1::HIS3*	This study	3-11 B, C, D
GV 1870	*MATa/ MATalpha, ho::LYS2, lys2, leu2::hisG, his4X::LEU2-URA3, ura3, arg4-nsp, dmc1D::ARG4, TRP1, iml3::KANMX*	This study	3-5 B, 3-7 D
GV 1906	*MATa/ MATalpha, ho::LYS2, lys2, leu2::hisG, his4X::LEU2-URA3, ura3, ARG4, TRP1, dmc1D::ARG4, nkp2D::KanMX6*	This study	3-7 C, 3-7 D
GV 1908	*MATa/ MATalpha, ho::LYS2, lys2, leu2::hisG, his4X::LEU2-URA3, ura3, ARG4 (?), TRP1, dmc1D::ARG4, nkp1D::KanMX6, arg4(-nsp)*	This study	3-7 C, 3-7 D

Table 7-1 continued.

Strain	Genotype	Reference	Figure
GV 1912	*MATa/ MATalpha, ho::LYS2, lys2, leu2::hisG, his4X::LEU2-URA3, ura3, arg4(-nsp), TRP1, dmc1D::ARG4, ctf19D::KanMX6, ARG4 (?)*	This study	3-4 C, 3-5 B, 3-6 B, 3-7 D, 3-8 D, 3-10, 3-12 D, 3-15, 3-16
GV 1913	*MATa/ MATalpha, ho::LYS2, lys2, leu2::hisG, his4X::LEU2-URA3, ura3, arg4(-nsp), TRP1, dmc1D::ARG4, ctf3D::KanMX6*	This study	3-6 B, 3-7 D
GV 1914	*MATa/ MATalpha, ho::LYS2, lys2, leu2::hisG, his4X::LEU2-URA3, ARG4, ura3, trp1::hisG, dmc1D::ARG4, mcm16D::KanMX6, TRP1*	This study	3-6 C, 3-7 D
GV 1971	*MATa/ MATalpha, ho::LYS2, lys2(?), ura3, leu2::hisG, his3::hisG, trp1::hisG, his4B::LEU2, , arg4-Bgl2/ARG4 (?), mcm22D::KanMX, dmc1D::ARG4*	This study	3-6 C, 3-7 D
GV 2029	*MATa/ MATalpha, ho::LYS2, lys2, leu2::hisG, his4B::LEU2, ura3, ARG4, TRP, HIS, dmc1D::ARG4, cnn1D::HphMX*	This study	3-7 B, 3-7 D
GV 2050	*MATa/ MATalpha, ho::LYS2, lys2, leu2::hisG, ura3, arg4-Bgl2/ARG4 (?),dmc1D::ARG4, mcm21::KANMX his4B::LEU2*	This study	3-4 C, 3-7 D, 3-9, 3-14 E
GV 2127	*MATa/ MATalpha, ho::LYS2, lys2, leu2::hisG, his4X::LEU2-URA3, ura3, arg4(-nsp), TRP1, dmc1D::ARG4, ctf3D::KanMX6, spo11-Y135F-HA-URA3*	This study	3-6 B

Table 7-1 continued.

Strain	Genotype	Reference	Figure
GV 2128	*MATa/ MATalpha, ho::LYS2, lys2, leu2::hisG, ura3, ARG4 (?), TRP1, dmc1D::ARG4, ctf19D::KanMX6, spo11-Y135F-HA-URA3*	This study	3-4 C
GV 2135	*MATa/ MATalpha, ho::LYS2, lys2, leu2::hisG, his4B::LEU2, ura3, arg4-Bgl2, TRP1, dmc1D::ARG4, rts1del::KanMX6*	This study	3-15 B
GV 2139	*MATa/ MATalpha, ho::LYS2, lys2, leu2::hisG, his4X::LEU2-URA3, ura3, arg4-nsp, dmc1D::ARG4, TRP1, ARG4, chl4::KANMX*	This study	3-5 B
GV 2140	*MATa/ MATalpha, ho::LYS2, lys2, leu2::hisG, trp1::hisG, ura3, arg4-Bgl2(?), dmc1D::ARG4, sgo1D::KanMX6*	This study	3-15 B
GV 2145	*MATa/ MATalpha, ho::LYS2, lys2, leu2::hisG, ura3, arg4-Bgl2, dmc1D::ARG4, sgo1(Y47A,Q50A, S52A)-6HA::TRP1*	This study	3-15 B
GV 2205	*MATa/ MATalpha, ho::LYS2, lys2, ura3::hisG, leu2::hisG, his4X, TRP1, spo11-Y135F-HA-URA3, arg4-Bgl2/ARG4 (?),dmc1D::ARG4, mcm21::KANMX*	This study	3-4 C
GV 2275	*MATa/ MATalpha, ho::LYS2, lys2, ura3, leu2::hisG, his3::hisG, trp1::hisG, tor1-1::HIS3, RPL13A-2XFKBP12::TRP1, fpr1::KanMX4, CTF19-FRB-GFP::KanMX6*	This study	3-11 B, C, D
GV 2283	*MATalpha, ho::LYS2, lys2, ura3, leu2::hisG, his3::hisG, trp1::hisG, tor1-1::HIS3, RPL13A-2XFKBP12::TRP1, fpr1::KanMX4, Ctf19-FRB-GFP::KanMX6, mad2::KanMX*	This study	3-11 B

Table 7-1 continued.

Strain	Genotype	Reference	Figure
GV 2286	*MATa/ MATalpha, ho::LYS2, lys2, his4B::LEU2, ura3, arg4-Bgl2/ARG4 (?), dmc1D::ARG4, mcm21::KANMX, rec8::HIS3MX6*	This study	3-9
GV 2203	*MATa/ MATalpha, ho::LYS2, lys2, ura3, leu2::hisG, his3::hisG, trp1::hisG, RPL13A-2XFKBP12::TRP1, fpr1::KanMX4, tor1-1::HIS3, ORC2-FRB::KanMX6*	This study	3-11 B
GV 2305	*MATa/ MATalphs, ho::LYS2, lys2, ura3, leu2::hisG, his3::hisG, trp1::hisG, Scc4::HIS3, his4X::LEU2-URA3, ura3, arg4-nsp, dmc1D::ARG4, TRP1, ARG4*	This study	3-10
GV 2354	*MATa/ MATalpha, ho::LYS2, lys2, ura3, leu2::hisG, his3::hisG, trp1::hisG, tor1-1::HIS3, RPL13A-2XFKBP12::TRP1, fpr1::KanMX4, CTF19-FRB-GFP::KanMX6, dmc1D::ARG4*	This study	3-12 D, E, F
GV 2367	*MATa/ MATalpha, ho::LYS2, lys2, leu2::hisG, ura3, arg4-Bgl2, his3::hisG, trp1::hisG, RPL13A-2XFKBP12::TRP1, fpr1::KanMX4, tor1-1::HIS3, dmc1D::ARG4*	This study	3-12 D, E, F
GV 2514	*MATa/ MATalpha, ho::LYS2, lys2, leu2::hisG, ura3, his3::hisG?, trp1::hisG, TRP, arg4-nsp (?), ndt80D::LEU2 (?), mtw1::pCLB2-3HA-MTW1::KanMX6, dmc1D::ARG4, ARG4, REC8-3HA::URA3*	This study	3-8 D
GV 2533	*MATa/ MATalpha, ho::LYS2, lys2, ura3, leu2::hisG, his3::hisG, trp1::hisG, Scc4-F324A_K327D_K331D_K541A_K542A::HIS3, arg4-nsp, dmc1D::ARG4, TRP1, ARG4 his4X::LEU2-URA3*	This study	3-10

Table 7-1 continued.

Strain	Genotype	Reference	Figure
GV 2548	*MATa/ MATalpha, ho::LYS2, lys2, leu2::hisG, ura3, his3::hisG?, trp1::hisG, TRP, arg4-nsp (?), REC8-3HA::URA3 (?), dsn1::pCLB2-3HA-DSN1::KanMX6, dmc1D::ARG4, ARG4*	This study	3-8 D
GV 2734	*MATa/ MATalpha, ho::LYS2, lys2, leu2::hisG, his4X::LEU2::URA3, ura3, his3::hisG, zip1::LYS2, dmc1D::HIS3*	Hochwagen's laboratory	3-14 E
GV 2913	*MATa/ MATalpha, ho::LYS2, lys2, leu2::hisG, his4X::LEU2-URA3, ura3, arg4-nsp (?), dmc1Δ::ARG4, TRP1, ARG4 , IRC20Δ::HphMX4, TRP1*	This study	3-16
GV 2921	*MATa/ MATalpha, ho::LYS2, lys2, leu2::hisG, his4X::LEU2-URA3, ura3, arg4-nsp (?), dmc1Δ::ARG4, TRP1, YTA7Δ::HphMX4*	This study	3-16
GV 2930	*MATa/ MATalpha, ho::LYS2, lys2, leu2::hisG, ura3 (?), arg4-nsp, dmc1Δ::ARG4, htz1::KanMX*	This study	3-16
GV 2931	*MATa/ MATalpha, ho::LYS2, lys2, leu2::hisG, his4X::LEU2-URA3 (?), ura3, arg4-nsp, dmc1Δ::ARG4, ARG4, ARP8Δ::HphMX*	This study	3-16
GV 2943	*MATa/ MATalpha, ho::LYS2, lys2, leu2::hisG, his4X::LEU2-URA3, ura3, arg4-nsp, dmc1Δ::ARG4, TRP1 (?), ARG4 (?), ISW1Δ::HphMX*	This study	3-16
GV 2950	*MATa/ MATalpha, ho::LYS2, lys2, ura3, leu2::hisG, his3::hisG, trp1::hisG, ARG trp::p11_pHOP1_3xFLAG-dCas9::TRP*	This study	3-17 B, C
GV 2953	*MATa/ MATalpha, ho::LYS2, lys2, ura3, leu2::hisG, his3::hisG, trp1::hisG, ARG trp::p11_pHOP1_IML3_3xFLAG-dCas9::TRP*	This study	3-17 B, C, 3-19
GV 2958	*MATa/ MATalpha, ho::LYS2, lys2, leu2::hisG, his4X::LEU2-URA3, ura3, arg4-nsp, dmc1Δ::ARG4, TRP1, FUN30Δ::HphMX*	This study	3-16

Table 7-1 continued.

Strain	Genotype	Reference	Figure
GV 2960	*MATa/ MATalpha, ho::LYS2, lys2, ura3, leu2::hisG, his3::hisG, trp1::hisG, ARG trp::p11_pHOP1_CTF19_3xFLAG-dCas9::TRP*	This study	3-17 B, C, 3-18
GV 3049	*MATa/ MATalpha, ho::LYS2, lys2, leu2::hisG, his4X::LEU2-URA3, ura3, arg4, TRP1, ctf19D::KanMX6*	This study	3-18
GV 3086	*MATa/ MATalpha, ho::LYS2, lys2, ura3, leu2::hisG, his3::hisG, trp1::hisG, arg4, iml3::KANMX*	This study	3-19
GV 3095	*MATa/ MATalpha, ho::LYS2, lys2, ura3, leu2::hisG, his3::hisG, ARG trp1::p11_pHOP1_CTF19_3xFLAG-dCas9::TRP1, ctf19Δ::KanMX6, dmc1Δ::ARG4 (?), ARG4(?)*	This study	3-18
GV 3128	*MATa/ MATalpha, ho::LYS2, lys2, ura3, leu2::hisG, his3::hisG, trp1::hisG, trp::p11_pHOP1_IML3_3xFLAG-dCas9::TRP, iml3::KANMX, ARG4*	This study	3-19
GV 3129	*MATa/ MATalpha, ho::LYS2, lys2, ura3, leu2::hisG, his3::hisG, trp1::hisG, trp::p11_pHOP1_3xFLAG-dCas9::TRP, ura3:: sgRNA expression cassette_sequence 5) chromosome arm8::URA3 THR1::pYKL050c-CFP::TRP SGD. 150521-151070::pYKL050c-RFP::LEU (~10kb to right of ARG4)/ ARG4::pYKL050c-GFP*::URA*	This study	3-20 C, D, E, 3-21 C, D
GV 3166	*MATa/ MATalpha, ho::LYS2, lys2, ura3, leu2::hisG, his3::hisG, trp1::hisG, trp::p11_pHOP1_CTF19_3xFLAG-dCas9::TRP, ura3:: sgRNA expression cassette_sequence 5) chromosome arm8::URA3 THR1::pYKL050c-CFP::TRP ARG4::pYKL050c-GFP*::URA/ SGD. 150521-151070::pYKL050c-RFP::LEU (~10kb to right of ARG4)*	This study	3-20 C, D, E, 3-21 C, D

Table 7-1 continued.

Strain	Genotype	Reference	Figure
GV 3179	*MATa/ MATalpha, ho::LYS2, lys2, ura3, leu2::hisG, his3::hisG, trp1::hisG, trp::p11_pHOP1_IML3_3xFLAG-dCas9::TRP (fusion protein Iml3-dCas9), ura3:: sgRNA expression cassette_sequence 5) chromosome arm8::URA3 THR1::pYKL050c-CFP::TRP SGD. 150521-151070::pYKL050c-RFP::LEU (~10kb to right of ARG4)/ ARG4::pYKL050c-GFP*::URA*	This study	3-20 C, D, E
GV 3272	*MATa/ MATalpha, ho::LYS2, lys2, ura3, leu2::hisG, his3::hisG, trp1::hisG,ARG4, Mcm21-6HA::TRP1 trp::p11_pHOP1_CTF19_3xFLAG-dCas9::TRP, ura3:: sgRNA expression cassette_sequence 5) chromosome arm8::URA3*	This study	3-21 A, C
GV 3308	*MATa/ MATalpha, ho::LYS2, lys2, ura3, leu2::hisG, his3::hisG, trp1::hisG, Mcm21-6HA::TRP1, ura3:: sgRNA expression cassette_sequence 5) chromosome arm8::URA3*	This study	3-21 A
GV 3311	*MATa/ MATalpha, ho::LYS2, lys2, ura3, leu2::hisG, his3::hisG, trp1::hisG, ARG trp::p11_pHOP1_CTF19_3xFLAG-dCas9::TRP, ura3:: sgRNA expression cassette w/out 20mer guide sequence::URA3 THR1::pYKL050c-CFP::TRP ARG4::pYKL050c-GFP*::URA/ SGD. 150521-151070::pYKL050c-RFP::LEU (~10kb to right of ARG4)*	This study	3-20 C, D

Table 7-1 continued.

Strain	Genotype	Reference	Figure
GV 3433	*MATa/ MATalpha, ho::LYS2, lys2, ura3, leu2::hisG, his3::hisG, trp1::hisG, CHL4-6HA::k1TRP1 trp::p11_pHOP1_CTF19_dCas9::TRP (fusion protein Ctf19-dCas9) ura3:: sgRNA expression cassette_sequence 5) chromosome arm8::URA3*	This study	3-21 B, C
GV 3449	*MATa/ MATalpha, ho::LYS2, lys2, ura3, leu2::hisG, his3::hisG, trp1::hisG, trp::p11_pHOP1_IML3_3xFLAG-dCas9::TRP, ura3:: sgRNA expression cassette_sequence 1) YCR047C::URA3 THR1::pYKL050c-CFP::TRP ARG4::pYKL050c-GFP*::URA/ SGD. 150521-151070::pYKL050c-RFP::LEU (~10kb to right of ARG4)*	This study	3-20 C, D
GV 3450	*MATa/ MATalpha, ho::LYS2, lys2, ura3, leu2::hisG, his3::hisG, trp1::hisG, trp::p11_pHOP1_3xFLAG-dCas9::TRP, ura3:: sgRNA expression cassette_sequence 1) YCR047C::URA3 THR1::pYKL050c-CFP::TRP ARG4::pYKL050c-GFP*::URA/ SGD. 150521-151070::pYKL050c-RFP::LEU (~10kb to right of ARG4)*	This study	3-20 C, D
GV 3451	*MATa/ MATalpha, ho::LYS2, lys2, ura3, leu2::hisG, his3::hisG, trp1::hisG, trp::p11_pHOP1_CTF19_exFLAG-dCas9::TRP (fusion protein Ctf19-dCas9) ura3:: sgRNA expression cassette_sequence 1) YCR047C::URA3 THR1::pYKL050c-CFP::TRP ARG4::pYKL050c-GFP*::URA/ SGD. 150521-151070::pYKL050c-RFP::LEU (~10kb to right of ARG4)*	This study	3-20 C, D

Table 7-1 continued.

Strain	Genotype	Reference	Figure
GV 3360	*MATa/ MATalpha, ho::LYS2, lys2, ura3, leu2::hisG, his3::hisG, trp1::hisG, ARG trp::p11_pHOP1_IML3_3xFLAG-dCas9::TRP, ura3:: sgRNA expression cassette w/out 20mer guide sequence::URA3 THR1::pYKL050c-CFP::TRP ARG4::pYKL050c-GFP*::URA/ SGD. 150521-151070::pYKL050c-RFP::LEU (~10kb to right of ARG4)*	This study	3-20 C, D
GV 3522	*MATa/ MATalpha, ho::LYS2, lys2, ura3, leu2::hisG, his3::hisG, trp1::hisG, trp::p11_pHOP1_dCas9::TRP (negative ctrl), ura3:: sgRNA expression cassette_sequence 5) chromosome arm8::URA3 THR1::pYKL050c-CFP::TRP ARG4::pYKL050c-GFP*::URA/ SGD. 150521-151070::pYKL050c-RFP::LEU (~10kb to right of ARG4) iml3::KANMX*	This study	3-21 D
GV 3523	*MATa/ MATalpha, ho::LYS2, lys2, ura3, leu2::hisG, his3::hisG, trp1::hisG, trp::p11_pHOP1_CTF19_3xFLAG-dCas9::TRP, ura3:: sgRNA expression cassette_sequence 5) chromosome arm8::URA3 THR1::pYKL050c-CFP::TRP SGD. 150521-151070::pYKL050c-RFP::LEU (~10kb to right of ARG4)/ ARG4::pYKL050c-GFP*::URA iml3::KANMX*	This study	3-21 D

Table 7-1 continued.

Strain	Genotype	Reference	Figure
GV 3527	*MATa/ MATalpha, ho::LYS2, lys2, ura3, leu2::hisG, his3::hisG, trp1::hisG, CHL4-6HA::k1TRP1, ura3:: sgRNA expression cassette_sequence 5) chromosome arm8::URA3*	This study	3-21 B, C
GV 3535	*MATa/ MATalpha, ho::LYS2, lys2, ura3, leu2::hisG, his3::hisG, trp1::hisG, trp::p11_pHOP1_3xFLAG-dCas9::TRP, ura3:: sgRNA expression cassette_sequence 5) chromosome arm8::URA3 CHL4-6HA::k1TRP1*	This study	3-21 C
GV 3543	*MATa/ MATalpha, ho::LYS2, lys2, ura3, leu2::hisG, his3::hisG, trp1::hisG, trp::p11_pHOP1_3xFLAG-dCas9::TRP, ura3:: sgRNA expression cassette_sequence 5) chromosome arm8::URA3 Mcm21-6HA::TRP1*	This study	3-21 C

Table 7-2 Synthetic oligonucleotides used for qPCR and cloning (Gibson assembly)

Number/ Name	Sequence (5' → 3')	Figure
GV 2249/ p11_pHOP1_GENE_ 3xFLAG-dCas9-STOP-CYC1_p11	tacgccaagcttgcatgcctgcaggtcgacTGAAAATGAACCAGGTAACAAATCTGGTGAAATC	3-17 B
GV 2250/ p11_pHOP1_CTF19_ 3xFLAG-dCas9-STOP-CYC1_p11	AACAGCTTTATCTCAGAAAAGTCAGGAATTATGGATTTTACGTCTGATACGACGAATTCG	3-17 B
GV 2251/ p11_pHOP1_CTF19_ 3xFLAG-dCas9-STOP-CYC1_p11	GTTTGCCTATTCCCGGACATGTACGCCAGGGACTACAAAGACCATGACGGTGATTATAAAG	3-17 B
GV 2252/ p11_pHOP1_GENE_ 3xFLAG-dCas9-STOP-CYC1_p11	ggttttgggacgctcgaaggctttaatttgGgatccccgggtaccgagctcgaattcactg	3-17 B
GV 2253/ p11_pHOP1_IML3_3 xFLAG-dCas9-STOP-CYC1_p11	AACAGCTTTATCTCAGAAAAGTCAGGAATTATGCCTTATACTTGGAAGTTTTTAGGAATC	3-17 B
GV 2254/ p11_pHOP1_IML3_3 xFLAG-dCas9-STOP-CYC1_p11	GTACTCCAATCGATTCAGTTTACCAGCGAGGACTACAAAGACCATGACGGTGATTATAAAG	3-17 B
GV 2277/ p11_pHOP1_3xFLAG -dCas9-STOP-CYC1_p11	AACAGCTTTATCTCAGAAAAGTCAGGAATTATGGACTACAAAGACCATGACGGTGATTATAAAG	3-17 B
GV 2468/ YCR047C target3)	TGTGTCCCTCGCAAGCCCTT	3-20 C
GV 2472/ Chr arm 8_ target2)	TAA ATG TAC CTT ACC ATG TTG	3-20 C
GV 2569/ CEN3_ChIP-qPCR	GATCAGCGCCAAACAATATGGAAAATCC	3-20 C

DNA sequences (5' → 3') of the single guide RNA expression cassettes used for CRISPR/ dCas9 based technology:

The single guide RNA expression cassettes are flanked by restriction sites for *SacII* and *EagI.* For cloning, plasmids containing the single guide RNA expression cassettes were digested with *SacII* and *EagI* according to Laughery et al. (2015).

SacII CCGCGG

EagI CGGCGG

target-specific complementary sequence

1. single guide RNA expression cassette of "*sgRNA-VIII*" (target-specific complementary sequence of the intergenic region between the genes *YHR020w* and *YHR021c* on chromosome *VIII*):

```
  1 CCGCGGacaaTCTTTGAAAAGATAATGTATGATTATGCTTTCACTCATAT
 51 TTATACAGAAACTTGATGTTTTCTTTCGAGTATATACAAGGTGATTACAT
101 GTACGTTTGAAGTACAACTCTAGATTTTGTAGTGCCCTCTTGGGCTAGCG
151 GTAAAGGTGCGCATTTTTTCACACCCTACAATGTTCTGTTCAAAAGATTT
201 TGGTCAAACGCTGTAGAAGTGAAAGTTGGTGCGCATGTTTCGGCGTTCG
251 AAACTTCTCCGCAGTGAAAGATAAATGATCAGACCTTTATAGTACTGTTA
301 GTTTTAGAGCTAGAAATAGCAAGTTAAAATAAGGCTAGTCCGTTATCAAC
351 TTGAAAAAGTGGCACCGAGTCGGTGGTGCTTTTTTTGTTTTTTATGTCTT
401 CGAGTCATGTAATTAGTTATAAAGCATGTGAGCTAAGACACTGTAATTGC
451 CAATCTAAACGATACCACGGCGG
```

2. single guide RNA expression cassette of "*sgRNA-III*" (target-specific complementary sequence of the intergenic region between the genes *YCR045c* and *YCR046c* on chromosome *III*):

```
  1 CCGCGGacaaTCTTTGAAAAGATAATGTATGATTATGCTTTCACTCATAT
 51 TTATACAGAAACTTGATGTTTTCTTTCGAGTATATACAAGGTGATTACAT
101 GTACGTTTGAAGTACAACTCTAGATTTTGTAGTGCCCTCTTGGGCTAGCG
151 GTAAAGGTGCGCATTTTTTCACACCCTACAATGTTCTGTTCAAAAGATTT
201 TGGTCAAACGCTGTAGAAGTGAAAGTTGGTGCGCATGTTTCGGCGTTCG
251 AAACTTCTCCGCAGTGAAAGATAAATGATCTCTTATATACAGGAGATGGG
301 GTTTTAGAGCTAGAAATAGCAAGTTAAAATAAGGCTAGTCCGTTATCAAC
351 TTGAAAAAGTGGCACCGAGTCGGTGGTGCTTTTTTTGTTTTTTATGTCTT
401 CGAGTCATGTAATTAGTTATAAAGCATGTGAGCTAAGACACTGTAATTGC
451 CAATCTAAACGATACCACGGCGG
```

3. single guide RNA expression cassette of "*sgRNA-mock*" (no target-specific complementary sequence):

```
  1 CCGCGGacaaTCTTTGAAAAGATAATGTATGATTATGCTTTCACTCATAT
 51 TTATACAGAAACTTGATGTTTTCTTTCGAGTATATACAAGGTGATTACAT
101 GTACGTTTGAAGTACAACTCTAGATTTTGTAGTGCCCTCTTGGGCTAGCG
151 GTAAAGGTGCGCATTTTTTCACACCCTACAATGTTCTGTTCAAAAGATTT
201 TGGTCAAACGCTGTAGAAGTGAAAGTTGGTGCGCATGTTTCGGCGTTCG
251 AAACTTCTCCGCAGTGAAAGATAAATGATCGAATCGATGCGTTTTAGA
301 GCTAGAAATAGCAAGTTAAAATAAGGCTAGTCCGTTATCAACTTGAAAAA
351 GTGGCACCGAGTCGGTGGTGCTTTTTTTGTTTTTTATGTCTTCGAGTCAT
401 GTAATTAGTTATAAAGCATGTGAGCTAAGACACTGTAATTGCCAATCTAA
451 ACGATACCACGGCGG
```

Bibliography

Alberts, B., Johnson, A., Lewis, J., Raff, M., Roberts, K., Walter, P. (2008). Molecular Biology of the Cell- 5th edition. *Garland Science, Taylor & Francis Group, LLC.*

Aleksenko, A., Nielsen, ML., Clutterbuck, AJ. (2001). Genetic and physical mapping of two centromere-proximal regions of chromosome IV in Aspergillus nidulans. *Fungal genetics and biology* 32(1):45-54.

Alipour, E., Marko, JF. (2012). Self-organization of domain structures by DNA-loop-extruding enzymes. *Nucleic acids research* 40(22):11202-12.

Allers, T., Lichten, M. (2001). Differential timing and control of noncrossover and crossover recombination during meiosis. *Cell* 106(1):47-57.

Almouzni, G., Probst, AV. (2011). Heterochromatin maintenance and establishment: lessons from the mouse pericentromere. *Nucleus* 2(5):332-8.

Anderson, CM., Chen, SY., Dimon, MT., Oke, A., DeRisi, JL., Fung, JC. (2011). ReCombine: a suite of programs for detection and analysis of meiotic recombination in whole-genome datasets. *Plos one* 6(10):e25509.

Arora, C., Kee, K., Maleki, S., Keeney, S. (2004). Antiviral protein Ski8 is a direct partner of Spo11 in meiotic DNA break formation, independent of its cytoplasmic role in RNA metabolism. *Molecular Cell* 13(4):549-59.

Bailis, JM., Roeder, GS. (1998). Synaptonemal complex morphogenesis and sister-chromatid cohesion require Mek1-dependent phosphorylation of a meiotic chromosomal protein. *Genes & development* 12(22):3551-63.

Bardhan, A., Chuong, H., Dawson, DS. (2010). Meiotic cohesin promotes pairing of nonhomologous centromeres in early meiotic prophase. *Molecular biology of the cell* 21(11):1799-809.

Barrangou, R., Fremaux, C., Deveau, H., Richards, M., Boyaval, P., Moineau, S., Romero, DA., Horvath, P. (2007). CRISPR provides acquired resistance against viruses in prokaryotes. *Science* 315(5819):1709-12.

Barrington, C., Finn, R., Hadjur, S. (2017). Cohesin biology meets the loop extrusion model. *Chromosome research* 25(1):51-60.

Baudat, F., Buard, J., Grey, C., Fledel-Alon, A., Ober, C., Przeworski, M., Coop, G., de Massy, B. (2010). PRDM9 is a major determinant of meiotic recombination hotspots in humans and mice. *Science* 327(5967):836-40.

Baudat, F., Imai, Y., de Massy, B. (2013). Meiotic recombination in mammals: localization and regulation. *Nature reviews genetics* 14(11):794-806.

Baudat, F., Nicolas, A. (1997). Clustering of meiotic double-strand breaks on yeast chromosome III. *Proceedings of national academy of sciences* 94(10):5213-8.

Beadle, GW. (1932). A Possible Influence of the Spindle Fibre on Crossing-Over in Drosophila. *Preceedings of the national acedamy of sciences* 18(2):160-5.

Bell, SP., Kobayashi, R., Stillman, B. (1993). Yeast origin recognition complex functions in transcription silencing and DNA replication. *Science* 262(5141):1844-9.
Belmont, AS. (2001). Visualizing chromosome dynamics with GFP. *Trends in cell biology* 11(6):250-7.

Belmont, AS., Straight, AF. (1998). In vivo visualization of chromosomes using lac operator-repressor binding. *Trends in cell biology* 8(3):121-4.

Belton, JM., McCord, RP., Gibcus, JH., Naumova, N., Zhan, Y., Dekker, J. (2012). Hi-C: a comprehensive technique to capture the conformation of genomes. *Methods* 58(3):268-76.

Betts Lindroos, HB., Ström, L., Itoh, T., Shirahige, K., Sjögren, C. (2006). Chromosomal association of the Smc5/6 complex reveals that it functions in differently regulated pathways. *Molecular cell* 22(6):755-67.

Bergerat, A., de Massy, B., Gadelle, D., Varoutas, PC., Nicolas, A., Forterre, P. (1997). An atypical topoisomerase II from Archaea with implications for meiotic recombination. *Nature* 386(6623):414-7.

Bhalla, N., Dernburg, AF. (2005). A conserved checkpoint monitors meiotic chromosome synapsis in Caenorhabditis elegans. *Science* 310(5754):1683-6.

Bhaya, D., Davison, M., Barrangou, R. (2011). CRISPR-Cas systems in bacteria and archaea: versatile small RNAs for adaptive defense and regulation. *Annual review of genetics* 45:273-97.

Biggins, S. (2013). The composition, functions, and regulation of the budding yeast kinetochore. *Genetics* 194(4):817-46.

Bishop, DK., Park, D., Xu, L., Kleckner, N. (1992). DMC1: a meiosis-specific yeast homolog of E. coli recA required for recombination, synaptonemal complex formation, and cell cycle progression. *Cell* 69(3):439-56.

Blat, Y., Protacio, RU., Hunter, N., Kleckner, N. (2002). Physical and functional interactions among basic chromosome organizational features govern early steps of meiotic chiasma formation. Cell 111(6):791-802.

Blitzblau, HG., Bell, GW., Rodriguez, J., Bell, SP., Hochwagen, A. (2007). Mapping of meiotic single-stranded DNA reveals double-stranded-break hotspots near centromeres and telomeres. *Current biology* 17(23):2003-12.

Blitzblau, HG., Hochwagen, A. (2013). ATR/Mec1 prevents lethal meiotic recombination initiation on partially replicated chromosomes in budding yeast. *Elife* 2:e00844.

Borde, V., Robine, N., Lin, W., Bonfils, S., Géli, V., Nicolas, A. (2009). Histone H3 lysine 4 trimethylation marks meiotic recombination initiation sites. *The embo journal* 28(2):99-111.

Bousset, K., Diffley, JF. (1998). The Cdc7 protein kinase is required for origin firing during S phase. *Genes & development* 12(4):480-90.

Börner, GV., Cha, RS. (2015). Analysis of Yeast Sporulation Efficiency, Spore Viability, and Meiotic Recombination on Solid Medium. *Cold spring harbor protocols* 2015(11):1003-8.

Börner, GV., Kleckner, N., Hunter, N. (2004). Crossover/noncrossover differentiation, synaptonemal complex formation, and regulatory surveillance at the leptotene/zygotene transition of meiosis. *Cell* 117(1):29-45.

Brar, GA., Amon, A. (2008). Emerging roles for centromeres in meiosis I chromosome segregation. *Nature reviews genetics* 9(12):899-910.

Brar, GA., Kiburz, BM., Zhang, Y., Kim, JE., White, F., Amon, A. (2006). Rec8 phosphorylation and recombination promote the step-wise loss of cohesins in meiosis. *Nature* 441(7092):532-6.

Buhler, C., Borde, V., Lichten, M. (2007). Mapping meiotic single-strand DNA reveals a new landscape of DNA double-strand breaks in Saccharomyces cerevisiae. *Plos biology* 5(12):e324.

Buonomo, SB., Clyne, RK., Fuchs, J., Loidl, J., Uhlmann, F., Nasmyth, K. (2000). Disjunction of homologous chromosomes in meiosis I depends on proteolytic cleavage of the meiotic cohesin Rec8 by separin. *Cell* 103(3):387-98.

Cao, L., Alani, E., Kleckner, N. (1990). A pathway for generation and processing of double-strand breaks during meiotic recombination in S. cerevisiae. *Cell* 61(6):1089-101.

Carballo, JA., Johson, AL., Sedgwick, SG., Cha, RS. (2008). Phosphorylation of the axial element protein Hop1 by Mec1/Tel1 ensures meiotic interhomolog recombination. *Cell* 132(5):758-70.

Chakraborty, P., Pankajam, AV., Lin, G., Dutta, A., Krishnaprasad, GN., Tekkedil, MM., Shinohara, A., Steinmetz, LM., Nishant, KT. (2017). Modulating Crossover Frequency and Interference for Obligate Crossovers in Saccharomyces cerevisiae Meiosis. *Genes, genomes, genetics* 7(5):1511-1524.

Chan, RC., Severson, AF., Meyer, BJ. (2004). Condensin restructures chromosomes in preparation for meiotic divisions. *The journal of cell biology* 167(4):613-25.

Charlie, TM., Amon, A. (2008). Meiosis I is established through division-specific translational control of a cyclin. *Cell* 133(2):280-91.

Carpenter, AT. (1987). Gene conversion, recombination nodules, and the initiation of meiotic synapsis. *Bioessays* 6(5):232-6.

Cheeseman, IM., Chappie, JS., Wilson-Kubalek, EM., Desai, A. (2006). The conserved KMN network constitutes the core microtubule-binding site of the kinetochore. *Cell* 127(5):983-97.

Cheeseman, IM., Desai, A. (2008). Molecular architecture of the kinetochore-microtubule interface. *Nature reviews molecular cell biology* 9(1):33-46.

Chen, SY., Tsubouchi, T., Rockmill, B., Sandler, JS., Richards, DR., Vader G., Hochwagen, A., Roeder, GS., Fung, JC. Global analysis of the meiotic crossover landscape. *Developmental cell* 15(3):401-15.

Cho, US., Harrison, SC. (2011). Ndc10 is a platform for inner kinetochore assembly in budding yeast. *Nature structural & molecular biology* 19(1):48-55.

Chu, S., DeRisi, J., Eisen, M., Mulholland, J., Botstein, D., Brown, PO., Herskowitz, I. (1998). The transcriptional program of sporulation in budding yeast. *Science* 282(5389):699-705.

Chu, S., Herskowitz, I. (1998). Gametogenesis in yeast is regulated by a transcriptional cascade dependent on Ndt80. *Molecular cell* 1(5):685-96.

Ciosk, R., Shirayama, M., Shevchenko, A., Tanaka, T., Toth, A., Shevchenko, A., Nasmyth, K. (2000). Cohesin's binding to chromosomes depends on a separate complex consisting of Scc2 and Scc4 proteins. *Molecular cell* 5(2):243-54.

Clapier, CR.,Cairns, BR. (2009). The biology of chromatin remodeling complexes. *Annual review of biochemistry* 78:273-304.

Clark, MW., Zhong, WW., Keng, T., Storms, RK., Barton, A., Kaback, DB., Bussey, H. (1992). Identification of a Saccharomyces cerevisiae homolog of the SNF2 transcriptional regulator in the DNA sequence of an 8.6 kb region in the LTE1-CYS1 interval on the left arm of chromosome I. *Yeast* 8(2):133-45.

Clift, D., Marston, AL. (2011). The role of shugoshin in meiotic chromosome segregation. *Cytogenetic and genome research* 133(2-4):234-42.

Clift, D., Schuh, M. (2013). Restarting life: fertilization and the transition from meiosis to mitosis. *Nature reviews molecular cell biology* 14(9):549-62.

Collins, I., Newlon, CS. (1994). Chromosomal DNA replication initiates at the same origins in meiosis and mitosis. *Molecular and cellular biology* 14(5):3524-34.

Cong, L., Ran, FA., Cox, D., Lin, S., Barretto, R., Habib, N., Hsu, PD., Wu, X., Jiang, W., Marraffini, LA., Zhang, F. (2013). Multiplex genome engineering using CRISPR/Cas systems. *Science* 339(6121):819-23.

Connelly, C., Hieter, P. (1996). Budding yeast SKP1 encodes an evolutionarily conserved kinetochore protein required for cell cycle progression. *Cell* 86(2):275-85.

Copenhaver, GP., Nickel, K., Kuromori, T., Benito, MI., Kaul, S., Lin, X., Bevan, M., Murphy, G., Harris, B., Parnell, LD., McCombie, WR., Martienssen, RA., Marra, M. (1999). Genetic definition and sequence analysis of Arabidopsis centromeres. *Science* 286(5449):2468-74.

Cooper, TJ., Garcia, V., Neale, MJ. (2016). Meiotic DSB patterning: A multifaceted process. *Cell cycle* 15(1):13-21.

Copsey, A., Tang, S., Jordan, PW., Blitzblau, HG., Newcombe, S., Chan, AC., Newnham, L., Li, Z., Gray, S., Herbert, AD., Arumugam, P., Hochwagen, A., Hunter, N., Hoffmann, E. (2013). Smc5/6 coordinates formation and resolution of joint molecules with chromosome morphology to ensure meiotic divisions. *Plos genetics* 9(12):e1004071.

D'Ambrosio, C., Schmidt, CK., Katou, Y., Kelly, G., Itoh, T., Shirahige, K., Uhlmann, F. (2008). Identification of cis-acting sites for condensin loading onto budding yeast chromosomes. *Genes & development* 22(16):2215-27.

Daniel, JA., Keyes, BE., Ng, YP., Freeman, CO., Burke, DJ. (2006). Diverse functions of spindle assembly checkpoint genes in Saccharomyces cerevisiae. *Genetics* 172(1):53-65.

Davis, CR., Kempainen, RR., Srodes, MS., McClung, CR. (1994). Correlation of the physical and genetic maps of the centromeric region of the right arm of linkage group III of Neurospora crassa. *Genetics* 136(4):1297-306.

De Massy, B. (2013). Initiation of meiotic recombination: how and where? Conservation and specificities among eukaryotes. *Annual review of genetics* 47:563-99.

de los Santos, T., Hollingsworth, NM. (1999). Red1p, a MEK1-dependent phosphoprotein that physically interacts with Hop1p during meiosis in yeast. *The journal of biological chemistry* 274(3):1783-90.

De Piccoli, G., Torres-Rosell, J., Aragōn, L. (2009). The unnamed complex: what do we know about Smc5-Smc6? *Chromosome research* 17(2):251-63.

De Wulf, P., McAinsh, AD., Sorger, PK. (2003). Hierarchical assembly of the budding yeast kinetochore from multiple subcomplexes. *Genes & development* 17(23):2902-21.

Déjardin, J. (2015). Switching between Epigenetic States at Pericentromeric Heterochromatin. *Trends in genetics* 31(11):661-72.

Drinnenberg, IA., deYoung, D., Henikoff, S., Malik, HS. (2014). Recurrent loss of CenH3 is associated with independent transitions to holocentricity in insects. *Elife* 3. doi: 10.

Dimitrova, YN., Jenni, S., Valverde, R., Khin, Y., Harrison, SC. (2016). Structure of the MIND Complex Defines a Regulatory Focus for Yeast Kinetochore Assembly. *Cell* 167(4):1014-1027.

Drinnenberg, IA., Henikoff, S., Malik, HS. (2016). Evolutionary Turnover of Kinetochore Proteins: A Ship of Theseus? *Trends in cell biology* 26(7):498-510.

Dirick, L., Goetsch, L., Ammerer, G., Byers, B. (1998). Regulation of meiotic S phase by Ime2 and a Clb5,6-associated kinase in Saccharomyces cerevisiae. *Science* 281(5384):1854-7.

Dobzhansky T. (1930). Translocations Involving the Third and the Fourth Chromosomes of DROSOPHILA MELANOGASTER. *Genetics* 15(4):347-99.

Dominguez, AA., Lim, WA., Qi, LS. (2015). Beyond editing: repurposing CRISPR-Cas9 for precision genome regulation and interrogation. *Nature reviews molecular cell biology* 17(1):5-15.

Donaldson, AD., Fangman, WL., Brewer, BJ. (1998). Cdc7 is required throughout the yeast S phase to activate replication origins. *Genes & development* 12(4):491-501.

Dorn, JF., Maddox, PS. (2012). Kinetochore dynamics: how protein dynamics affect chromosome segregation. *Current opinion in cell biology* 24(1):57-63.

Durand-Dubief, M., Will, WR., Petrini, E., Therodorou, D., Harris, RR., Crawford, MR., Paszkiewicz, K., Krueger, F., Correra, RM., Vetter, AT., Miller, JR., Kent, NA.,

Varga-Weisz, P. (2012). SWI/SNF-like chromatin remodeling factor Fun30 supports point centromere function in S. cerevisiae. *Plos genetics* 8(9):e1002974.

Eckert, CA., Gravdahl, DJ., Megee, PC. (2007). The enhancement of pericentromeric cohesin association by conserved kinetochore components promotes high-fidelity chromosome segregation and is sensitive to microtubule-based tension. *Genes & development* 21(3):278-91.

Ellermeier, C., Higuchi, EC., Phadnis, N., Holm, L., Geelhood, JL., Thon, G., Smith, GR. (2010). RNAi and heterochromatin repress centromeric meiotic recombination. *Preceedings of the national academy of sciences* 107(19):8701-5.

Eshleman, HD., Morgan, DO. (2014). Sgo1 recruits PP2A to chromosomes to ensure sister chromatid bi-orientation during mitosis. *Journal of cell science* 127(Pt 22):4974-83.

Fan, QQ., Petes, TD. (1996). Relationship between nuclease-hypersensitive sites and meiotic recombination hot spot activity at the HIS4 locus of Saccharomyces cerevisiae. *Molecular and cellular biology* 16(5):2037-43.

Farmer, S., San-Segundo, PA., Aragõn, L. (2011). The Smc5-Smc6 complex is required to remove chromosome junctions in meiosis. *Plos one* 6(6):e20948.

Fernius, J., Marston, AL. (2009). Establishment of cohesion at the pericentromere by the Ctf19 kinetochore subcomplex and the replication fork-associated factor, Csm3. *Plos genetics* 5(9):e1000629.

Fernius, J., Nerusheva, OO>, Galander, S., Alves Fde, L., Rappsilber, J., Marston, AL. (2013). Cohesin-dependent association of scc2/4 with the centromere initiates pericentromeric cohesion establishment. *Current biology* 23(7):599-606.

Fink, GR., Petes, TD. (1984). Gene conversion in the absence of reciprocal recombination. *Nature* 310(5980):728-9.

Fitzgerald-Hayes, M., Clarke, L., Carbon, J. (1982). Nucleotide sequence comparisons and functional analysis of yeast centromere DNAs. *Cell* 29(1):235-44.

Flaus, A., Martin, DM., Barton, GJ., Owen-Hughes, T. (2006). Identification of multiple distinct Snf2 subfamilies with conserved structural motifs. *Nucleic acids research* 34(10):2887-905.

Flaus, A., Owen-Hughes, T. (2011). Mechanisms for ATP-dependent chromatin remodelling: the means to the end. *The febs journal* 278(19):3579-95.

Fowler, KR., Sasaki, M., Milman, N., Keeney, S., Smith, GR. (2014). Evolutionarily diverse determinants of meiotic DNA break and recombination landscapes across the genome. *Genome research* 24(10):1650-64.

Freeman, L., Aragon-Alcaide, L., Strunnikov, A. (2000). The condensin complex governs chromosome condensation and mitotic transmission of rDNA. *The journal of cell biology* 149(4):811-24.

Freemont, PS. (2000). RING for destruction? *Current biology* 10(2):R84-7.

Freese, EB., Chu, MI., Freese, E. (1982). Initiation of yeast sporulation of partial carbon, nitrogen, or phosphate deprivation. *Journal of Bacteriology* 149(3):840-51.

Fudenberg, G., Imakaev, M., Lu, C., Goloborodko, A., Abdennur, N., Mirny, LA. (2016). Formation of Chromosomal Domains by Loop Extrusion. *Cell reports* 15(9):2038-49.

Fukagawa, T., Earnshaw, WC. (2014). The centromere: chromatin foundation for the kinetochore machinery. *Developmental cell* 30(5):496-508.

Gangaraju, VK., Bartholomew, B. (2007). Mechanisms of ATP dependent chromatin remodeling. *Mutation research* 618(1-2):3-17.

Gardner, RD., Poddar, A., Yellman, C., Tavormina, PA., Monteagudo, MC., Burke, DJ. (2001). The spindle checkpoint of the yeast Saccharomyces cerevisiae requires kinetochore function and maps to the CBF3 domain. *Genetics* 157(4):1493-502.

Gasiunas, G., Barrangou, R., Horvath, P., Siksnys, V. (2012). Cas9-crRNA ribonucleoprotein complex mediates specific DNA cleavage for adaptive immunity in bacteria. *Proceedings of the national academy of sciences* 109(39):E2579-86

Gassler, J., Brandão, HB., Imakaev, M., Flyamer, IM., Ladstätter, S. Bickmore, WA., Peters, JM., Mirny, LA., Tachibana, K. (2017). A mechanism of cohesin-dependent loop extrusion organizes zygotic genome architecture. *The embo journal* 36(24):3600-3618.

Gerald, JN., Benjamin, JM., Kron, SJ. (2002). Robust G1 checkpoint arrest in budding yeast: dependence on DNA damage signaling and repair. *Journal of cell science* 115(Pt 8):1749-57.

Gerton, JL., De Risi, J., Shroff, R., Lichten, M., Brown, PO., Petes, TD. (2000). Global mapping of meiotic recombination hotspots and coldspots in the yeast Saccharomyces cerevisiae. Proceedings of the national academy of sciences 97(21):11383-90.

Ghosh, SK., Poddar, A., Hajra, S., Sanyal, K., Sinha, P. (2001). The IML3/MCM19 gene of Saccharomyces cerevisiae is required for a kinetochore-related process during chromosome segregation. *Molecular genetics and genomics* 265(2):249-57.

Gibson, DG., Young, L., Chuang, RY., Venter, JC., Hutchison, CA, Smith, HO. (2009). Enzymatic assembly of DNA molecules up to several hundred kilobases. *Nature methods* 6(5):343-5.

Glynn, EF., Megee, PC., Yu, HG., Mistrot, C., Unal, E., Koshland, DE., DeRisi, JL., Gerton, JL. (2004). Genome-wide mapping of the cohesin complex in the yeast Saccharomyces cerevisiae. *Plos biology* 2(9):E259.

Goh, PY., Kilmartin, JV. (1993). NDC10: a gene involved in chromosome segregation in Saccharomyces cerevisiae. *The journal of cell biology* 121(3):503-12.

Gómez-Escoda, B., Wu, PY. (2017). Roles of CDK and DDK in Genome Duplication and Maintenance: Meiotic Singularities. *Genes* 8(3): 105.

Gonen, S., Akiyoshi, B., Iadanza, MG., Shi, D., Duggan, N., Biggins, S., Gonen, T. (2012). The structure of purified kinetochores reveals multiple microtubule-attachment sites. *Nature structural and molecular biology* 19(9):925-9.

Gore, MA., Chia, JM., Elshire, RJ., Sun, Q., Ersoz, ES., Hurwitz, BL., Peiffer, JA., McMullen, MD., Grills, GS., Ross-Ibarra, J., Ware, DH., Buckler, ES. (2009). A first-generation haplotype map of maize. *Science* 326(5956):1115-7.

Gradolatto, A., Rogers, RS., Lavender, H., Taverna, SD., Allis, CD., Aitchison, JD., Tackett, AJ. (2008). Saccharomyces cerevisiae Yta7 regulates histone gene expression. *Genetics* 179(1):291-304.

Grandin, N., Reed, SI. (1993). Differential function and expression of Saccharomyces cerevisiae B-type cyclins in mitosis and meiosis. *Molecular and cellular biology* 13(4):2113-25.

Grewal, SI., Jia, S. (2007). Heterochromatin revisited. *Nature reviews genetics* 8(1):35-46.

Goldfarb, T., Lichten, M. (2010). Frequent and efficient use of the sister chromatid for DNA double-strand break repair during budding yeast meiosis. *Plos biology* 8(10):e1000520.

Gray, S., Cohen, PE. (2016). Control of Meiotic Crossovers: From Double-Strand Break Formation to Designation. *Nature reviews genetics* 50:175-210.

Haarhuis, JHI, van der Weide, RH., Blomen, VA., Yañez-Cuna, JO., Amendola, M., van Ruiten, MS., Krijger, PHL., Teunissen, H., Medema, RH., van Steensel., B., Brummelkamp, TR., de Wit, E., Rowland, BD. (2017). The Cohesin Release Factor WAPL Restricts Chromatin Loop Extension. *Cell* 169(4):693-707.e14.

Haering, CH., Farcas, AM., Arumugam, P., Metson, J., Nasmyth, K. (2008). The cohesin ring concatenates sister DNA molecules. *Nature* 454(7202):297-301.

Haering, CH., Schoffnegger, D., Nishino, T., Helmhart, W., Nasmyth, K., Löwe, J. (2004). Structure and stability of cohesin's Smc1-kleisin interaction. *Molecular cell* 15(6):951-64.

Hartwell, LH., Weinert, TA. (1989). Checkpoints: controls that ensure the order of cell cycle events. *Science* 246(4930):629-34.

Haruki, H., Nishikawa, J., Laemmli, UK. (2008). The anchor-away technique: rapid, conditional establishment of yeast mutant phenotypes. *Molecular cell* 31(6):925-32.

Harvey, SH., Krien, MJ., O'Connell, MJ. (2002). Structural maintenance of chromosomes (SMC) proteins, a family of conserved ATPases. *Genome biology* 3(2):REVIEWS3003.

Hassold, T., Hunt, P. (2001). To err (meiotically) is human: the genesis of human aneuploidy. *Nature reviews genetics* 2(4):280-91.

Hauf, S., Waizenegger, IC., Peters, JM. (2001). Cohesin cleavage by separase required for anaphase and cytokinesis in human cells. *Science* 293(5533):1320-3.

Haupt, W., Fischer, TC., Winderl, S., Fransz, P., Torres-Ruiz, RA. (2001). The centromere1 (CEN1) region of Arabidopsis thaliana: architecture and functional impact of chromatin. *The plant journal* 27(4):285-96.

Hegemann, JH., Fleig, UN. (1993). The centromere of budding yeast. *Bioessays* 15(7):451-60.

He, X., Rines, DR., Espelin, CW., Sorger, PK. (2001). Molecular analysis of kinetochore-microtubule attachment in budding yeast. *Cell* 106(2):195-206.

Henderson, KA., Kee, K., Maleki, S., Santini, PA., Keeney, S. (2006). Cyclin-dependent kinase directly regulates initiation of meiotic recombination. *Cell* 125(7):1321-32.

Hieter, P., Pridmore, D., Hegemann, JH., Thomas, M., Davis, RW., Philippsen, P. (1985). Functional selection and analysis of yeast centromeric DNA. *Cell* 42(3):913-21.

Hinshaw, SM., Makrantoni, V., Harrison, SC., Marston, AL. (2017). The Kinetochore Receptor for the Cohesin Loading Complex. *Cell* 171(1):72-84.e13.

Hinshaw, SM., Makrantoni, V., Kerr, A., Marston, AL., Harrison, SC. (2015). Structural evidence for Scc4-dependent localization of cohesin loading. *Elife* 4:e06057.

Hirano, T. (2012). Condensins: universal organizers of chromosomes with diverse functions. *Genes & development* 26(15):1659-78.

Ho, HC., Burges, SM., (2011). Pch2 acts through Xrs2 and Tel1/ATM to modulate interhomolog bias and checkpoint function during meiosis. *Plos genetics* 7(11):e1002351.

Ho, KH., Tsuchiya, D., Oliger, AC., Lacefield, S. (2014). Localization and function of budding yeast CENP-A depends upon kinetochore protein interactions and is independent of canonical centromere sequence. *Cell reports* 9(6):2027-33.

Hochwagen, A. (2008). Meiosis. *Current biology* 18(15):R641-R645.

Hochwagen, A., Amon, A. (2006). Checking your breaks: surveillance mechanisms of meiotic recombination. *Current biology* 16(6):R217-28.

Hollingsworth, N. (2010). Phosphorylation and the creation of interhomolog bias during meiosis in yeast. *Cell cycle* 9(3):436-7.

Hollingsworth, N., Goetsch, L., Byers, B. (1990). The HOP1 gene encodes a meiosis-specific component of yeast chromosomes. *Cell* 61(1):73-84.

Hornung, P., Maier, M., Alushin, GM., Lander, GC., Nogales, E., Westermann, S. (2011). Molecular architecture and connectivity of the budding yeast Mtw1 kinetochore complex. *Journal of molecular biology* 405(2):548-59.

Hornung, P., Troc, P., Malvezzi, F., Maier, M., Demianova, Z., Zimniak, T., Litos, G., Lampert, F., Schleiffer, A., Brunner, M., Mechtler, K., Herzog, F., Marlovits, TC., Westermann, S. (2014). A cooperative mechanism drives budding yeast kinetochore assembly downstream of CENP-A. *The journal of cell biology* 206(4):509-24.

Humphryes, N., Hochwagen, A. (2014). A non-sister act: recombination template choice during meiosis. *Experimental cell research* 329(1):53-60.

Hyland, KM., Kingsbury, J., Koshland, D., Hieter, P. (1999). Ctf19p: A novel kinetochore protein in Saccharomyces cerevisiae and a potential link between the kinetochore and mitotic spindle. *The journal of cell biology* 145(1):15-28.

Indjeian, VB., Stern, BM., Murray, AW. (2005). The centromeric protein Sgo1 is required to sense lack of tension on mitotic chromosomes. *Science* 307(5706):130-3.

Ishiguro, T., Tanaka, K., Sakuno, T., Watanabe, Y. (2010). Shugoshin-PP2A counteracts casein-kinase-1-dependent cleavage of Rec8 by separase. *Nature cell biology* 12(5):500-6.

Ito, M., Kugou, K., Fawcett, JA., Mura, S., Ikeda, S., Innan, H., Ohta, K. (2014). Meiotic recombination cold spots in chromosomal cohesion sites. *Genes to cells* 19(5):359-73.

Jackson, AL., Pahl, PM., Harrison, K., Rosamond, J, Sclafani, RA. (1993). Cell cycle regulation of the yeast Cdc7 protein kinase by association with the Dbf4 protein. *Molecular and cell biology* 13(5):2899-908.

Janssens, V., Goris, J. (2001). Protein phosphatase 2A: a highly regulated family of serine/threonine phosphatases implicated in cell growth and signalling. *Biochemical journal* 353(Pt 3):417-39.

Jasin, M., Rothstein, R. (2013). Repair of strand breaks by homologous recombination. *Cold spring harbor perspectives in biology* 5(11):a012740.

Jeppsson, K., Kanno, T., Shirahige, K., Sjögren, C. (2014). The maintenance of chromosome structure: positioning and functioning of SMC complexes. *Nature reviews molecular cell biology* 15(9):601-14.

Jinek, M., Chylinski, K., Fonfara, I., Hauer, M., Dounda, JA., Charpentier, E. (2012). A programmable dual-RNA-guided DNA endonuclease in adaptive bacterial immunity. *Science* 337(6096):816-21.

Joglekar, AP., Bouck, DC., Molk, JN., Bloom, KS., Salmon, ED. (2006). Molecular architecture of a kinetochore-microtubule attachment site. *Nature cell biology* 8(6):581-5.

Johnston, LH., Masai, H., Sugino, A. (1999). First the CDKs, now the DDKs. *Trends in cell biology* 9(7):249-52.

Jones, GH. (1984). The control of chiasma distribution. *Symposia of the society for experimental biology* 38:293-320.

Kabadi, AM., Ousterout, DG., Hilton, IB., Gersbach, CA., (2014). Multiplex CRISPR/Cas9-based genome engineering from a single lentiviral vector. *Nucleic acids research* 42(19):e147.

Kadyk, LC., Hartwell, LH. (1992). Sister chromatids are preferred over homologs as

substrates for recombinational repair in Saccharomyces cerevisiae. *Genetics* 132(2):387-402.

Kassir, Y., Granot, D., Simchen, G. (1998). IME1, a positive regulator gene of meiosis in S. cerevisiae. *Cell* 52(6):853-62.

Katis, VL., Galova, M., Rabitsch, KP., Gregan, J., Nasmyth, K. (2004). Maintenance of cohesin at centromeres after meiosis I in budding yeast requires a kinetochore-associated protein related to MEI-S332. *Current biology* 14(7):560-72.

Katis, VL., Lipp, JJ., Imre, R., Bogdanova, A., Okaz, E., Habermann, B., Mechtler, K., Nasmyth, K., Zachariae, W. (2010). Rec8 phosphorylation by casein kinase 1 and Cdc7-Dbf4 kinase regulates cohesin cleavage by separase during meiosis. *Developmental cell* 18(3):397-409.

Kato, H., Jiang, J., Zhou, BR., Rozendaal, M., Feng, H., Ghirlando, R., Xiao, TS., Straight, AF., Bai, Y. (2013). A conserved mechanism for centromeric nucleosome recognition by centromere protein CENP-C. *Science* 340(6136):1110-3.

Kauppi, L., Jeffreys, AJ., Keeney, S. (2004). Where the crossovers are: recombination distributions in mammals. *Nature reviews genetics* 5(6):413-24.

Kawashima, SA., Yamagishi, Y., Honda, T., Ishiguro, K., Watanabe, Y. (2010). Phosphorylation of H2A by Bub1 prevents chromosomal instability through localizing shugoshin. *Science* 327(5962):172-7.

Keeney, S. (2001). Mechanism and control of meiotic recombination initiation. *Current topics in developmental biology* 52:1-53.

Keeney, S., Giroux, CN., Kleckner, N. (1997). Meiosis-specific DNA double-strand breaks are catalyzed by Spo11, a member of a widely conserved protein family. *Cell* 88(3):375-84.

Keeney, S., Kleckner, N. (1995). Covalent protein-DNA complexes at the 5' strand termini of meiosis-specific double-strand breaks in yeast. *Preceedings of the national academy of sciences* 92(24):11274-8.

Keeney, S., Neale, MJ. (2006). Initiation of meiotic recombination by formation of DNA double-strand breaks: mechanism and regulation. *Biochemical society transactions* 34(Pt 4):523-5.

Kegel, A., Betts Lindroos, H., Kanno, T., Jeppsson, K., Ström, L., Katou, Y., Itoh, T., Shirahige, K., Sjögren, C. (2011). Chromosome length influences replication-induced topological stress. *Nature* 471(7338):392-6.

Kerrebrock, AW., Miyazaki, WY., Birnby, D., Orr-Weaver, TL. (1992). The Drosophila mei-S332 gene promotes sister-chromatid cohesion in meiosis following kinetochore differentiation. *Genetics* 130(4):827-41.

Kerrebrock, AW., Moore, DP., Wu, JS., Orr-Weaver, TL. (1995). Mei-S332, a Drosophila protein required for sister-chromatid cohesion, can localize to meiotic centromere regions. *Cell* 83(2):247-56.

Kiermaier, E., Woehrer, S., Peng, Y., Mechtler, K., Westermann, S. (2009). A Dam1-based artificial kinetochore is sufficient to promote chromosome segregation in budding yeast. *Nature cell biology* 11(9):1109-15.

Kim, KP., Weiner, BM., Zhang, L., Jordan, A., Dekker, J., Kleckner, N. (2010). Sister cohesion and structural axis components mediate homolog bias of meiotic recombination. *Cell* 143(6):924-37.

Kiburz, BM., Amon, A., Marston, AL. (2008). Shugoshin promotes sister kinetochore biorientation in Saccharomyces cerevisiae. *Molecular biology of the cell* 19(3):1199-209.

Kiburz, BM., Reynolds, DB., Megee, PC., Marston, AL., Lee, BH., Lee, TI., Levine, SS., Young, RA., Amon, A. (2005). The core centromere and Sgo1 establish a 50-kb cohesin-protected domain around centromeres during meiosis I. *Genes & development* 19(24):3017-30.

Klein, F., Mahr, P., Galova, M., Buonomo, SB., Michaelis, C., Nairz, K., Nasmyth, K. (1999). A central role for cohesins in sister chromatid cohesion, formation of axial elements, and recombination during yeast meiosis. *Cell* 98(1):91-103.

Kniewel, R., Keeney, S. (2009). Histone methylation sets the stage for meiotic DNA breaks. *The embo journal* 28(2):81-3.

Koehler, KE., Hawley, RS, Sherman, S., Hassold, T. (1996). Recombination and nondisjunction in humans and flies. *Human molecular genetics* 1495-504.

Kogut, I., Wang, J., Guacci, V., Mistry, RK., Megee, PC. (2009). The Scc2/Scc4 cohesin loader determines the distribution of cohesin on budding yeast chromosomes. *Genes & development* 23(19):2345-57.

Lacefield, S., Lau, DT., Murray, AW. (2009). Recruiting a microtubule-binding complex to DNA directs chromosome segregation in budding yeast. *Nature cell biology* 11(9):1116-20.

Lam, I., Keeney, S. (2014). Mechanism and regulation of meiotic recombination initiation. *Cold spring harbor persectives in biology* 7(1):a016634.

Lamb, NE., Sherman, SL., Hassold, TJ. (2005). Effect of meiotic recombination on the production of aneuploid gametes in humans. *Cytogenetic and genome research* 111(3-4):250-5.

Lambie, EJ., Roeder, GS. (1986). Repression of meiotic crossing over by a centromere (CEN3) in Saccharomyces cerevisiae. *Genetics* 114(3):769-89.

Lampert, F., Westermann, S. (2011). A blueprint for kinetochores - new insights into the molecular mechanics of cell division. *Nature reviews molecular cell biology* 12(7):407-12.

Laughery, MF., Hunter, T., Brown, A., Hoopes, J., Ostbye, T., Shumaker, T., Wyrick, JJ. (2015). New vectors for simple and streamlined CRISPR-Cas9 genome editing in Saccharomyces cerevisiae. *Yeast* 32(12):711-20.

Lechward, K., Awotunde, OS., Swiatek, W., Muszynska, G. (2001). Protein phosphatase 2A: variety of forms and diversity of functions. *Acta Biochimica Polonica* 48(4):921-33.

Lee, N., Amon, A. (2001). Meiosis: how to create a specialized cell cycle. *Current opinion in cell biology* 13(6):770-7.

Lee, BH., Amon, A. (2003). Role of Polo-like kinase CDC5 in programming meiosis I chromosome segregation. *Science* 300(5618):482-6.

Lengronne, A., Mclntyre, J., Katou, Y., Kanoh, Y., Hopfner, KP., Shirahige, K., Uhlmann, F. (2006). Establishment of sister chromatid cohesion at the S. cerevisiae replication fork. *Molecular cell* 23(6):787-99.

Li, J., Hooker, GW., Roeder, GS. (2006). *Saccharomyces cerevisiae* Mer2, Mei4 and Rec114 Form a Complex Required for Meiotic Double-Strand Break Formation. *Genetics* 173(4): 1969–1981.

Li, R., Murray, AW. (1991). Feedback control of mitosis in budding yeast. *Cell* 66(3):519-31.

Lichten, M., Goldman, AS. (1995). Meiotic recombination hotspots. *Annual review of genetics* 29:423-44.

Liu, H., Rankin, S., Yu, H. (2013). Phosphorylation-enabled binding of SGO1-PP2A to cohesin protects sororin and centromeric cohesion during mitosis. *Nature cell biology* 15(1):40-9.

London, N., Ceto, S., Ranish, JA., Biggins, S. Phosphoregulation of Spc105 by Mps1 and PP1 regulates Bub1 localization to kinetochores. *Current biology* 22(10):900-6.

Longhese, MP., Foiani, M., Muzi-Falconi, M., Lucchini, G., Plevani, P. (1998). DNA damage checkpoint in budding yeast. *The embo journal* 17(19):5525-8.

Losada, A., Hirano, M., Hirano, T. (2002). Cohesin release is required for sister chromatid resolution, but not for condensin-mediated compaction, at the onset of mitosis. *Genes & development* 16(23):3004-16.

Lydall, D., Nikolsky, Y., Bishop, DK., Weinert, T. (1996). A meiotic recombination checkpoint controlled by mitotic checkpoint genes. *Nature* 383(6603):840-3.

Lynn, A., Soucek, R., Börner, GV. (2007). ZMM proteins during meiosis: crossover artists at work. *Chromosome research* 15(5):591-605.

MacQueen, AJ., Hochwagen, A. (2011). Checkpoint mechanisms: the puppet masters of meiotic prophase. *Trends in cell biology* 21(7):393-400.

Mahtani, MM., Willard, HF. (1998). Physical and genetic mapping of the human X chromosome centromere: repression of recombination. *Genome research* 8(2):100-10.

Maleki, S., Neale, MJ., Arora, C., Henderson, KA., Keeney, S. (2007). Interactions between Mei4, Rec114, and other proteins required for meiotic DNA double-strand break formation in Saccharomyces cerevisiae. *Chromosoma* 116(5):471-86.

Marmorstein, R., Trievel, RC. (2009). Histone modifying enzymes: structures, mechanisms, and specificities. *Biochimicha et Biophysica Acta* 1789(1):58-68.

Marston, AL. (2015). Shugoshins: tension-sensitive pericentromeric adaptors safeguarding chromosome segregation. *Molecular and cell biology* 35(4):634-48.

Marston, AL., Amon, A. (2004). Meiosis: cell-cycle controls shuffle and deal. *Nature reviews molecular cell biology* 5(12):983-97.

Marston, AL., Tham, WH., Shah, H., Amon, A. (2004). A genome-wide screen identifies genes required for centromeric cohesion. *Science* 303(5662):1367-70.

Martini, E., Diaz, RL., Hunter, N., Keeney, S. (2006). Crossover homeostasis in yeast meiosis. *Cell* 126(2):285-95.

Maskell, DP., Hu, XW., Singleton, MR. (2010). Molecular architecture and assembly of the yeast kinetochore MIND complex. *The journal of cell biology* 190(5):823-34.

Masson, JY., West, SC. (2001). The Rad51 and Dmc1 recombinases: a non-identical twin relationship. *Trends in biochemical sciences* 26(2):131-6.

Mather, K. (1939). Crossing over and Heterochromatin in the X Chromosome of Drosophila Melanogaster. *Genetics* 24(3):413-35.

McAinsh, AD., Meraldi, P. (2011). The CCAN complex: linking centromere specification to control of kinetochore-microtubule dynamics. *Seminars in cell and developmental biology* 22(9):946-52.

McAinsh, AD., Tytell, JD., Sorger, PK. (2003). Structure, function, and regulation of budding yeast kinetochores. *Annual review of cell and developmental biology* 19:519-39.

McGuinness, BE., Hirato, T., Kudo, NR., Peters, JM., Nasmyth, K. (2005). Shugoshin prevents dissociation of cohesin from centromeres during mitosis in vertebrate cells. *Plos biology* 3(3):e86.

McKinley, KL., Cheeseman, IM. (2016). The molecular basis for centromere identity and function. *Nature reviews molecular cell biology* 17(1):16-29.

Measday, V., Hailey, DW., ot, I., Givan, SA., Hyland, KM., Cagney, G., Fields, S., Davis, TN., Hieter, P. (2002). Ctf3p, the Mis6 budding yeast homolog, interacts with Mcm22p and Mcm16p at the yeast outer kinetochore. *Genes & development* 16(1):101-13.

Medhi, D., Goldman, AS., Lichten, M. (2016). Local chromosome context is a major determinant of crossover pathway biochemistry during budding yeast meiosis. *Elife* 5. pii: e19669.

Megee, PC., Mistrot, C., Guacci, V., Koshland, D. (1999). The centromeric sister chromatid cohesion site directs Mcd1p binding to adjacent sequences. *Molecular cell* 4(3):445-50.

Mehta, GD., Agarwal, M., Ghosh, SK. (2014). Functional characterization of kinetochore protein, Ctf19 in meiosis I: an implication of differential impact of Ctf19 on the assembly of mitotic and meiotic kinetochores in Saccharomyces cerevisiae. *Molecular microbiology* 91(6):1179-99.

Meller, J., Morillon, A. (2004). ISWI complexes in Saccharomyces cerevisiae. *Biochica et Biophysica Acta* 1677(1-3):100-12.

Meyer, RE, Chuong, HH., Hild, M., Hanson, CL., Kinter, M., Dawson, DS. (2015). Ipl1/Aurora-B is necessary for kinetochore restructuring in meiosis I in Saccharomyces cerevisiae. *Molecular biology of the cell* 26(17):2986-3000.

Michaelis, C., Ciosk, R., Nasmyth, K. (1997). Cohesins: chromosomal proteins that prevent premature separation of sister chromatids. *Cell* 91(1):35-45.

Miller, MP., Unal, E., Brar, GA., Amon, A. (2012). Meiosis I chromosome segregation is established through regulation of microtubule-kinetochore interactions. *Elife* 1:e00117.

Miranda, JJ., De Wulf, P., Sorger, PK., Harrison, SC. (2005). The yeast DASH complex forms closed rings on microtubules. *Nature structural & molecular biology* 12(2):138-43.

Mitchell, AP. (1994). Control of meiotic gene expression in Saccharomyces cerevisiae. *Microbiological reviews* 58(1):56-70.

Mitchell, AP. (1988). Two switches govern entry into meiosis in yeast. *Progress in clinical and biological research* 267:47-66.

Murakami, H., Keeney, S. (2008). Regulating the formation of DNA double-strand breaks in meiosis. *Genes & development* 22(3):286-92.

Murray, A. (1994). Cell cycle checkpoints. *Current opinion in cell biology* 6(6):872-6.
Musacchio, A. (2011). Spindle assembly checkpoint: the third decade. *Philosophical transactions of the royal society of London* 366(1584):3595-604.

Musacchio, A., Desai, A. (2017). A Molecular View of Kinetochore Assembly and Function. *Biology* 6(1). pii: E5.

Musacchio, A., Salmon, ED. (2007). The spindle-assembly checkpoint in space and time. *Nature reviews molecular cell biology* 8(5):379-93.

Nakaseko, Y., Adachi, Y., Funahashi, S., Niwa, O., Yanagida, M. (1986). Chromosome walking shows a highly homologous repetitive sequence present in all the centromere regions of fission yeast. *The embo journal* 5(5):1011-21.

Nambiar, M., Smith, GR. (2016). Repression of harmful meiotic recombination in centromeric regions. *Seminars in cell and developmental biology* 54:188-97.

Nasmyth, K. (2001). Disseminating the genome: joining, resolving, and separating sister chromatids during mitosis and meiosis. *Annual review of genetics* 35:673-745.

Natsume, T., Müller, CA., Katou, Y., Retkute, R., Gierlinski, M., Araki, H., Blow, JJ., Shirahige, K., Nieduszynski, CA., Tanaka, TU. (2013). Kinetochores coordinate pericentromeric cohesion and early DNA replication by Cdc7-Dbf4 kinase recruitment. *Molecular cell* 50(5):661-74.

Nerusheva, OO., Galander, S., Fernius, J., Kelly, D., Marston, AL. (2014). Tension-dependent removal of pericentromeric shugoshin is an indicator of sister chromosome biorientation. *Genes & development* 28(12):1291-309.

Ng, TM., Waples, WG., Lavoie, BD., Biggins, S. (2009). Pericentromeric sister chromatid cohesion promotes kinetochore biorientation. *Molecular biology of the cell* 20(17):3818-27.

Niu, H., Li, X., Job, E., Park, C., Moazed, D., Gygi, SP., Hollingsworth, N. (2007). Mek1 kinase is regulated to suppress double-strand break repair between sister chromatids during budding yeast meiosis. *Molecular and cellular biology* 27(15):5456-67.

Niu, H., Wan, L., Baumgartner, B., Schaefer, D., Loidl, J., Hollingsworth, N. (2005). Partner choice during meiosis is regulated by Hop1-promoted dimerization of Mek1. *Molecular biology of the cell* 16(12):5804-18.

Niu, H., Wan, L., Busygina, V., Kwon, Y., Allen, JA., Li, X., Kunz, RC., Kubota, K., Wang, B., Sung, P., Shokat, KM., Gygi, SP., Hollingsworth, N. (2009) Regulation of meiotic recombination via Mek1-mediated Rad54 phosphorylation. *Molecular cell* 36(3):393-404.

Ocampo, J., Chereji, RV., Eriksson, PR., Clark, DJ. (2016). The ISW1 and CHD1 ATP-dependent chromatin remodelers compete to set nucleosome spacing in vivo. *Nucleic acids research* 44(10):4625-35.

Ogino, K., Masai, H. (2006). Rad3-Cds1 mediates coupling of initiation of meiotic recombination with DNA replication. Mei4-dependent transcription as a potential target of meiotic checkpoint. *The journal of biological chemistry* 281(3):1338-44.

Oke, A., Anderson, CM., Yam, P., Fung, JC. (2014). Controlling meiotic recombinational repair - specifying the roles of ZMMs, Sgs1 and Mus81/Mms4 in crossover formation. *Plos genetics* 10(10):e1004690.

Oritz, J., Stemmann, O., Rank, S., Lechner, J. (1999). A putative protein complex consisting of Ctf19, Mcm21, and Okp1 represents a missing link in the budding yeast kinetochore. *Genes & development* 13(9):1140-55.

Orr, B., Godek, KM., Compton, D. (2015). Aneuploidy. Current biology 25(13):R538-42.

Page, SL., Hawley, RS. (2004). The genetics and molecular biology of the synaptonemal complex. *Annual review of cell and developmental biology* 20:525-58.

Pagliuca, C., Draviam, VM., Marco, E., Sorger, PK., De Wulf, P. (2009) Roles for the conserved spc105p/kre28p complex in kinetochore-microtubule binding and the spindle assembly checkpoint. *Plos one* 4(10):e7640.

Pan, J., Sasaki, M., Kniewel, R., Murakami, H., Blitzblau, HG., Tischfield, SE., Zu, X., Neale, MJ., Jasin, M., Socci, ND., Hochwagen, A., Keeney, S. (2011). A hierarchical combination of factors shapes the genome-wide topography of yeast meiotic recombination initiation. *Cell* 144(5):719-31.

Pangilinan, F., Spencer, F. (1996). Abnormal kinetochore structure activates the spindle assembly checkpoint in budding yeast. *Molecular biology of the cell* 7(8):1195-208.

Panizza, S., Mendoza, MA., Berlinger, M., Huang, L., Nicolas, A., Shirahige, K., Klein, F. (2011). Spo11-accessory proteins link double-strand break sites to the chromosome axis in early meiotic recombination. *Cell* 146(3):372-83.

Pekgöz Altunkaya, G., Malvezzi, F., Demianova, Z., Zimniak, T., Litos, G., Weissmann, F., Mechtler, K., Herzog, F., Westermann, S. (2016). CCAN Assembly Configures Composite Binding Interfaces to Promote Cross-Linking of Ndc80 Complexes at the Kinetochore. *Current biology* 26(17):2370-8.

Petes, TD. (2001). Meiotic recombination hot spots and cold spots. *Nature reviews genetics* 2(5):360-9.

Petronczki, M., Siomos, MF., Nasmyth, K. (2003). Un ménage à quatre: the molecular biology of chromosome segregation in meiosis. *Cell* 112(4):423-40.

Phadnis, N., Hyppa, RW., Smith, GR. (2011). New and old ways to control meiotic recombination. *Trends in genetics* 27(10):411-21.

Pinsky, BA., Tasutani, SY., Collins, KA., Biggins, S. (2003). An Mtw1 complex promotes kinetochore biorientation that is monitored by the Ipl1/Aurora protein kinase. *Developmental cell* 5(5):735-45.

Pot, I., Measday, V., Snydsman, B., Cagney, G., Fields, S., Davis, TN., Muller, EG., Hieter, P. (2003). Chl4p and iml3p are two new members of the budding yeast outer kinetochore. *Molecular biology of the cell* 14(2):460-76.

Potapova, T., Gorbsky, GJ. (2017). The Consequences of Chromosome Segregation Errors in Mitosis and Meiosis. *Biology* 6(1).

Powers, AF., Franck, AD., Gestaut, DR., Cooper, J., Gracyzk, B., Wei, RR., Wordeman, L., Davis, TN., Asbury, CL. (2009). The Ndc80 kinetochore complex forms load-bearing attachments to dynamic microtubule tips via biased diffusion. *Cell* 136(5):865-75.

Prieler, S., Penkner, A., Borde, V., Klein, F. (2005). The control of Spo11's interaction with meiotic recombination hotspots. *Genes & development* 19(2):255-69.

Puechberty, J., Laurent, AM., Gimenez, S., Billault, A., Brun-Laurent, ME., Calenda, A., Marcais, B., Prades, C., Ioannou, P., Yurov, Y., Roizès, G. (1999). Genetic and physical analyses of the centromeric and pericentromeric regions of human chromosome 5: recombination across 5cen. *Genomics* 56(3):274-87.

Qi, LS., Larson, MH., Gilbert, LA., Doudna, JA., Weissman, JS., Arkin, AP., Lim, WA. (2013). Repurposing CRISPR as an RNA-guided platform for sequence-specific control of gene expression. *Cell* 152(5):1173-83.

Rabitsch KP., Gregan, J., Schleiffer, A., Javerzat, JP., Eisenhaber, F., Nasmyth, K. (2004). Two fission yeast homologs of Drosophila Mei-S332 are required for chromosome segregation during meiosis I and II. *Current biology* 14(4):287-301.

Richardson, A., Gardner, RG., Prelich, G. (2013). Physical and genetic associations of the Irc20 ubiquitin ligase with Cdc48 and SUMO. *Plos one* 8(10):e76424.

Riedel, CG., Katis, VL., Katou, Y., Mori, S., Itoh, T., Helmhart, W., Gálová, M., Petronczki, M., Gregan, J., Cetin, B., Mudrak, I., Ogris, E., Mechtler, K., Pelletier, L., Buchholz, F., Shirahige, K., Nasmyth, K. (2006). Protein phosphatase 2A protects centromeric sister chromatid cohesion during meiosis I. *Nature* 441(7089):53-61.

Robine, N., Uematsu, N., Amiot, X., Barillot, E., Nicolas, A., Borde, V. (2006). Genome-wide redistribution of meiotic double-strand breaks in Saccharomyces cerevisiae. *Molecular and cellular biology* 27(5):1868-80.

Rockmill, B., Voelkel-Meiman, K., Roeder, GS. (2006). Centromere-proximal crossovers are associated with precocious separation of sister chromatids during meiosis in Saccharomyces cerevisiae. *Genetics* 174(4):1745-54.

Romao, M., Tanaka, K., Sibarita, JB., Ly-Hartig, NT., Tanaka, TU., Antony, C. (2008). Three-dimensional electron microscopy analysis of ndc10-1 mutant reveals an aberrant organization of the mitotic spindle and spindle pole body defects in Saccharomyces cerevisiae. *Journal of structural biology* 163(1):18-28.

Roeder, GS., Bailis, JM. (2000). The pachytene checkpoint. *Trends in genetics* 16(9):395-403.

Roy, MA., Dhanaraman, T., D'Amours, D. (2015). The Smc5-Smc6 heterodimer associates with DNA through several independent binding domains. *Scientific reports* 5:9797.

Saintenac, C., Falque, M., Martin, OC., Paux, E., Feuillet, C., Sourdille, P. (2009). Detailed recombination studies along chromosome 3B provide new insights on crossover distribution in wheat (Triticum aestivum L.). *Genetics* 181(2):393-403.

San-Segundo, PA., Roeder, GS. (1999). Pch2 links chromatin silencing to meiotic checkpoint control. *Cell* 97(3):313-24.

Santaguida, S., Musacchio, A. (2009). The life and miracles of kinetochores. *The embo journal* 28(17):2511-31.

Sasaki, M., Lange, J., Keeney, S. (2010). Genome destabilization by homologous recombination in the germ line. *Nature reviews molecular cell biology* 11(3):182-95.

Sasanuma, H., Murakami, H., Fukuda, T., Shibata, T., Nicolas, A., Ohta, K. (2007). Meiotic association between Spo11 regulated by Rec102, Rec104 and Rec114. *Nucleic acids research* 35(4):1119-33.

Schalbetter, SA., Goloborodko, A., Fudenberg, G., Belton, JM., Miles, C., Yu, M., Dekker, J., Mirny, L., Baxter, J. (2016). Cohesin dependent compaction of mitotic chromosomes. *Biorxiv*

Schleiffer, A., Maier, M., Litos, G., Lampert, F., Hornung, P., Mechtler, K., Westermann, S. (2012). CENP-T proteins are conserved centromere receptors of the Ndc80 complex. *Nature cell biology* 14(6):604-13.

Schmitzberger, F., Harrison, SC. (2012). RWD domain: a recurring module in kinetochore architecture shown by a Ctf19-Mcm21 complex structure. *Embo reports* 13(3):216-22.

Schmitzberger, F., Richter, MM., Gordiyenko, Y., Robinson, CV., Dadlez, M., Westermann, S. (2017). Molecular basis for inner kinetochore configuration through RWD domain-peptide interactions. *The embo journal* 36(23):3458-3482.

Schwacha, A., Kleckner, N. (1994). Identification of joint molecules that form frequently between homologs but rarely between sister chromatids during yeast meiosis. *Cell* 76(1):51-63.

Schwacha, A., Kleckner, N. (1997). Interhomolog bias during meiotic recombination: meiotic functions promote a highly differentiated interhomolog-only pathway. *Cell* 90(6):1123-35.

Sclafani, RA. (2000). Cdc7p-Dbf4p becomes famous in the cell cycle. *Journal of cell science 113* (Pt 12):2111-7.

Sehorn, MG., Sung, P. (2004). Meiotic recombination: an affair of two recombinases. *Cell cycle* 3(11):1375-7.

Simchen, G. (1974). Are mitotic functions required in meiosis? *Genetics* 76(4):745-53.

Shen, X., Ranallo, R., Choi, E., Wu, C. (2003). Involvement of actin-related proteins in ATP-dependent chromatin remodeling. *Molecular cell* 12(1):147-55.

Shinohara, A., Ogawa, H., Ogawa, T. (1992). Rad51 protein involved in repair and recombination in S. cerevisiae is a RecA-like protein. *Cell* 69(3):457-70.

Sjögren, C., Nasmyth, K. (2001). Sister chromatid cohesion is required for postreplicative double-strand break repair in Saccharomyces cerevisiae. *Current biology* 11(12):991-5.

Smith, BJ., (1984). SDS Polyacrylamide Gel Electrophoresis of Proteins. *Methods in molecular biology* 1:41-55.

Smith, MM. (2002). Centromeres and variant histones: what, where, when and why? *Current opinion in cell biology* 14(3):279-85.

Smith, AV., Roeder, GS., (1997). The yeast Red1 protein localizes to the cores of meiotic chromosomes. *The journal of cell biology* 136(5):957-67.

Smith, HE., Su, SS., Neigeborn, L., Driscoll, SE., Mitchell, AP. (1990). Role of IME1 expression in regulation of meiosis in Saccharomyces cerevisiae. *Molecular and cell biology* 10(12):6103-13.

Sourirajan, A., Lichten, M. (2008). Polo-like kinase Cdc5 drives exit from pachytene during budding yeast meiosis. *Genes & development* 22(19):2627-32.

Sorger, PK., Severin, FF., Hyman, AA. (1994). Factors required for the binding of reassembled yeast kinetochores to microtubules in vitro. *The journal of cell biology* 127(4):995-1008.

Stephens, AD., Haase, J., Vicci, L., Taylor, RM., Bloom, K. (2011). Cohesin, condensin, and the intramolecular centromere loop together generate the mitotic chromatin spring. *The journal of cell biology* 193(7):1167-80.

Stoler, S. Rogers, K., Weitze, S., Morey, L., Fitzgerald-Hayes, M., Baker, RE. (2007). Scm3, an essential Saccharomyces cerevisiae centromere protein required for G2/M progression and Cse4 localization. *Proceedings of the national academy of sciences* 104(25):10571-6.

Storlazzi, A., Tessé, S., Gargano, S., James, F., Kleckner, N., Zickler, D. (2003). Meiotic double-strand breaks at the interface of chromosome movement, chromosome remodeling, and reductional division. *Genes & development* 17(21):2675-87.

Storlazzi, A., Xu, L., Cao, L., Kleckner, N. (1995). Crossover and noncrossover recombination during meiosis: timing and pathway relationships. *Proceedings of the national academy of sciences* 92(18):8512-6.

Ström, L., Betts Lindroos, HB., Shirahige, K., Sjögren, C. (2004). Postreplicative recruitment of cohesin to double-strand breaks is required for DNA repair. *Molecular cell* 16(6):1003-15.

Ström, L., Sjörgen, C. (2007). Chromosome segregation and double-strand break repair - a complex connection. *Current opinion in cell biology* 19(3):344-9.

Stuart, D., Wittenberg, C. (1998). CLB5 and CLB6 are required for premeiotic DNA replication and activation of the meiotic S/M checkpoint. *Genes & development* 12(17):2698-710.

Subramanian, VV., Hochwagen, A. (2014). The meiotic checkpoint network: step-by-step through meiotic prophase. *Cold spring harbor perspectives in biology* 6(10):a016675.

Subramanian, VV., Mac Queen, AJ., Vader, G., Shinohara, M., Sanchez, A., Borde, V., Shinohara, A., Hochwagen, A. (2016). Chromosome Synapsis Alleviates Mek1-Dependent Suppression of Meiotic DNA Repair. *Plos biology* 14(2):e1002369.

Subramanian, VV., Markowitz, TE., Vale-Silva, LA., San-Segundo, PA., Hollingsworth, N., Hochwagen, A. (2017). Persistent DNA-break potential near telomeres increases initiation of meiotic recombination on small chromosomes. *Biorxiv*

Sumara, I., Vorlaufer, E., Stukenberg, PT., Kelm, O., Redemann, N., Nigg, EA., Peters, JM. (2002). The dissociation of cohesin from chromosomes in prophase is regulated by Polo-like kinase. *Molecular cell* 9(3):515-25.

Sun, X., Huang, L., Markowitz, TE., Blitzblau, HG., Chen, D., Klein, F., Hochwagen, A. (2015). Transcription dynamically patterns the meiotic chromosome-axis interface. *Elife* 4,

Sun, SC., Kim, NH. (2012). Spindle assembly checkpoint and its regulators in meiosis. *Human reproduction update* 18(1):60-72.

Sym, M., Engebrecht, JA., Roeder, GS. (1993). ZIP1 is a synaptonemal complex protein required for meiotic chromosome synapsis. *Cell* 72(3):365-78.

Talbert, PB., Henikoff, S. (2010). Centromeres convert but don't cross. *Plos biology* 8(3):e1000326.

Tanaka, T., Cosma, MP., Wirth, K., Nasmyth, K. (1999). Identification of cohesin association sites at centromeres and along chromosome arms. *Cell* 98(6):847-58.

Tang, Z., Shu, H., Qi, W., Mahmood, NA., Mumby, MC., Yu, H. (2006). PP2A is required for centromeric localization of Sgo1 and proper chromosome segregation. *Develpomental cell* 10(5):575-85.

Tanksley, SD., Ganal, MW., Prince, JP., de Vicente, MC., Bonierbale, MW., Broun, P., Fulton, TM., Giovannoni, JJ., Grandillo, S., Martin, GB., et al. (1992). High density molecular linkage maps of the tomato and potato genomes. *Genetics* 132(4):1141-60.

Terentyev, Y., Johnson, R., Neale, RMJ., Khisroon, M., Bishop-Bailey, A., Goldman, AS. (2010). Evidence that MEK1 positively promotes interhomologue double-strand break repair. *Nucleic acids research* 38(13):4349-60.

Thacker, D., Lam, I., Knop, M., Keeney, S. (2011). Exploiting spore-autonomous fluorescent protein expression to quantify meiotic chromosome behaviors in Saccharomyces cerevisiae. *Genetics* 189(2):423-39.

Tischfield, SE., Keeney, S. (2012). Scale matters: the spatial correlation of yeast meiotic DNA breaks with histone H3 trimethylation is driven largely by independent colocalization at promoters. *Cell Cycle* 11(8):1496-503.

Tonami, Y., Murakami, H., Shirahige, K., Nakanishi, M. (2005). A checkpoint control linking meiotic S phase and recombination initiation in fission yeast. *Proceedings of the national academy of sciences* 102(16):5797-801.

Tsubouchi, T., Roeder, GS. (2005). A synaptonemal complex protein promotes homology-independent centromere coupling. *Science* 308(5723):870-3.

Uhlmann, F. (2016). SMC complexes: from DNA to chromosomes. *Nature reviews cell biology* 17(7):399-412.

Uhlmann, F., Lottspeich, F., Nasmyth, K. (1999). Sister-chromatid separation at anaphase onset is promoted by cleavage of the cohesin subunit Scc1. *Nature* 400(6739):37-42.

Uhlmann, F., Nasmyth, K. (1998). Cohesion between sister chromatids must be established during DNA replication. *Current biology* 8(20):1095-101.

Usui, T., Ohta, T., Oshiumi, H., Tomizawa, J., Ogawa, H., Ogawa, T. (1998). Complex formation and functional versatility of Mre11 of budding yeast in recombination. *Cell* 95(5):705-16.

Vader, G. (2015). Pch2(TRIP13): controlling cell division through regulation of HORMA domains. *Chromosoma* 124(3):333-9.

Vader, G., Blitzblau, HG., Tame, MA., Falk, JE., Curtin, L., Hochwagen, A. (2011). Protection of repetitive DNA borders from self-induced meiotic instability. *Nature* 477(7362):115-9.

Van Berkum, NL., Lieberman-Aiden, E., Williams, L., Imakaev, M., Gnitke, A., Mirny, LA., Dekker, J., Lander, ES. (2010). Hi-C: A Method to Study the Three-dimensional Architecture of Genomes. *Journal of visualized experiments* (39): 1869.

Van Werven, FJ., Amon, A. (2011). Regulation of entry into gametogenesis. *Philosophical transactions of the royal society of London* 366(1584):3521-31.

Vary, JC Jr., Gangaraju, VK., Qin, J., Landel, CC., Kooperberg, C., Bartholomew, B., Tsukiyama, T. (2003). Yeast Isw1p forms two separable complexes in vivo. *Molecular and cellular biology* 23(1):80-91.

Verdaasdonk, JS., Bloom, K. (2011). Centromeres: unique chromatin structures that drive chromosome segregation. *Nature reviews molecular cell biology* 12(5):320-32.

Vershon, AK., Hollingsworth, NM., Johnson, AD. (1992). Meiotic induction of the yeast HOP1 gene is controlled by positive and negative regulatory sites. *Molecular and cellular biology* 12(9):3706-14.

Vershon, AK., Pierce, M. (2000). Transcriptional regulation of meiosis in yeast. *Current opinion in cell biology* 12(3):334-9.

Verzijlbergen, KF., Nerusheva, OO., Kelly, D., Kerr, A., Clift, D., de Lima Alves, F., Rappsilber, J., Marston, AL. (2014). Shugoshin biases chromosomes for biorientation through condensin recruitment to the pericentromere. *Elife* 3:e01374.

Vincenten, N., Kuhl, LM., Lam, I., Oke, A., Kerr, ARW., Hochwagen, A., Fung, J., Keeney, S., Vader, G., Marston, AL. (2015). The kinetochore prevents centromere-proximal crossover recombination during meiosis. *Elife* 4: e10850.

Vissel, B., Choo, KH. (1989). Mouse major (gamma) satellite DNA is highly conserved and organized into extremely long tandem arrays: implications for recombination between nonhomologous chromosomes. *Genomics* 5(3):407-14.

Waizenegger, IC., Hauf, S., Meinke, A., Peters, JM. (2000). Two distinct pathways remove mammalian cohesin from chromosome arms in prophase and from centromeres in anaphase. *Cell* 103(3):399-410.

Wan, L., de los Santos, T., Zhang, C., Shokat, K., Hollingsworth, N. (2004). Mek1 kinase activity functions downstream of RED1 in the regulation of meiotic double strand break repair in budding yeast. *Molecular biology of the cell* 15(1):11-23.

Wan, L., Niu, H., Futcher, B., Zhang, C., Shokat, KM., Boulton, SJ., Hollingsworth, N. (2008). Cdc28-Clb5 (CDK-S) and Cdc7-Dbf4 (DDK) collaborate to initiate meiotic recombination in yeast. *Genes & development* 22(3):386-97.

Wang, Y., Burke, DJ. (1995). Checkpoint genes required to delay cell division in response to nocodazole respond to impaired kinetochore function in the yeast Saccharomyces cerevisiae. *Molecular and cellular biology* 15(12):6838-44.

Watanabe, Y. (2012). Geometry and force behind kinetochore orientation: lessons from meiosis. *Nature reviews molecular cell biology* 13(6):370-82.

Watanabe, Y., Kitajima, TS. (2005). Shugoshin protects cohesin complexes at centromeres. *Philosophical transactions of the royal society of London* 360(1455):515-21.

Weber, SA., Gerton, JL., Polancic, JE., DeRisi, JL., Koshland, D., Megee, PC. (2004). The kinetochore is an enhancer of pericentric cohesin binding. *Plos biology* 2(9):E260.

Weinert, T. (1998). DNA damage checkpoints update: getting molecular. *Current opinion in genetics & development* 8(2):185-93.

Westermann, S., Avila-Sakar, A., Wang, HW., Niederstrasser, H., Wong, J., Drubin, DG., Nogales, E., Barnes, G. (2005). Formation of a dynamic kinetochore-microtubule interface through assembly of the Dam1 ring complex. *Molecular cell* 17(2):277-90.

Westermann, S., Drubin, DG., Barnes, G. (2007). Structures and functions of yeast kinetochore complexes*. Annual review of biochemistry* 76:563-91.

Westermann, S., Schleiffer, A. (2013). Family matters: structural and functional conservation of centromere-associated proteins from yeast to humans. *Trends in cell biology* 23(6):260-9.

Westhorpe, FG., Straight, AF. (2013). Functions of the centromere and kinetochore in chromosome segregation. *Current opinion in cell biology* 25(3):334-40.

Westphal, T., Reuter, G. (2002). Recombinogenic effects of suppressors of position-effect variegation in Drosophila. *Genetics* 160(2):609-21.

Wiedenheft, B., Sternberg, SH., Doudna, JA. (2012). RNA-guided genetic silencing systems in bacteria and archaea. *Nature* 482(7385):331-8.

Woltering, D., Baumgartner, B., Bagchi, S., Larkin, B., Loidl, J., de los Santos, T., Hollingsworth, N. (2000). Meiotic segregation, synapsis, and recombination checkpoint functions require physical interaction between the chromosomal proteins Red1p and Hop1p. *Molecular and cellular biology* 20(18):6646-58.

Wu, HY., Burgess, SM. (2006). Two distinct surveillance mechanisms monitor meiotic chromosome metabolism in budding yeast. *Current biology* 16(24):2473-9.

Xiong, B. (2011). Spc25: How the kinetochore protein plays during oocyte meiosis. *Cell cycle* 10(7):1031-1030.

Xu, Z., Cetin, B., Anger, M., Cho, US., Helmhart, W., Nasmyth, K.Xu, W. (2009). Structure and function of the PP2A-shugoshin interaction. *Molecular cell* 35(4):426-41.

Yamagishi, Y., Sakuno, T., Goto, Y., Watanabe, Y. (2014). Kinetochore composition and its function: lessons from yeasts. *Fems microbiology reviews* 38(2):185-200.

Yu, HG., Koshland, DE. (2003). Meiotic condensin is required for proper chromosome compaction, SC assembly, and resolution of recombination-dependent chromosome linkages. *The journal of cell biology* 163(5):937-47.

Zickler, D., Kleckner, N. (2015). Recombination, Pairing, and Synapsis of Homologs during Meiosis. *Cold spring harbor perspectives in biology* 7(6). pii: a016626.

Acknowledgements

First and foremost, I would like to express my deepest gratitude to my supervisor Dr. Gerben Vader for giving me the opportunity to carry out my doctoral research study in his lab. I am forever indebted to him for his continuous support, guidance and encouragement in the course of this project. In the lab he did not only introduce me to various techniques in yeast genetics but also helped me to troubleshoot problems concerning my practical work. I am also thankful for his scientific discussions and ideas as well as sharing his immense knowledge about meiosis.

I would like to thank Prof. Dr. Andrea Musacchio and Prof. Dr. Stefan Westermann not only for their suggestions and feedback on my progress throughout my PhD work but also for taking the time to be examiners of my PhD thesis.

I want to express my sincere gratitude to Dr. Nadine Vincenten and Dr. Adèle Marston, Dr. Isabel Lam and Dr. Scott Keeney, Dr. Ashwini Oke and Dr. Jennifer Fung as well as Dr. Andreas Hochwagen for collaborating with us and contributing their data to our publication. In particular, I would like to acknowledge Dr. Adèle Marston for her collaboration with us in the past and present. I am thankful to her for sharing data and reagents as well as scientific knowledge.

I am grateful to past and present members of “AG Vader” and “AG Bird” not only for scientific discussions and ideas in our common group meetings but also for their friendship throughout my PhD. I am particularly thankful to Dr. Richard Cardoso da Silva for introducing me to chromatin immunoprecipitation analysis and real-time quantitative PCR. I would also like to acknowledge him for his advices regarding my project. My thanks go to Dr. Arnaud Rondelet for his help in choosing target sequences for the CRISPR-dCas9 system and Divya Singh for a detailed introduction to the DeltaVision microscope. I would also like to express my thankfulness to all members of Department I for a nice working atmosphere and making me feel welcome.

Finally, I would like to acknowledge my family for believing in me and being supportive throughout my whole life. Without them, I would not have made it this far. The last word of my acknowledgements goes to my husband Nicolai Kuhl, who has been a constant source of strength and encouragement during this adventurous “PhD journey”. He is always by my side and keeps a strong faith in me during hard times. Without him this thesis would not have been possible.

Affidavit

Hiermit erkläre ich, Lisa-Marie Kuhl, gem. § 7 Abs. (2) d) + f) der Promotionsordnung der Fakultät für Biologie zur Erlangung des Dr. rer. nat., dass ich die vorliegende Dissertation selbstständig verfasst und mich keiner anderen als der angegebenen Hilfsmittel bedient, bei der Abfassung der Dissertation nur die angegebenen Hilfsmittel benutzt und alle wörtlich oder inhaltlich übernommen Stellen als solche gekennzeichnet habe.

Essen, den Unterschrift:

Hiermit erkläre ich, Lisa-Marie Kuhl, gem. § 7 Abs. (2) e) + g) der Promotionsordnung der Fakultät für Biologie zur Erlangung des Dr. rer. nat., dass ich keine anderen Promotionen bzw. Promotionsversuche in der Vergangenheit durchgeführt habe und dass diese Arbeit von keiner anderen Fakultät/ Fachbereich abgelehnt worden ist.

Essen, den Unterschrift:

Hiermit erkläre ich, Prof. Dr. Andrea Musacchio, gem. § 6 Abs. (2) g) der Promotionsordnung der Fakultät für Biologie zur Erlangung des Dr. rer. nat., dass ich das Arbeitsgebiet, dem das Thema “Kinetochore-driven control of meiotic DNA break formation and recombination at centromere-proximal regions” zuzuordnen ist, in Forschung und Lehre vertrete und den Antrag von Lisa-Marie Kuhl befürworte und die Betreuung auch im Falle eines Weggangs, wenn nicht wichtige Gründe dem entgegenstehen, weiterführen werde.

Essen, den Unterschrift: